EVALUATING BENDING AND TRANSLATIONAL BEHAVIOR OF SANDWICH PANELS AT AMBIENT AND ELEVATED TEMPERATURES

Von der Fakultät für Architektur, Bauingenieurwesen und Stadtplanung der

Brandenburgischen Technischen Universität Cottbus-Senftenberg zur Erlangung des

akademischen Grades eines

Doktor der Ingenieurwissenschaften (Dr.-Ing.)

genehmigte Dissertation

vorgelegt von

M.Sc.-Ing.

Ashkan Shoushtarian Mofrad

aus Isfahan, Iran

Gutachter:	Prof. Dr.-Ing. habil. Hartmut Pasternak
Gutachter:	Prof. Dr.-Ing. Meri Cvetkovska
Gutachter:	Prof. Dr.-Ing. Mikko Malaska

Tag der Disputation: 25.03.2022

Schriftenreihe Stahlbau 2022, Heft 20, ISSN 1611-5023

DECLARATION

I declare that this thesis represents my own work, except where due acknowledgment is made. It has not been previously included in a thesis, dissertation or report submitted to this University or any other institution for a degree, diploma or other qualification.

ACKNOWLEDGEMENT

First and foremost, I am grateful to my supervisor, Professor Dr.- Eng. habil. Hartmut Pasternak for his supervision, valuable guidance, counsel, continuous support, patience and encouragement throughout the period of my Ph.D. research. I would like to thank him for believing in me and supporting me in doing my research.

I am thankful to Prof. Dr.-Ing. Meri Cvetkovska and Prof. Dr.-Ing. Mikko Malaska for the time that they have invested in assessing the work.

I wish to express my warm and sincere thanks to the German Academic Exchange Service (DAAD) for their financial support. A special thank goes to Mrs. Maren Grande and Mrs. Dagmar Hosseini-Razi for their valuable advice and friendly help.

I would like to thank Prof. Wald and his colleagues from the Department of Steel and Timber Structures, Czech Technical University in Prague, who carried out the bending and translational tests in the laboratory of the Faculty of Civil Engineering. I would also appreciate all the STABFI project partners who contributed to the project's testing phase (Tampere University, Czech Technical University in Prague, City, University of London, Budapest University of Technology and Economics, Brandenburg University of Technology, HAMK University of Applied Sciences, Ruukki Construction, Kingspan and SFS Intec).

I am grateful to all my colleagues at the Department of Steel and Timber Structures at the Brandenburg University of Technology Cottbus-Senftenberg for all kinds of support and help.

Last but not least, I would like to thank my parents and my sister for their understanding, support, and encouragement during my Ph.D. study.

ABSTRACT

Steel cladding structures such as sandwich panels can replace bracing systems to provide further stability to individual structural members such as beams and columns. Previous researches studied the stabilizing effects of sandwich panels on the whole structure at ambient temperatures. It was shown that considerable savings could be achieved in the case of using steel cladding systems. In the STABFI (Steel Cladding Systems for Stabilisation of Steel Buildings in Fire) project, the primary objective was to study the stabilizing behavior of cladding systems in the fire. The current thesis is a part of the STABFI project focusing on the bending and translational stiffness of sandwich panels at ambient and elevated temperatures.

The thesis consists of two separate parts, the bending and translational performance of sandwich panels at ambient and elevated temperatures. Sandwich panels are typically composites of two thin steel sheets and a core of higher thickness and lower density. They are valued for their excellent thermal properties. This research employs two different materials, including mineral wool (MW) and Polyisocyanurate (PIR), as a core.

In the first part of the thesis, the bending tests carried out in Prague are described. The experimental results are presented in the first phase of this part. A finite element (FE) model is developed to validate simulations with experimental results, and then a comprehensive parametric study is carried out. During the parametric study, different factors such as panel thickness, width, span, the thickness of steel sheets, and the fire's influence on panels' mechanical behavior are investigated. Moreover, the analytical solutions obtained from Eurocodes (EN 14509, 2013) at ambient temperature are employed to predict the bending stiffness values. The analytical solutions are then developed to apply at elevated temperatures by incorporating the reduction factors into the equations. Eventually, the accuracy of suggested analytical equations is compared with numerical results.

In the second part of the thesis, after presenting the translational tests which also conducted in Prague and validation of FE models, an extensive parametric study on the decisive factors such as the steel sheet thicknesses, screw diameters and temperature effects on the sandwich panel connections behavior is performed. The parametric study shows how each parameter affects the shear resistance and stiffness of sandwich panel connections. Furthermore, the deterioration of shear performance at elevated temperatures is evaluated. The analytical solutions achieved from the ECCS manual are used to estimate the shear stiffness and resistance of connections at

ambient temperatures. At elevated temperatures, the equations are developed to anticipate the abovementioned values in the fire case. Finally, the safety and accuracy of proposed analytical solutions are assessed.

ZUSAMMENFASSUNG

Stahlverkleidungskonstruktionen wie Sandwichelemente können Aussteifungssysteme ersetzen, um einzelnen Bauteilen wie Trägern und Stützen zusätzliche Stabilität zu verleihen. Frühere Forschungen untersuchten die stabilisierende Wirkung von Sandwichelementen auf die gesamte Struktur bei Raumtemperaturen. Es wurde gezeigt, dass bei der Verwendung von Stahlverkleidungssystemen erhebliche Einsparungen erzielt werden können. Im Projekt STABFI (Steel Cladding Systems for Stabilisation of Steel Buildings in Fire) war das primäre Ziel die Untersuchung des stabilisierenden Verhaltens von Bekleidungssystemen im Brandfall. Die vorliegende Arbeit ist ein Teil des STABFI-Projekts und beschäftigt sich mit der Biege- und Translationssteifigkeit von Sandwichpaneelen bei Raum- und erhöhten Temperaturen.

Die Arbeit besteht aus zwei separaten Teilen, dem Biege- und dem Translationsverhalten von Sandwichpaneelen bei Umgebungs- und erhöhter Temperatur. Sandwichpaneele sind typischerweise Verbundwerkstoffe aus zwei dünnen Stahlblechen und einem Kern mit höherer Dicke und verringerter Dichte. Sie werden wegen ihrer hervorragenden thermischen Eigenschaften geschätzt. In dieser Untersuchung werden zwei verschiedene Materialien, darunter Mineralwolle (MW) und Polyisocyanurat (PIR), als Kern verwendet.

Im ersten Teil der Arbeit werden die in Prag durchgeführten Biegeversuche beschrieben. Die experimentellen Ergebnisse werden in der ersten Phase dieses Teils vorgestellt. Ein Finite-Elemente-Modell (FE) wird entwickelt, um die Simulationen mit den experimentellen Ergebnissen zu validieren, danach wird eine umfassende parametrische Studie durchgeführt. Während der parametrischen Studie werden verschiedene Faktoren wie Plattendicke, Breite, Spannweite, die Dicke der Stahlbleche und der Einfluss des Feuers auf das mechanische Verhalten der Platten untersucht. Außerdem werden die analytischen Lösungen aus den Eurocodes (EN 14509, 2013) bei Umgebungstemperatur verwendet, um die Biegesteifigkeitswerte vorherzusagen. Die analytischen Lösungen werden dann für die Anwendung bei erhöhten Temperaturen entwickelt, indem die Reduktionsfaktoren in die Gleichungen aufgenommen werden. Schließlich wird die Genauigkeit der vorgeschlagenen analytischen Gleichungen mit numerischen Ergebnissen verglichen.

Im zweiten Teil der Arbeit wird nach der Vorstellung der ebenfalls in Prag Translationsversuche und der Validierung der FE-Modelle eine umfangreiche parametrische Studie zu den entscheidenden Faktoren wie den Stahlblechdicken, Schraubendurchmessern und Temperatureffekten auf das Verhalten der Sandwichelementverbindungen durchgeführt. Die

parametrische Studie zeigt, wie sich die einzelnen Parameter auf die Scherfestigkeit und Steifigkeit von Sandwichelementverbindungen auswirken. Darüber hinaus wird die Verschlechterung des Scherverhaltens bei erhöhten Temperaturen bewertet. Die analytischen Lösungen aus dem ECCS-Handbuch werden verwendet, um die Schersteifigkeit und den Widerstand der Verbindungen bei Raumtemperaturen abzuschätzen. Bei erhöhten Temperaturen werden die Gleichungen entwickelt, um die oben genannten Werte für den Brandfall zu antizipieren. Abschließend werden die Sicherheit und Genauigkeit der vorgeschlagenen analytischen Lösungen bewertet.

CONTENTS

LIST OF FIGURES

LIST OF TABLES

NOMENCLATURE

v	Poisson's ratio
E_{ii}	Young's modulus in i direction
E	Young's modulus
E_θ	Young's modulus at θ temperature
θ	Temperature
θ_a	Steel temperature
λ	Thermal conductivity
λ_a	Steel thermal conductivity
c	Specific heat
c_a	Steel specific heat
f_y	Yield stress
$f_{y,\theta}$	Yield stress at θ temperature
f_u	Ultimate tensile stress
$f_{u,\theta}$	Ultimate tensile stress at θ temperature
σ_{true}	True stress
$\sigma_{enginnering}$	Engineering stress
ε_{true}	True strain
$\varepsilon_{enginnering}$	Engineering strain
F_{max}	Maximum load
k_b	Bending stiffness
$NT11$	Temperature (°C)
v_{max}	Maximum deflection
G	Shear modulus
G_c	Shear modulus of core material
A_c	Cross-sectional areas of the core
A_{F1}	Cross-sectional areas of the external faces
A_{F2}	Cross-sectional areas of the external faces
e	Distance between centroids of faces
q	Uniform load
E_{F1}	Young's modulus of the external faces
E_{F2}	Young's modulus of the internal faces
F	Concentrated load

L	Span of panels
b	Width of core materials
D	Thickness of panels
B_{F1}	Bending stiffness of the external face with respect to its own axis
I	Moment of inertia
I_{F1}	Moment of inertia of the external face
B	Width of panels
t_{F1}	Thickness of external faces
t_{F2}	Thickness of internal faces
U_x	Displacement in x-direction
U_y	Displacement in y-direction
U_z	Displacement in z-direction
V	Shear resistance
k_v	Shear stiffness
d_s	Diameter of screws
$t_{cor,F2}$	Core thickness of internal faces
$t_{cor,sup}$	Thickness of substructure
d_1	Minor diameter of the threaded part of a fastener
$f_{u,F2}$	Ultimate tensile stress of internal faces
C_{sup}	Stiffness of clamping of fasteners in the substructure
k_F	Stiffness of face sheets
k	Reduction factors

Chapter 1: INTRODUCTION

1.1 Background

In the STABFI (Steel cladding systems for stabilization of steel buildings in fire) project, it has been shown that sandwich panels can efficiently be employed to provide additional stability to individual structural members and entire building frames. Sandwich panels consist of two thin and stiff facing sheets of dense material separated by a thick layer of low density, less stiff and less strong material as the core. The use of sandwich panels as roof and wall claddings has increased considerably in recent times. A comprehensive guidance set is currently provided in design codes at ambient temperature. However, knowledge on the stabilizing effect of cladding structures in a fire situation is still lacking. The primary purpose of the STABFI project was to produce enough data on the stabilizing behavior of sandwich panels in a fire such that the stabilizing effect could be considered in the design.

This thesis is a part of the STABFI project focusing on the bending and translational behavior of sandwich panels at ambient and elevated temperatures. The STABFI project results associated with sandwich panels' bending and translational behavior are developed and reported in this thesis. The thesis includes experimental, numerical and analytical models. The bending and translational behavior of sandwich panels are investigated in separate chapters.

1.2 Problem Statement and objectives

The aim of this research is to understand and evaluate the bending and translational (shear) performance of sandwich panels at ambient and elevated temperatures. This research is carried out mainly through finite element (FE) simulations using the ABAQUS software and analytical solutions.

The specific objectives of the research project are as follows:

- To provide detailed experimental information on bending tests;
- To validate and compare numerical models with bending tests;
- To establish accurate FE models for parametric study of bending specimens;

- To compare analytical solutions with numerical results for bending models at ambient temperature and develop them at elevated temperatures;
- To provide detailed experimental information for translational tests;
- To validate and compare numerical models with translational tests;
- To create accurate FE models for parametric study of translational specimens;
- To compare analytical solutions with numerical results at ambient temperature and extend them at elevated temperatures.

1.3 Outline of the thesis

This thesis contains the following chapters:

Chapter 1 gives a general introduction to the research background, the scope, and the thesis outline.

Chapter 2 introduces sandwich panels, their functions and applications and their material properties at ambient and elevated temperatures. Additionally, a summary of similar investigations conducted by other researchers is presented.

Chapter 3 presents details of bending tests and validates the numerical results with experimental ones. The details of numerical models created using ABAQUS are described in this chapter. The validation includes both thermal and mechanical results.

Chapter 4 performs a comprehensive parametric study according to the verified bending models. The influence of different parameters such as height, width and length of panels on the bending performance of models is evaluated. Then, the analytical results of existing design codes are compared with simulations at ambient temperature. Furthermore, the analytical solutions are developed to apply at elevated temperatures. The results of suggested analytical solutions at the fire are compared with numerical results.

Chapter 5 provides accurate information about translational tests. The details of numerical models are presented in this chapter. Afterward, the numerical results are validated against the experimental ones.

Chapter 6 conducts an extensive parametric study to investigate different efficient factors on sandwich panels' translational behavior. An analytical model is then established to compare the analytical and numerical results at ambient temperature. Therefore, the analytical solutions are

modified to be applicable at elevated temperatures. Eventually, the accuracy and safety of suggested solutions to predict the translational stiffness and resistance are evaluated at elevated temperatures.

Chapter 7 compares single-story buildings stabilized with bracings and sandwich panels to show the practical aspect of the current research.

Chapter 8 presents a summary of the work carried out in this research. The main conclusions from this research are stated, and probable future research topics are identified.

Chapter 2: LITERATURE REVIEW

2.1 Sandwich panels

Sandwich panels, typically composed of two thin reinforced steel sheets bonded on each side of a thick and lightweight foam core, are used in industrial and commercial buildings. They can be applied as an alternative for diagonal bracings to resist lateral loads and are easily adapted to walls and roofs. The core has sufficient stiffness in a direction normal to the sheets. The core is usually rubber, solid plastic material, rigid polymeric foam material (polyisocyanurate or polyurethane), mineral wool and honeycombs. The face sheets' static function is to carry bending and in-plane forces, while the core keeps the face sheets together and carries transverse shear loads. The facings are steel, aluminum or non-metallic material such as plywood particleboard or glass-reinforced plastic [1–6].

Various panel systems can be produced by combining different facings and core materials. In this research, the steel sheets, together with polyisocyanurate (PIR) and mineral wool (MW) as core materials, are employed (see Figure 2.1).

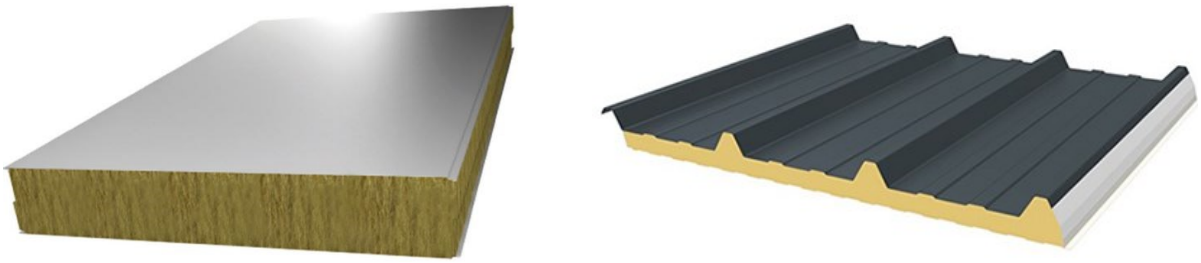

(a) (b)

Figure 2.1. Sandwich panels: a) MW panels, b) PIR panels

In addition to mechanical properties, the sandwich panels provide adequate acoustic insulation and excellent fire resistance. Generally, sandwich panels are used as external claddings, insulated internal envelopes and partitions and fire-resisting compartment walls [6,7].

2.2 Applications of sandwich panels

Sandwich panels can be employed efficiently to provide further stability to individual structural members (beams and columns) and entire building frames. In the STABFI project, it has been

shown that in the case of fixed column bases and unprotected columns, the fire resistance of steel frames with steel claddings (no bracings) is 22% higher than with only traditional bracings (Figure 2.2). It shows that the steel claddings systems provide better stabilization in a fire case [8]. Sandwich panels can decrease the problem of lateral-torsional buckling of this substructure of beams or purlins by providing stabilization either by shear stiffness or torsional restraint [9,10].

When sandwich panels are subjected to external loads, they can transfer the loadings to substructures such as beams, columns and purlins through the bending, translational and torsional performances.

(a)

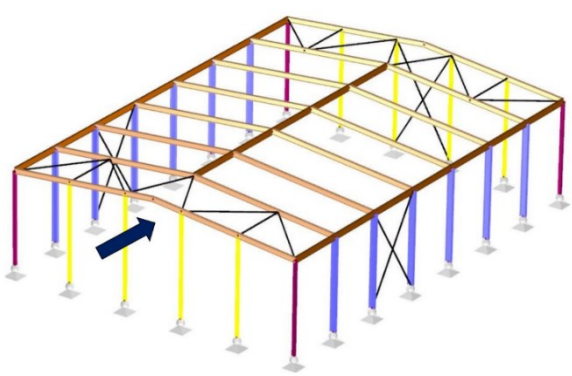

(b)

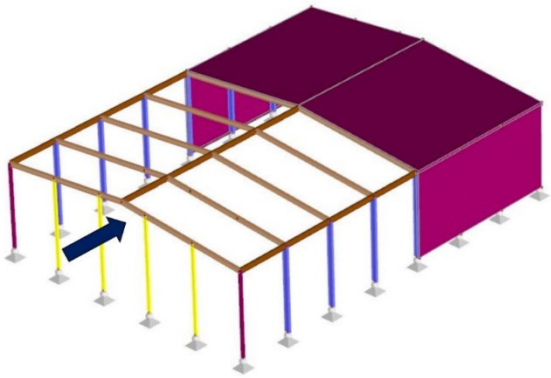

(c)

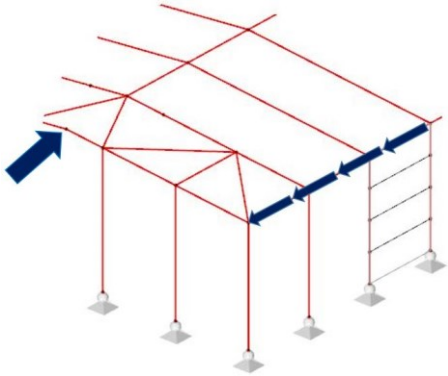

(d)

Figure 2.2. Portal frame structure: a) horizontal panels in practice, b) without steel claddings with the bracing system, c) without bracing system with steel claddings, d) reaction to the lateral force

2.2.1 Bending performance

Sandwich panels are mainly used in abattoirs, food stores, restaurants and meat packaging factories. In such applications, they are under wind, snow and self-weight loads; therefore, it is necessary to understand and evaluate the sandwich panels' performance under uniform loads [11]. The separation of face sheets by a core material increases the moment of inertia of the structure, resulting in higher bending stiffness, which is the sandwich structure's main characteristic [12]. The central core in panels provides stiffness against bending and buckling [13–15].

2.2.2 Shear performance

Sandwich panels are typically connected to the supporting structure by screws only at the transverse edges. They do not have connections at the longitudinal edges, which allows each panel to act as an individual element. Sandwich panels transfer shear loads to supporting members (substructures), which are usually columns, beams or purlins, through self-tapping or self-drilling screws. The head of the screw and the washer lie on the external face sheet, separated from the substructure by the core layer (Figure 2.3). The load-bearing capacity and stiffness of sandwich panels' fastenings are usually determined by testing, and they exist in national approvals. The stiffness of a sandwich panel's fastening to a steel substructure depends on the fastener and internal face sheet, which in between the inner sheet plays a determining role [9,16,17].

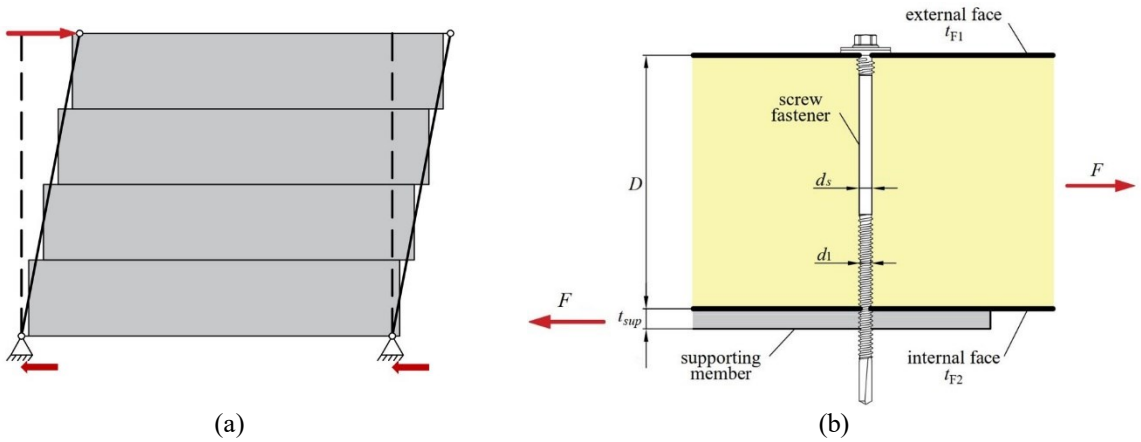

Figure 2.3. a) deformation of unidirectionally spanning sandwich panels, b) sandwich panels under shear loading

2.2.3 Torsional performance

Sandwich panels increase the supporting structure's resistance against lateral torsional buckling and buckling by restraining the lateral displacements and rotations. The leading cause of the torsion is the application of additional load on the eccentric. The torsional restraint is governed by the sandwich panel's stiffness connection to the supporting structure [18–20]. Many researchers have investigated the torsional restrain provided by sandwich panels [21–23]. The torsional restraint by sandwich panels can be calculated using a torsion spring's mechanical model with a spring stiffness. This spring stiffness combines the attached panel's bending stiffness, the connection's stiffness, and the beam's distortional stiffness. The behavior of the joint depends on the rotational direction. The joint produces smaller torsional restraint if the screw is placed on the compression side (Figure 2.4b).

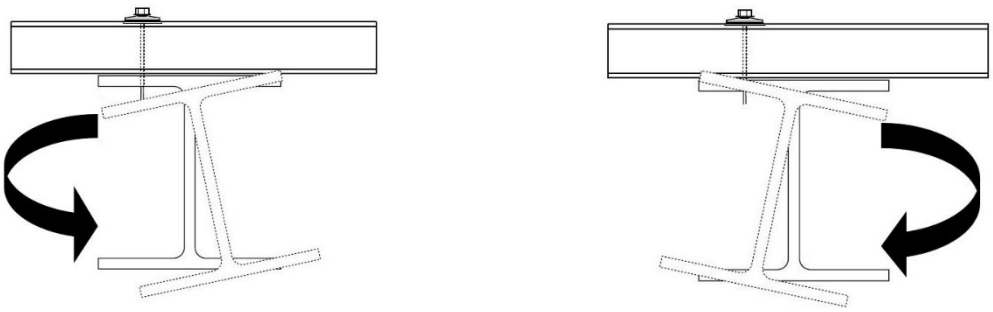

(a) (b)

Figure 2.4. Sandwich panels under torsional loading: a) screw on the tension side, b) screw on the compression side [9]

2.3 Fire safety of buildings

Throughout history, fire has been the most common way to endanger buildings. While buildings were growing in size and height, many questions emerged. For example, how the fire spread within and between buildings or the structural sufficiency under fire exposure. These questions led the NRC (National Research Council of Canada) to create the Division of Building Research (IRC). According to the NRC, the temperature decreases after the initial growth in real fire scenarios, while the temperature follows an increasing trend in a standard fire. The comparison of the ISO 834 parametric curve and a temperature curve of a real fire case is shown in Figure 2.5. The ISO 834 curve neglects the growth period and does not include the decay period [24,25].

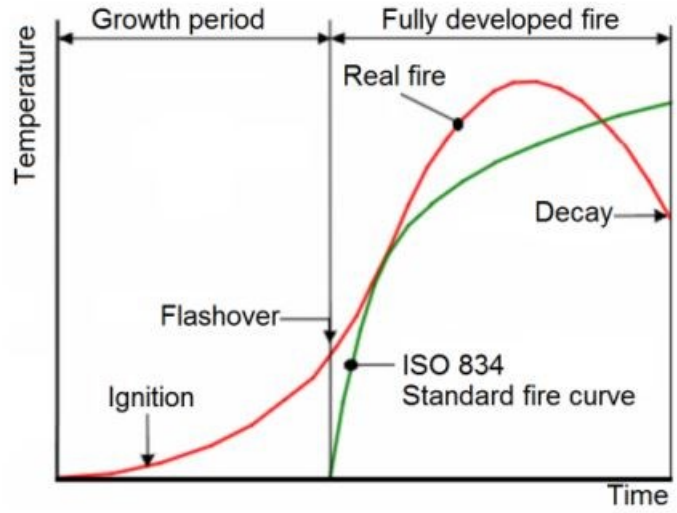

Figure 2.5. Comparison of a real fire and ISO 834 standard fire [26]

Fire compartments are areas of a building varying in dimension from a single room to a whole floor area. Physical barriers such as walls and ceilings are employed to withstand the spread of the fire for a while [25]. By understanding the characteristic features of compartments fires, the designer can better predetermine the nature of fire and choose the most suitable approach to deal with it. They can either design compartments for minimum structural damage without installing special equipment (defensive approach) or provide special equipment for detecting and suppressing the fire (offensive approach) [27].

A fire can always be a threat to the neighboring buildings. Limiting the number and size of openings in a structure and separating the building by a clear space requiring buildings to be non-combustible are some measures to decrease the risk of fire spreading to the neighboring buildings. The findings of NBCC (The National Building Code of Canada) requirements showed that the radiation levels from buildings with combustible interiors were double those where non-combustible interiors were employed. Peak radiation levels at some distance from the building were directly dependent on the percentage of openings in the exterior wall. Furthermore, it was concluded that the maximum radiation levels were not greatly affected by the type of exterior claddings [24,25].

Using the SAFIR program, Moss et al. [28] conducted a study into the fire behavior of steel portal frame buildings at elevated temperatures. It was shown that the bases of the steel portal frames at the foundations must be designed with some level of fixity to ensure that the structure will deform acceptably during a fire. In order to avoid sideways, steel portal frame columns don't need to be fire-protected unless the designer wants to ensure that the columns and wall panels remain in place during and after the fire.

Jiang et al. [29] investigated the disproportionate collapse behavior of three-dimensional steel-framed gravity buildings subjected to traveling fires. The effect of fire curves (burning rate) and fire spreading speeds on the collapse behavior was studied. It was indicated that the duration of the heating phase has a great effect on the building collapses, and the structure may collapse during the cooling phase. A “long-cool” fire curve (slow-burning rate) was more dangerous than mild (average burning rate) and “short-hot” fire curves (fast burning rate). They concluded that fire traveling speed plays a significant role in the failure sequence of columns, range of damage and collapse mode of structures. Utilization of bracing systems can prevent collapse of structures under a slow travelling fire, but not for a fast travelling fire. They recommended the consideration of the possible fire scenarios when determining the fire-resistance rating, and increase the fire-resistance rating of components to three hours to prevent collapse under a travelling fire with a “long-cool” fire curve.

Gernay and Elhami [30] studied steel framed buildings with composite floor slabs and presented an analysis of the structure under fire. The scenarios were single- and multi-compartment fires and fire as a secondary event after a column loss. Single slab, single slab with restraint, and full building models were investigated to realize the influence of continuity in the boundary conditions. The full building model showed the most desirable behavior, while the single panel model without horizontal restraint was the most conservative. They illustrated that performance-based fire design can use advanced computational models to study the fire-structure behavior for multiple design alternatives and hazard scenarios.

2.4 Material properties of employed cores

2.4.1 Mineral wool core

The mineral wools (MW) are the most common insulation materials; they are characterized by small thermal conductivity values to impair hit transfer from one side of the panel to the other. The properties of MW cores relate closely to the properties of the network's constituents (fiber and binder) and the fibers' structure inside the products. For example, the fibers' orientation is known to substantially impact MW products' mechanical properties. Collection of the fibers during production results in a laminar structure of the MW product [31,32].

In this research, the MW core material properties are obtained from the compressive tests conducted by the manufacturers. Table 2.1 presents the MW cores' elastic properties at ambient

temperature, while Figure 2.6 shows their stress-strain curves. The density of the MW core is considered 87 kg/m^3.

Table 2.1. Measured material properties of MW cores

Core	Young's modulus (MPa)			Poisson's ratio		
	E_{11}	E_{22}	E_{33}	v_{12}	v_{13}	v_{23}
MW	3.44	0.20	9.01	0.05	0.03	0.14

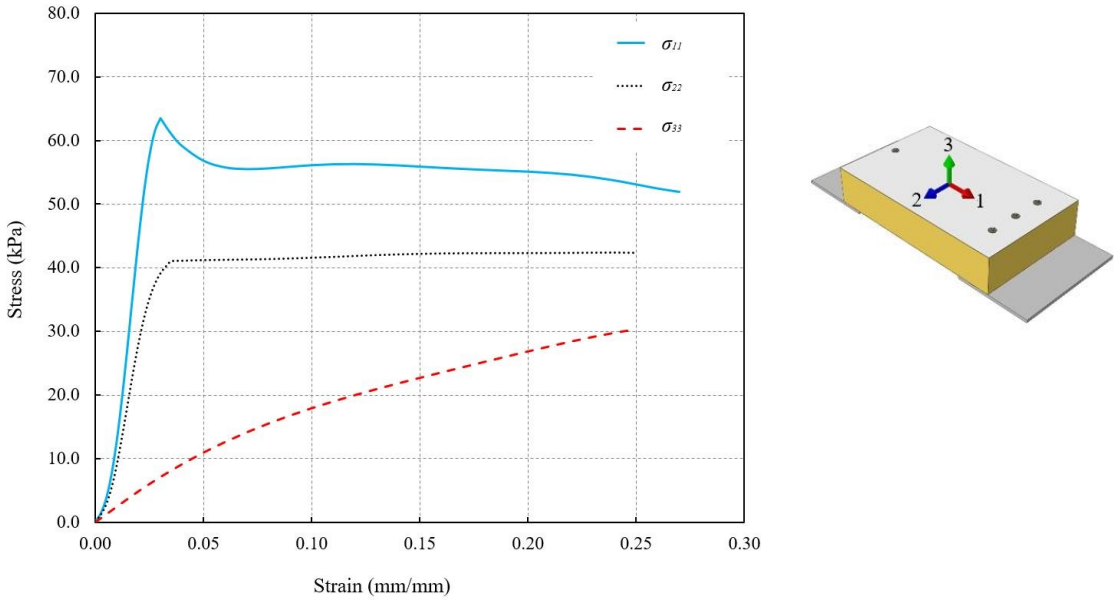

Figure 2.6. Stress-strain curves for MW cores at ambient temperature

The mineral wool's specific heat is not sensitive to temperature; therefore, a constant value of 840 kJ/(kg·°C) is adopted [33]. The thermal conductivity for the MW recommended by Wang [34] is used in this research (see Table 2.2).

Table 2.2. Thermal conductivity of MW core [34]

Temperature (°C)	10	50	150	200	300	350	400	450	550	600
Thermal conductivity (W/m.°C)	0.034	0.037	0.054	0.066	0.097	0.108	0.113	0.150	0.320	0.520

2.4.2 Polyisocyanurate foam

The Polyisocyanurate (PIR) foam differs from the traditional Polyurethane (PUR) foam in the more robust molecular structure. PIR is a modified PUR with dominance in the isocyanate group system and another polyol ratio. PIR-foams are obtained in a ratio of 1:2 (polyol and isocyanate), PUR-foams in proportions of 1:1. PIR's molecular structure makes it more suitable than PUR in the thermal stability, flame retardance, and mechanical behavior of foam material [35–41].

The PIR core material properties are received from the compressive tests conducted by the manufacturers in this research. Table 2.3 and Figure 2.7 indicate the PIR cores' elastic properties at ambient temperature and stress-strain curves. The density of the MW core is 40 kg/m^3.

Table 2.3. Measured material properties of PIR cores

Core	Young's modulus (MPa)			Poisson's ratio		
	E_{11}	E_{22}	E_{33}	ν_{12}	ν_{13}	ν_{23}
PIR	12.44	3.40	4.10	0.03	0.05	0.04

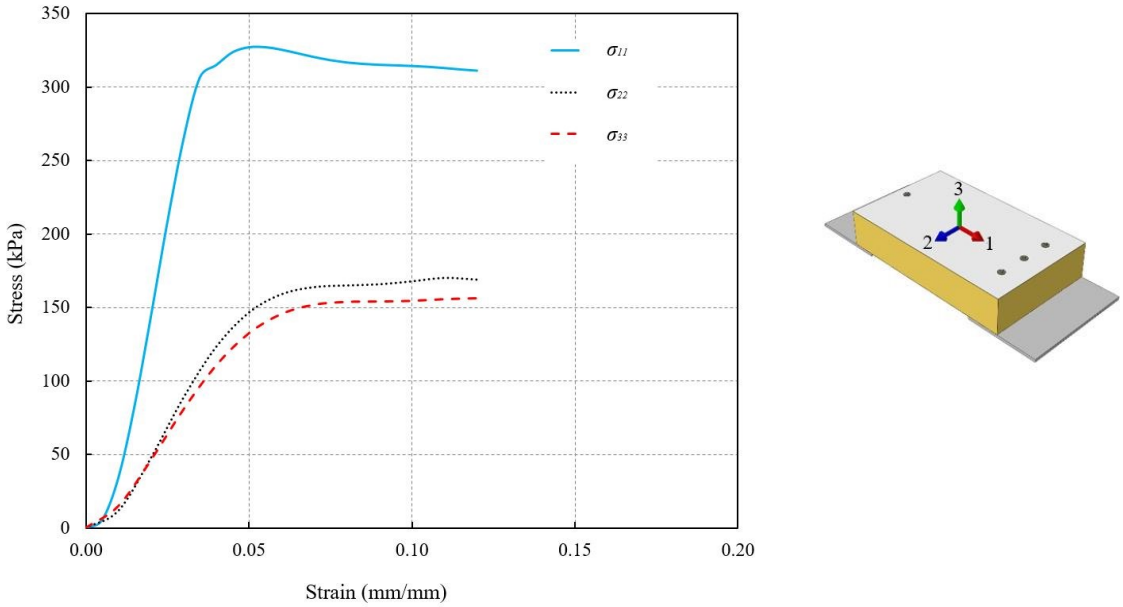

Figure 2.7. Stress-strain curves for PIR cores at ambient temperature

The PIR foam's specific heat is 1400 J/kg.K, which is independent of temperature [42]. Table 2.4 illustrates the thermal conductivity of PIR cores applied in this research and suggested by [43].

Table 2.4. Thermal conductivity of PIR core [43]

Temperature (°C)	1	20	50	100	200	300	400	500	600	700
Thermal conductivity (W/m.°C)	0.029	0.031	0.034	0.039	0.051	0.065	0.083	0.104	0.130	0.162

2.5 Material properties employed steels

2.5.1 Material properties of applied steels

The material properties used as facings are S280GD with a density of 7.85×10^{-6} kg/mm^3. To obtain steel material characteristics of the facings, a tensile coupon test was performed in the laboratory of the Department of Structural Engineering, Budapest University of Technology and Economics, at ambient temperature (Figure 2.8).

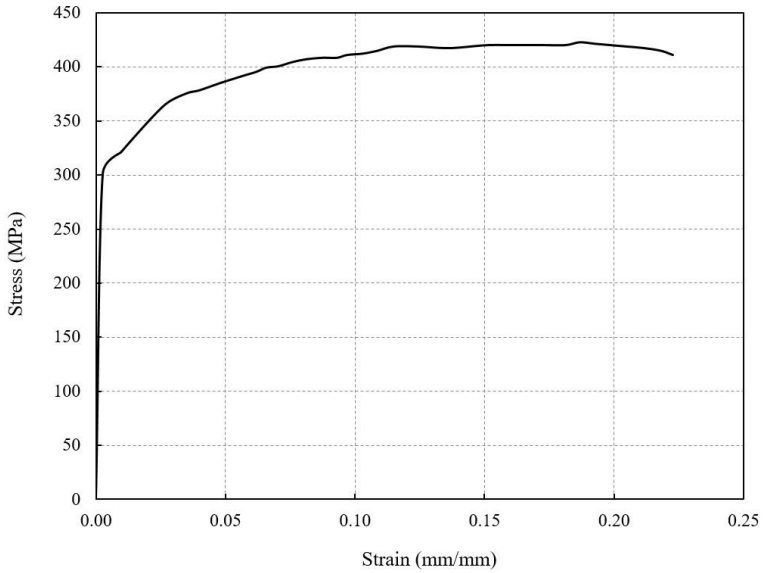

Figure 2.8. Stress-strain curve for the steel sheet at normal condition

Moreover, Figure 2.9 shows the stainless bolts' material properties at ambient temperature, obtained from tensile coupon tests and determined at the laboratory of the Brandenburg University of Technology by the Chair of Steel and Timber Structures. The density of the bolt is 9.85×10^{-6} kg/mm^3.

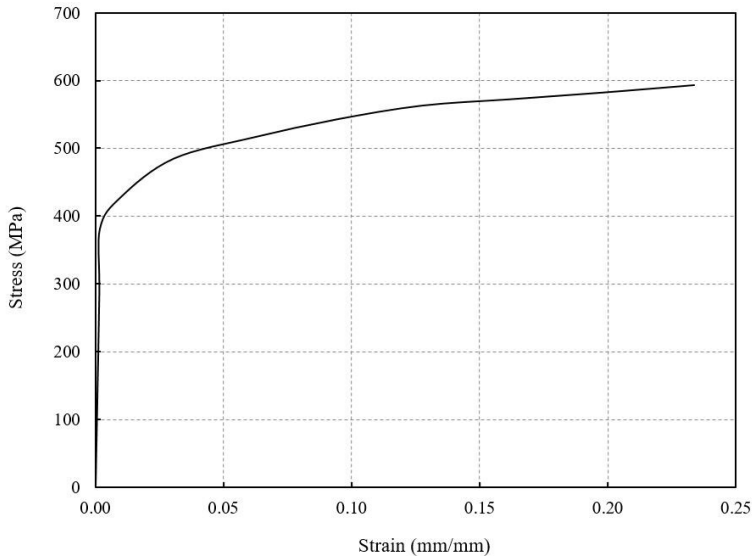

Figure 2.9. Stress-strain curve for the stainless steel bolts at ambient temperature

The material for the supporting plates is steel S355 with a density of 7.85×10^{-6} kg/mm^3. Figure 2.10 illustrates material properties for S355 taken from EN 1993-1-1 [44].

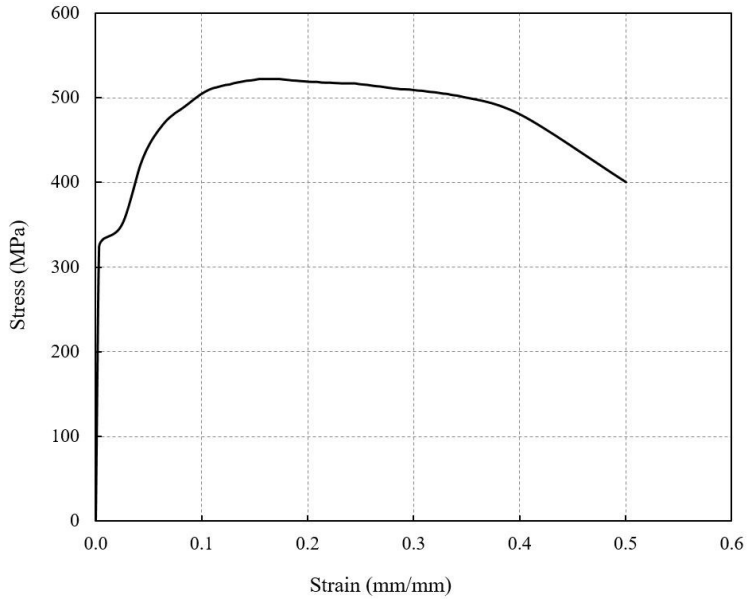

Figure 2.10. Stress-strain curve for steel S355 at ambient temperature

The thermal properties, including thermal conductivity and specific heat, of carbon steels are in accordance with Eq. (2.1) and (2.2) [45].

$$\lambda_a = \begin{cases} 54 - 3.33 \times 10^{-2}\theta_a \; W/mK & for\ 20°C \leq \theta_a < 800\ °C \\ 27.3\ W/mK & for\ 800°C\ \leq \theta_a \leq 1200°C \end{cases} \tag{2.1}$$

$$c_a = \begin{cases} 425 + 0.773 \times \theta_a - 0.00169 \times \theta_a^2 + 2.22 \times 10^{-6}\theta_a^3 \dfrac{J}{kgK} \\ \qquad for\ 20°C \leq \theta_a < 600°C \\ 666 + \dfrac{13002}{738 - \theta_a} \dfrac{J}{kgK} \qquad for\ 600°C\ \leq \theta_a < 735°C \end{cases} \tag{2.2}$$

where θ_a (°C) is the steel temperature and λ_a and c_a represent thermal conductivity and specific heat.

According to EN 1993-1-2 [45], Eq. (2.3) and (2.4) display thermal conductivity and specific heat of stainless steel.

$$\lambda_a = 14.6 + 1.27 \times 10^{-2}\theta_a \frac{W}{mK} \tag{2.3}$$

$$c_a = 450 + 0.208 \times \theta_a - 2.91 \times 10^{-4}\theta_a^2 + 1.34 \times 10^{-7}\theta_a^3 \frac{J}{kgK} \tag{2.4}$$

Generally, the specific heat of steel increases when the temperature elevates. However, the temperature elevation increases stainless steel's thermal conductivity and decreases carbon steels' thermal conductivity.

Table 2.5 shows the values for thermal conductivity and specific heat of employed steels in this research up to the maximum temperature of 600 °C.

Table 2.5. Thermal conductivity and specific heat for steels [45]

Temperature (°C)	20	100	200	300	400	500	600
Stainless steel bolt							
Thermal conductivity (W/m.K)	14.85	15.87	17.14	18.41	19.68	20.95	22.22
Specific heat (kJ/kg.K)	455.50	475.20	495.40	511.40	524.00	534.00	542.20
Carbon steel S355 and S280GD							
Thermal conductivity (W/m.K)	53.33	50.67	47.34	44.01	40.68	37.35	34.02
Specific heat (kJ/kg.K)	439.80	487.62	529.76	564.74	605.88	666.50	759.92

2.5.2 Reduction factors of steel material properties at elevated temperatures

The deterioration of mechanical properties, such as modulus of elasticity and yield strength, with temperature elevation is a determining issue in assessing the steel structural elements' performance in the fire. Craveiro et al. [46] conducted an experimental campaign to determine the mechanical and thermal properties of the S280GD steel at temperatures ranging from 20 to 800 °C. Some researches were performed on the mechanical properties of cold-formed steels at elevated temperatures with different thicknesses [47–49].

Table 2.6 presents the suggested reduction factors by [46] for the yield strength, modulus of elasticity, ultimate strength and proportional limit for the S280GD steel at elevated temperatures. The reduction factors suggested by EN 1993-1-2 [45] for the yield strength and elastic modulus of class 4 hot-rolled steel at elevated temperatures are illustrated in Table 2.7.

Table 2.6. Reduction factors of yield strength, modulus of elasticity and ultimate strength of the S280GD steel [46]

Temperature (°C)	20	100	200	300	400	500	600
S280GD (Craveiro et al.)							
$f_{y,\theta}/f_{y,20}$	1.00	0.962	0.898	0.728	0.592	0.370	0.253
E_θ/E_{20}	1.00	0.980	0.841	0.703	0.593	0.414	0.305
$f_{u,\theta}/f_{u,20}$	1.00	0.979	1.111	0.937	0.687	0.391	0.205

Table 2.7. Reduction factors of yield strength and modulus of elasticity of class 4 hot-rolled steel [45]

Temperature (°C)	20	100	200	300	400	500	600
EN 1993-1-2							
$f_{y,\theta}/f_{y,20}$	1.00	1.00	0.89	0.78	0.65	0.53	0.30
E_θ/E_{20}	1.00	1.00	0.90	0.80	0.70	0.60	0.31

Figure 2.11 compares the reduction factors provided by EN 1993-1-2 [45] against the reduction factors determined in [46] for both yield strength and modulus of elasticity of steel S280GD. It is obvious that the EN 1993-1-2 [45] overestimates the reduction factors for yield strength and modulus of elasticity for steel S280GD. Therefore, the reduction factors for steel sheets are taken from [23] in this research.

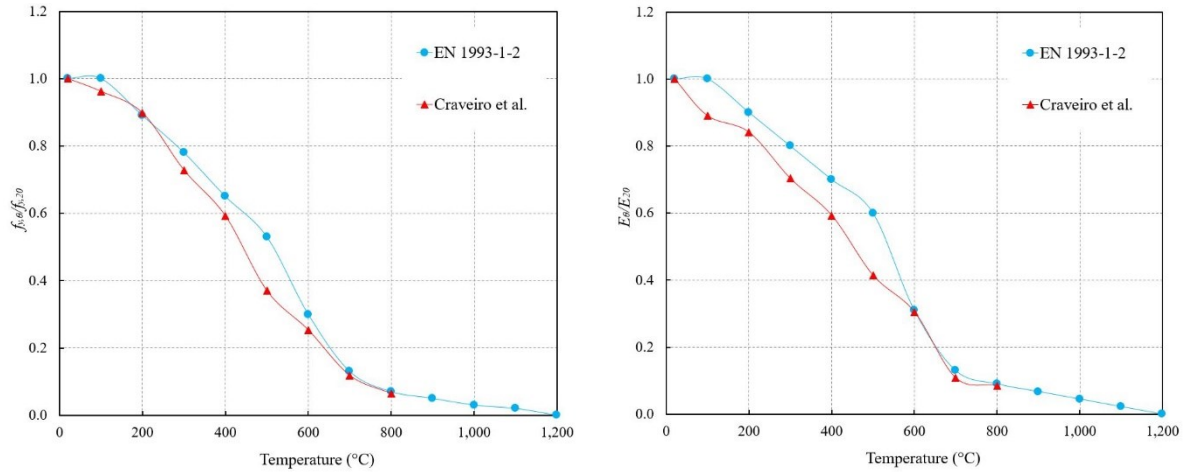

Figure 2.11. Comparison between the reduction factors in Craveiro et al. [46] research and the current design standards [45]: a) yield strength reduction factors, b) modulus of elasticity reduction factors.

Since the material of screws are stainless steels, the reduction factors for yield strength, modulus of elasticity, and ultimate strength are in accordance with Table C.1, Annex C of EN 1993-1-2 [45]. In this research, the reduction factors for S280GD, S355 and stainless steels are according to Table 2.6, Table 2.7 and Table 2.8, respectively.

Table 2.8. Reduction factors of yield strength, modulus of elasticity and ultimate strength of stainless steel [45]

Temperature (°C)	20	100	200	300	400	500	600
Stainless steel screw (EN 1993-1-2)							
$f_{y,\theta}/f_{y,20}$	1.00	0.82	0.68	0.64	0.60	0.54	0.49
E_θ/E_{20}	1.00	0.96	0.92	0.88	0.84	0.80	0.76
$f_{u,\theta}/f_{u,20}$	1.00	0.87	0.77	0.73	0.72	0.67	0.58

2.6 Summary of literature review

Since sandwich panels are commonly subjected to lateral loading, the study and understanding of their bending behavior are necessary [50]. Many researchers have studied the behavior of sandwich panels subjected to bending loads [51–66]. Zhang et al. [67] presented an experimental investigation of composite sandwich panels' bending performance with a new mixed core subjected to a four-point bending load. The results showed that the mixed core could change the failure mode of sandwich panels. For instance, the failure mode of wooden panels is characterized by the tensile failure of bottom wood. In contrast, the failure mode of composite sandwich panels with wood and polyurethane foam mixed core is the web's shear failure.

Iyer et al. [68] carried out a comparative study between three-point and four-point bending of glass-epoxy skin sandwich panels. Flexural properties like flexural rigidity and bending strength were determined and compared for each case. The three-point bend setup was

commonly used to study flexure in a structure, while the four-point bend setup was preferred for longer spans and rigid structures. The flexural moduli obtained from three-point and four-point bending tests for the same specimen are different [69]. Semi-empirical strength and stiffness optimization studies for honeycomb sandwich panels under four-point bending load were performed by Murthy et al. [70]. It is observed that the use of expensive core materials does not provide significant improvement in mechanical properties [71].

Srivaro et al. [72] studied the bending stiffness and strength of oil palmwood (OPW) core sandwich panel overlaid with rubberwood veneer under center point bending. Linear elastic beam theory was employed to predict the bending performance of the panels. Results showed that the linear elastic beam theory adequately predicted the sandwich beams' stiffness and bending strength. Stiffness and strength values of sandwich panels under bending loading depend on the properties of their faces, core materials and geometry. Linear elastic beam theory has been employed to predict the sandwich panel's stiffness and strength [73–77]. Joseph et al. [78] carried out experimental and analytical studies to understand and compare concrete sandwich panels' flexural behavior under two different loading conditions: punching and four-point bending. The experimental study illustrated that loading conditions significantly affect the concrete sandwich panels' flexural behavior.

During storms and cyclones, low-rise steel buildings are subjected to uplift pressures on roof claddings and lateral pressures on wall claddings. The lateral pressures can be resisted by the shear strength and stiffness of sandwich panel systems under in-plane shear forces [79]. Connecting systems, self-tapping, and self-drilling screws generally play a role in both the shear strength and stiffness of sandwich panels [80]. Misiek et al. [81] investigated the parameters to choose the materials for fastening screws used in connections involving thin-walled sections and thin sheeting.

Studies on bolted connections for connecting cold-formed steel members showed the typical failure modes loaded in shear at both ambient and elevated temperatures are: bearing failure, shear-out failure, net-section failure of the connecting plate, and shear fracture of the fastener [82–87]. The ultimate resistance of cold-formed profiled steel roof sheeting connected to the top chord of a steel roof truss through self-tapping screws at both ambient and elevated temperatures is predicted by [88].

Lu et al. [89] showed that the failure modes of the connection between the metal deck roofing system and the low-pitched roof area for both ambient and elevated temperatures bear the

thinner sheet's failure. Degradation of material at elevated temperatures reduces the strength and stiffness of the connections.

Chapter 3: EXPERIMENTAL STUDY AND VALIDATION OF THE FE MODELING FOR BENDING TESTS OF SANDWICH PANELS

3.1 Introduction

In this chapter, the bending tests of sandwich panels are presented. All steps, including the tests arrangement, the geometry of employed specimens, boundary conditions and loadings, and the measured parameters, are described in this chapter. The experiments' outputs are load-displacement curves at different temperatures, which determine the bending stiffness and load-bearing capacity of specimens. Therefore, the numerical models are created in ABAQUS software to compare with experimental results. Detailed information about the finite element models is presented. The main objective of this chapter is to validate the numerical models with the experimental results to provide valid results for further numerical investigations.

3.2 Experimental program for bending tests

3.2.1 Test arrangement

The experimental program's main purpose was to determine sandwich panels' bending stiffness under bending loading at normal and elevated temperatures. The tests were carried out at the Czech Technical University in Prague. The inner and outer sheet thicknesses for MW panels are 0.5 mm and 0.6 mm, and for PIR panels, 0.4 mm and 0.5 mm, respectively. Figure 3.1 displays the cross-section of MW and PIR sandwich panels. Table 3.1 presents the temperature and dimensions of the tested specimens. The specimens were tested at temperatures of the inner sheet (20 °C, 200 °C, 300 °C, 450 °C and 600 °C) and loaded by mechanical load.

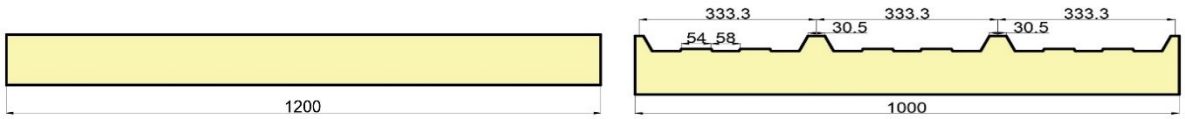

(a) (b)

Figure 3.1. The cross-section of sandwich panels in bending tests, a) MW panels, b) PIR panels, dimensions in mm

Table 3.1. Dimensions and temperature of specimens for bending tests

Panel	Specimen size (mm×mm)	Panel thickness (mm)	Temperature (°C)
MW sandwich panels	1200×2500	100	20 300 450 600
	1200×2500	230	20 300 450 600
PIR sandwich panels	1000×2500	100	20 200 250 300
	1000×2500	160	20 200 300

3.2.2 Loading and boundary conditions

As shown in Figure 3.2, the bottom of the panel was fixed on both sides at a length of 150 mm, and the load was applied by a hydraulic jack from the upper side through four HEA120 beams. The loading rate was set to a constant value of 0.050 mm per second (mm/s) or 0.075 mm/s. A system of ceramic heating pads was employed to heat the bottom surface of the inner steel sheet. The heating pads were uniformly distributed on the inner sheet of the panel (Figure 3.3). The temperature of the inner panel face was controlled by coated thermocouples [90].

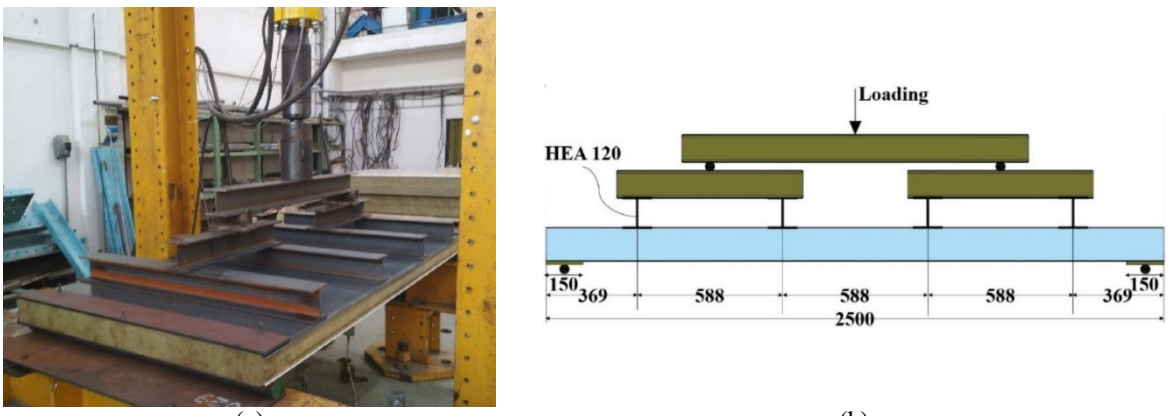

(a) (b)

Figure 3.2. Test arrangement of MW panel, a) test [8], b) front view, dimensions in mm

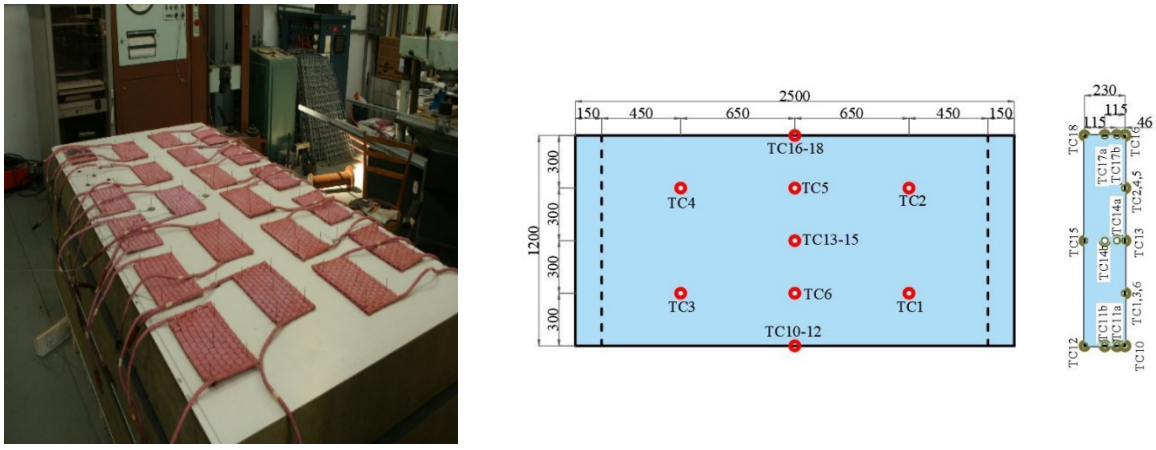

(a) (b)

Figure 3.3. a) Distribution of ceramic heating pad on the panel face [8], b) location of thermocouples for MW panels dimensions in mm

During the tests, the displacements, the loading forces and the temperatures were measured. Temperatures were recorded by coated thermocouples, and deflections were measured by transducers. The transducers were located in the mid-span of the panel (P1, P3 and P5) and one-fourth of the panel span (P2 and P4). The steel sheet temperature was increased by a system of ceramic heating pads generated by machine Mannings HTC 70 kVA. The applied force was taken by the testing machine. Nine coated thermocouples recorded the inner sheet's temperature (lower side during the test). The outer sheet's temperature was measured by three thermocouples. The temperature of the panel core was recorded with six thermocouples (Figure 3.3b) [8]. The machine generates heat until a defined temperature. Therefore, it maintained a constant temperature until the end of the test. Using insulation materials on the heating pads helps to keep the temperature constant (Figure 3.4). The panel's mechanical loading started when the inner panel sheet's temperature reached the defined temperature and was constant [91].

Figure 3.4. Applying insulation materials to avoid temperature loss [8]

3.2.3 Experimental results and main observations

During the tests, the displacements, the loading forces and the temperatures were measured. Temperatures were recorded by coated thermocouples, and deflections were measured by transducers. The collapse of MW panels was usually caused by shear. At 600 °C temperature, the panel showed a deformation caused by bending without any panel failure. The PIR panels demonstrated similar behavior such as MW panels. In fact, they experienced shear failure at lower temperatures and bending deformation at 300 °C (Figure 3.5).

(a) (b)

Figure 3.5. Shear failure of a) MW panels and b) PIR panels at normal conditions [8]

Figure 3.6 and Figure 3.7 show the load-displacement curves for MW and PIR panels obtained from the bending tests. The PIR panels have a higher resistance at ambient and elevated temperatures than MW panels when the thickness is 100 mm. There are two main reasons for this behavior; first, PIR cores' material properties are stiffer than MW cores; second, the PIR panels consist of trapezoidal sheetings while the sheetings of MW panels are flat. MW panels have a milder decrease of load after reaching the maximum load. However, PIR panels have very sharp resistance peaks due to the brittle behavior of the PIR core. During the tests, the loadings were stopped at some intervals to control the experimental conditions. These pauses caused some jumping (sharp movement) in the experimental curves. In Section 3.4, the experimental results are discussed and compared to the numerical results [90,91].

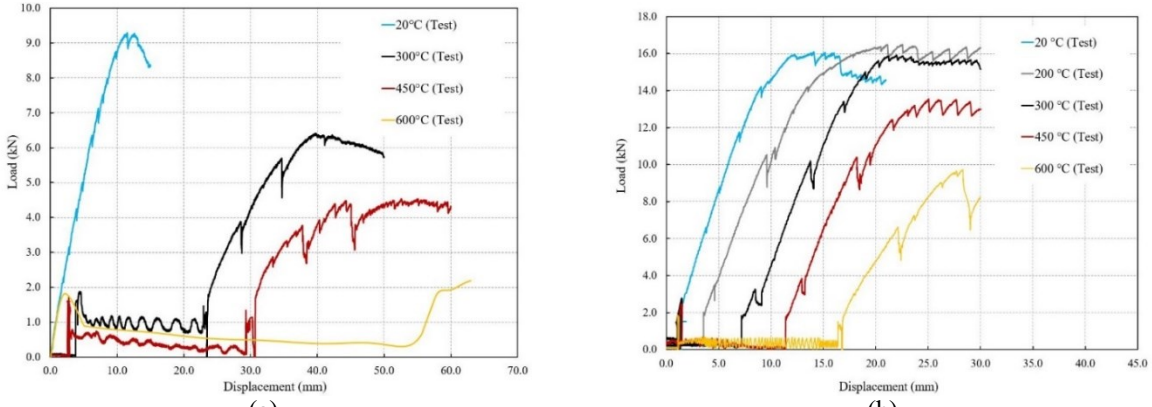

(a) (b)

Figure 3.6. Load-displacement curves for MW panels a) 100 mm and b) 230 mm at different temperatures for experimental results

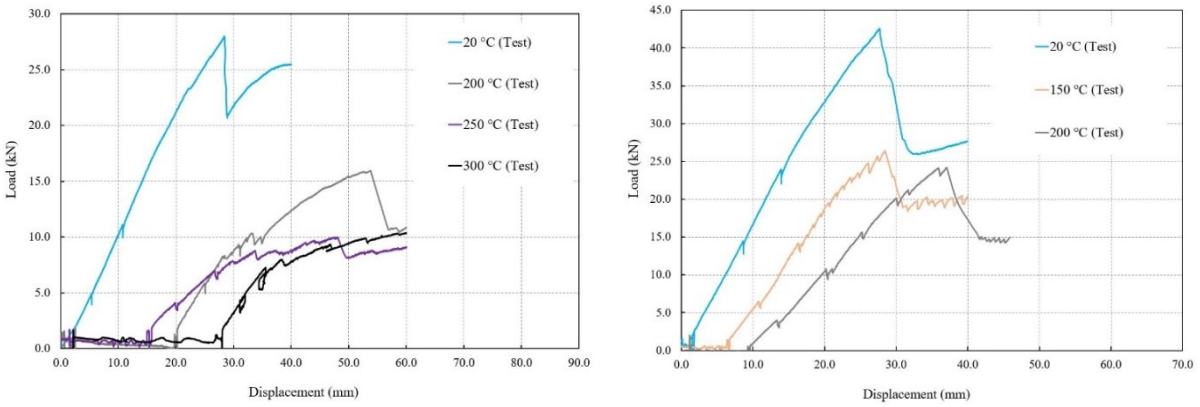

(a) (b)

Figure 3.7. Load-displacement curves for PIR panels a) 100 mm and b) 160 mm at different temperatures for experimental results

3.3 Validation of numerical modeling with bending tests

3.3.1 General introduction of ABAQUS

The ABAQUS is one of the most powerful and modern commercial finite element (FE) software used in structural engineering research. It provides two types of solutions for simulation: implicit analysis and explicit analysis. Whereas implicit analysis must iterate to determine the solution to a non-linear problem, explicit analysis determines the solution without iterating by explicitly advancing the kinematic state from the end of the previous increment. The implicit analysis employs an iterative solution to solve a set of simultaneous non-linear equations. It is used commonly to solve static problems that are not time-related. The Newton-Raphson method (General static analysis) is applied until the stiffness matrix's determinant becomes zero or negative. The explicit method is designed to solve the dynamic impact problems that are time-related. It uses explicit integrations to solve non-linear complicated contact problems. In this research, the implicit static method is employed for analysis. This section presents the main points of the numerical models.

3.3.2 Model description

The main objective of the numerical study herein is to verify the simulations with experiments and then conduct a parametric study and compare the numerical results with analytical ones. To simulate the behavior of experimental specimens, a combination of heat transfer and mechanical analysis is performed. Indeed, the outputs of heat transfer analysis determine the

temperature distributions of specimens, which are applied as mechanical analysis inputs. Load-displacement curves at different temperatures are the final outputs of the analysis. The main components of the developed finite element models for bending simulations are core and internal and external facings. The geometrical and material nonlinearity, as well as initial imperfection for the model, is incorporated. The dimensions of all models are created accurately in accordance with the geometry of experiments (Section 3.2). In fact, the MW and PIR cores dimensions are 2500×1200×100 (or 230) mm and 2500×1000×100 (or 160) mm, respectively.

3.3.3 Material properties

It should be mentioned that the data obtained from tensile coupon tests are engineering stress and strain. They should be converted into corresponding true stresses and true plastic strains for different temperatures, according to Eq. (3.1) and (3.2):

$$\sigma_{true} = \sigma_{engineering} \times (1 + \varepsilon_{engineering}) \quad (3.1)$$

$$\varepsilon_{true} = ln(1 + \varepsilon_{engineering}) \quad (3.2)$$

The facing material is steel S280GD, with a density of 7850 kg/m^3 (see Figure 2.8). For simulation, a non-linear isotropic/ kinematic hardening model is employed for both steel facings. This model adopts a typical elastic-plastic isotropic model, which follows the von Mises yielding criteria to define its isotropic yielding. The tensile stress-strain behaviors of steel materials consider the strain hardening effect. Since no experiments are carried out at elevated temperatures within this research, the mechanical properties of steel are reduced according to the reduction factors presented by Craveiro et al. (Section 2.5). The steel facings' thermal properties, such as thermal conductivity and specific heat, are taken from EN 1993-1-2 (Section 2.5).

The mechanical characteristics of polymer products may be described based on their density [92–95]. For this reason, the mechanical properties of MW and PIR cores were achieved by manufacturers. MW and PIR cores are orthotropic (Figure 2.6 and Figure 2.7). The density for MW and PIR core is 87 and 40 kg/m^3. The degradation of core materials at elevated temperatures is based on the suggested reduction factors for Young's modulus (Table 3.2).

Table 3.2. Suggested reduction factors for Young's modulus of cores

MW core					
Temperature (°C)	20	150	300	450	600
Reduction factor for Young's modulus	1	0.75	0.5	0.25	0.25
PIR core					
Temperature (°C)	20	150	300	450	600
Reduction factor for Young's modulus	1	0.67	0.45	0.15	0.15

The thermal properties of MW and PIR cores are according to Section 2.4. All the engineering stresses and engineering strains are converted into the corresponding true stresses and true plastic strains for different FE models' temperatures.

3.3.4 Contact interaction

In bending simulations, there are interactions between the core and upper and lower facings. The delamination of the exposed (fire) side of the steel face from the panel's core is crucial for analyzing at elevated temperatures. For this reason, the interaction between the core and the lower facing is modeled with surface-to-surface contact, with Normal and Tangential behaviors. The type of Normal behavior is "Hard Contact," which allows the separation of components after contact. To simulate the debonding of the surfaces at elevated temperature, in the Tangential behavior, the friction between the surfaces is modeled as temperature-dependent, with complete friction at ambient temperature and reduced friction at elevated temperatures. For PIR panels, the debonding of the steel sheet from the core material is observed at a temperature of 300 °C. For MW panels, debonding occur at 450°C in the heated area [8]. Since the temperature of the upper facing did not increase during the heating of the panel, the contact between the unexposed (cold) side of the steel face and the core material is defined as the "Tie" constraint, where the facing is the master surface and the core slave surface. By "Tie" interaction, every slippage or movement between the two parts is prevented. The above solution seems sufficiently acceptable when comparing the numerical and experimental results.

3.3.5 Loading and boundary conditions

Boundary conditions need to be made as simple as possible to reduce the run time of simulations. In order to simplify the numerical model, the load-transferring mechanism, including HEA120 beams and steel sections fixed to the sandwich panels, is removed. As an alternative, the loadings are directly applied to the panel's upper side in four bands in the vertical direction. The magnitude of each surface load is 0.05 N/mm², and the loading area corresponds to the outer surface of the beam flange (HEA 120), which is 1200 (or 1000) mm × 120 mm. Simultaneously, all plates and rods from the test creating the support for the test specimens are discarded. Moreover, the boundary conditions are precisely applied to the lower surface of sandwich elements. The boundary conditions are defined so that edge areas of

150 mm × 1000 mm (for PIR) and 150 mm × 1200 mm (for MW) of the sandwich panel are fixed in the X, Y and Z directions (see Figure 3.8).

The loading-heating order is as follows: first, a pre-load is applied by a displacement-controlled method, then the panel is heated up to the defined limit temperature, and finally, the mechanical loading is again applied. In the heat transfer analysis, the heating is assigned uniformly to the bottom side (the exposed side) of sandwich panels. The other parts of the specimens are in contact with ambient temperature. At the same time, the mechanical loading is applied to the top sheet in the four bands at distances of 588 mm from each other (Figure 3.8).

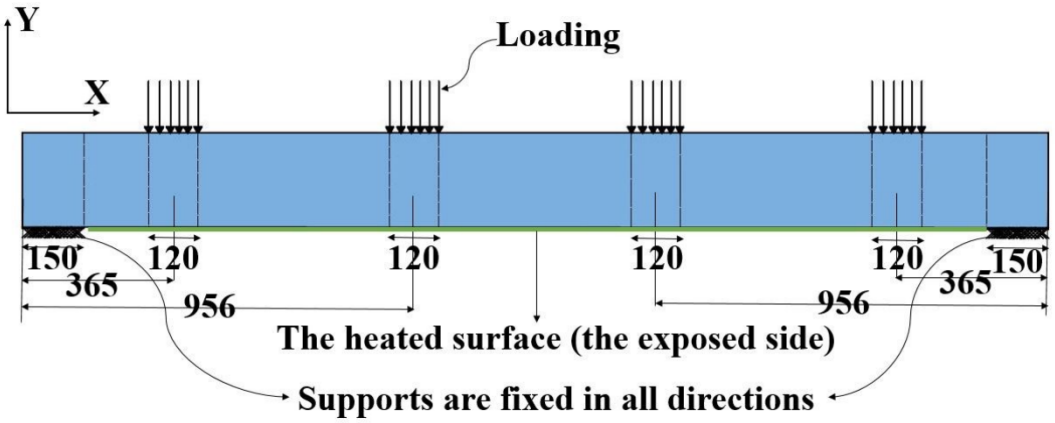

(a)

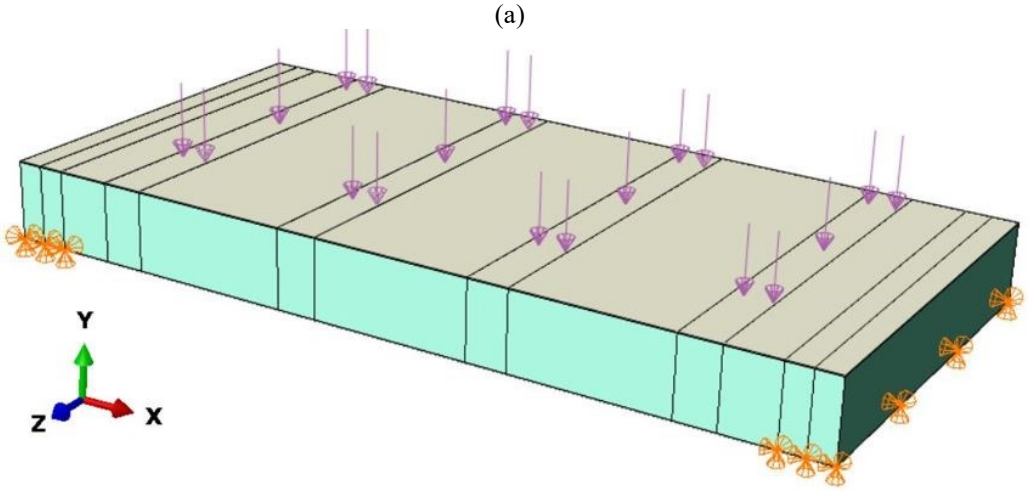

(b)

Figure 3.8. Loading and boundary conditions for sandwich panels: a) side view, dimensions in mm, b) 3D FE model

3.3.6 Element types and mesh size

The continuum element C3D8R with hourglass control and reduced integration point is adopted to simulate the mechanical analysis's core material to improve computational efficiency. The C3D8R element is a three-dimensional 8-node linear brick element [96–98]. This element is

suitable for applying linear and non-linear analysis at large strain and deformation. The reduced integration gives reasonable control of the hourglass effect and decreases calculation time. The facings' element type is the S4R shell element, a 4-node doubly curved thin or thick shell with reduced integration, hourglass control, and finite membrane strains [96,99,100].

In the heat transfer analysis, the DCC3D8 element is adopted for the core. The DCC3D8 is an 8-node convection/diffusion brick solid element, the upper and lower facings are simulated by the DS4 element, a 4-node heat transfer quadrilateral shell [96,100,101].

A smaller mesh size gives better accuracy to simulation results while increasing calculations time. Optimal mesh size should be employed to achieve the best accuracy with the minimum time consumption. For this reason, mesh verification and sensitivity analyses are conducted to optimize the number of elements and meet good quality (see Figure 3.9). In both heat transfer and mechanical analyses of each specimen, the size and number of the elements are accurately similar. In general, the mesh size is recommended 30 mm × 20 mm × 10 mm in the X, Y and Z directions, respectively (Figure 3.10). However, in an area with 428 mm length in the X direction from both ends of the panel, the element size is reduced to 10 mm × 20 mm × 10 mm. The area mentioned above is selected because of the observation from the experiments. Almost all failures and cracks initiation of panels have occurred within this area.

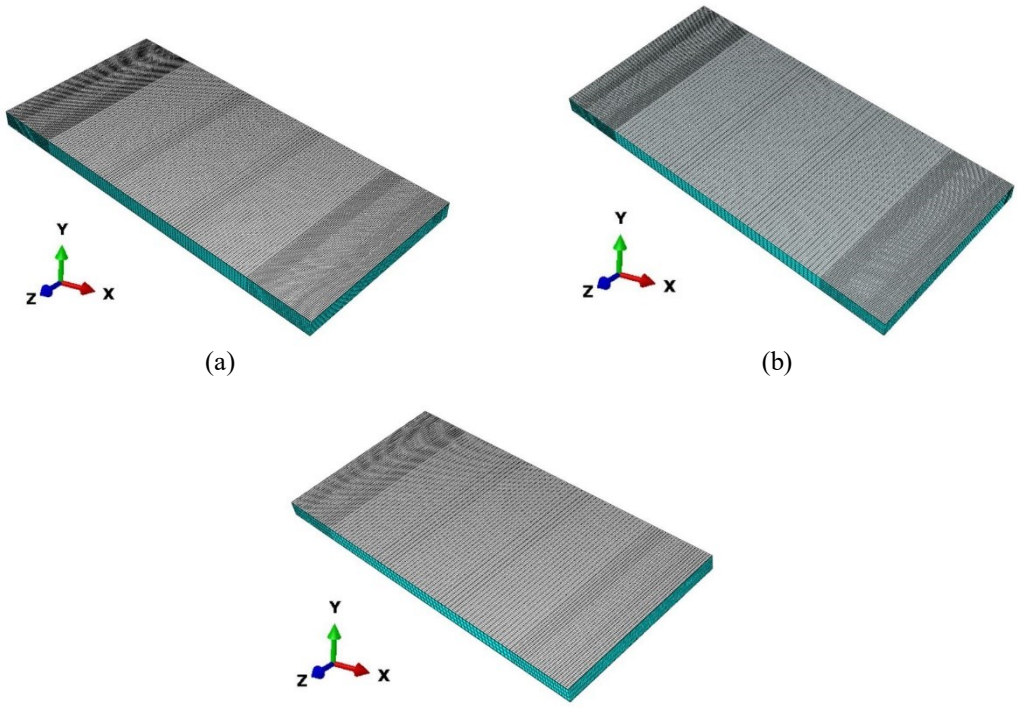

(a) (b)

(c)

Figure 3.9. MW panels with the mesh size: a) 20 mm × 10 mm × 10 mm (207360 elements), b) 30 mm × 20 mm × 10 mm (40320 elements), c) 30 mm × 30 mm × 20 mm (20000 elements)

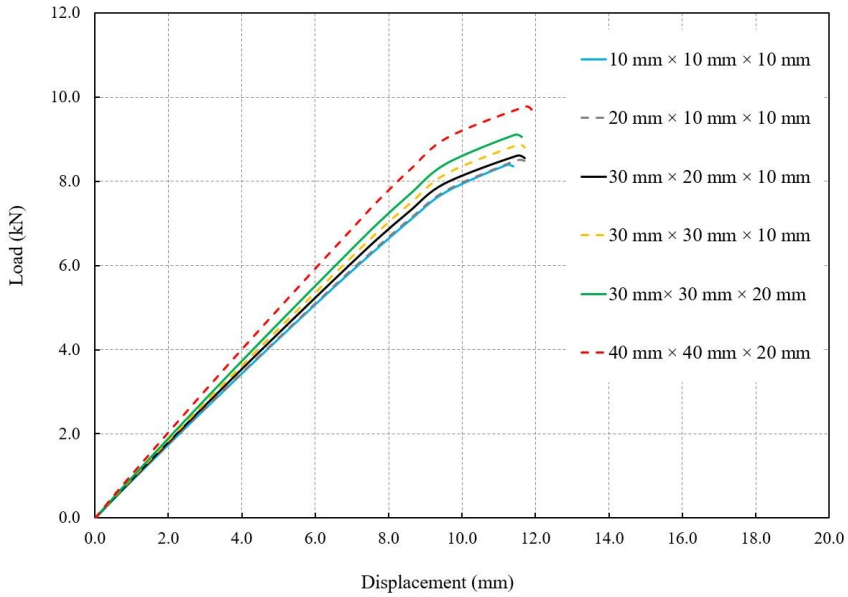

Figure 3.10. Load-displacement curves for MW panels 100 mm with different element sizes

3.4 Comparison between simulation and test results

In order to progress the research more efficiently, numerical models are validated against the experimental results presented in Section 3.2.3. Thermal and mechanical responses can be investigated separately. Therefore, the temperature distributions obtained from heat transfer analysis and load-displacement curves attained from the mechanical analysis are compared to the corresponding experimental results. The simulations are run until the critical cross-section in each case reaches its load-bearing capacity. This approach enables the determination of the initial stiffness and ultimate load. The ultimate load is defined as the maximum load-bearing capacity of the curves, and the bending stiffness is calculated by dividing 50% of the maximum force into the corresponding displacement.

3.4.1 Temperature distribution for MW sandwich panels

Figure 3.11 shows the temperature distribution of experimental and numerical results for the sandwich panel with an MW core of 100 mm and 230 mm thickness and the exposed side temperature of 600 °C. The results are evaluated for the experiment and the simulation in the middle of the plate. The evaluation takes place in the middle of the core thickness for the core material. During the simulation, the plate's lower surface (exposed surface) is exposed to the experiment's measured temperature (blue curve in Figure 3.11). Ambient temperature is assigned to all other component surfaces at the beginning of the simulation. As shown in

Figure 3.11, there is an excellent agreement between the measured and simulated temperature profiles.

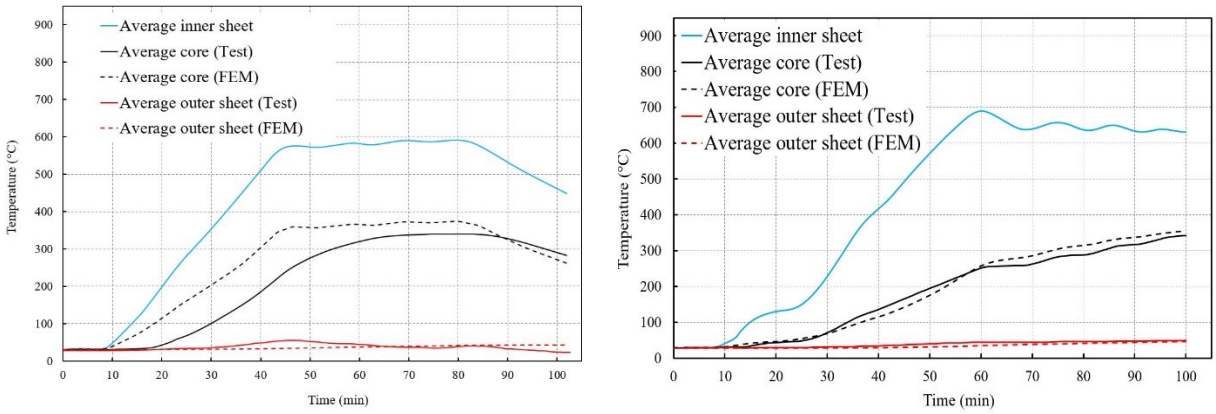

Figure 3.11. Temperature distribution from experiment and simulation for MW core, a) 100 mm, and b) 230 mm with temperature 600 °C.

In Figure 3.12, the temperature changes through the plate's thickness between the exposed (600 °C) and unexposed (ambient temperature) sides of the plate are illustrated.

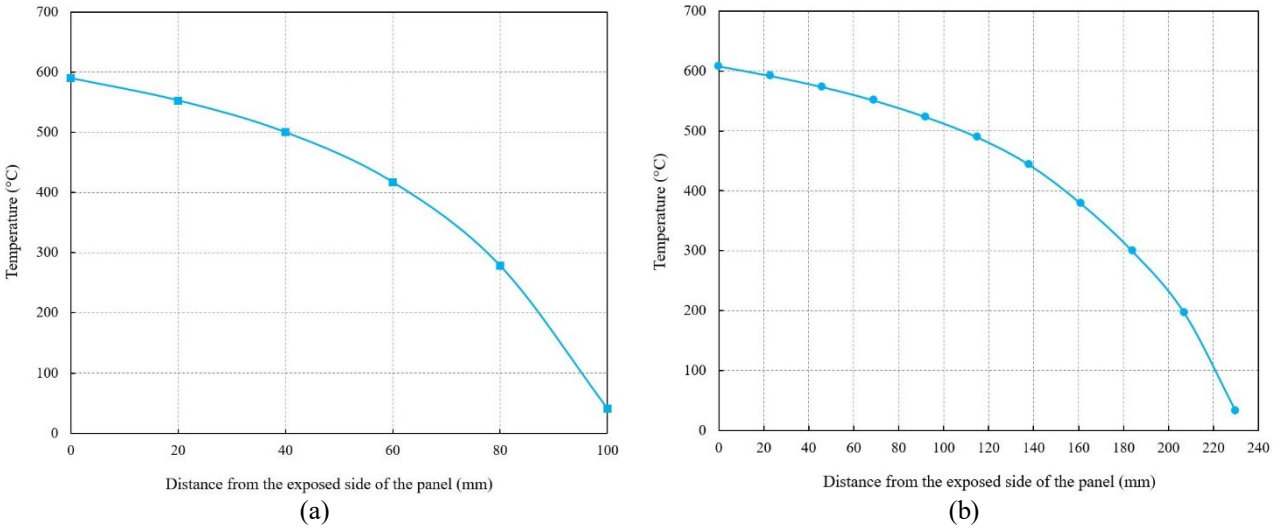

Figure 3.12. Temperature gradient for MW panels through the thickness: a) 100 mm, b) 230 mm

3.4.2 Load-displacement curves for MW sandwich panels

The mode of failure is applied to compare the experimental and numerical models. The collapse of MW sandwich panels is usually caused by shear failure. Figure 3.13 compares the failure mode of the test and a corresponding finite element model at ambient temperature. As can be seen, the area in the vicinity of the supports has the maximum stress.

The load-deformation curves derived from the experiments are used to validate the numerical models for the mechanical analyses. The displacement is measured in the lower plate's mid-span, and the force is recorded from supports. The load-displacement curves obtained from the tests and the simulations are compared for MW panels of 100 mm and 230 mm in Figure 3.14 and Figure 3.15.

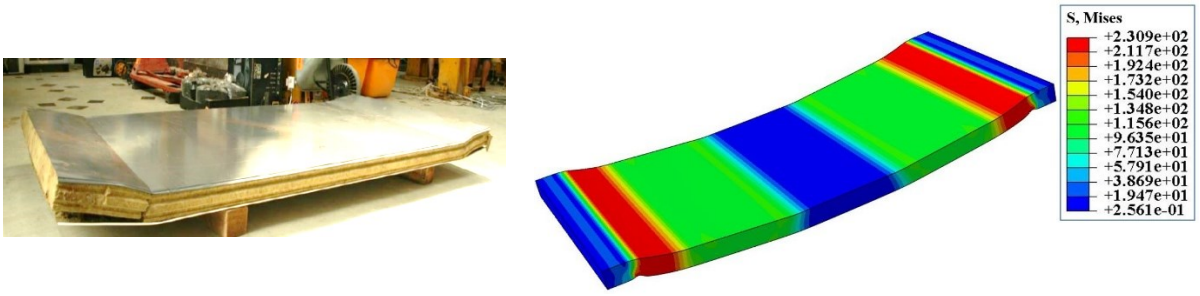

(a) (b)

Figure 3.13. The failure mode for a) the test [8], b) the simulation (in MPa)

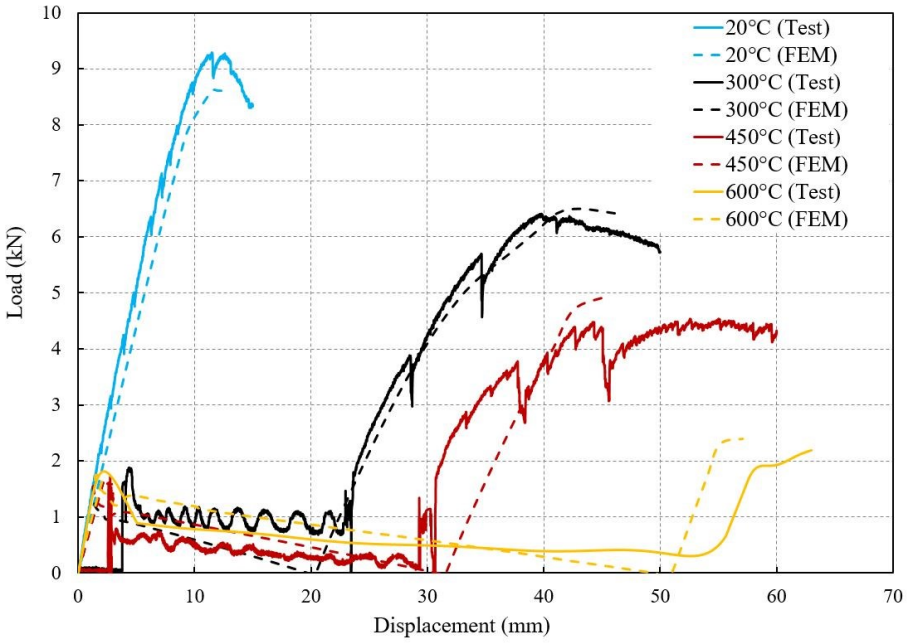

Figure 3.14. Validation of load-displacement curves for MW panel 100 mm

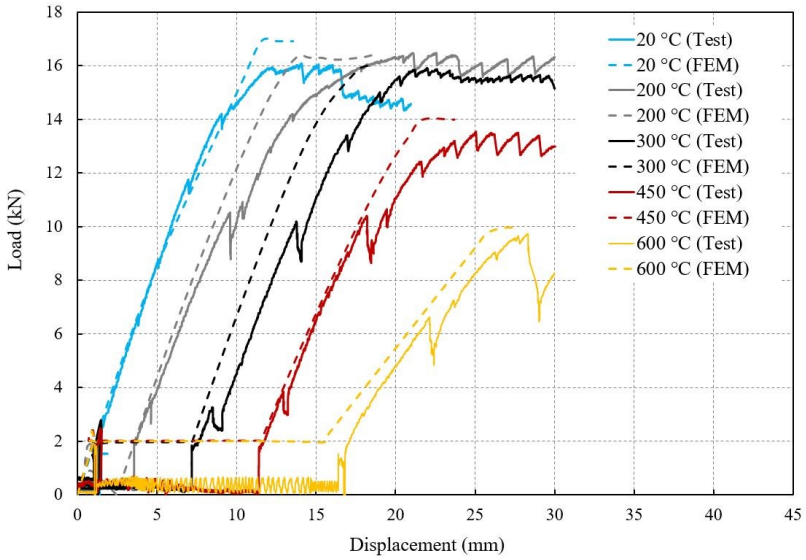

Figure 3.15. Validation of load-displacement curves for MW panel 230 mm

It is observed that the bending stiffness and bearing strengths predicted from FE models are in good agreement with the test results. Both the ultimate load and bending stiffness of the panel decrease as the temperature increases. However, this reduction in stiffness and strength does not follow a linear pattern dependent on the temperature rise. The stiffness and the load-bearing capacity become higher when the panel thickness increases, which was expected.

The numerical results show that for MW panels with 100 mm thickness, the maximum load for 300 °C, 450 °C and 600 °C is 75%, 57% and 28% of the load capacity at ambient temperature, respectively. For MW panels with 230 mm thickness, the maximum load is 95%, 82% and 59% of the maximum load at ambient temperature for 300 °C, 450 °C and 600 °C, respectively.

Table 3.3 presents the maximum load and the stiffness of sandwich panels at different temperatures, where F_{max} and k_b are the maximum loads and the bending stiffness of sandwich panels for experimental and numerical results.

Table 3.3. The maximum load and stiffness of sandwich panels at various temperatures tests

Specimen	T (°C)	D (mm)	$F_{max,FEM}$ (kN)	$F_{max,EXP}$ (kN)	$F_{max,FEM}/F_{max,EXP}$	$k_{b,\ FEM}$ (kN/mm)	$k_{b,\ EXP}$ (kN/mm)	$k_{b,\ FEM}/k_{b,EXP}$
MW sandwich panel	20	100	8.60	9.28	0.92	0.82	0.84	0.97
	300	100	6.50	6.41	1.01	0.53	0.44	1.20
	450	100	4.95	4.53	1.09	0.37	0.32	1.15
	600	100	2.39	2.19	1.09	0.25	0.24	1.04
					Avg: 1.03			Avg: 1.09
					SD: 0.07			SD: 0.10
	20	230	16.91	16.51	1.02	1.49	1.55	0.96
	200	230	16.60	16.50	1.00	1.45	1.47	0.98
	300	230	16.05	15.90	1.00	1.44	1.46	0.98
	450	230	13.95	13.50	1.03	1.29	1.29	1.00
	600	230	9.95	9.73	1.02	0.75	0.83	0.90
					Avg: 1.02			Avg: 0.96
					SD: 0.01			SD: 0.03

Table 3.3 shows that average ultimate loads for simulations are around 3% and 2% (for 100 mm and 230 mm thicknesses, respectively) higher than those for experiments. This ratio for bending stiffness is about 9% for the panels with 100 mm thickness. Nonetheless, the average bending stiffness of panels with 230 mm thickness for numerical results is 4% less than experimental results. In general, the difference between numerical and experimental results is negligible.

3.4.3 Temperature distribution for PIR sandwich panels

A good agreement exists between the measured and simulated temperature profiles for the PIR core panel of 100 mm thickness at 300 °C (Figure 3.16). The results are evaluated for the experiment and the simulation in the middle of the plate and the core thickness. During the simulation, the plate's lower surface (exposed surface) is exposed to the experiment's measured temperature (blue curve in Figure 3.16). Ambient temperature is given to all other component surfaces at the start of the simulation. Figure 3.17 indicates the temperature changes through the plate's thickness between the exposed (300 °C) and unexposed (ambient temperature) sides of the PIR core plate.

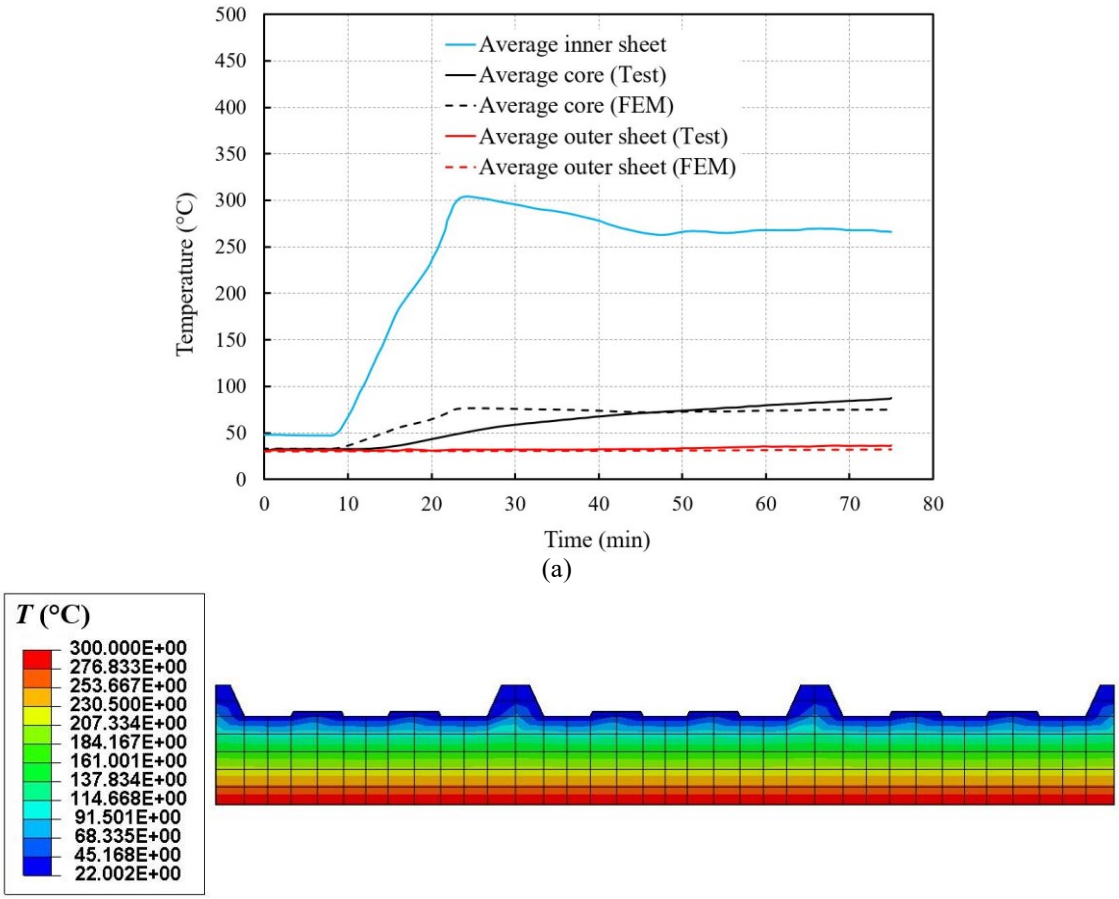

(a)

(b)

Figure 3.16. Temperature distribution for PIR core 100 mm with temperature 300 °C: a) validation, b) FE model

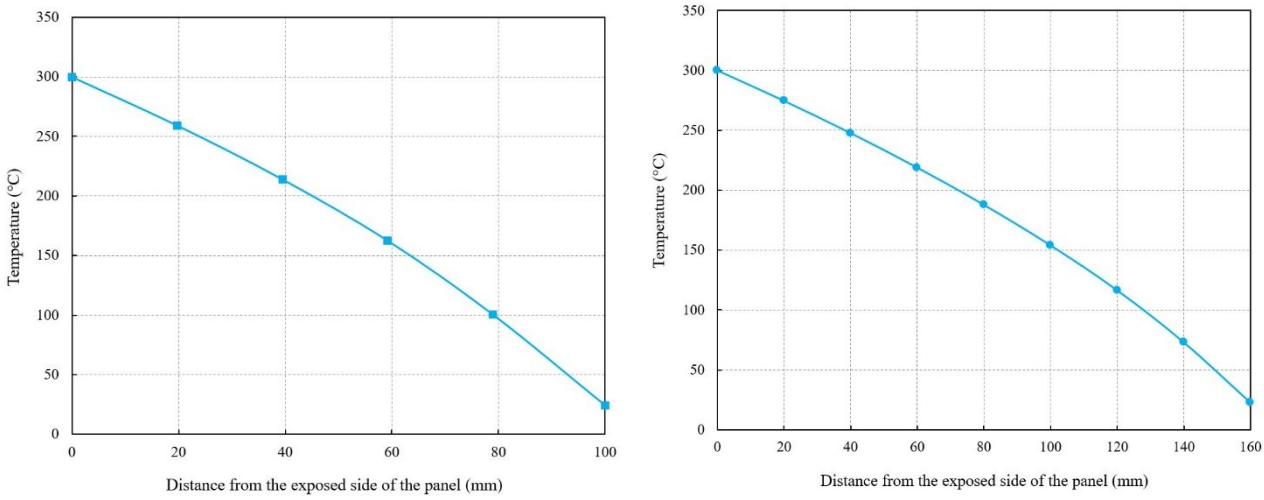

Figure 3.17. Temperature gradient for PIR panels through the thickness: a) 100 mm, b) 160 mm

3.4.4 Load-displacement curves for PIR sandwich panels

Figure 3.18 and Figure 3.19 compare the load-deformation curves achieved from the experiments and simulations for PIR sandwich panels to validate the numerical results. Such as MW panels, the displacement is measured in the lower plate's mid-span, and the force is recorded from supports.

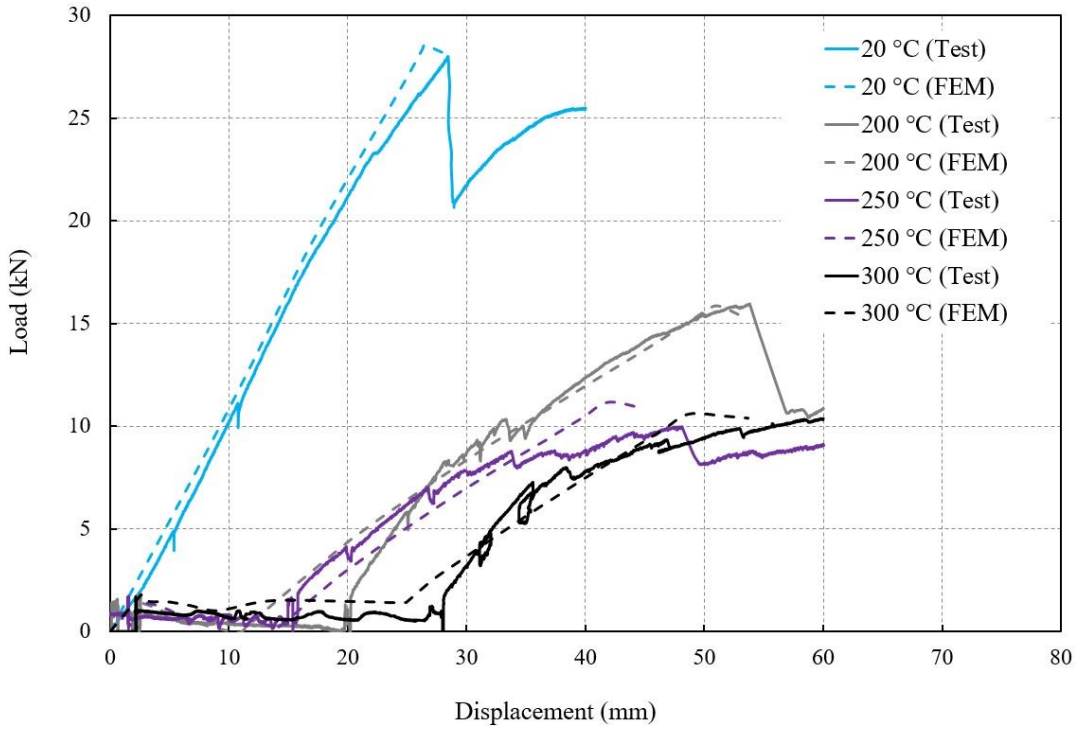

Figure 3.18. Validation of load-displacement curves for PIR panel 100 mm

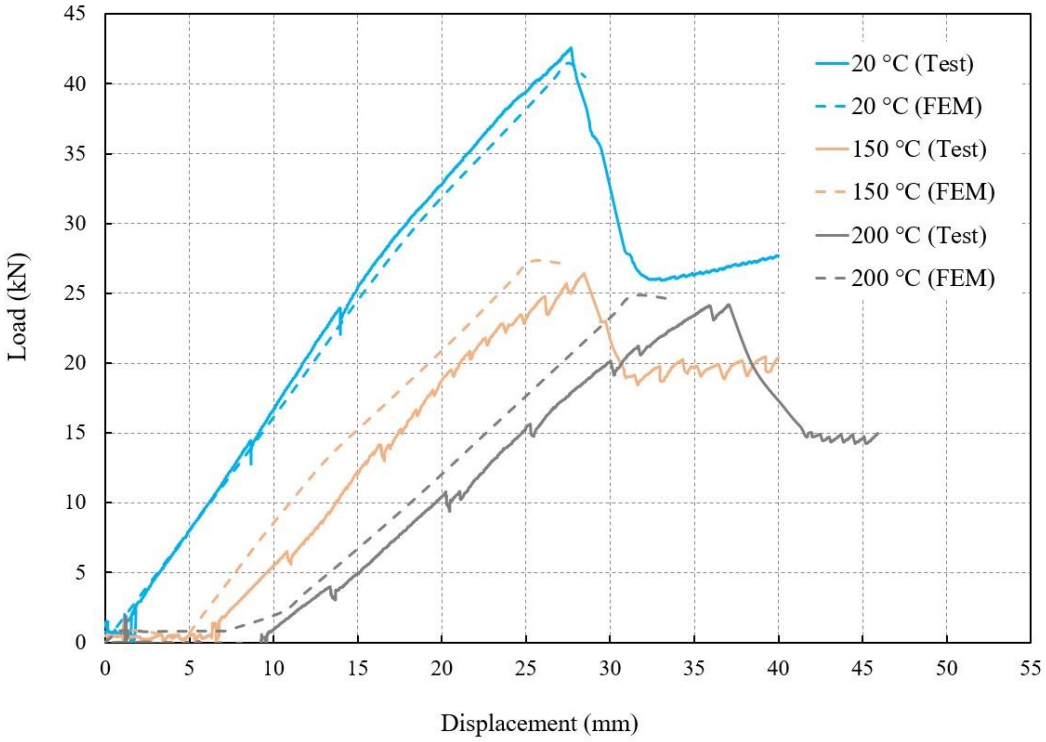

Figure 3.19. Validation of load-displacement curves for PIR panel 160 mm

From the Figures above, it can be concluded that, quite expectedly, the temperature decreases the ultimate load and bending stiffness of the panels. The numerical and experimental results are in satisfying agreement in terms of the initial stiffness and ultimate load.

In PIR sandwich panels at ambient temperature, changing the thickness from 100 mm to 160 mm leads to an increase of the numerically calculated capacity of 44%; furthermore, the numerically calculated bending stiffness of the panel rises by around 55%.

The numerical results show that for the PIR panel with 100 mm thickness, the maximum load for 200 °C, 250 °C and 300 °C is 55%, 39% and 38% of the load capacity at ambient temperature, respectively. A similar relationship can be observed for the PIR panel with 160 mm thickness. Here, the maximum force's decrease is 34% and 40% for the temperatures 150 °C and 200 °C compared to the maximum force at ambient temperature.

Table 3.4 displays the maximum load and stiffness of sandwich panels at different temperatures. F_{max} and k_b are the maximum load and bending stiffness of sandwich panels for experimental and numerical results. The results illustrate that average ultimate loads for simulations are around 2% for panels 100 mm higher and 1% for panels 160 mm less than those for experiments. However, the disparency for average bending stiffness with different thicknesses is greater than maximum force. In fact, the numerical results present higher bending stiffness

than the experimental results, especially at elevated temperatures. The reason can be due to the evaporation of adhesive material for PIR panels at elevated temperatures.

Table 3.4. The maximum load and stiffness of sandwich panels at different temperatures tests

Specimen	T (°C)	D (mm)	$F_{max,FEM}$ (kN)	$F_{max,EXP}$ (kN)	$F_{max,FEM}/F_{max,EXP}$	$k_{b,\,FEM}$ (kN/mm)	$k_{b,\,EXP}$ (kN/mm)	$k_{b,\,FEM}/k_{b,\,EXP}$
PIR sandwich panel	20	100	28.56	28.00	1.02	1.21	1.08	1.12
	200	100	15.85	15.96	0.99	0.94	0.47	2.00
	250	100	11.16	10.16	1.10	0.86	0.31	2.77
	300	100	10.58	10.83	0.97	0.76	0.30	2.53
					Avg: 1.02			Avg: 2.10
					SD: 0.05			SD: 0.73
	20	160	41.49	44.38	0.93	1.87	1.65	1.13
	150	160	27.30	26.44	1.03	1.66	1.22	1.36
	200	160	24.84	24.19	1.02	1.24	0.89	1.39
					Avg: 0.99			Avg: 1.29
					SD: 0.05			SD: 0.14

3.5 Conclusion

This chapter investigated MW and PIR sandwich panels' bending stiffnesses at ambient and elevated temperatures under bending loadings. A FE model was developed to verify simulations with experimental results. Due to the testing procedure, a two-stage analysis process was required for the thermo-mechanical simulation. According to the experimental setup, boundary conditions (loadings and supports) were specified in the numerical model. With the help of a mesh sensitivity study, the optimal mesh was determined.

The following conclusions can be drawn:

- The numerical results were in good agreement with experimental results for maximum forces at ambient and elevated temperatures for MW and PIR sandwich panels. Averagely, the difference between numerical and experimental results was around 2.5%
- The PIR panels showed a higher resistance at ambient and elevated temperatures than MW panels when the thickness was similar.
- There was a decrease in the load-bearing capacity and bending stiffness with increasing specimen temperature for both MW and PIR panels.
- The validation of bending tests also provided the required knowledge to simulate translational tests.

Chapter 4: ANALYTICAL AND PARAMETRIC STUDY FOR BENDING TESTS OF SANDWICH PANELS

4.1 Introduction

In this chapter, sandwich panels' bending stiffness obtained from Eurocodes (EN 14509, 2013) [102] for both MW and PIR panels is presented. These formulas predict the bending stiffness of panels at ambient temperature. Afterward, in order to predict the bending stiffness of panels at elevated temperatures with a reasonable accuracy, two methods called "average solution" and "maximum solution" are developed. Moreover, a parametric study in ABAQUS for ambient and elevated temperatures is carried out. During the parametric study, the decisive components such as height, span, and width of the panel and the sheets' thickness are changed and investigated. This chapter's main objective is to validate the proposed solutions with the numerical results achieved from the parametric study to provide valid formulas for further analytical investigations at elevated temperatures.

4.2 Analytical study for MW sandwich panels

This section describes an analytical solution to predict MW sandwich panels' bending stiffness with flat facings at ambient and elevated temperatures. The analytical solution employs Eurocodes (EN 14509, 2013) [102].

4.2.1 Formula from Eurocode for normal condition

The MW sandwich panels studied in this research have flat or slightly profiled faces. The maximum deflection of a sandwich panel with flat or slightly profiled faces is presented in Table E.10.1 (EN 14509, 2013). The maximum deflection of single-span sandwich panels at ambient temperature is according to Eq. (4.1).

$$\nu_{max} = \frac{5qL^4}{384B_s}(1 + 3.2k) \tag{4.1}$$

where B_S and k (correction factor) are defined with Eq. (4.2) and (4.3).

$$B_S = e^2 \frac{E_{F1}A_{F1}.E_{F2}A_{F2}}{(E_{F1}A_{F1} + E_{F2}A_{F2})} \quad (4.2)$$

$$k = \frac{3B_S}{L^2 G_c A_c} = \frac{3B_S}{L^2 G_c bD} \quad (4.3)$$

Eq. (4.1) to (4.3) employ the following notations:

G_c	shear modulus of core material
A_c	the cross-sectional area of the core
E_{F1}, E_{F2}	young's modulus of the external and internal faces, respectively
A_{F1}, A_{F2}	cross-sectional areas of the external and internal faces, respectively
e	the distance between the centroids of faces
L	the span of the panel
b, D	the width and height of the core
q	the uniform load
v_{max}	the maximum deflection

In this research, the internal face (exposed side) is subjected to fire, while the external face (unexposed side) is at ambient temperature. The uniform load is converted to a concentrated force through Eq. (4.4). Since stiffness is the extent to which an object resists deformation in response to an applied force, the bending stiffness (k_b) for MW sandwich panels is calculated with Eq. (4.5).

$$F = q.L \quad (4.4)$$

$$k_b = \frac{F}{v_{max}} = \frac{q.L}{v_{max}} = \frac{384B_s}{5L^3(1 + 3.2k)} \quad (4.5)$$

where k_b is the bending stiffness of sandwich panels at ambient temperature. In the analytical solutions, in order to make core materials compatible with the abovementioned equations, they are considered isotropic materials. The shear modulus is obtained from Eq. (4.6), where G, E and v represent the shear modulus, Young's modulus and Poisson's ratio [103].

$$E = 2G.(1 + \nu) \quad (4.6)$$

4.2.2 Average and maximum solution for elevated temperatures

In the fire case, the analytical formulation is modified by replacing Young's modulus of the exposed face and the shear modulus of the core material with the corresponding values at elevated temperatures.

Due to the thin thickness of the inner steel sheet, the whole sheet thickness's temperature is constant (exposed temperature). As a result, Young's modulus of the inner sheet is a specific value calculated by the degradation of steel materials. However, the temperature distribution along the core thickness is different. As a matter of fact, the heat varies between the maximum temperature (exposed side) and ambient temperature (unexposed side). In such a case, it is proposed to use an average shear modulus of the core. This average value is computed according to the thickness ratio of each temperature layer. As a conservative approach, the shear modulus value can be calculated based on the shear modulus at the maximum core temperature. $k_{b,theory\text{-}avg}$ ("average solution") and $k_{b,theory\text{-}max}$ ("maximum solution"), respectively, indicate the bending stiffness calculated by the average shear modulus of the core and the shear modulus at the highest core temperature. It is evident that the "average" and "maximum" solutions give similar results at ambient temperature.

Following the explanations above, Eq. (4.5) should be modified at elevated temperatures for two parameters, $E_{F2,\theta}$ and $G_{C,\theta}$ in the form of Eq. (4.7) and (4.8), which show their influence in k and B_S.

$$E_{F2,\theta} = E_{F2} \times k_{E,\theta} \tag{4.7}$$

$$G_{C,\theta} = G_C \times k_{Gc,\theta} \tag{4.8}$$

where $k_{E,\theta}$ is the reduction factor for Young's modulus of carbon steel according to Section 2.5.2, and $k_{GC,\theta}$ is the reduction factor for the shear modulus of the MW core material, which is based on the proposed reduction factor and shown in Table 4.1.

Table 4.1. The proposed reduction factor for shear modulus of the MW core at elevated temperatures

Temperature (°C)	20	150	300	450	600
Reduction factor	1	0.75	0.5	0.25	0.25

As a consequence, Eq. (4.2), (4.3) and (4.5) are modified to Eq. (4.9), (4.10) and (4.11), respectively, for MW sandwich panels at elevated temperatures.

$$B_{S,\theta} = e^2 \frac{E_{F1}A_{F1}.E_{F2,\theta}A_{F2}}{(E_{F1}A_{F1} + E_{F2,\theta}A_{F2})} \tag{4.9}$$

$$k_\theta = \frac{3B_{S,\theta}}{L^2 G_{c,\theta} A_c} = \frac{3B_{S,\theta}}{L^2 G_{c,\theta} bD} \tag{4.10}$$

$$k_{b,\theta} = \frac{384B_{s,\theta}}{5L^3(1 + 3.2k_\theta)} \tag{4.11}$$

Eq. (4.11) presents the bending stiffness of MW panels at elevated temperatures. If the shear modulus of the core material is computed based on an average degradation, the outputs demonstrate "average solution" results. When applying the maximum reduction factor for the core material, outputs present "maximum solution" results.

An example is provided in Appendix A to show how the bending stiffness of MW panels is calculated at ambient and elevated temperatures for both "average solution" and "maximum solution".

4.3 Analytical study for PIR sandwich panels

This section describes an analytical solution to predict PIR sandwich panels' bending stiffness with one profiled facing and one flat facing at ambient and elevated temperatures. The analytical solution employs Eurocodes (EN 14509, 2013) [102].

4.3.1 Formula from Eurocode for ambient temperature

The PIR sandwich panels studied in this research have one flat facing and one profiled (trapezoidal) face. The maximum deflection of a sandwich panel with one profiled face and one flat or lightly profiled face is presented in Table E.10.2 (EN 14509, 2013). The maximum deflection of single-span sandwich panels at ambient temperature is according to Eq. (4.12).

$$v_{max} = \frac{5qL^4}{384B_s}(1 + 3.2k)(1 - \beta) \tag{4.12}$$

where

$$\beta = \frac{B_{F1}}{B_{F1} + \frac{B_s}{1 + 3.2k}} \tag{4.13}$$

Eq. (4.12) and (4.13) employ the notations in Section 4.2.1. B_{F1} displays the bending stiffness of the external face with respect to its own axis and is calculated according to Eq. (4.14):

$$B_{F1} = E_{F1}I_{F1} \tag{4.14}$$

where E_{F1} and I_{F1} are Young's modulus and the second moment of area of the external face.

In this case, the flat face (exposed side) is subjected to fire, while the trapezoidal face (unexposed side) is at ambient temperature. Moreover, the bending stiffness (k_b) of PIR sandwich panels is calculated with Eq. (4.15):

$$k_b = \frac{384 B_s}{5L^3(1+3.2k)(1-\beta)} \tag{4.15}$$

Other parameters, such as B_S and k, are calculated according to Eq. (4.2) and (4.3).

4.3.2 Average and maximum solution for elevated temperatures

In the fire case, the analytical formulation for PIR panels is modified by replacing Young's modulus of the exposed face and the shear modulus of the core material with the corresponding values at elevated temperatures.

In fact, the process of determining the bending stiffness is similar to the MW panels. Eq. (4.16) displays the bending stiffness of the PIR panels at elevated temperatures.

$$k_{b,\theta} = \frac{384 B_{s,\theta}}{5L^3(1+3.2k_\theta)(1-\beta_\theta)} \tag{4.16}$$

$B_{S,\theta}$ and k_θ are calculated by Eq. (4.9) and (4.10), while β_θ is obtained from Eq. (4.17).

$$\beta_\theta = \frac{B_{F1}}{B_{F1} + \frac{B_{S,\theta}}{1+3.2k_\theta}} \tag{4.17}$$

B_{F1}, $B_{S,\theta}$ and k_θ are achieved from the formulas of Sections 4.2.2 and 4.3.1. Since the same material of facing steel for both MW and PIR panels is employed, the reduction factor for Young's carbon steel modulus is similar to those applied for MW panels. The reduction factor for the shear modulus of the PIR core material is based on the proposed reduction factor shown in Table 4.2.

Table 4.2. The proposed reduction factor for shear modulus of the PIR core at elevated temperatures

Temperature (°C)	20	150	300	450	600
Reduction factor	1	0.67	0.45	0.12	0.12

The "average solution" and "maximum solution" are calculated in a way explained in Section 4.2.2. An example is shown in Appendix B to show how PIR panels' bending stiffness is calculated at ambient and elevated temperatures for "average solution" and "maximum solution".

4.4 Parametric study for MW sandwich panels

4.4.1 General

After validating numerical simulations against the experimental results, an extensive number of finite element analyses are performed to determine MW sandwich panels' bending stiffness under bending loads at ambient and elevated temperatures. The investigated parameters include the width, thickness and span of panels and the thickness of facings. The changes in dimensions of specimens are based on the commonly existing parts in the industry. For example, the facing thickness of sandwich panels usually ranges from 0.40 mm to 1.00 mm, or the core thickness changes between 50 mm and 300 mm. The steel facings' material properties and the core in the parametric study are identical to those of the tests.

In Table 4.3, the numerical and analytical results for MW panels are presented and compared at different temperatures, where the specimens are labeled in the way [panel]-B-D-L-t_{F2}- t_{F1}-θ. B, D, L, t_{F2}, t_{F1} and θ are the width, thickness, span of panels, inner thickness facing, outer thickness facing, and the exposed side's temperature. The specimens are mainly categorized into groups according to their temperatures and investigated parameters. For instance, the label "MW-1200-100-2500-0.5-0.6-20" defines as follows: an MW panel with 1200 mm width, 100 mm thickness, 2500 mm span, 0.5 mm inner sheet thickness, 0.6 mm outer sheet thickness, which is exposed to 20 °C temperature. $k_{b,FEM}$ is the bending stiffness of panels obtained from the numerical results. According to Section 4.2.2, the bending stiffness of panels calculated by the analytical formulation is based on the two methods of $k_{b,theory\text{-}avg}$ ("average solution") and $k_{b,theory\text{-}max}$ ("maximum solution"). They indicate the bending stiffness calculated by the average shear modulus of the core and the shear modulus at the highest core temperature. It is evident that the "average" and "maximum" solutions give similar results at ambient temperature. In Appendix E, the load-displacement curves obtained from FE models for some of the specimens under bending loading at ambient and elevated temperatures are presented.

Table 4.3. Comparison of the bending stiffness of MW sandwich panels calculated by numerical and analytical methods

Case	$k_{b,theory\text{-}avg}$ (kN/mm)	$k_{b,FEM}$ (kN/mm)	$k_{b,theory\text{-}avg}$ / $k_{b,FEM}$	$k_{b,theory\text{-}max}$ (kN/mm)	$k_{b,theory\text{-}max}$ / $k_{b,FEM}$
MW-600-100-2500-0.5-0.6-20	0.36	0.41	0.88	0.36	0.88
MW-900-100-2500-0.5-0.6-20	0.54	0.62	0.87	0.54	0.87
MW-1200-100-2500-0.5-0.6-20	0.72	0.83	0.87	0.72	0.87
MW-1500-100-2500-0.5-0.6-20	0.90	1.04	0.87	0.90	0.87
MW-2500-100-2500-0.5-0.6-20	1.50	1.50	1.00	1.50	1.00
MW-1200-100-2500-0.4-0.6-20	0.70	0.81	0.86	0.70	0.86
MW-1200-100-2500-0.5-0.6-20	0.72	0.83	0.87	0.72	0.87
MW-1200-100-2500-0.7-0.6-20	0.74	0.85	0.87	0.74	0.87
MW-1200-100-2500-1.0-0.6-20	0.76	0.87	0.87	0.76	0.87

MW-1200-100-2500-0.5-0.4-20	0.69	0.80	0.86	0.69	0.86
MW-1200-100-2500-0.5-0.6-20	0.72	0.83	0.87	0.72	0.87
MW-1200-100-2500-0.5-0.7-20	0.73	0.84	0.87	0.73	0.87
MW-1200-100-2500-0.5-1.0-20	0.74	0.86	0.86	0.74	0.86
MW-1200-100-1000-0.5-0.6-20	2.13	1.97	1.08	2.13	1.08
MW-1200-100-1875-0.5-0.6-20	1.07	1.30	0.82	1.07	0.82
MW-1200-100-2500-0.5-0.6-20	0.72	0.83	0.87	0.72	0.87
MW-1200-100-3125-0.5-0.6-20	0.51	0.64	0.80	0.51	0.80
MW-1200-100-4500-0.5-0.6-20	0.27	0.34	0.79	0.27	0.79
MW-1200-100-6000-0.5-0.6-20	0.14	0.20	0.70	0.14	0.70
MW-1200-50-2500-0.5-0.6-20	0.30	0.38	0.79	0.30	0.79
MW-1200-100-2500-0.5-0.6-20	0.72	0.83	0.87	0.72	0.87
MW-1200-160-2500-0.5-0.6-20	1.24	1.31	0.95	1.24	0.95
MW-1200-230-2500-0.5-0.6-20	1.85	1.73	1.07	1.85	1.07
MW-1200-300-2500-0.5-0.6-20	2.47	2.06	1.20	2.47	1.20
MW-600-100-2500-0.5-0.6-300	0.25	0.27	0.93	0.19	0.70
MW-1200-100-2500-0.5-0.6-300	0.50	0.53	0.94	0.38	0.72
MW-2500-100-2500-0.5-0.6-300	1.04	1.11	0.94	0.80	0.72
MW-1200-100-2500-0.4-0.6-300	0.49	0.52	0.94	0.38	0.73
MW-1200-100-2500-0.5-0.6-300	0.50	0.53	0.94	0.38	0.72
MW-1200-100-2500-0.7-0.6-300	0.52	0.55	0.95	0.39	0.71
MW-1200-100-2500-1.0-0.6-300	0.53	0.57	0.93	0.40	0.70
MW-1200-100-2500-0.5-0.4-300	0.48	0.52	0.92	0.37	0.71
MW-1200-100-2500-0.5-0.6-300	0.50	0.53	0.94	0.38	0.72
MW-1200-100-2500-0.5-0.7-300	0.50	0.54	0.93	0.39	0.72
MW-1200-100-2500-0.5-1.0-300	0.51	0.55	0.93	0.39	0.71
MW-1200-100-1000-0.5-0.6-300	1.44	1.33	1.08	1.08	0.81
MW-1200-100-1875-0.5-0.6-300	0.73	0.83	0.88	0.56	0.67
MW-1200-100-2500-0.5-0.6-300	0.50	0.53	0.94	0.38	0.72
MW-1200-100-3125-0.5-0.6-300	0.36	0.42	0.86	0.28	0.67
MW-1200-100-4500-0.5-0.6-300	0.19	0.24	0.79	0.16	0.67
MW-1200-100-6000-0.5-0.6-300	0.11	0.15	0.73	0.09	0.60
MW-1200-50-2500-0.5-0.6-300	0.22	0.25	0.88	0.17	0.68
MW-1200-100-2500-0.5-0.6-300	0.50	0.53	0.94	0.38	0.72
MW-1200-160-2500-0.5-0.6-300	0.85	0.83	1.02	0.65	0.78
MW-1200-230-2500-0.5-0.6-300	1.26	1.16	1.09	0.95	0.82
MW-1200-300-2500-0.5-0.6-300	1.68	1.36	1.24	1.26	0.93
MW-600-100-2500-0.5-0.6-450	0.19	0.19	1.00	0.10	0.53
MW-1200-100-2500-0.5-0.6-450	0.38	0.37	1.03	0.20	0.54
MW-2500-100-2500-0.5-0.6-450	0.79	0.76	1.04	0.42	0.55
MW-1200-100-2500-0.4-0.6-450	0.37	0.36	1.03	0.19	0.53
MW-1200-100-2500-0.5-0.6-450	0.38	0.37	1.03	0.20	0.54
MW-1200-100-2500-0.7-0.6-450	0.39	0.37	1.05	0.20	0.54
MW-1200-100-2500-1.0-0.6-450	0.40	0.40	1.00	0.20	0.50
MW-1200-100-2500-0.5-0.4-450	0.37	0.36	1.03	0.20	0.56
MW-1200-100-2500-0.5-0.6-450	0.38	0.37	1.03	0.20	0.54
MW-1200-100-2500-0.5-0.7-450	0.38	0.37	1.03	0.20	0.54
MW-1200-100-2500-0.5-1.0-450	0.39	0.37	1.05	0.20	0.54
MW-1200-100-1000-0.5-0.6-450	1.09	0.90	1.21	0.54	0.60
MW-1200-100-1875-0.5-0.6-450	0.56	0.57	0.98	0.28	0.49
MW-1200-100-2500-0.5-0.6-450	0.38	0.37	1.03	0.20	0.54
MW-1200-100-3125-0.5-0.6-450	0.27	0.29	0.93	0.15	0.52
MW-1200-100-4500-0.5-0.6-450	0.15	0.17	0.88	0.09	0.53
MW-1200-100-6000-0.5-0.6-450	0.08	0.11	0.73	0.05	0.45
MW-1200-50-2500-0.5-0.6-450	0.16	0.17	0.94	0.09	0.53
MW-1200-100-2500-0.5-0.6-450	0.38	0.37	1.03	0.20	0.54
MW-1200-160-2500-0.5-0.6-450	0.65	0.55	1.18	0.33	0.60
MW-1200-230-2500-0.5-0.6-450	0.96	0.66	1.45	0.48	0.73
MW-1200-300-2500-0.5-0.6-450	1.28	0.86	1.49	0.64	0.74
MW-600-100-2500-0.5-0.6-600	0.13	0.14	0.93	0.09	0.64
MW-1200-100-2500-0.5-0.6-600	0.27	0.27	1.00	0.19	0.70

MW-2500-100-2500-0.5-0.6-600	0.58	0.56	1.04	0.40	0.71
MW-1200-100-2500-0.4-0.6-600	0.27	0.27	1.00	0.19	0.70
MW-1200-100-2500-0.5-0.6-600	0.27	0.27	1.00	0.19	0.70
MW-1200-100-2500-0.7-0.6-600	0.29	0.28	1.04	0.20	0.71
MW-1200-100-2500-1.0-0.6-600	0.29	0.29	1.00	0.20	0.69
MW-1200-100-2500-0.5-0.4-600	0.27	0.27	1.00	0.19	0.70
MW-1200-100-2500-0.5-0.6-600	0.27	0.27	1.00	0.19	0.70
MW-1200-100-2500-0.5-0.7-600	0.28	0.27	1.04	0.19	0.70
MW-1200-100-2500-0.5-1.0-600	0.28	0.28	1.00	0.19	0.68
MW-1200-100-1000-0.5-0.6-600	0.80	0.63	1.27	0.53	0.84
MW-1200-100-1875-0.5-0.6-600	0.41	0.42	0.98	0.28	0.67
MW-1200-100-2500-0.5-0.6-600	0.27	0.27	1.00	0.19	0.70
MW-1200-100-3125-0.5-0.6-600	0.20	0.22	0.91	0.14	0.64
MW-1200-100-4500-0.5-0.6-600	0.10	0.13	0.77	0.08	0.62
MW-1200-100-6000-0.5-0.6-600	0.06	0.08	0.75	0.05	0.63
MW-1200-50-2500-0.5-0.6-600	0.12	0.13	0.92	0.08	0.62
MW-1200-100-2500-0.5-0.6-600	0.27	0.27	1.00	0.19	0.70
MW-1200-160-2500-0.5-0.6-600	0.47	0.42	1.12	0.32	0.76
MW-1200-230-2500-0.5-0.6-600	0.70	0.47	1.49	0.47	1.00
MW-1200-300-2500-0.5-0.6-600	0.93	0.65	1.43	0.63	0.97

4.4.2 Effect of inner and outer sheet thickness

The sheet thickness of sandwich panels varies between 0.40 mm and 1.00 mm. According to Table 4.3, it can be concluded that the sheet thickness within the range above does not play a significant role in changing the bending stiffness of specimens. For example, at ambient temperature, when the inner sheet thickness changes from 0.40 mm to 1.00 mm, the stiffness of FE models increases only 7.4%. This growth for analytical results is 8.5%. Consequently, the sheet thickness of panels is not considered as a determining parameter to influence the bending stiffness. Comparing the numerical and analytical results shows that the analytical solution's stiffness is favorably less than the numerical ones (Figure 4.1). In fact, the analytical results lead to a safe prediction for bending stiffness. Furthermore, the growth rate of both methods (analytical and FE approaches) is almost similar.

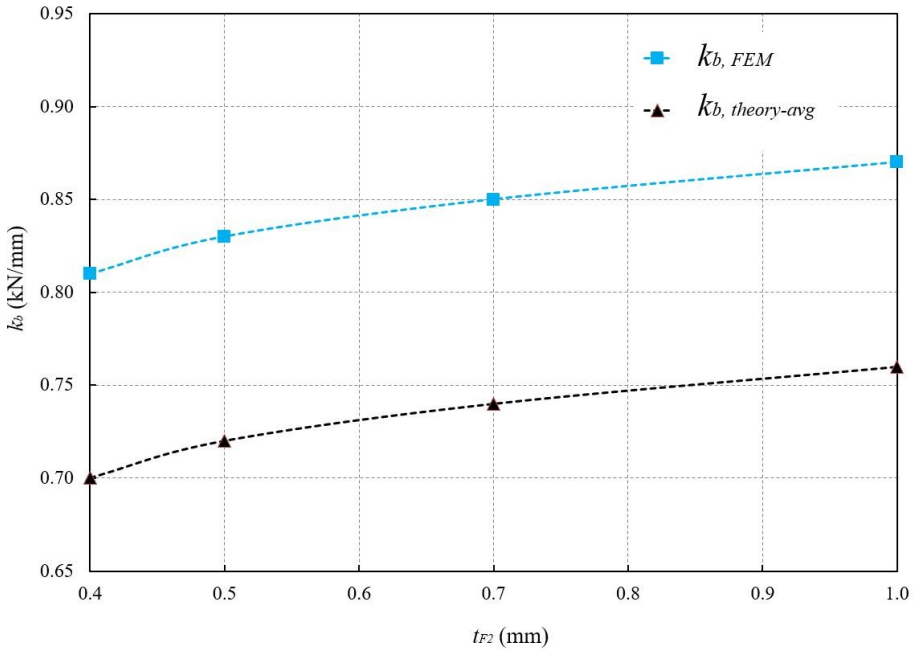

Figure 4.1. Bending stiffness of numerical and analytical results with different inner sheet thicknesses at ambient temperature (MW-1200-100-2500-t_{F2}-0.6-20)

4.4.3 Effect of panel thickness

One of the significant parameters to determine the bending stiffness is the sandwich panel thickness. Figure 4.2 indicates the load-displacement curves of MW-1200-*D*-2500-0.5-0.6-20 specimens taken from simulations with different panel thicknesses at ambient temperature. As expected, with the increase of the thickness, the stiffness increases. For instance, a panel's stiffness with 300 mm thickness is around 5.4 times greater than the same panel with 50 mm thickness. The bending stiffness values calculated by the analytical and numerical methods are very similar for the panels with thickness less than 160 mm (see Figure 4.3). However, for the panels thicker than 160 mm, numerical results' values are less than analytical results. The results from analytical solutions follow a linear trend within the range above, while the FE results are linear just to 160 mm, and after that, the slope of the curve decreases.

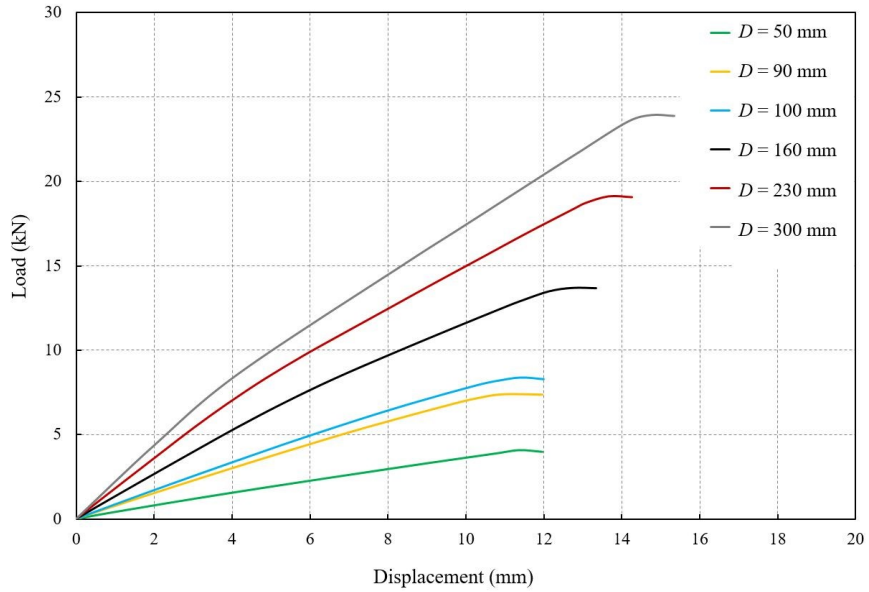

Figure 4.2. Load-displacement curves for MW-1200-*D*-2500-0.5-0.6-20 specimen with different panel thicknesses at ambient temperature

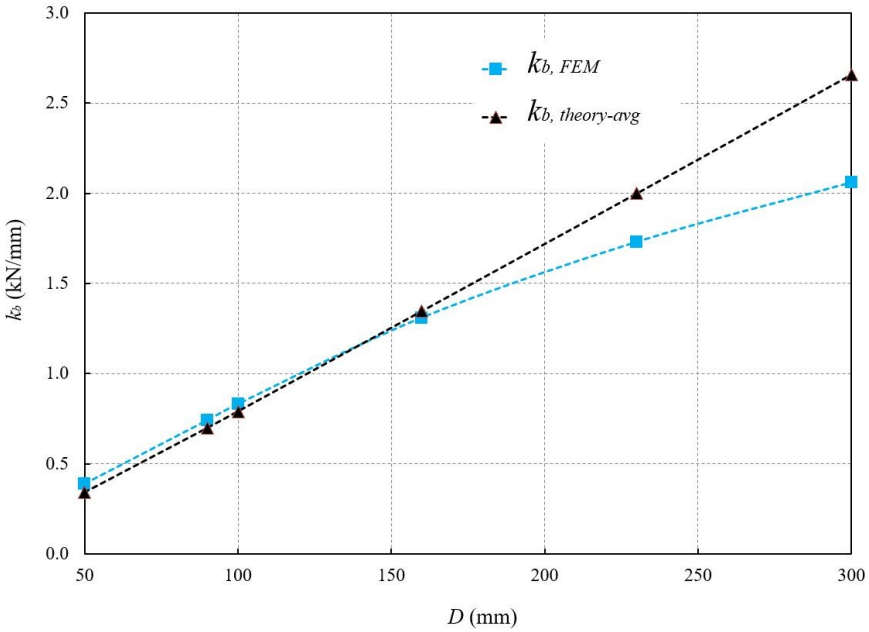

Figure 4.3. Bending stiffness of numerical and analytical results with different panel thicknesses at ambient temperature (MW-1200-*D*-2500-0.5-0.6-20)

4.4.4 Effect of panel widths

In this study, the panel width varies from 600 mm to 2500 mm. Figure 4.4 demonstrates that the panel width directly affects the bending stiffness. When the panel width increases around 67%, the stiffness grows about 68%. Figure 4.5 illustrates an almost linear relationship between the panel width and bending stiffness for analytical and numerical results. Furthermore, it can

be concluded that up to 1800 mm width, the analytical results are on the safe side, while for higher values, the analytical results are non-conservative compared to the simulations.

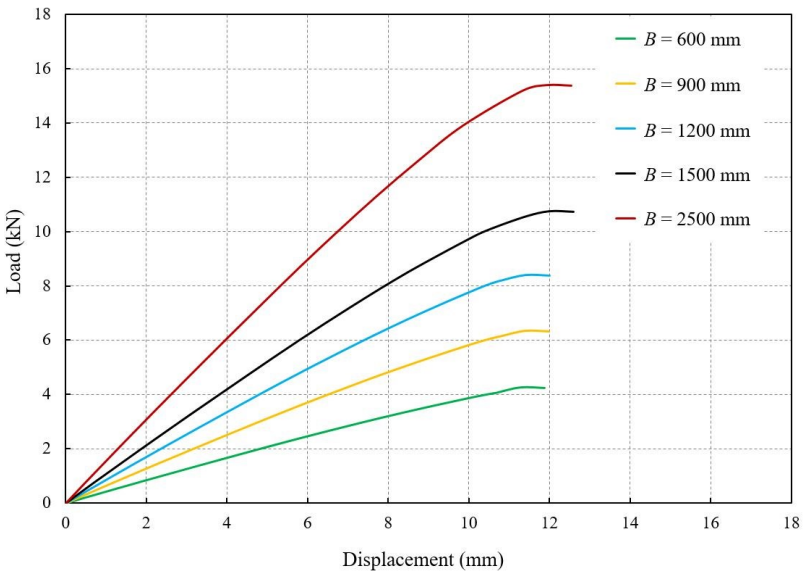

Figure 4.4. Load-displacement curves for MW-*B*-100-2500-0.5-0.6-20 specimen with different panel widths at ambient temperature

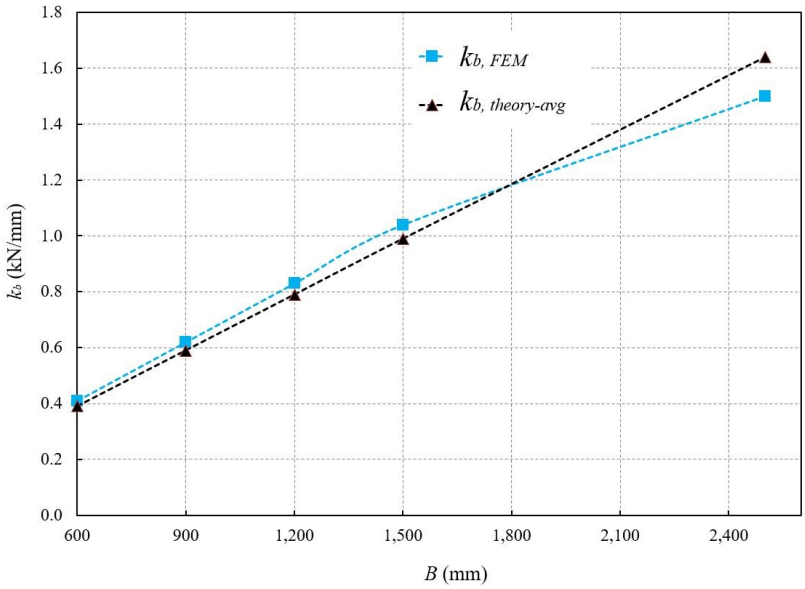

Figure 4.5. Bending stiffness of numerical and analytical results with different panel widths at ambient temperature (MW-*B*-100-2500-0.5-0.6-20)

4.4.5 Effect of panel spans

According to the results obtained from the finite element models, it is found that changing the panel span has a substantial influence on the bending stiffness of panels. In fact, it can be said that the stiffness decreases with the enlargement of the span. At ambient temperature, the panel's bending stiffness with 1875 mm length is 1.30 kN/mm, which with increasing the length to

2500 mm and 6000 mm, the bending stiffness of panels reduces to 0.83 kN/mm and 0.20 kN/mm, respectively. As shown in Figure 4.6, the process of changing stiffness is similar for both analytical and numerical results, and the analytical results for all amounts are slightly less than simulations. Therefore, it can be concluded that the analytical solution is safe for all spans lengths.

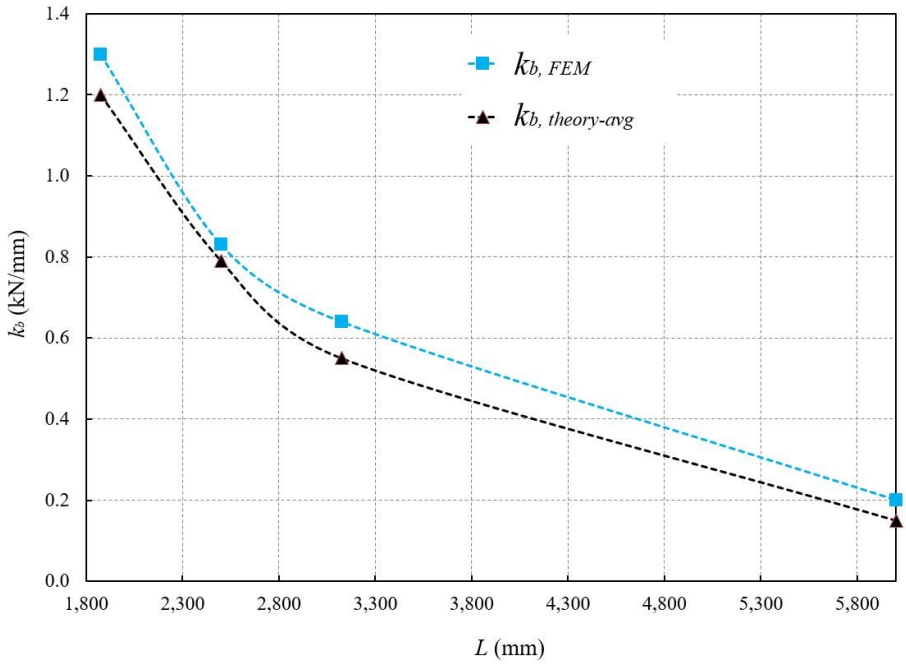

Figure 4.6. Bending stiffness of numerical and analytical results with different panel spans at ambient temperature (MW-1200-100-*L*-0.5-0.6-20)

4.4.6 Effect of temperature

As shown in Table 4.3, different temperatures are assigned to the lower sheet of panels to evaluate the fire's effect on the bending stiffness. As expected, at elevated temperatures, the stiffness and the load-bearing capacity are reduced for numerical and analytical results. This decrease is due to the degradation in the lower sheet and the core mechanical properties. Figure 4.7, as an example, illustrates the numerical results for MW-1200-100-2500-0.5-0.6-θ specimens at different temperatures.

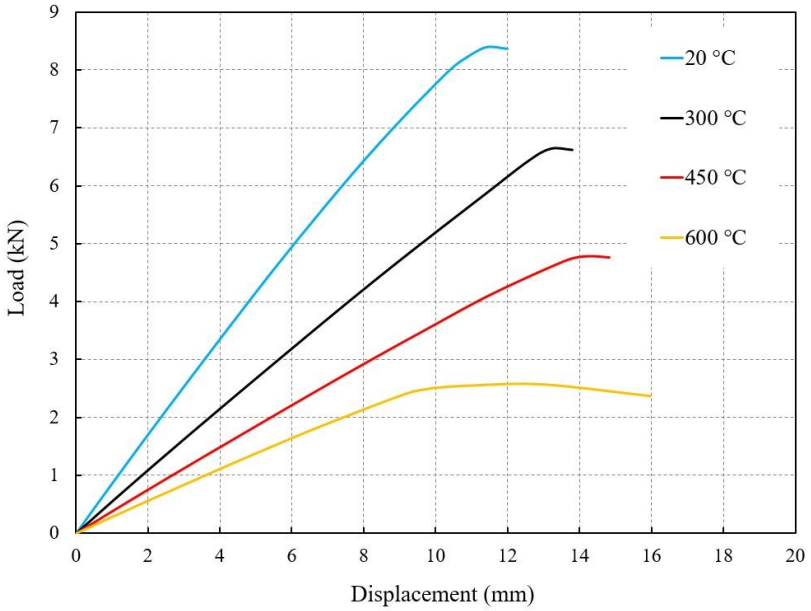

Figure 4.7. Load-displacement curves for MW-1200-100-2500-0.5-0.6-θ specimen at different temperatures

Figure 4.8 indicates the degradation of bending stiffness of numerical and analytical results for MW-1200-100-2500-0.5-0.6-θ specimens at different temperatures. The stiffness calculated by all methods decreases with increasing the temperature. Nevertheless, the rate of reduction varies for them. In the case of the "average solution," although the decrease of bending stiffness for the numerical results is higher than the analytical results, the difference in the curves' slope is just 9%. However, up to 450 °C, the stiffness drop of the analytical results calculated by the "maximum solution" is greater than the numerical results and "average solution." Therefore, it is clear that at elevated temperatures, the results obtained from the "average solution" and numerical results are closer to each other than the "maximum solution."

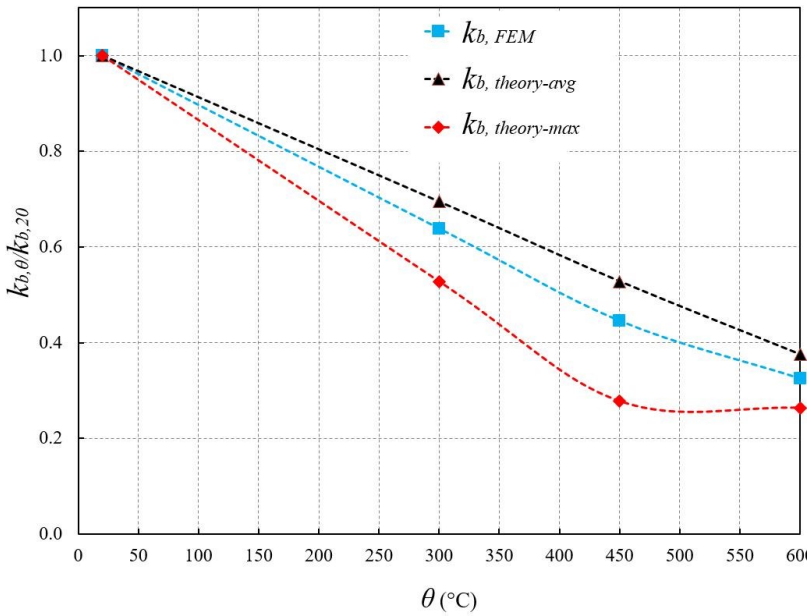

Figure 4.8. Bending stiffness of numerical and analytical results for MW-1200-100-2500-0.5-0.6-θ specimen at different temperatures

4.4.7 Comparison of numerical and analytical results at elevated temperatures for MW panels

In the previous sections, the effect of each parameter at ambient temperature was investigated. In this part, parameter changes in the bending stiffness at different temperatures for simulations and analytical solutions are studied and compared. The bending stiffness of panels with various panel thicknesses at different temperatures is shown by the results achieved from numerical and analytical approaches (see Figure 4.9). In this section, when the analytical solution is mentioned, it refers to the "average solution". As shown in Figure 4.9, the difference between bending stiffness values of the panels with various thicknesses decreases with increasing temperature. In other words, at higher temperatures, the stiffness values tend to converge. The same phenomenon happens for panels with different spans and widths. Indeed, as the temperature elevates, the bending stiffness values approach (see Figure 4.10). However, the degradation of the bending stiffness ratio at elevated temperatures for different thicknesses or different spans of panels is similar, which means they are independent of the geometry (see Figure 4.11).

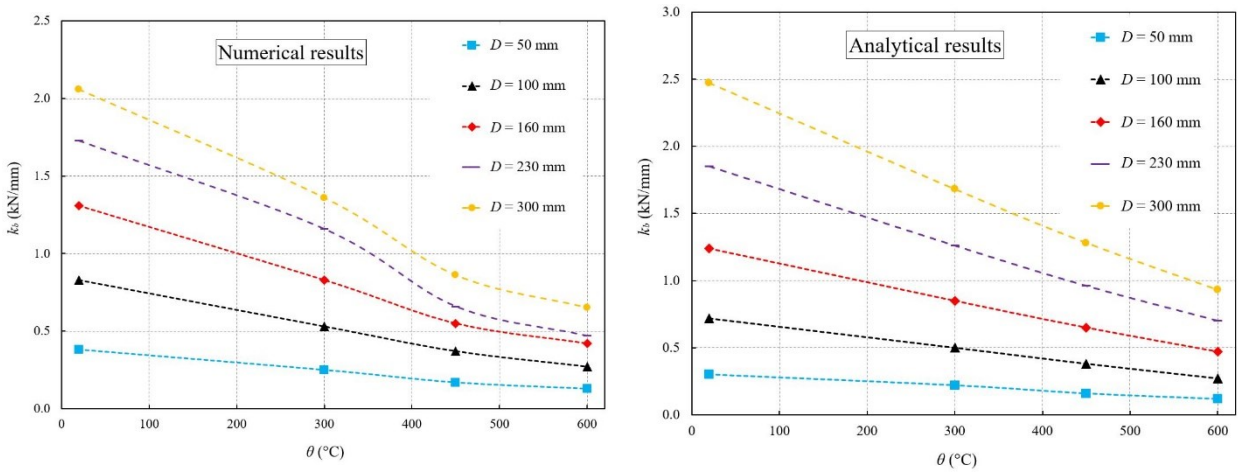

(a) (b)

Figure 4.9. Bending stiffness of MW sandwich panels with various thicknesses at different temperatures, a) numerical results, and b) analytical results

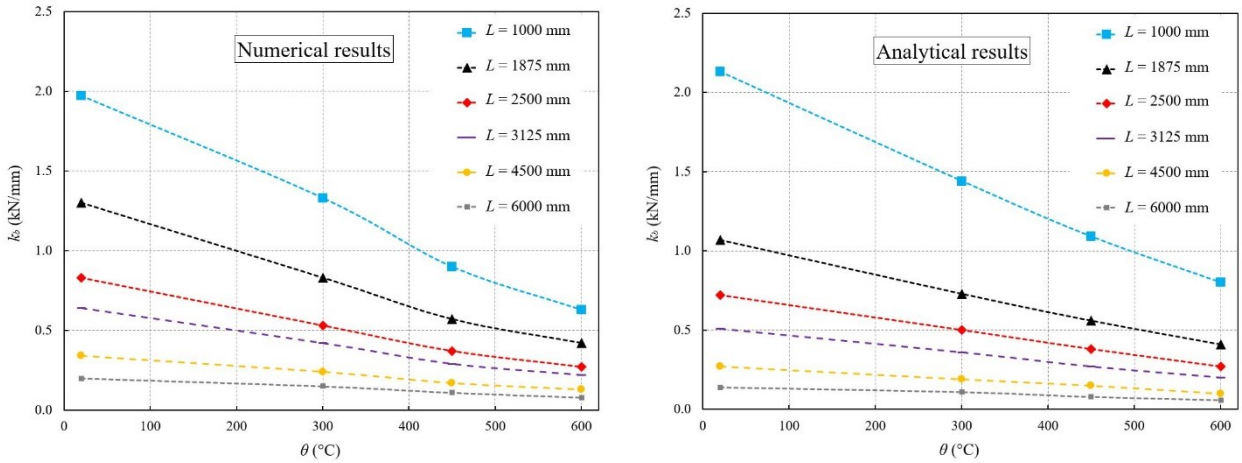

Figure 4.10. Bending stiffness of MW sandwich panels with various spans at different temperatures, a) numerical results, and b) analytical results

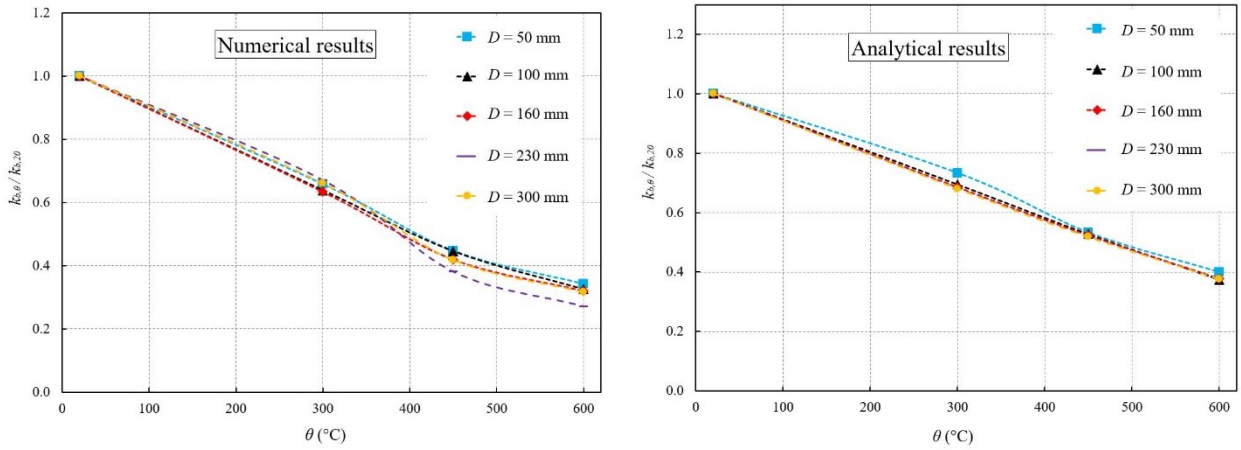

Figure 4.11. Degradation of bending stiffness for MW panels with varying panel thickness: a) numerical results; b) analytical results

To evaluate the proposed solutions at elevated temperatures, Figure 4.12 compares the stiffness calculated by the simulation, the "average solution," and the "maximum solution" for the panels with different widths of 600 mm, 1200 mm and 2500 mm. It is observed that the results calculated by the "average solution" for different widths are very close to the stiffness values achieved from simulations. However, at higher temperatures (450 °C and 600 °C) for the wider panels, the "average solution" values are slightly greater than numerical values. Nevertheless, the "maximum solution" can be considered as an utterly conservative method.

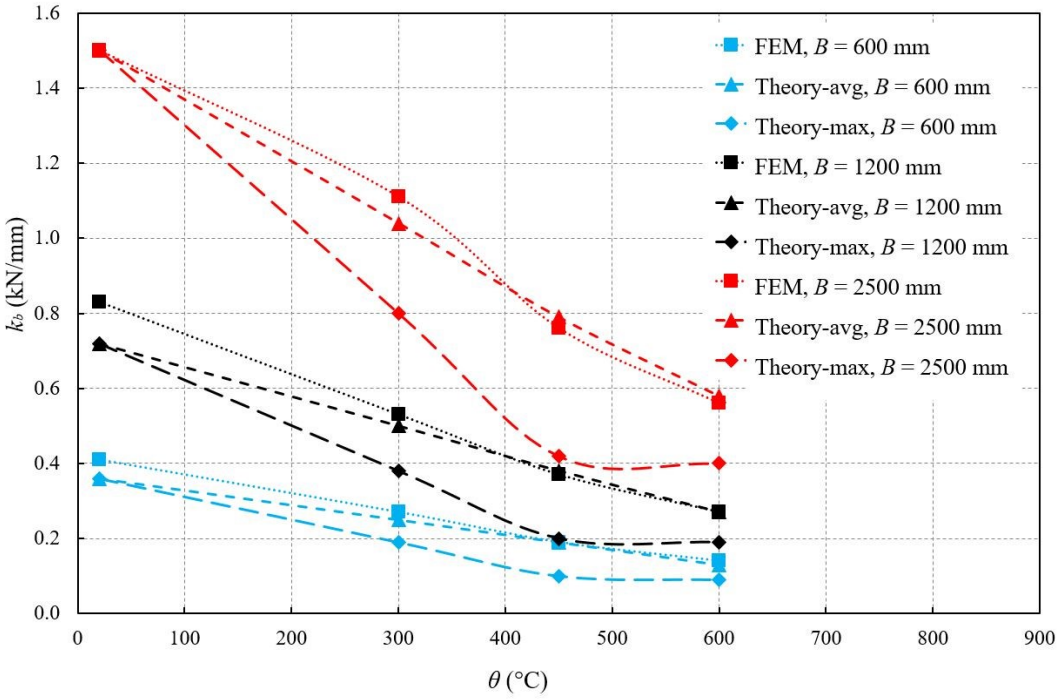

Figure 4.12. Bending stiffness of MW sandwich panels with various widths at different temperatures calculated by three methods

4.5 Parametric study for PIR sandwich panels

4.5.1 General

Such as MW panels, after validating numerical simulations against the experimental results, an extensive number of finite element analyses are performed to determine PIR sandwich panels' bending stiffness under bending loads at ambient and elevated temperatures. Since the PIR panels' experiments were conducted until 300 °C, the parametric study was performed up to the maximum temperature of 300 °C. The objective of this section is to compare the numerical and analytical results at different conditions. The investigated parameters include the width, thickness and span of panels and the thickness of facings. The steel facings' material properties and the core in the parametric study are identical to those of the tests.

In Table 4.4, the numerical and analytical results for PIR panels are presented and compared at different conditions. The applied notations and the label of specimens are determined exactly according to Section 4.4.1. B, D and L are the width, thickness, and span of panels, respectively, and t_{F2} and t_{F1} present the lower and upper facings' thickness. In fact, the label "PIR-1000-100-2500-0.4-0.5-300" defines as follows: a PIR panel with 1000 mm width, 100 mm thickness, 2500 mm span, 0.4 mm inner sheet thickness, 0.5 mm outer sheet thickness, which is exposed to 300 °C temperature. $k_{b,FEM}$ is the bending stiffness of panels obtained from the numerical

results, and $k_{b,theory\text{-}avg}$ and $k_{b,theory\text{-}max}$ show the bending stiffness calculated by the "average solution" and "maximum solution," respectively. In Appendix E, the load-displacement curves obtained from FE models for some of the specimens under bending loading at ambient and elevated temperatures are presented.

Table 4.4. Comparison of the bending stiffness of PIR sandwich panels calculated by numerical and analytical methods

Case	$k_{b,theory\text{-}avg}$ (kN/mm)	$k_{b,FEM}$ (kN/mm)	$k_{b,theory\text{-}avg}$ / $k_{b,FEM}$	$k_{b,theory\text{-}max}$ (kN/mm)	$k_{b,theory\text{-}max}$ / $k_{b,FEM}$
PIR-600-100-2500-0.4-0.5-20	0.59	0.74	0.80	0.59	0.80
PIR-1000-100-2500-0.4-0.5-20	1.07	1.20	0.89	1.07	0.89
PIR-2500-100-2500-0.4-0.5-20	2.94	3.12	0.94	2.94	0.94
PIR-1000-100-2500-0.4-0.5-20	1.06	1.20	0.88	1.06	0.88
PIR-1000-100-2500-0.7-0.5-20	1.13	1.27	0.89	1.13	0.89
PIR-1000-100-2500-1.0-0.5-20	1.16	1.33	0.87	1.16	0.87
PIR-1000-100-2500-0.4-0.5-20	1.07	1.20	0.89	1.07	0.89
PIR-1000-100-2500-0.4-0.7-20	1.14	1.29	0.88	1.14	0.88
PIR-1000-100-2500-0.4-1.0-20	1.22	1.38	0.88	1.22	0.88
PIR-1000-100-1000-0.4-0.5-20	4.16	4.00	1.04	4.16	1.04
PIR-1000-100-2500-0.4-0.5-20	1.07	1.20	0.89	1.07	0.89
PIR-1000-100-4500-0.4-0.5-20	0.32	0.34	0.94	0.32	0.94
PIR-1000-100-6000-0.4-0.5-20	0.16	0.18	0.89	0.16	0.89
PIR-1000-50-2500-0.4-0.5-20	0.51	0.65	0.78	0.51	0.78
PIR-1000-100-2500-0.4-0.5-20	1.07	1.20	0.89	1.07	0.89
PIR-1000-160-2500-0.4-0.5-20	1.78	1.89	0.94	1.78	0.94
PIR-1000-230-2500-0.4-0.5-20	2.64	2.65	1.00	2.64	1.00
PIR-1000-300-2500-0.4-0.5-20	3.51	3.37	1.04	3.51	1.04
PIR-600-100-2500-0.4-0.5-300	0.42	0.53	0.79	0.31	0.58
PIR-1000-100-2500-0.4-0.5-300	0.78	0.88	0.89	0.58	0.66
PIR-2500-100-2500-0.4-0.5-300	2.18	2.25	0.97	1.66	0.74
PIR-1000-100-2500-0.4-0.5-300	0.78	0.88	0.89	0.58	0.66
PIR-1000-100-2500-0.7-0.5-300	0.82	0.91	0.90	0.6	0.66
PIR-1000-100-2500-1.0-0.5-300	0.84	0.93	0.90	0.61	0.66
PIR-1000-100-2500-0.4-0.5-300	0.78	0.88	0.88	0.58	0.66
PIR-1000-100-2500-0.4-0.7-300	0.84	0.94	0.89	0.63	0.67
PIR-1000-100-2500-0.4-1.0-300	0.91	1.01	0.90	0.7	0.69
PIR-1000-100-1000-0.4-0.5-300	3.27	2.81	1.16	2.63	0.94
PIR-1000-100-2500-0.4-0.5-300	0.78	0.88	0.89	0.58	0.66
PIR-1000-100-4500-0.4-0.5-300	0.24	0.32	0.75	0.19	0.59
PIR-1000-100-6000-0.4-0.5-300	0.12	0.16	0.75	0.1	0.63
PIR-1000-50-25000-.4-0.5-300	0.4	0.46	0.87	0.32	0.70
PIR-1000-100-2500-0.4-0.5-300	0.78	0.88	0.89	0.58	0.66
PIR-1000-160-2500-0.4-0.5-300	1.27	1.31	0.97	0.91	0.69
PIR-1000-230-2500-0.4-0.5-300	1.86	1.77	1.05	1.3	0.73
PIR-1000-300-2500-0.4-0.5-300	2.45	2.25	1.09	1.69	0.75

4.5.2 Effect of inner and outer sheet thickness

The outer sheet thickness of PIR sandwich panels varies between 0.50 mm and 1.00 mm. As shown in Table 4.4, the sheet thickness within the range above does not lead to a significant change in specimens' bending stiffness compared to other parameters. For example, at ambient temperature, when the outer sheet thickness changes from 0.50 mm to 1.00 mm, the stiffness of FE models increases only around 15%. This growth for analytical results is about 14%. Similar to MW panels, it should be said that the sheet thickness of panels is not considered as a determining parameter to influence the bending stiffness. Comparing the numerical and analytical results shows that the analytical solution's stiffness is favorably less than the numerical ones (see Figure 4.13).

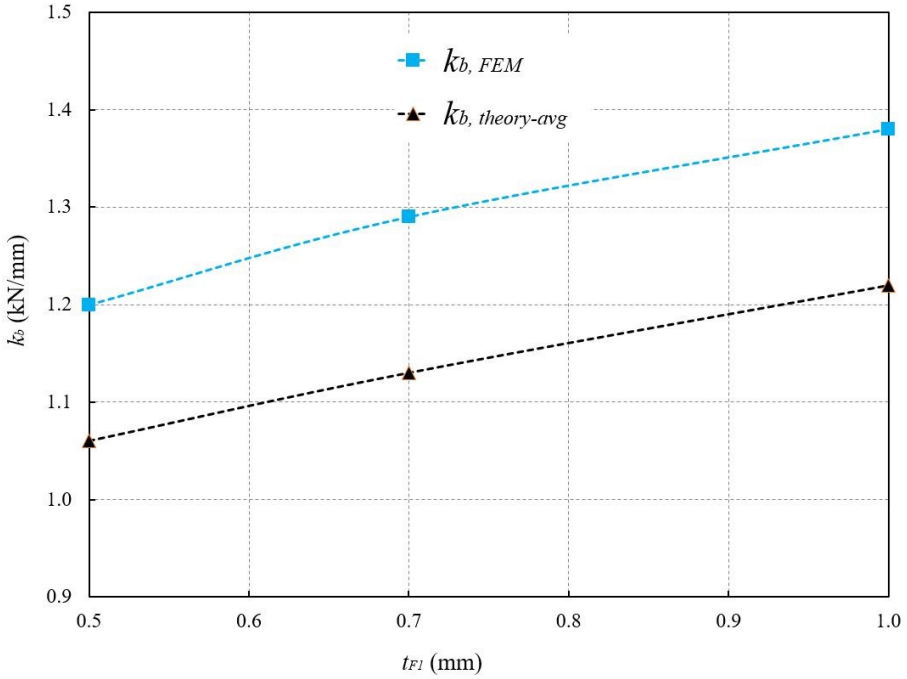

Figure 4.13. Bending stiffness of numerical and analytical results with different outer sheet thicknesses at ambient temperature (PIR-1000-100-2500-0.4-t_{Fl}-20)

4.5.3 Effect of panel thickness

Figure 4.14 shows that thicker panels have a higher bending stiffness than thinner ones. Indeed, there is a linear relationship between panel thickness and bending stiffness for both numerical and analytical results at ambient temperature (see Figure 4.15). Nevertheless, the slope of the analytical curve is slightly greater than the numerical one. Figure 4.15 indicates that the intersection between numerical and analytical results is at 230 mm thickness. For thickness values less than 230 mm, the analytical solutions are on the safe side. However, there is no significant difference between numerical and analytical results within the whole curve. By

increasing the panel thickness from 50 mm to 300 mm at ambient temperature, the bending stiffness increases 5.2 and 6.9 times for numerical and analytical results, respectively, at ambient temperature.

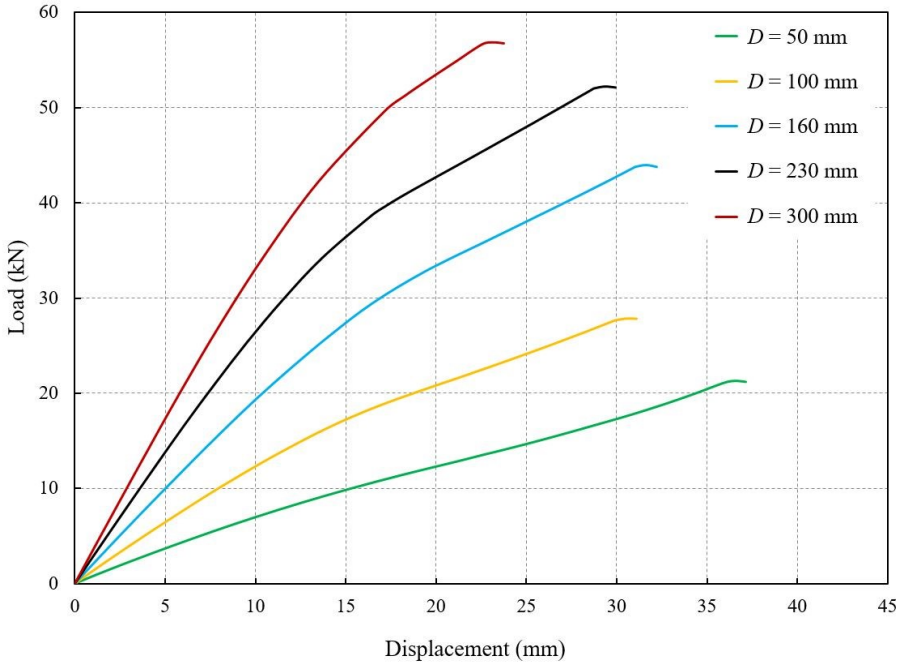

Figure 4.14. Load-displacement curves for PIR-1000-*D*-2500-0.4-0.5-20 specimen with different panel thicknesses at ambient temperature

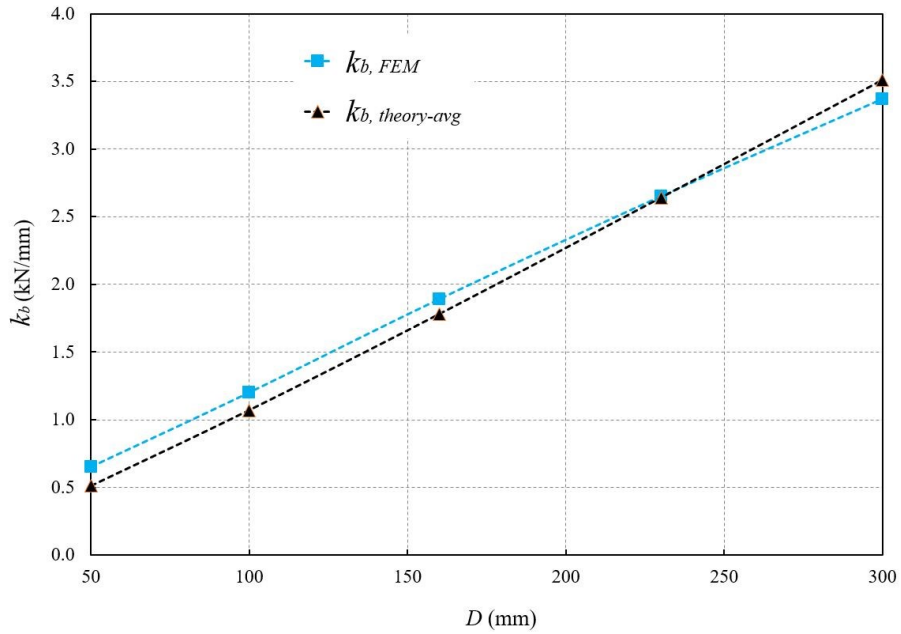

Figure 4.15. Bending stiffness of numerical and analytical results with different panel widths at ambient temperature (PIR-1000-*D*-2500-0.4-0.5-20)

4.5.4 Effect of panel widths

Figure 4.16 displays the load-displacement curve for PIR panels with different widths at ambient temperature. The linear relationship between numerical and analytical results is evident (see Figure 4.17). When the panel width increases around 67%, the stiffness grows about 62% for the FE model. It should be said that there is almost a specific difference between numerical and analytical results for 600 mm, 1000 mm and 2500 mm widths, and favorably the predicted analytical values are less than numerical values.

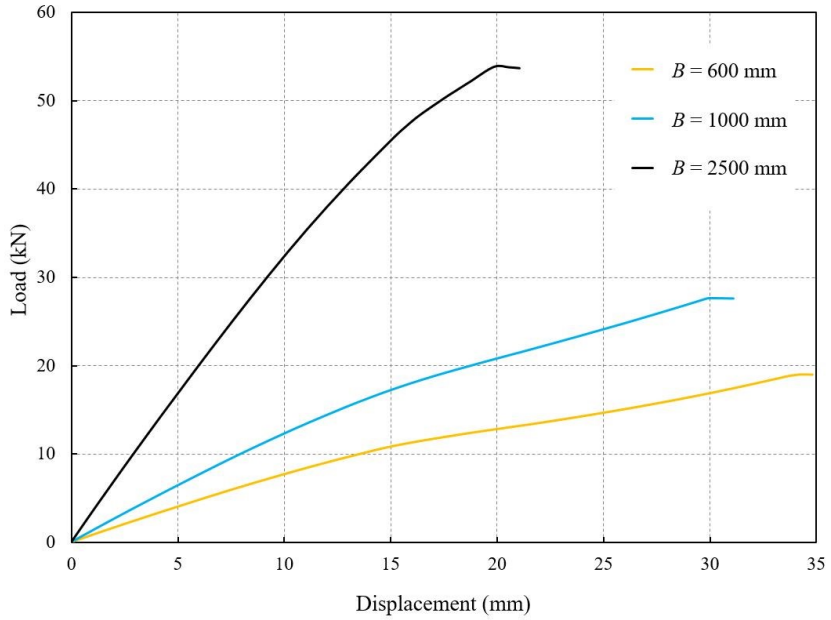

Figure 4.16. Load-displacement curves for PIR-*B*-100-2500-0.4-0.5-20 specimen with different panel widths at ambient temperature

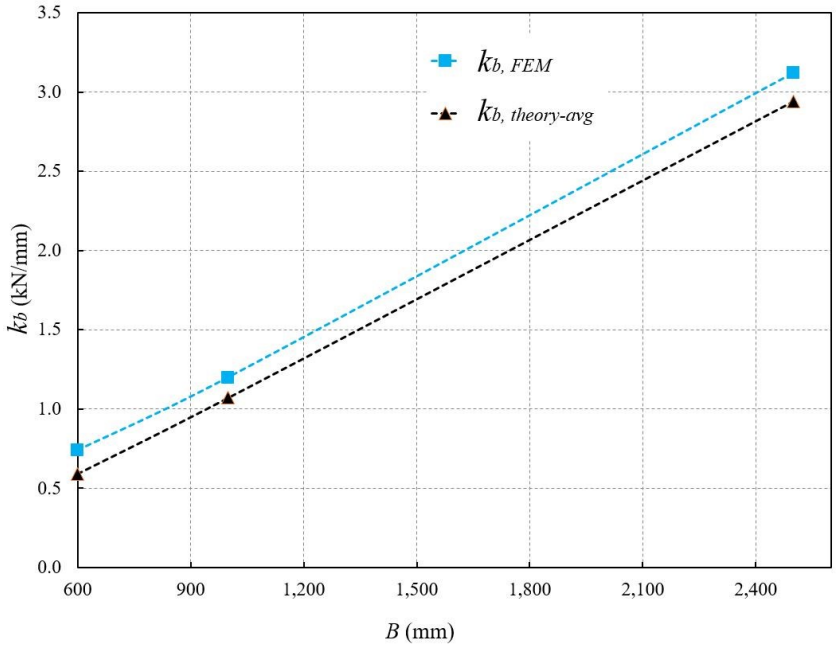

Figure 4.17. Bending stiffness of numerical and analytical results with different panel widths at ambient temperature (PIR-*B*-100-2500-0.4-0.5-20)

4.5.5 Effect of panel spans

The numerical and analytical results show that the span length substantially influences the panels' bending stiffness (see Figure 4.18). As expected, the panels with shorter spans demonstrate higher stiffness. For example, the panel span increases from 2500 mm to 4500 mm, the stiffness decreases around 72% and 70% for numerical and analytical values at ambient temperature, respectively. Actually, the numerical results are very well predicted by the analytical ones. The intersection of the two curves is at around 1700 mm span length. Unlike panel width and thickness, there is no linear relationship between the panel span and bending stiffness. It is observed that the stiffness's change rate for the panels with spans shorter than 2500 mm is higher than the panels with spans longer than 2500 mm (Figure 4.18). At ambient temperature, for 1000 mm span length, the analytical solution predicts the FE results slightly non-conservative. However, the estimation of analytical solution of numerical values is acceptable in all spans.

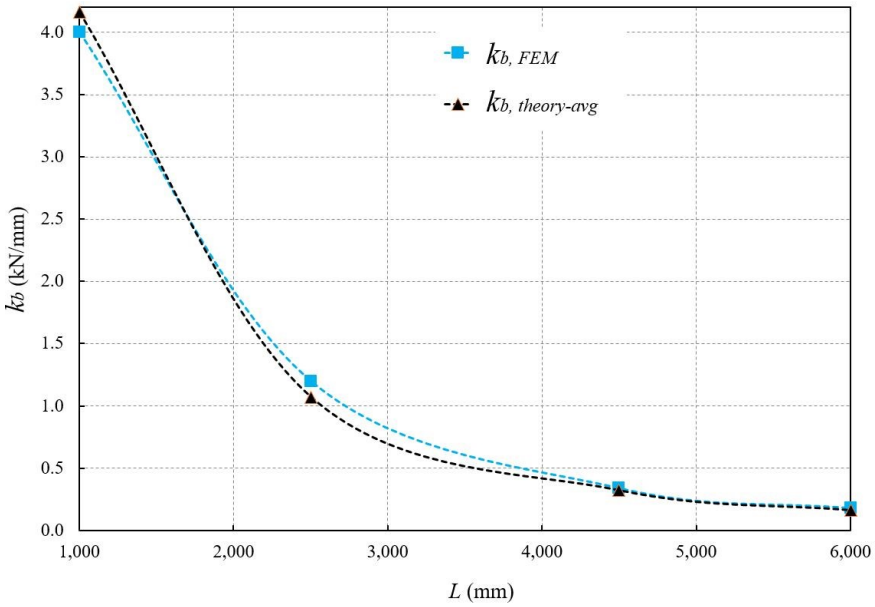

Figure 4.18. Bending stiffness of numerical and analytical results with diverse panel spans at ambient temperature (PIR-1000-100-*L*-0.4-0.5-20)

4.5.6 Effect of temperature

Since the PIR sandwich panels were tested until the maximum temperature of 300 °C (due to experimental conditions) and the availability of experimental results at elevated temperatures in order to validate simulations is essential, the parametric study was investigated at the same

temperature. Because of the degradation of steel and core materials at elevated temperatures, the bending stiffness is reduced for numerical and analytical results.

Figure 4.19 indicates the bending stiffness of numerical and analytical results PIR-1000-100-2500-0.4-0.5-θ specimens at 20 °C and 300 °C. As shown in Figure 4.19, The stiffness calculated by all methods decreases when the temperature elevates. Nonetheless, the reduction rate is different for them. The stiffness decreases around 26.6% for the FE model when temperatures rise from 20 °C to 300 °C. However, for the "average solution" and "maximum solution", this reduction is about 26.4% and 45.3%. Therefore, it can be concluded that the "average solution" gives a better estimation of the numerical model. It is clear that the stiffness value at 20 °C for the "average solution" and "maximum solution" are equal.

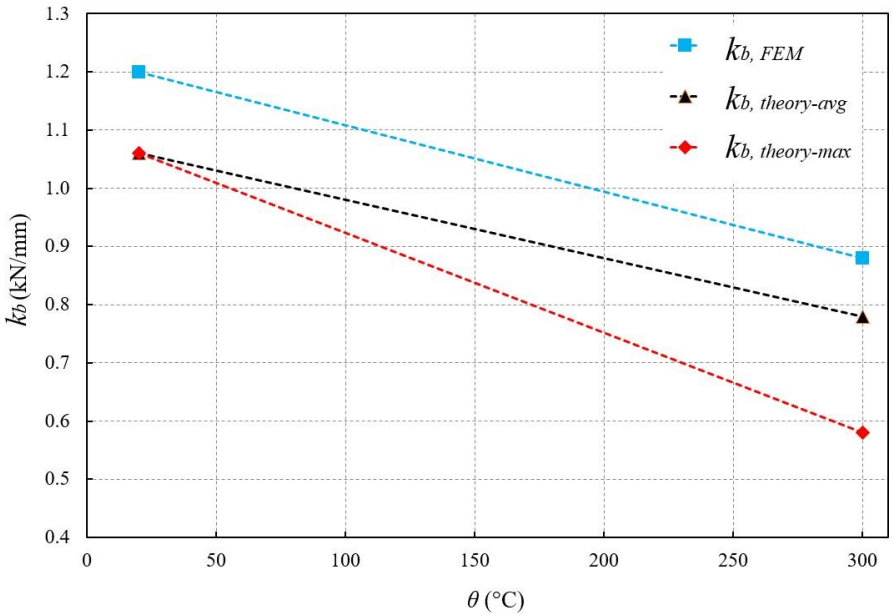

Figure 4.19. Bending stiffness of numerical and analytical results for PIR-1000-100-2500-0.4-0.5-θ specimen at different temperatures

4.5.7 Comparison of numerical and analytical results at elevated temperatures for PIR panels

In this section, the influence of panel thickness and span on the bending stiffness at 20 °C and 300 °C is investigated. Figure 4.20 indicates the bending stiffness of PIR panels for different thickness values for numerical and analytical results. In simulations, for the panel with 300 mm thickness, when the temperature elevates to 300 °C, the bending stiffness reduces by around 33%. However, for the panel with 50 mm thickness, this reduction is about 29%. This trend also applies to analytical results. In fact, by increasing the temperature to 300 °C, the bending stiffness obtained from the analytical solution decreases 30.2% and 21.5% for 300 mm and

50 mm thickness, respectively. In this section, the analytical results refer to the "average solution."

Similarly, the influence of the temperature on PIR panels' bending stiffness with different spans is observed for numerical and analytical results (see Figure 4.21). It can be concluded that the panels with longer spans are less affected by the temperature rise compared to the panels with shorter spans. In numerical results, at elevated temperatures, the stiffness reduces around 30% for the panel with 1000 mm length, while this reduction for the panel with 6000 mm is almost 11%.

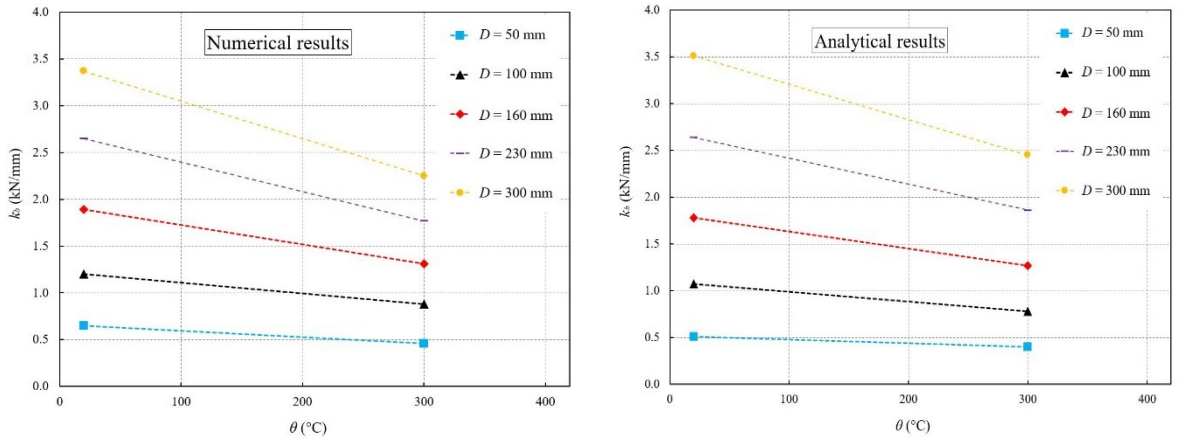

Figure 4.20. Bending stiffness of PIR sandwich panels with various thicknesses at different temperatures, a) numerical results, and b) analytical results

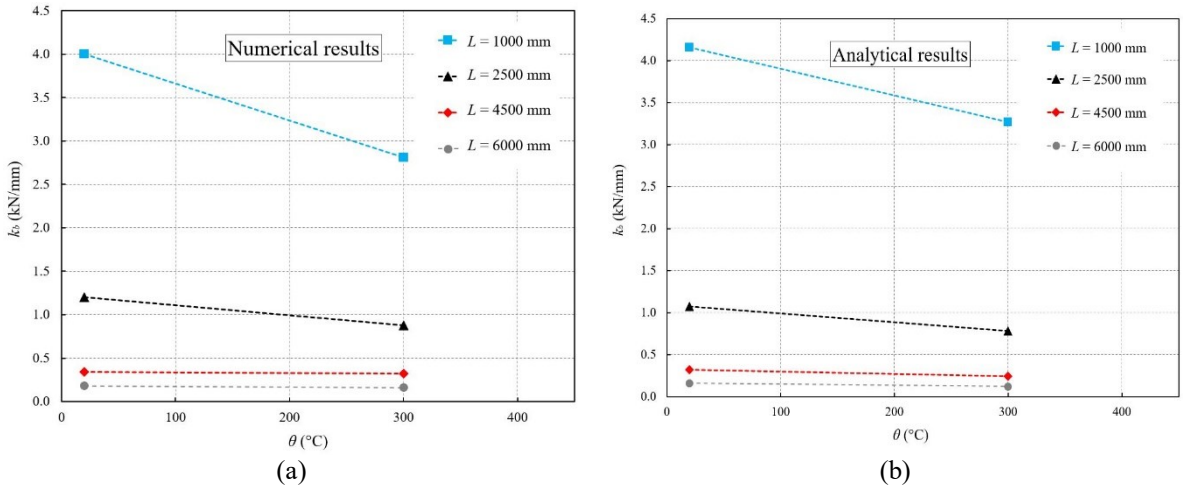

Figure 4.21. Bending stiffness of PIR sandwich panels with various spans at different temperatures, a) numerical results, and b) analytical results

The bending stiffness obtained from FE models, the "average solution," and the "maximum solution" for the panels with 600 mm, 1000 mm and 2500 mm are compared in Figure 4.22. It is clear that the "average solution" better estimates FE results than the "maximum solution" in

approximately all cases. For higher temperatures, the "maximum solution" presents very conservative results. Therefore, it is recommended to employ the "average solution" within the 20 °C to 300 °C.

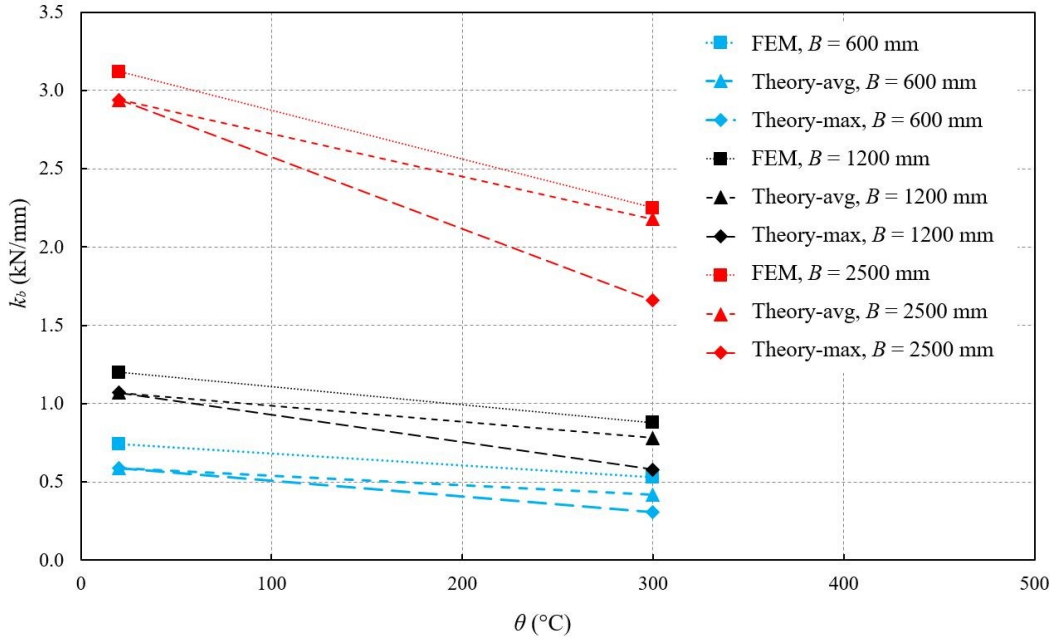

Figure 4.22. Bending stiffness of PIR sandwich panels with various widths at different temperatures calculated by three methods

4.6 Conclusion

In this chapter, sandwich panels' bending stiffness under bending loadings at ambient and elevated temperatures was investigated. A comprehensive parametric study at different temperatures was performed to investigate the effect of various parameters, such as panel span, width and thickness, on the bending stiffness of specimens. Then, the numerical results were compared with the analytical formulations provided by Eurocodes (EN 14509, 2013) at ambient temperature [102]. Moreover, the analytical formulations were developed to apply at elevated temperatures. For that reason, two methods called "average solution" and "maximum solution" were proposed.

The following conclusions can be drawn:

- Although the panels became stiffer as the inner and outer sheets' thickness increased, such a change was not noticeable. That could be because a change in sheet thickness does not lead to a significant difference in the moment of inertia for the panel cross-section. Since the panels' stiffness depends strongly on the moment of inertia of the

panel cross-section, no significant change was observed in this case. The stiffness growth was similar for numerical and analytical results within the range of 0.4 mm to 1.0 mm thickness.

- The thickness of the panels was one of the most influential parameters to determine panel stiffness. At ambient temperature, when the thickness of the MW panel increased from 50 mm to 100 mm, the bending stiffness calculated by simulation increased 2.18 times. For PIR panels, this value increased 1.85 times. Up to 160 mm panel thickness, the stiffness values calculated by numerical and analytical methods for MW panels gave approximately the same results at ambient conditions; however, the analytical results were slightly higher than numerical ones for thicker panels. Therefore, it could be concluded that the analytical solutions have better accuracy for the panels with a thickness of less than 160 mm. For PIR panels, up to 230 mm panel thickness, the numerical results were slightly higher than analytical ones; however, in 300 mm thickness, the analytical solution gave an unsafe prediction.
- Increasing the width of panels led to the higher bending stiffness values of sandwich panels. There was an almost linear relationship between bending stiffness and panel width for analytical and numerical results. However, the growth rate of analytical results was slightly higher than the numerical results for MW panels. It was observed that the growth rate for analytical and numerical results was almost similar for PIR panels.
- There was an inverse relationship between the panel span and the bending stiffness of panels. Indeed, the increase in panel span caused a reduction in the stiffness of panels. Nevertheless, this decrease was not linear. It is observed that for various span lengths, the analytical results were less than numerical ones for both MW and PIR panels. Just in one case, for the PIR panel with a span of 1000 mm, the analytical solution was slightly higher than the numerical result.
- In general, at higher temperatures, the stiffness of panels reduces. On the other hand, the differences between stiffness values of various parameters decrease at elevated temperatures. For instance, the difference in bending stiffness values between the MW panels with different thicknesses at ambient temperature was higher than the difference between those stiffness values at 600 °C. This fact is also applied to the span and width values of MW and PIR panels.
- The ratio degradation of bending stiffness was independent of specimens' geometry, such as panel thickness, width and span. For example, the reduction ratio of the bending stiffness for the panels with different thicknesses was approximately similar.

- Two analytical solutions were proposed for elevated temperatures. The "average solution" offered a good approximation of numerical results. For MW panels, at temperatures higher than 450 °C, the "average solution" showed greater values than numerical results; nonetheless, this difference is not significant. The "maximum solution" presented very conservative results compared to the simulations, especially at temperatures higher than 450 °C. Consequently, applying the "average solution" seems reasonable to estimate sandwich panels' bending stiffness.

Chapter 5: EXPERIMENTAL STUDY AND VALIDATION OF FE MODELING OF TRANSLATIONAL TESTS OF SANDWICH PANEL CONNECTIONS

5.1 Introduction

In this chapter, the translational tests of sandwich panels are presented. Tests arrangement, the geometry of employed specimens, boundary conditions and loadings, and the measured parameters, are explained in this chapter. The numerical models are created in ABAQUS to compare with the experimental results. The applied material properties, the interaction between different specimens, and employed elements are accurately described in this chapter. The objective of this chapter is to validate the simulations against the experimental results.

Consequently, the load-displacement and time-temperature curves obtained from the tests and simulations are the outputs of this chapter. The comparison between experimental and numerical results is conducted for mechanical and thermal analyses. The results provided in this chapter are applied for further numerical investigations.

5.2 Experimental program for translational tests

5.2.1 Test arrangement

The main objective of translational tests was to determine the load-bearing capacity and translational stiffness of sandwich panels under shear loads at normal and elevated temperatures. The tests were carried out at the Czech Technical University in Prague. The inner and outer sheet thickness for MW panels is 0.5 mm and 0.6 mm, and for PIR panels, 0.4 mm and 0.5 mm, respectively. The screw diameter for all specimens is 5.5 mm. Figure 5.1 shows the cross-section of the MW and PIR sandwich panels. The given temperature and dimensions of the specimens are presented in Table 5.1. The specimens were tested at temperatures of the inner sheet (20 °C, 200 °C, 250 °C, 300 °C, 450 °C and 600 °C).

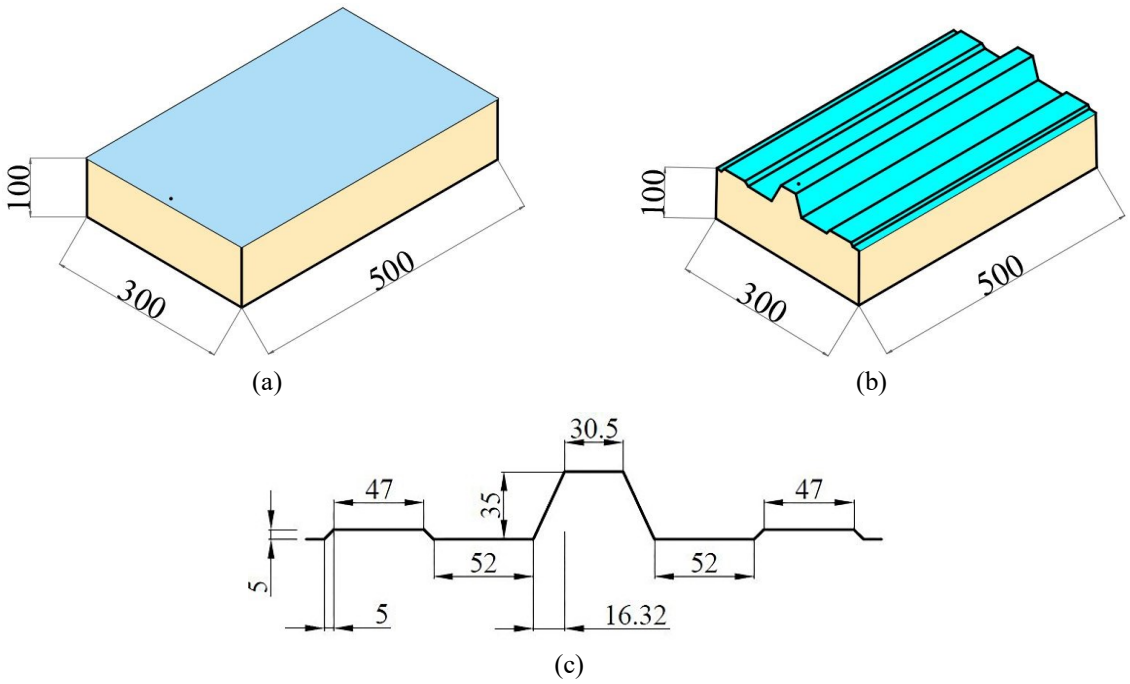

Figure 5.1. The cross-section of sandwich panels in translational tests, a) MW panels, b) PIR panels, c) trapezoidal sheeting, dimensions in mm

Table 5.1. Dimensions and temperature of specimens for translational tests

Panel	Specimen size (mm×mm)	Panel thickness (mm)	Supporting member thickness (mm)	Temperature (°C)
MW sandwich panels	500×300	100	8	20
			8	300
			8	450
			8	600
PIR sandwich panels	500×300	100	8	20
			8	200
			8	300
			8	450

5.2.2 Loading and boundary conditions

As shown in Figure 5.2, the lower end of the samples was fixed while the upper end was free to move in the loading direction (upward movement). The load applied by a displacement-controlled method was increased monotonically until failure. The lower end of the supporting member was fixed to the machine frame using a pin and rod of 50 mm diameter. A loading rate of 1 mm/min was applied. The connection's displacement was measured using an optical extensometer with optic sensors placed at the connection's central axis.

A ceramic heating pads system was employed to heat half of the sandwich panel's inner steel sheet close to the lower side and the supporting steel member's bottom surface with Manning's heating pads. The heating rate was set to around 17 °C/min. After reaching the required temperature, the temperature was kept constant, and the specimen's loading was started. In order

to keep the temperature constant and uniform on the exposed sides, the same approach as bending tests was applied (Section 3.2.2).

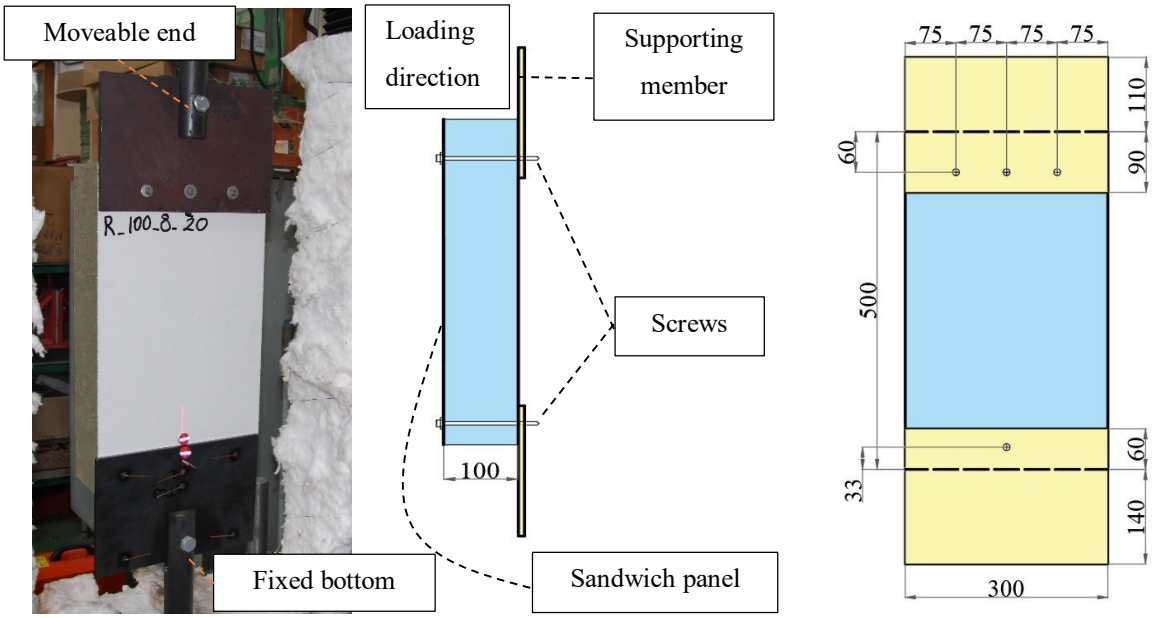

Figure 5.2. Experimental arrangement of panels in translational tests, a) test [8], b) section view, c) front view, dimensions in mm

During the tests, the displacements, the loading forces and the temperatures were measured. Five thermocouples recorded the temperature of the sample specimen during heating. Another two thermocouples were used to control the temperatures of the heating machines (see Figure 5.3). Displacement of the connection was measured with the help of an optical extensometer.

The optical extensometer employed laser light to measure the difference between the two sensors placed on the sample specimen. The two sensors were located close to the connection on the central axis of the specimen. One sensor was placed on the non-movable steel plate of the supporting member, and the second sensor was located in contact with the face of the steel sheet of the sandwich panel, moving in the direction of the loading. At elevated temperatures, the optical extensometer was set to zero before the start of loading.

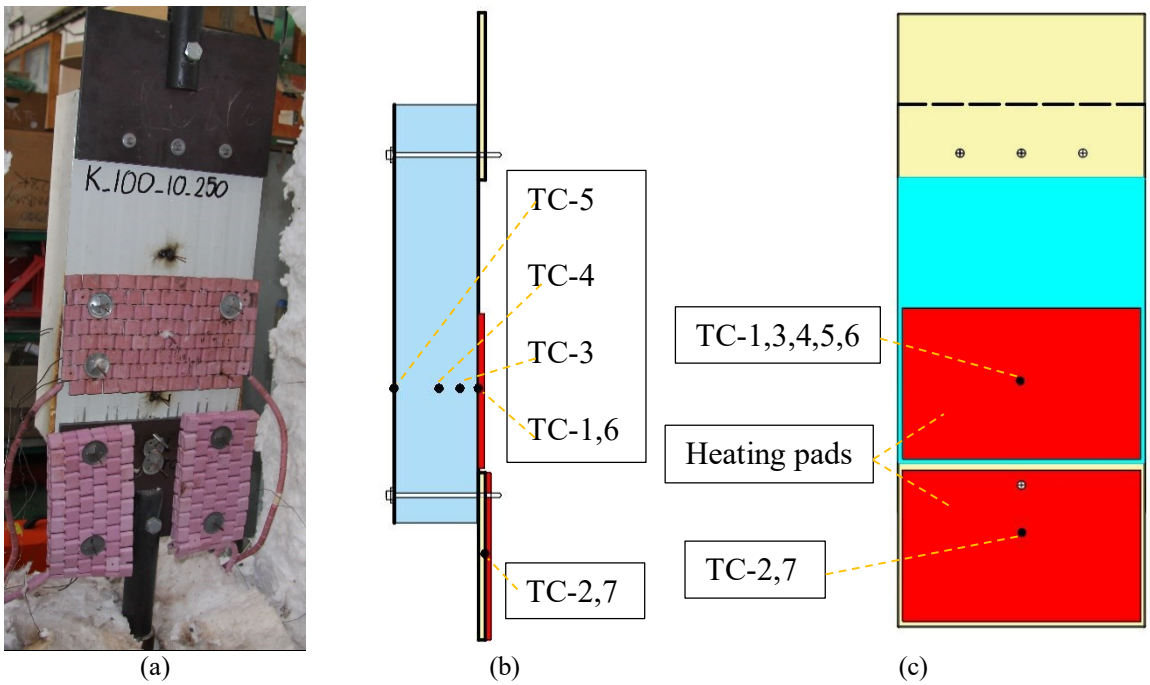

Figure 5.3. a) distribution of ceramic heating pad on the panel's face and supporting member's face, a) test [8], b) section view, c) front view

5.2.3 Experimental results and main observations

The temperatures, the loading forces and the displacements were measured during the tests. The primary failure for all the experiments was a bearing failure of the sandwich panel's inner face near the hole of the screw connection (see Figure 5.4). At both ambient and elevated temperatures, the sheets ruptured in a narrow path with a small fold of the steel sheet. However, at elevated temperatures, the steel sheet tore off on a broader area.

Figure 5.4. Failure of the inner sheet of MW sandwich panels at ambient temperature [8]

Figure 5.5 shows the load-displacement curves for MW and PIR panels obtained from the translational tests. The load-displacement curves are interpreted and smoothed according to the experimental results and main conclusions of the EASIE project [17]. Both the strength and

stiffness of the connections are reduced when the temperature elevates. At elevated temperatures, the shear stiffness decreases due to the material's degradation. Because of laboratory limitations, the PIR sandwich panels were heated up to 450 °C. In Section 5.4, the experimental results are compared and validated with numerical results.

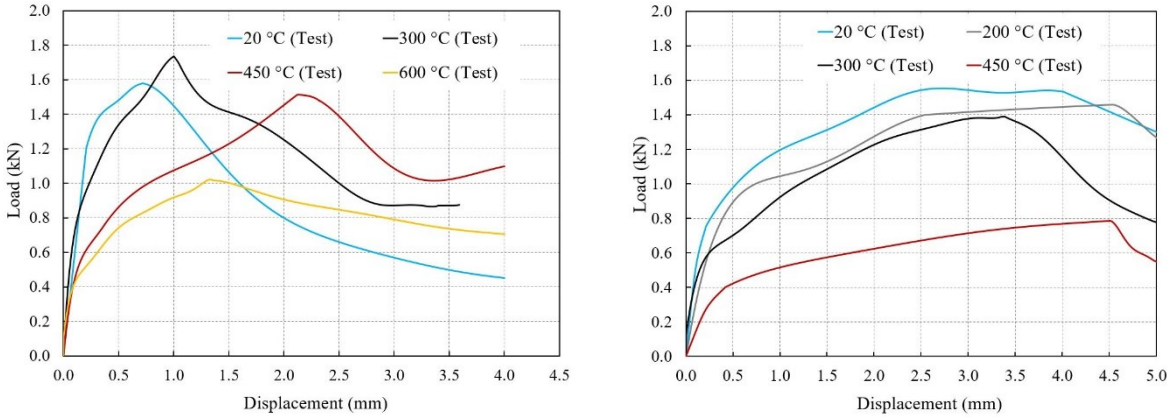

Figure 5.5. Load-displacement curves with a) MW and b) PIR panels of 100 mm thickness and 8 mm supporting member at different temperatures

5.3 Validation of numerical modeling with translational tests

5.3.1 Model description

The primary aim of this section is to validate FE models with the experimental results. In fact, the validation of simulation provides the validity of a comprehensive parametric in the next chapter. Such as bending simulations, a combination of heat transfer and mechanical analysis is conducted to simulate experimental specimens' behavior. The model incorporates geometrical and material nonlinearity. The main components developed in FE models for translational simulations are core, internal and external facings, screws and supporting members. The geometry of created models is accurately in accordance with experimental specimens (Section 5.2). For both MW and PIR specimens, the panel's dimensions are 500 mm×300 mm×100 mm.

5.3.2 Material properties

True stresses and true plastic strains are employed in ABAQUS, while the tests provide engineering stress and strain. For this reason, Eq. (3.1) and (3.2) are applied to convert the engineering stress and strain into true stresses and strains.

The steel sheets and MW and PIR cores' material properties are similar to the bending tests (see Section 2.4). The supporting member's materials are steel grade S355 (Figure 2.10). To determine the mechanical properties of S355 steels and stainless steel bolts at high temperatures, Young's modulus, yield stress and ultimate stress of supporting members are reduced by the reduction factors given in EN 1993-1-2 (Section 2.5.2).

Regarding thermal properties, the most critical parameters consist of thermal conductivity, specific heat and density. The thermal properties of the screws and supporting members are taken from EN 1993-1-2 [45] and [46] (see Section 2.5.1).

5.3.3 Contact interaction

In simulations, the interaction between the core and steel sheets is similar to bending simulations (Section 3.3.4). The interfaces between the screws as well as the core and supporting members are modeled by surface-to-surface contact. The tougher surface with finer mesh is defined as a master surface in each contact, while the other is a slave surface. For example, in the interaction between the screws and the core, the screws are considered master surfaces, and the core surfaces are the slave. The surface-to-surface contact is defined by properties of normal behavior and tangential behavior. The type of normal behavior is chosen as "Hard contact," which avoids any components' penetration. The friction coefficient of 0.4 is used between the supporting and internal sheet at ambient and elevated temperatures in tangential behavior [104].

5.3.4 Loading and boundary conditions

The boundary conditions of the FE model are identical to those in the tests. According to the tests, the temperature is assigned to the investigated supporting member's bottom surface and half of the lower facing (Figure 5.6). The initial temperatures of all components are assigned to 20 °C. In the mechanical analysis, the backside of the investigated supporting member is in all translational directions constrained ($Ux=Uy=Uz=0$), where U is displacement, whereas the front side of another supporting member is just fixed in the vertical and lateral directions ($Uy=Uz=0$) and free in the loading direction (Figure 5.6).

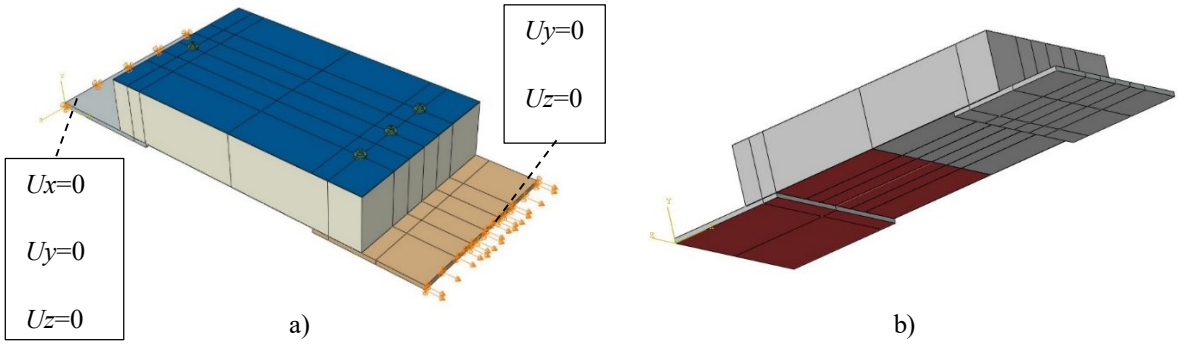

Figure 5.6. Loading and boundary conditions of FE models, a) restrained surfaces, b) heated surfaces.

5.3.5 Element types and mesh size

In the mechanical analysis, to simulate the core material, screws and supporting members, the C3D8R element with hourglass control and reduced integration point is adopted. The S4R shell element is applied for facings. The features of these elements are described in Section 3.3.6. In the heat transfer analysis, the core material, screws and supporting members are simulated with the DCC3D8 element, while facings employ the DS4 element (Section 3.3.6).

Mesh verification and sensitivity analyses are performed to reach the optimal mesh size. The size and number of the elements are accurately similar in both heat transfer and mechanical analysis. The applied mesh size is 10 mm×10 mm, which was refined to 2 mm×2 mm in the areas with high stress and temperature gradients and 1 mm×1 mm in the screws and vicinity of holes. Figure 5.7 shows three different mesh sizes of specimens. The MW and the PIR panels and also the connection area are meshed according to Figure 5.8. The mesh sensitivity study for translational models is presented in Figure 5.9.

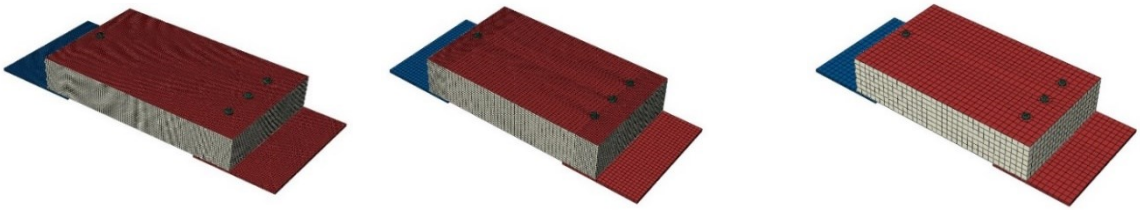

Figure 5.7. Meshing of the entire connection, a) 171502 elements, b) 49246 elements (recommended), c) 11970 elements

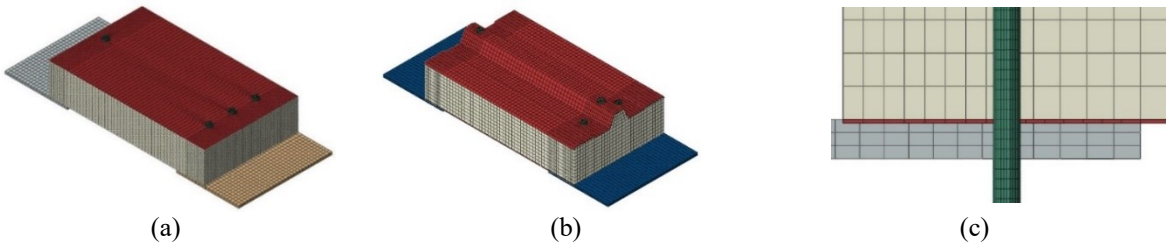

Figure 5.8. Meshing, a) the whole MW specimen, b) the whole PIR specimen, c) connection area

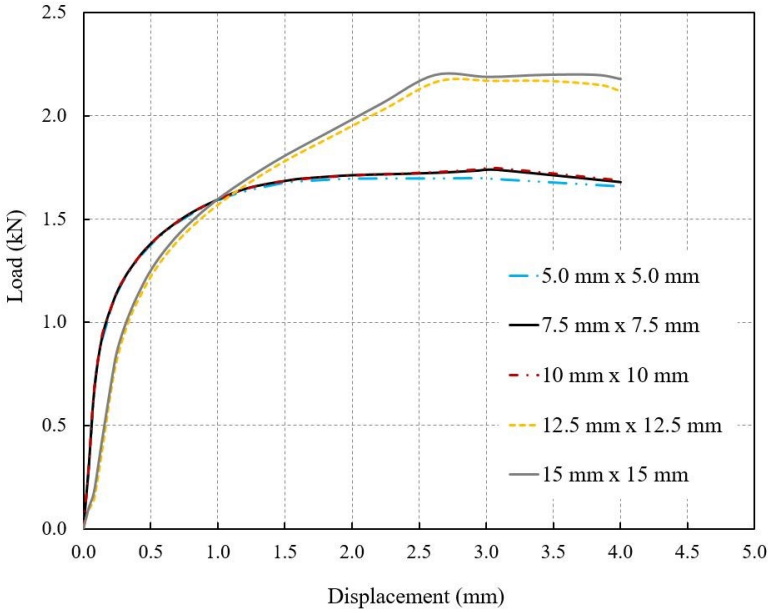

Figure 5.9. The load-displacement curves with different mesh sizes

5.4 Comparison between simulation and test results

In this section, the numerical models are validated with translational tests. The load-displacement and time-temperature curves obtained from experimental and numerical results are compared. The numerical results determine the initial stiffness and load-bearing capacity of connections.

5.4.1 Temperature distribution for MW and PIR sandwich panels

Figure 5.10 compares the experimental and numerical results obtained from heat transfer analysis for MW and PIR sandwich panels. The internal face and the supporting member curves show the assigned temperature at the exposed side. Therefore, there is no difference between experiments and simulations. The core and the external face temperatures are obtained from the middle of the panel's core and the unexposed side in the indicated section in Figure 5.11.

Figure 5.12 illustrates the temperature changes through the plate's thickness between the exposed (600 °C) and unexposed (ambient temperature) sides of the plate for MW and PIR panels. Although there is no tremendous difference between the temperature of the two panels' unexposed sides due to the vicinity of ambient temperatures, the PIR panel shows a higher fire resistance than the MW panel.

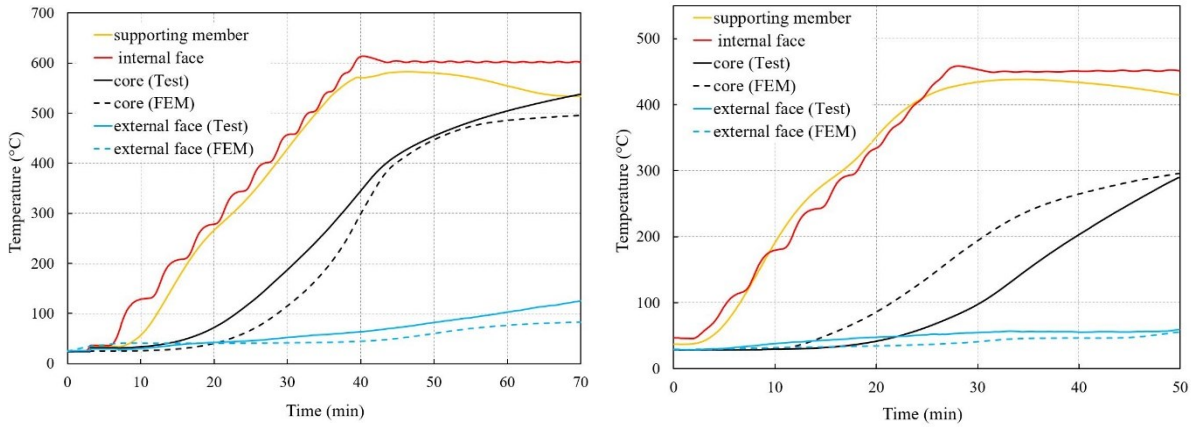

Figure 5.10. The time-temperature curve of experiment and simulation for a) MW panel 100 mm thickness at 600 °C, b) PIR panel 100 mm thickness at 450 °C

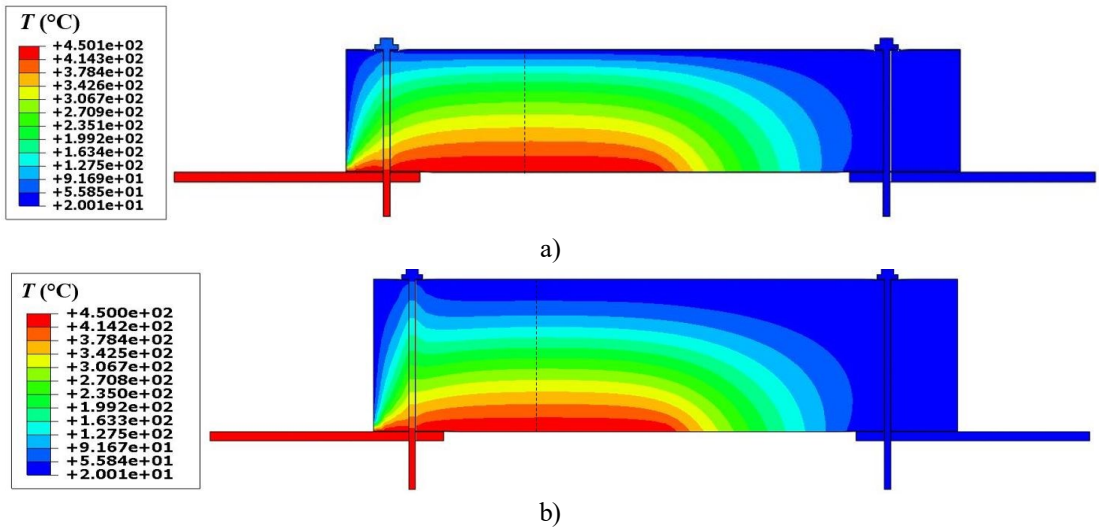

Figure 5.11. FE models of temperature distribution for a) MW cores 100 mm at 450 °C and b) PIR cores 100 mm at temperature 450 °C

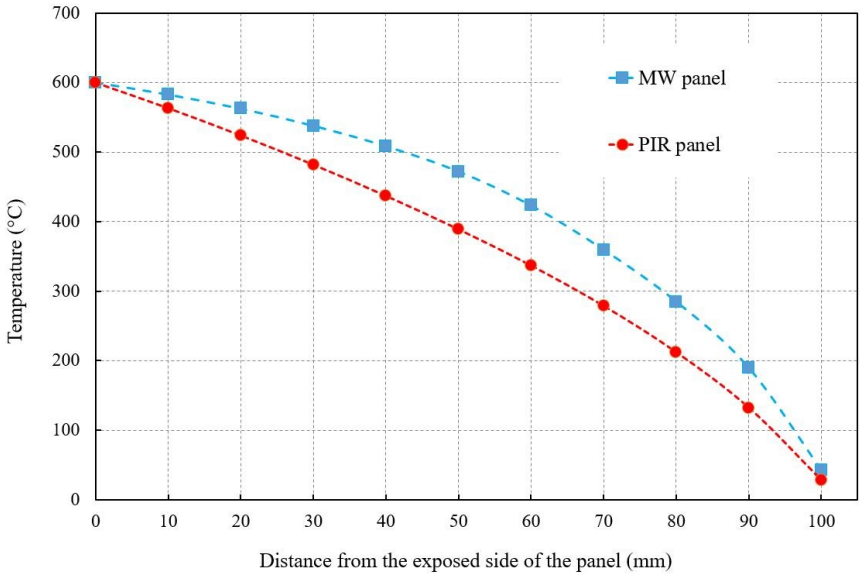

Figure 5.12. Temperature gradient for MW and PIR panels through the thickness

5.4.2 Validation of load-displacement curves for MW and PIR sandwich panels

As mentioned earlier, the main failure mode for all specimens is a bearing failure of the sandwich panel's inner face near the hole of the screw connection. Figure 5.13 displays the failure mode of the test and a corresponding FE model at ambient temperature (comparable with Figure 5.4). As can be seen, the area near the investigated inner face hole experiences higher stresses.

Figure 5.14 and Figure 5.15 show the load-displacement curves from the translational experiments and simulations for MW and PIR specimens. The force is recorded from supports. The displacement is obtained from the difference in the supporting member's movement and the inner sheet's movement of the investigated connection in the load direction.

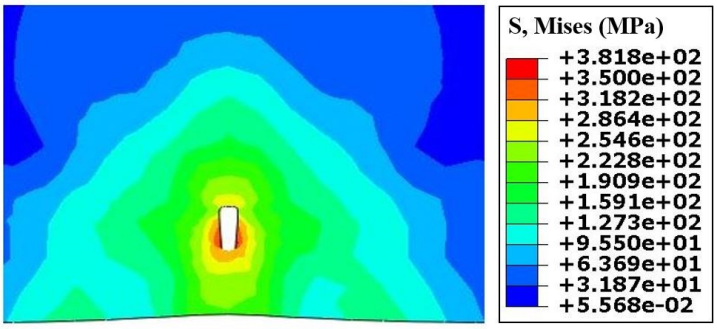

Figure 5.13. The failure mode for the FE model

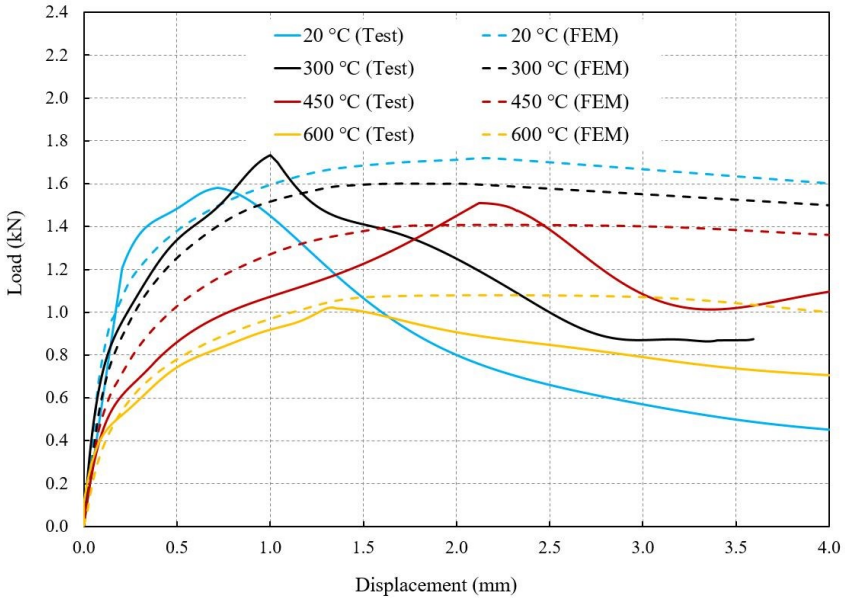

Figure 5.14. Validation of numerical results against tests for MW panels 100 mm thickness and 8 mm supporting member

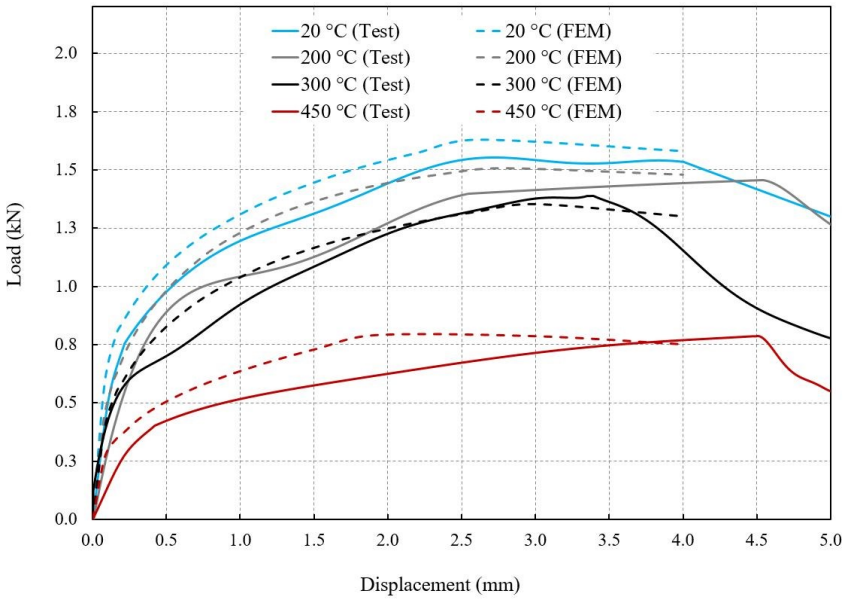

Figure 5.15. Validation of numerical results against tests for PIR panels 100 mm thickness and 8 mm supporting member

It is clear that the ultimate load and bending stiffness of the panel decrease as the temperature increases. This decrease is due to the degradation of materials at elevated temperatures.

In models, the shear resistance is obtained as the maximum load of displacement-force curves. Since the load level, $0.5V_{FEM}$ is within the linear part of the load-displacement curve, 50% of the maximum force is divided into the corresponding displacement to calculate the initial stiffness of connections [105].

The numerical results show that for MW panels, the shear resistance for 300 °C, 450 °C and 600 °C is 93.5%, 81.8% and 62.5% of the load capacity at ambient temperature. This trend for stiffness is 61.7%, 45.7% and 33.6% respectively. PIR panels' shear resistance decreases 7.3%, 17.1% and 51.5% for numerical results at 200 °C, 300 °C and 450 °C. This reduction for stiffness is 30.4%, 47.8% and 67.9% respectively.

Table 5.2 presents the shear resistance and stiffness of sandwich panels at different temperatures, where V and k_v are the shear resistance and translational stiffness of sandwich panels for experimental and numerical results. The connections are named in the way [panel]-D-d_s-t_{F2}-θ.

As can be seen, there is a good agreement, on averagely maximum of 2% difference, between the numerical and experimental results of PIR and MW sandwich panels for shear resistance. However, the FE model overestimates the shear stiffness of both the MW and PIR connections. The material properties of the FE model did not include damage properties that would allow the tearing of the internal face and lead to higher stiffness at later stages of loading. The very

complex behavior of the analyzed connection, including several sources of imperfection and the unavoidable uncertainties of the material properties and thermal loading, cause the difference in shear stiffness between numerical and experimental results.

Table 5.2. Shear resistance and stiffness of sandwich panels at different temperatures

Specimen	θ (°C)	$k_{v,exp}$ (kN/mm)	$k_{v,FEM}$ (kN/mm)	$k_{v,FEM}/\ k_{v,exp}$	V_{exp} (kN)	V_{FEM} (kN)	$V_{FEM}/\ V_{exp}$
MW-100-5.5-0.5-20	20	3.65	7.58	2.07	1.58	1.71	1.08
MW-100-5.5-0.5-300	300	5.51	4.68	0.85	1.74	1.60	0.92
MW-100-5.5-0.5-450	450	2.05	3.47	1.69	1.51	1.40	0.93
MW-100-5.5-0.5-600	600	1.62	2.55	1.57	1.02	1.07	1.05
				Avg: 1.55			Avg: 1.00
				SD: 0.51			SD: 0.08
PIR-100-5.5-0.4-20	20	3.25	4.37	1.34	1.55	1.63	1.05
PIR-100-5.5-0.4-200	200	2.22	3.04	1.37	1.46	1.51	1.03
PIR-100-5.5-0.4-300	300	1.44	2.28	1.58	1.39	1.35	0.97
PIR-100-5.5-0.4-450	450	0.58	1.40	2.41	0.79	0.79	1.00
				Avg: 1.68			Avg: 1.02
				SD: 0.50			SD: 0.04

5.5 Conclusion

This chapter investigated MW and PIR sand panels' translational stiffness under shear loadings at ambient and elevated temperatures. A FE model was developed to validate simulations with experimental results. A two-stage analysis process was required for the thermo-mechanical simulation. Boundary conditions, including loadings and supports, were defined in the numerical model in accordance with the experimental setup. The optimal mesh was specified with the help of a mesh sensitivity study.

The following conclusions can be drawn:

- The numerical models were able to predict the temperature distribution of different components of experimental specimens rather accurately.
- There was an excellent agreement, an average maximum of 2% difference, between the shear resistance of numerical and experimental results at ambient and elevated temperatures.
- The tests and FE models showed the same failure mode, which is a bearing failure of the sandwich panel's inner face near the hole of the screw connection.

- By increasing the temperature, the shear resistance and translational stiffness of MW and PIR panels due to the degradation of materials decreased.
- At elevated temperatures, the decrease in MW and PIR panels' translational stiffness was higher than shear resistance for both numerical and experimental results.

Chapter 6: ANALYTICAL AND PARAMETRIC STUDY FOR TRANSLATIONAL TESTS OF SANDWICH PANEL CONNECTIONS

6.1 Introduction

This chapter presents sandwich panels' translational resistance and stiffness obtained from the ECCS manual [9]. The shear resistance and the translational stiffness of sandwich panels are calculated at ambient temperatures. Subsequently, the equations presented in the ECCS are developed to predict the shear resistance and the translational stiffness of sandwich panels at elevated temperatures. Moreover, a parametric study in ABAQUS at ambient and elevated temperatures is conducted. The decisive parameters to influence the shear stiffness and resistance, such as the screw diameter, the inner sheet thickness and the temperature, are investigated. This chapter compares the analytical solutions with the numerical results achieved from the parametric study to validate the developed formulas for further analytical investigations at elevated temperatures.

6.2 Analytical study for translational behavior of sandwich panel connections

In this section, the analytical solutions to calculate the shear resistance and translational stiffness of sandwich panel connections at ambient temperatures are presented according to the ECCS manual [9] to design sandwich panels (ECCS, 2014). After that, the formulas obtained from the ECCS are developed to apply at elevated temperatures.

6.2.1 Analytical solution for shear resistance at ambient and elevated temperatures

The shear resistance of sandwich panel connections is calculated by Eq. (6.1). According to the ECCS manual, the shear resistance's characteristic value is provided by the internal face sheet.

$$V_{ECCS} = 4.2\sqrt{t_{cor,F2}^3 . d_1} . f_{u,F2} \quad (6.1)$$

V_{ECCS}, $t_{cor,F2}$, d_1 and $f_{u,F2}$ are the shear resistance, the core thickness of the inner face (the inner sheet thickness of steel facing), the fastener diameter and the inner face's tensile strength [9].

At elevated temperatures, the tensile strength of the inner face is decreased according to two approaches. The first approach (Approach 1) is to apply the reduction factors presented in Section 2.5.2, which are similar to those employed in numerical simulations. The second approach (Approach 2) uses the tensile strength at elevated temperature (Eq. (6.2)) provided in Annex A of EN 1993-1-2, which presents the ultimate resistance of carbon steel as a function of its yield strength $f_{y,F2,\theta}$.

$$f_{u,F2,\theta} = \begin{cases} 1.25 f_{y,F2,\theta}, & for\ \theta < 300\,°C \\ (2 - 0.0025\theta) f_{y,F2,\theta}, & for\ 300\,°C \le \theta < 400\,°C \\ f_{y,F2,\theta}, & for\ \theta \ge 400\,°C \end{cases} \quad (6.2)$$

The yield strength of the inner face is calculated as Eq. (6.3).

$$f_{y,F2,\theta} = f_{y,F2} . k_{y,\theta} \quad (6.3)$$

The only parameter changing at elevated temperatures is the inner face's tensile strength for the shear resistance. Therefore, the shear resistance at elevated temperatures can be calculated according to Eq. (6.4).

$$V_{ECCS,\theta} = 4.2\sqrt{t_{cor,F2}^3 . d_1} . f_{u,F2,\theta} \quad (6.4)$$

6.2.2 Analytical solution for shear stiffness at ambient and elevated temperatures

According to the ECCS, The translational stiffness of a connection with a self-drilling or self-tapping screw fastener can be calculated with Eq. (6.5).

$$k_v = \frac{1}{\frac{x_F}{k_{F2}} + \frac{t_{cor,sup}^2 + 2.(1 - x_F).D.t_{cor,sup}}{4C_{sup}} + \frac{3.(1 - x_F).D.t_{cor,sup}^2 + t_{cor,sup}^3}{24EI}} \quad (6.5)$$

where

$$x_F = 1 - \frac{\frac{1}{k_{F2}} - \frac{D.t_{cor,sup}}{2C_{sup}} - \frac{D.t_{cor,sup}^2}{8EI}}{\frac{1}{k_{F2}} + \frac{D^2}{C_{sup}} + \frac{D^2.(2D + 3t_{cor,\mathrm{sup}})}{6EI}} \quad (6.6)$$

$$EI = 200000N/mm^2.\frac{\pi.d_s^4}{64} \tag{6.7}$$

$$C_{sup} = 2400N/mm^2.\sqrt{t_{cor,sup}.d_1^5} \tag{6.8}$$

$$k_{F2} = \begin{cases} 6.93.\dfrac{f_{u,F2}.\sqrt{t_{cor,F2}^3.d_1}}{0.26mm + 0.8t_{F2}} \; for\; 0.40mm \le t_{cor,F2} \le 0.70mm \\ 4.20.\dfrac{f_{u,F2}.\sqrt{t_{cor,F2}^3.d_1}}{0.373mm} \; for\; 0.70mm \le t_{cor,F2} \le 1.00mm \end{cases} \tag{6.9}$$

Eq. (6.1) to (6.9) employ the following notations:

$t_{cor,F2}$	core thickness of the internal face
$t_{cor,sup}$	core thickness of the supporting structure (thickness of supporting member)
d_1	the minor diameter of the threaded part of the fastener
d_S	the diameter of the unthreaded shank
$f_{u,F2}$	tensile strength of the internal face
D	the thickness of the panel at the point of fastening

Eq. (6.1) to (6.9) apply within the application range, determined in Table 6.1. For the parameters not included in the application range, tests should be conducted to determine the stiffness and resistance [9].

Table 6.1. Application range of used parameters in shear stiffness and resistance [9]

5.5 mm ≤ d ≤ 8.0 mm	nominal diameter of the fastener
40 mm ≤ D	panel thickness
0.40 mm ≤ $t_{cor,F2}$ ≤ 1.00 mm	core sheet thickness of the face layers
1.50 mm ≤ $t_{cor,sup}$ ≤ 10.0 mm	core thickness of the supporting structure

At elevated temperatures, the stiffness is calculated by reducing Young's modulus of fasteners and decreasing the internal face's tensile strength. The reduction factors for Young's modulus are presented in Section 2.5.2. The results indicate that the reduction of Young's modulus leads only to a slight decrease in connection stiffness, even at high temperatures. The internal face's tensile strength is decreased according to the two approaches mentioned in Section 6.2.1. As an example, the shear resistance and stiffness of sandwich panels at ambient and elevated temperatures are calculated in Appendix C and Appendix D, respectively.

6.3 Definition of load-bearing capacity and translational stiffness

According to the Preliminary European Recommendations for the testing and design of fastenings for sandwich panels, Eq. (6.10) defines the ultimate load.

$$V = min\{V_{max}, V_{3mm}, V_1\} \tag{6.10}$$

where

V_{max} is the maximum load recorded during the test,

V_{3mm} is the load corresponding to a displacement of 3 mm; if this occurs on the rising part of the curve,

V_1 is the load at which the first decrease in load is observed in the load-displacement curve.

In this research, the ultimate load is mainly determined by the maximum load, usually in a displacement of less than 3 mm. After determining the ultimate load, the connection's stiffness is calculated by dividing 50% of the maximum force into the corresponding displacement. $0.5V_{FEM}$ is within the linear part of the load-displacement curve, giving a reasonable estimation of the initial stiffness of connections (see Figure 6.1) [17].

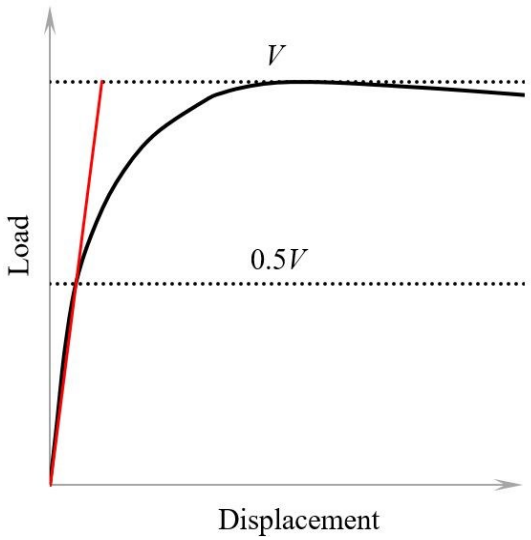

Figure 6.1. Determination of stiffness of the connection

6.4 Parametric study for sandwich panels

6.4.1 General

Regarding the results obtained from the comparison between simulations and the experiments, a vast number of finite element analyses are performed to determine the translational stiffness

and load-bearing capacity of sandwich panels at ambient and elevated temperatures. The investigated parameters include the inner sheet thickness and the screw diameter.

According to the results obtained from the finite element models, changing the thickness of the supporting member did not play any crucial role in the load and shear stiffness of connections. The panel thicknesses were varied between 100, 160 and 230 mm, the most commonly used panels in the industry. However, the results were approximately coincident (see Figure 6.2 and Figure 6.3). Besides, the variation of the outer sheet thickness did not cause any noticeable discrepancy between load-displacement curves. For that reason, the parameters mentioned above are not investigated further. Therefore, all specimens studied in this section have a thickness of 100 mm and a supporting member of 8 mm. The outer sheet thickness for MW and PIR panels are 0.6 mm and 0.5 mm, respectively.

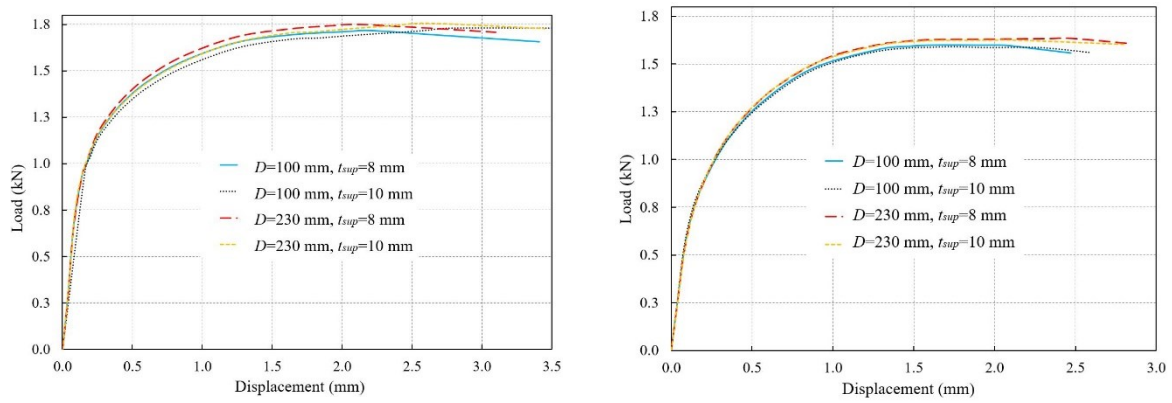

a) b)

Figure 6.2. Load-displacement curves for MW panels at a) 20 °C and b) 300 °C

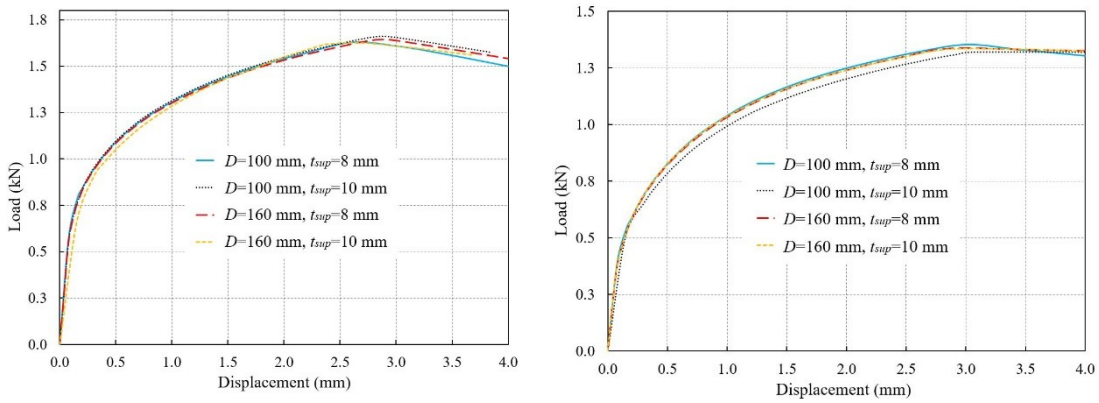

a) b)

Figure 6.3. Load-displacement curves for PIR panels at a) 20 °C and b) 300 °C

Table 6.2 to Table 6.5 present and compare the numerical and analytical results for sandwich panels at different temperatures, where the specimens are labeled in the way [panel]-D-d-t_{F2}-θ. D, d, t_{F2} and θ display the thickness of panels, the screw diameter, the thickness of the inner facing, and the exposed side's temperature. The specimens are categorized according to their

foam material, screw diameter and temperatures. For instance, the label "MW-100-4.2-0.4-20" defines as follows: an MW panel with 100 mm thickness, 4.2 mm screw diameter, 0.4 mm inner sheet thickness, which is exposed to 20 °C temperature. $V_{1,ECCS}$ and $V_{2,ECCS}$ show the load-bearing capacity calculated by the first and second approaches of the analytical solution. V_{FEM} indicates the load-bearing capacity obtained from the FE models. The same labels are employed to illustrate the shear stiffness of specimens. In fact, $k_{V1,ECCS}$, $k_{V2,ECCS}$ and k_{FEM} show the shear stiffness calculated by the first and second approaches of the analytical solution and obtained from the FE models. All load-displacement curves obtained from FE models at ambient and elevated temperatures are presented in Appendix F.

Table 6.2. Load-bearing capacity of MW sandwich panels at different temperatures calculated by numerical and analytical methods

Case	$V_{1,ECCS}$ (kN)	$V_{2,ECCS}$ (kN)	V_{FEM} (kN)	$V_{1,ECCS}/V_{FEM}$	$V_{2,ECCS}/V_{FEM}$
MW-100-4.2-0.4-20	0.88	0.67	1.38	0.64	0.48
MW-100-4.2-0.5-20	1.28	0.96	1.68	0.76	0.57
MW-100-4.2-0.6-20	1.71	1.29	1.93	0.89	0.67
MW-100-4.2-0.7-20	2.19	1.65	2.20	1.00	0.75
MW-100-4.2-1.0-20	3.85	2.90	2.72	1.41	1.06
MW-100-5.5-0.4-20	1.01	0.76	1.46	0.69	0.52
MW-100-5.5-0.5-20	1.46	1.10	1.72	0.85	0.64
MW-100-5.5-0.6-20	1.96	1.48	1.99	0.99	0.74
MW-100-5.5-0.7-20	2.51	1.89	2.26	1.11	0.84
MW-100-5.5-1.0-20	4.40	3.31	3.02	1.46	1.10
MW-100-6.3-0.4-20	1.08	0.81	1.53	0.71	0.53
MW-100-6.3-0.5-20	1.56	1.18	1.82	0.86	0.65
MW-100-6.3-0.6-20	2.10	1.58	2.09	1.00	0.76
MW-100-6.3-0.7-20	2.69	2.02	2.31	1.16	0.87
MW-100-6.3-1.0-20	4.71	3.55	3.13	1.50	1.13
MW-100-8.0-0.4-20	1.22	0.92	1.66	0.73	0.55
MW-100-8.0-0.5-20	1.76	1.33	2.03	0.87	0.65
MW-100-8.0-0.6-20	2.37	1.78	2.37	1.00	0.75
MW-100-8.0-0.7-20	3.03	2.28	2.62	1.16	0.87
MW-100-8.0-1.0-20	5.31	4.00	3.28	1.62	1.22
MW-100-4.2-0.4-300	0.85	0.22	1.28	0.67	0.17
MW-100-4.2-0.5-300	1.23	0.32	1.52	0.81	0.21
MW-100-4.2-0.6-300	1.66	0.42	1.72	0.96	0.25
MW-100-4.2-0.7-300	2.12	0.54	1.89	1.12	0.29
MW-100-4.2-1.0-300	3.72	0.95	2.19	1.70	0.44
MW-100-5.5-0.4-300	0.98	0.25	1.36	0.72	0.18
MW-100-5.5-0.5-300	1.41	0.36	1.60	0.88	0.23
MW-100-5.5-0.6-300	1.90	0.49	1.85	1.03	0.26
MW-100-5.5-0.7-300	2.43	0.62	2.08	1.17	0.30

MW-100-5.5-1.0-300	4.26	1.09	2.68	1.59	0.41
MW-100-6.3-0.4-300	1.05	0.27	1.43	0.73	0.19
MW-100-6.3-0.5-300	1.51	0.39	1.67	0.91	0.23
MW-100-6.3-0.6-300	2.03	0.52	1.90	1.07	0.27
MW-100-6.3-0.7-300	2.60	0.67	2.14	1.21	0.31
MW-100-6.3-1.0-300	4.55	1.17	2.84	1.61	0.41
MW-100-8.0-0.4-300	1.18	0.30	1.55	0.76	0.19
MW-100-8.0-0.5-300	1.70	0.44	1.75	0.97	0.25
MW-100-8.0-0.6-300	2.29	0.59	1.98	1.16	0.30
MW-100-8.0-0.7-300	2.93	0.75	2.33	1.26	0.32
MW-100-8.0-1.0-300	5.13	1.32	2.92	1.76	0.45
MW-100-4.2-0.4-450	0.50	0.14	1.09	0.45	0.13
MW-100-4.2-0.5-450	0.72	0.20	1.33	0.54	0.15
MW-100-4.2-0.6-450	0.96	0.27	1.54	0.62	0.17
MW-100-4.2-0.7-450	1.23	0.34	1.71	0.72	0.20
MW-100-4.2-1.0-450	2.16	0.60	2.10	1.03	0.28
MW-100-5.5-0.4-450	0.57	0.16	1.15	0.50	0.14
MW-100-5.5-0.5-450	0.82	0.23	1.40	0.58	0.16
MW-100-5.5-0.6-450	1.10	0.30	1.66	0.66	0.18
MW-100-5.5-0.7-450	1.41	0.39	1.89	0.74	0.21
MW-100-5.5-1.0-450	2.47	0.68	2.45	1.01	0.28
MW-100-6.3-0.4-450	0.61	0.17	1.15	0.53	0.15
MW-100-6.3-0.5-450	0.88	0.24	1.38	0.64	0.18
MW-100-6.3-0.6-450	1.18	0.33	1.66	0.71	0.20
MW-100-6.3-0.7-450	1.51	0.42	1.96	0.77	0.21
MW-100-6.3-1.0-450	2.64	0.73	2.59	1.02	0.28
MW-100-8.0-0.4-450	0.68	0.19	1.27	0.54	0.15
MW-100-8.0-0.5-450	0.99	0.27	1.42	0.70	0.19
MW-100-8.0-0.6-450	1.33	0.37	1.74	0.76	0.21
MW-100-8.0-0.7-450	1.70	0.47	2.11	0.81	0.22
MW-100-8.0-1.0-450	2.98	0.82	2.77	1.08	0.30
MW-100-4.2-0.4-600	0.22	0.10	0.83	0.27	0.12
MW-100-4.2-0.5-600	0.32	0.14	1.06	0.30	0.14
MW-100-4.2-0.6-600	0.43	0.19	1.24	0.35	0.15
MW-100-4.2-0.7-600	0.55	0.25	1.38	0.40	0.18
MW-100-4.2-1.0-600	0.97	0.43	1.64	0.59	0.26
MW-100-5.5-0.4-600	0.25	0.11	0.81	0.31	0.14
MW-100-5.5-0.5-600	0.37	0.16	1.07	0.34	0.15
MW-100-5.5-0.6-600	0.49	0.22	1.32	0.37	0.17
MW-100-5.5-0.7-600	0.63	0.28	1.61	0.39	0.18
MW-100-5.5-1.0-600	1.11	0.49	2.12	0.52	0.23
MW-100-6.3-0.4-600	0.27	0.12	0.77	0.35	0.16
MW-100-6.3-0.5-600	0.39	0.18	1.01	0.39	0.17
MW-100-6.3-0.6-600	0.53	0.24	1.33	0.40	0.18

MW-100-6.3-0.7-600	0.68	0.30	1.63	0.41	0.18
MW-100-6.3-1.0-600	1.18	0.53	2.25	0.53	0.23
MW-100-8.0-0.4-600	0.31	0.14	0.73	0.42	0.19
MW-100-8.0-0.5-600	0.44	0.20	0.89	0.50	0.22
MW-100-8.0-0.6-600	0.59	0.27	1.19	0.50	0.22
MW-100-8.0-0.7-600	0.76	0.34	1.46	0.52	0.23
MW-100-8.0-1.0-600	1.33	0.60	2.11	0.63	0.28

Table 6.3. Shear stiffness of MW sandwich panels at different temperatures calculated by numerical and analytical methods

Case	$k_{V1,ECCS}$ (kN/mm)	$k_{V2,ECCS}$ (kN/mm)	k_{FEM} (kN/mm)	$k_{V1,ECCS}/ k_{FEM}$	$k_{V2,ECCS}/ k_{FEM}$
MW-100-4.2-0.4-20	2.21	1.73	6.36	0.35	0.27
MW-100-4.2-0.5-20	2.68	2.11	7.70	0.35	0.27
MW-100-4.2-0.6-20	3.08	2.45	8.93	0.35	0.27
MW-100-4.2-0.7-20	4.12	3.34	10.06	0.41	0.33
MW-100-4.2-1.0-20	5.95	4.99	12.66	0.47	0.39
MW-100-5.5-0.4-20	2.73	2.10	5.32	0.51	0.39
MW-100-5.5-0.5-20	3.36	2.60	7.35	0.46	0.35
MW-100-5.5-0.6-20	3.93	3.05	8.64	0.45	0.35
MW-100-5.5-0.7-20	5.47	4.29	9.84	0.56	0.44
MW-100-5.5-1.0-20	8.52	6.85	12.71	0.67	0.54
MW-100-6.3-0.4-20	2.99	2.29	4.57	0.65	0.50
MW-100-6.3-0.5-20	3.70	2.84	6.48	0.57	0.44
MW-100-6.3-0.6-20	4.35	3.35	7.89	0.55	0.42
MW-100-6.3-0.7-20	6.14	4.77	9.61	0.64	0.50
MW-100-6.3-1.0-20	9.85	7.80	12.59	0.78	0.62
MW-100-8.0-0.4-20	3.46	2.64	2.58	1.34	1.02
MW-100-8.0-0.5-20	4.32	3.29	2.97	1.45	1.11
MW-100-8.0-0.6-20	5.10	3.89	5.86	0.87	0.66
MW-100-8.0-0.7-20	7.32	5.61	8.05	0.91	0.70
MW-100-8.0-1.0-20	12.18	9.45	12.28	0.99	0.77
MW-100-4.2-0.4-300	2.13	0.62	4.48	0.48	0.14
MW-100-4.2-0.5-300	2.58	0.77	5.61	0.46	0.14
MW-100-4.2-0.6-300	2.97	0.91	7.15	0.42	0.13
MW-100-4.2-0.7-300	3.97	1.30	7.85	0.51	0.17
MW-100-4.2-1.0-300	5.71	2.12	10.82	0.53	0.20
MW-100-5.5-0.4-300	2.64	0.73	3.44	0.77	0.21
MW-100-5.5-0.5-300	3.25	0.91	4.53	0.72	0.20
MW-100-5.5-0.6-300	3.79	1.08	6.52	0.58	0.16
MW-100-5.5-0.7-300	5.27	1.55	7.69	0.69	0.20
MW-100-5.5-1.0-300	8.18	2.62	10.69	0.77	0.24
MW-100-6.3-0.4-300	2.89	0.79	2.90	1.00	0.27
MW-100-6.3-0.5-300	3.58	0.98	3.86	0.93	0.25

MW-100-6.3-0.6-300	4.20	1.16	5.41	0.78	0.22
MW-100-6.3-0.7-300	5.93	1.69	7.54	0.79	0.22
MW-100-6.3-1.0-300	9.48	2.87	10.61	0.89	0.27
MW-100-8.0-0.4-300	3.35	0.91	2.05	1.63	0.44
MW-100-8.0-0.5-300	4.18	1.13	3.57	1.17	0.32
MW-100-8.0-0.6-300	4.93	1.34	4.49	1.10	0.30
MW-100-8.0-0.7-300	7.07	1.94	6.12	1.15	0.32
MW-100-8.0-1.0-300	11.75	3.33	10.34	1.14	0.32
MW-100-4.2-0.4-450	1.31	0.40	3.18	0.41	0.12
MW-100-4.2-0.5-450	1.60	0.49	4.62	0.35	0.11
MW-100-4.2-0.6-450	1.86	0.58	6.01	0.31	0.10
MW-100-4.2-0.7-450	2.54	0.84	7.00	0.36	0.12
MW-100-4.2-1.0-450	3.83	1.40	9.30	0.41	0.15
MW-100-5.5-0.4-450	1.58	0.46	2.50	0.63	0.18
MW-100-5.5-0.5-450	1.96	0.58	3.26	0.60	0.18
MW-100-5.5-0.6-450	2.30	0.69	4.59	0.50	0.15
MW-100-5.5-0.7-450	3.25	0.99	6.44	0.50	0.15
MW-100-5.5-1.0-450	5.21	1.69	9.18	0.57	0.18
MW-100-6.3-0.4-450	1.72	0.50	2.36	0.73	0.21
MW-100-6.3-0.5-450	2.14	0.63	3.10	0.69	0.20
MW-100-6.3-0.6-450	2.53	0.74	3.88	0.65	0.19
MW-100-6.3-0.7-450	3.60	1.08	5.18	0.70	0.21
MW-100-6.3-1.0-450	5.90	1.84	9.10	0.65	0.20
MW-100-8.0-0.4-450	1.98	0.58	1.22	1.63	0.48
MW-100-8.0-0.5-450	2.48	0.72	2.12	1.17	0.34
MW-100-8.0-0.6-450	2.93	0.85	3.46	0.85	0.25
MW-100-8.0-0.7-450	4.23	1.23	4.47	0.95	0.28
MW-100-8.0-1.0-450	7.12	2.12	8.80	0.81	0.24
MW-100-4.2-0.4-600	0.62	0.29	2.08	0.30	0.14
MW-100-4.2-0.5-600	0.77	0.36	2.98	0.26	0.12
MW-100-4.2-0.6-600	0.90	0.43	4.24	0.21	0.10
MW-100-4.2-0.7-600	1.27	0.61	5.10	0.25	0.12
MW-100-4.2-1.0-600	2.03	1.03	7.63	0.27	0.13
MW-100-5.5-0.4-600	0.73	0.34	2.14	0.34	0.16
MW-100-5.5-0.5-600	0.92	0.42	2.55	0.36	0.16
MW-100-5.5-0.6-600	1.08	0.50	3.35	0.32	0.15
MW-100-5.5-0.7-600	1.56	0.72	3.87	0.40	0.19
MW-100-5.5-1.0-600	2.59	1.24	7.45	0.35	0.17
MW-100-6.3-0.4-600	0.79	0.36	2.06	0.39	0.18
MW-100-6.3-0.5-600	0.99	0.45	2.53	0.39	0.18
MW-100-6.3-0.6-600	1.18	0.54	3.16	0.37	0.17
MW-100-6.3-0.7-600	1.70	0.78	3.58	0.47	0.22
MW-100-6.3-1.0-600	2.86	1.35	7.17	0.40	0.19
MW-100-8.0-0.4-600	0.91	0.42	1.51	0.60	0.28

MW-100-8.0-0.5-600	1.14	0.52	2.31	0.49	0.23
MW-100-8.0-0.6-600	1.35	0.62	2.72	0.50	0.23
MW-100-8.0-0.7-600	1.96	0.90	3.42	0.57	0.26
MW-100-8.0-1.0-600	3.35	1.55	7.07	0.47	0.22

Table 6.4. The load-bearing capacity of PIR sandwich panels at different temperatures calculated by numerical and analytical methods

Case	$V_{1,ECCS}$ (kN)	$V_{2,ECCS}$ (kN)	V_{FEM} (kN)	$V_{1,ECCS}/ V_{FEM}$	$V_{2,ECCS}/ V_{FEM}$
PIR-100-4.2-0.4-20	0.88	0.67	1.48	0.60	0.45
PIR-100-4.2-0.5-20	1.28	0.96	1.70	0.75	0.56
PIR-100-4.2-0.6-20	1.71	1.29	1.91	0.90	0.67
PIR-100-4.2-0.7-20	2.19	1.65	2.10	1.04	0.78
PIR-100-4.2-1.0-20	3.85	2.90	2.45	1.57	1.18
PIR-100-5.5-0.4-20	1.01	0.76	1.63	0.62	0.47
PIR-100-5.5-0.5-20	1.46	1.10	1.89	0.77	0.58
PIR-100-5.5-0.6-20	1.96	1.48	2.08	0.94	0.71
PIR-100-5.5-0.7-20	2.51	1.89	2.26	1.11	0.84
PIR-100-5.5-1.0-20	4.40	3.31	2.75	1.60	1.20
PIR-100-6.3-0.4-20	1.08	0.81	1.61	0.67	0.50
PIR-100-6.3-0.5-20	1.56	1.18	2.00	0.78	0.59
PIR-100-6.3-0.6-20	2.10	1.58	2.24	0.94	0.71
PIR-100-6.3-0.7-20	2.69	2.02	2.40	1.12	0.84
PIR-100-6.3-1.0-20	4.71	3.55	3.00	1.57	1.18
PIR-100-8.0-0.4-20	1.22	0.92	1.78	0.68	0.52
PIR-100-8.0-0.5-20	1.76	1.33	2.19	0.81	0.61
PIR-100-8.0-0.6-20	2.37	1.78	2.58	0.92	0.69
PIR-100-8.0-0.7-20	3.03	2.28	2.88	1.05	0.79
PIR-100-8.0-1.0-20	5.31	4.00	3.31	1.60	1.21
PIR-100-4.2-0.4-300	0.85	0.22	1.19	0.72	0.18
PIR-100-4.2-0.5-300	1.23	0.32	1.34	0.92	0.24
PIR-100-4.2-0.6-300	1.66	0.42	1.47	1.13	0.29
PIR-100-4.2-0.7-300	2.12	0.54	1.59	1.34	0.34
PIR-100-4.2-1.0-300	3.72	0.95	1.77	2.10	0.54
PIR-100-5.5-0.4-300	0.98	0.25	1.35	0.72	0.18
PIR-100-5.5-0.5-300	1.41	0.36	1.51	0.94	0.24
PIR-100-5.5-0.6-300	1.90	0.49	1.62	1.17	0.30
PIR-100-5.5-0.7-300	2.43	0.62	1.75	1.39	0.36
PIR-100-5.5-1.0-300	4.26	1.09	2.06	2.07	0.53
PIR-100-6.3-0.4-300	1.05	0.27	1.42	0.74	0.19
PIR-100-6.3-0.5-300	1.51	0.39	1.59	0.95	0.24
PIR-100-6.3-0.6-300	2.03	0.52	1.75	1.16	0.30
PIR-100-6.3-0.7-300	2.60	0.67	1.86	1.40	0.36
PIR-100-6.3-1.0-300	4.55	1.17	2.21	2.06	0.53

PIR-100-8.0-0.4-300	1.18	0.30	1.46	0.81	0.21
PIR-100-8.0-0.5-300	1.70	0.44	1.74	0.98	0.25
PIR-100-8.0-0.6-300	2.29	0.59	1.99	1.15	0.29
PIR-100-8.0-0.7-300	2.93	0.75	2.16	1.35	0.35
PIR-100-8.0-1.0-300	5.13	1.32	2.43	2.12	0.54
PIR-100-4.2-0.4-450	0.50	0.14	0.79	0.63	0.17
PIR-100-4.2-0.5-450	0.72	0.20	0.94	0.76	0.21
PIR-100-4.2-0.6-450	0.96	0.27	1.07	0.90	0.25
PIR-100-4.2-0.7-450	1.23	0.34	1.19	1.04	0.29
PIR-100-4.2-1.0-450	2.16	0.60	1.40	1.54	0.43
PIR-100-5.5-0.4-450	0.57	0.16	0.79	0.72	0.20
PIR-100-5.5-0.5-450	0.82	0.23	0.95	0.86	0.24
PIR-100-5.5-0.6-450	1.10	0.30	1.14	0.96	0.27
PIR-100-5.5-0.7-450	1.41	0.39	1.29	1.09	0.30
PIR-100-5.5-1.0-450	2.47	0.68	1.60	1.54	0.43
PIR-100-6.3-0.4-450	0.61	0.17	0.79	0.77	0.21
PIR-100-6.3-0.5-450	0.88	0.24	0.92	0.95	0.26
PIR-100-6.3-0.6-450	1.18	0.33	1.10	1.07	0.30
PIR-100-6.3-0.7-450	1.51	0.42	1.38	1.10	0.30
PIR-100-6.3-1.0-450	2.64	0.73	1.70	1.56	0.43
PIR-100-8.0-0.4-450	0.68	0.19	0.91	0.75	0.21
PIR-100-8.0-0.5-450	0.99	0.27	1.00	0.99	0.27
PIR-100-8.0-0.6-450	1.33	0.37	1.16	1.15	0.32
PIR-100-8.0-0.7-450	1.70	0.47	1.28	1.33	0.37
PIR-100-8.0-1.0-450	2.98	0.82	1.87	1.59	0.44
PIR-100-4.2-0.4-600	0.22	0.10	0.60	0.37	0.17
PIR-100-4.2-0.5-600	0.32	0.14	0.74	0.43	0.19
PIR-100-4.2-0.6-600	0.43	0.19	0.89	0.48	0.22
PIR-100-4.2-0.7-600	0.55	0.25	0.98	0.56	0.25
PIR-100-4.2-1.0-600	0.97	0.43	1.17	0.82	0.37
PIR-100-5.5-0.4-600	0.25	0.11	0.55	0.46	0.21
PIR-100-5.5-0.5-600	0.37	0.16	0.70	0.53	0.24
PIR-100-5.5-0.6-600	0.49	0.22	0.91	0.54	0.24
PIR-100-5.5-0.7-600	0.63	0.28	1.08	0.58	0.26
PIR-100-5.5-1.0-600	1.11	0.49	1.35	0.82	0.37
PIR-100-6.3-0.4-600	0.27	0.12	0.59	0.46	0.20
PIR-100-6.3-0.5-600	0.39	0.18	0.68	0.58	0.26
PIR-100-6.3-0.6-600	0.53	0.24	0.90	0.58	0.26
PIR-100-6.3-0.7-600	0.68	0.30	1.07	0.63	0.28
PIR-100-6.3-1.0-600	1.18	0.53	1.43	0.83	0.37
PIR-100-8.0-0.4-600	0.31	0.14	0.57	0.53	0.24
PIR-100-8.0-0.5-600	0.44	0.20	0.70	0.63	0.28
PIR-100-8.0-0.6-600	0.59	0.27	0.86	0.69	0.31
PIR-100-8.0-0.7-600	0.76	0.34	1.02	0.75	0.33

PIR-100-8.0-1.0-600	1.33	0.60	1.55	0.86	0.38

Table 6.5. Shear stiffness of PIR sandwich panels at different temperatures calculated by numerical and analytical methods

Case	$k_{V1,ECCS}$ (kN/mm)	$k_{V2,ECCS}$ (kN/mm)	k_{FEM} (kN/mm)	$k_{V1,ECCS}/ k_{FEM}$	$k_{V2,ECCS}/ k_{FEM}$
PIR-100-4.2-0.4-20	2.21	1.73	6.13	0.36	0.28
PIR-100-4.2-0.5-20	2.68	2.11	9.13	0.29	0.23
PIR-100-4.2-0.6-20	3.08	2.45	8.56	0.36	0.29
PIR-100-4.2-0.7-20	4.12	3.34	9.57	0.43	0.35
PIR-100-4.2-1.0-20	5.95	4.99	12.39	0.48	0.40
PIR-100-5.5-0.4-20	2.73	2.10	4.65	0.59	0.45
PIR-100-5.5-0.5-20	3.36	2.60	6.18	0.54	0.42
PIR-100-5.5-0.6-20	3.93	3.05	7.39	0.53	0.41
PIR-100-5.5-0.7-20	5.47	4.29	9.31	0.59	0.46
PIR-100-5.5-1.0-20	8.52	6.85	11.82	0.72	0.58
PIR-100-6.3-0.4-20	2.99	2.29	4.21	0.71	0.54
PIR-100-6.3-0.5-20	3.70	2.84	5.97	0.62	0.48
PIR-100-6.3-0.6-20	4.35	3.35	7.19	0.60	0.47
PIR-100-6.3-0.7-20	6.14	4.77	8.38	0.73	0.57
PIR-100-6.3-1.0-20	9.85	7.80	11.42	0.86	0.68
PIR-100-8.0-0.4-20	3.46	2.64	2.78	1.25	0.95
PIR-100-8.0-0.5-20	4.32	3.29	3.70	1.17	0.89
PIR-100-8.0-0.6-20	5.10	3.89	4.54	1.12	0.86
PIR-100-8.0-0.7-20	7.32	5.61	6.12	1.20	0.92
PIR-100-8.0-1.0-20	12.18	9.45	11.18	1.09	0.84
PIR-100-4.2-0.4-300	2.13	0.62	3.51	0.61	0.18
PIR-100-4.2-0.5-300	2.58	0.77	4.53	0.57	0.17
PIR-100-4.2-0.6-300	2.97	0.91	5.69	0.52	0.16
PIR-100-4.2-0.7-300	3.97	1.30	6.50	0.61	0.20
PIR-100-4.2-1.0-300	5.71	2.12	7.88	0.72	0.27
PIR-100-5.5-0.4-300	2.64	0.73	2.28	1.16	0.32
PIR-100-5.5-0.5-300	3.25	0.91	3.44	0.94	0.26
PIR-100-5.5-0.6-300	3.79	1.08	5.04	0.75	0.21
PIR-100-5.5-0.7-300	5.27	1.55	5.77	0.91	0.27
PIR-100-5.5-1.0-300	8.18	2.62	7.49	1.09	0.35
PIR-100-6.3-0.4-300	2.89	0.79	1.81	1.59	0.43
PIR-100-6.3-0.5-300	3.58	0.98	2.86	1.25	0.34
PIR-100-6.3-0.6-300	4.20	1.16	4.07	1.03	0.29
PIR-100-6.3-0.7-300	5.93	1.69	5.66	1.05	0.30
PIR-100-6.3-1.0-300	9.48	2.87	7.42	1.28	0.39
PIR-100-8.0-0.4-300	3.35	0.91	1.54	2.18	0.59
PIR-100-8.0-0.5-300	4.18	1.13	1.90	2.20	0.59
PIR-100-8.0-0.6-300	4.93	1.34	2.30	2.14	0.58

PIR-100-8.0-0.7-300	7.07	1.94	3.84	1.84	0.51
PIR-100-8.0-1.0-300	11.75	3.33	7.32	1.61	0.45
PIR-100-4.2-0.4-450	1.31	0.40	2.34	0.56	0.17
PIR-100-4.2-0.5-450	1.60	0.49	2.84	0.56	0.17
PIR-100-4.2-0.6-450	1.86	0.58	3.29	0.56	0.18
PIR-100-4.2-0.7-450	2.54	0.84	3.69	0.69	0.23
PIR-100-4.2-1.0-450	3.83	1.40	4.72	0.81	0.30
PIR-100-5.5-0.4-450	1.58	0.46	1.64	0.96	0.28
PIR-100-5.5-0.5-450	1.96	0.58	2.26	0.87	0.26
PIR-100-5.5-0.6-450	2.30	0.69	2.74	0.84	0.25
PIR-100-5.5-0.7-450	3.25	0.99	3.57	0.91	0.28
PIR-100-5.5-1.0-450	5.21	1.69	4.66	1.12	0.36
PIR-100-6.3-0.4-450	1.72	0.50	1.34	1.29	0.37
PIR-100-6.3-0.5-450	2.14	0.63	1.97	1.09	0.32
PIR-100-6.3-0.6-450	2.53	0.74	2.39	1.06	0.31
PIR-100-6.3-0.7-450	3.60	1.08	2.52	1.43	0.43
PIR-100-6.3-1.0-450	5.90	1.84	4.20	1.40	0.44
PIR-100-8.0-0.4-450	1.98	0.58	0.83	2.39	0.70
PIR-100-8.0-0.5-450	2.48	0.72	1.34	1.85	0.54
PIR-100-8.0-0.6-450	2.93	0.85	1.97	1.49	0.43
PIR-100-8.0-0.7-450	4.23	1.23	2.64	1.60	0.47
PIR-100-8.0-1.0-450	7.12	2.12	3.47	2.05	0.61
PIR-100-4.2-0.4-600	0.62	0.29	1.14	0.55	0.25
PIR-100-4.2-0.5-600	0.77	0.36	1.54	0.50	0.23
PIR-100-4.2-0.6-600	0.90	0.43	1.96	0.46	0.22
PIR-100-4.2-0.7-600	1.27	0.61	2.27	0.56	0.27
PIR-100-4.2-1.0-600	2.03	1.03	3.48	0.59	0.30
PIR-100-5.5-0.4-600	0.73	0.34	1.04	0.71	0.32
PIR-100-5.5-0.5-600	0.92	0.42	1.34	0.68	0.31
PIR-100-5.5-0.6-600	1.08	0.50	1.65	0.66	0.30
PIR-100-5.5-0.7-600	1.56	0.72	1.94	0.80	0.37
PIR-100-5.5-1.0-600	2.59	1.24	3.19	0.81	0.39
PIR-100-6.3-0.4-600	0.79	0.36	0.83	0.96	0.44
PIR-100-6.3-0.5-600	0.99	0.45	1.28	0.78	0.35
PIR-100-6.3-0.6-600	1.18	0.54	1.59	0.74	0.34
PIR-100-6.3-0.7-600	1.70	0.78	1.89	0.90	0.42
PIR-100-6.3-1.0-600	2.86	1.35	2.76	1.04	0.49
PIR-100-8.0-0.4-600	0.91	0.42	0.72	1.26	0.58
PIR-100-8.0-0.5-600	1.14	0.52	0.98	1.16	0.53
PIR-100-8.0-0.6-600	1.35	0.62	1.39	0.97	0.44
PIR-100-8.0-0.7-600	1.96	0.90	1.76	1.11	0.51
PIR-100-8.0-1.0-600	3.35	1.55	2.63	1.28	0.59

6.4.2 Effect of inner sheet thickness on connection performance

One of the most decisive parameters to determine the connection behavior is the thickness of the inner sheet. Figure 6.4 illustrates how increasing the inner sheet thickness affects the shear stiffness and load-bearing capacity of specimens at ambient temperature. At ambient temperature, it is shown that by changing the inner sheet thickness from 0.4 mm to 1.0 mm, FE models' load-bearing capacity increases 206% and 168% for MW and PIR panels. This increase in shear stiffness is 239% and 254%, respectively. Besides, it is obvious that the connections with a thinner sheet thickness experience more deformability than thicker sheet thickness. Generally, when the inner sheet thickness increases, the shear resistance and stiffness at all temperatures increase.

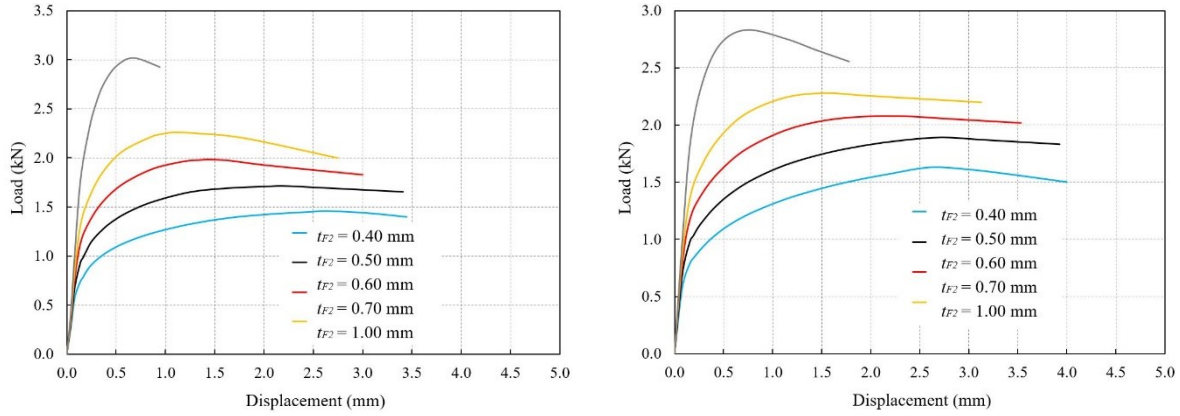

Figure 6.4. Load-displacement curves for sandwich panels with 5.5 mm screw diameter and different inner sheet thicknesses at ambient temperature, a) MW and b) PIR panels

6.4.3 Effect of screw diameter on connection performance

Figure 6.5 indicates the load-displacement curves for different screw diameters of MW and PIR sandwich panels with an inner sheet thickness of 0.5 mm at ambient temperature. When the screw diameter increases from 4.2 mm to 8 mm, the maximum load raises around 21% and 29% for MW and PIR panels, respectively. Nonetheless, compared to changes in the facing thickness, the rise is not substantial. This procedure for the shear stiffness is different. Indeed, the increase in the screw diameter from 4.2 mm to 8.0 mm results in a reduction of the shear stiffness. This reduction can be justified by the fact that as the screw diameter increases, so does the diameter of the hole on the steel sheet. As a result, the steel sheet is weakened and leads to a connection with the lower stiffness.

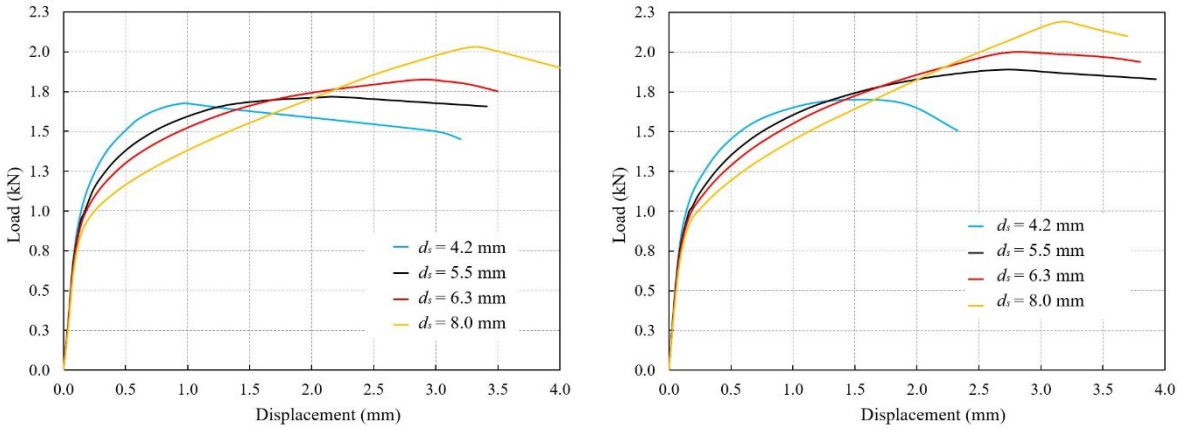

Figure 6.5. Load-displacement curves for sandwich panels with 0.5 mm inner sheet thickness and different screw diameters at ambient temperature, a) MW and b) PIR panels

Figure 6.6 shows that when the screw diameter increases, the load-bearing capacity rate of the connection grows. However, this increase depends on the inner sheet thickness of the panel. In fact, it is observed that the growth rate of shear resistance for thicker inner sheets can be higher than the panels with thinner inner sheets.

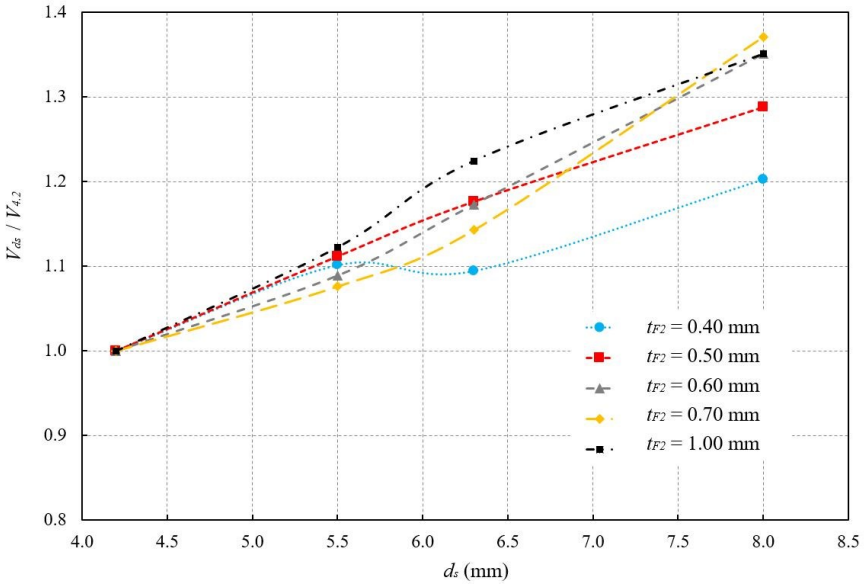

Figure 6.6. Shear resistance of PIR panels with different screw diameters and various inner sheet thicknesses at ambient temperature

6.4.4 Effect of temperature on connection performance

Different temperatures are applied to the inner sheet and supporting structures to observe the temperature effect on sandwich panel connections under shear loads. As expected, by the rise in the temperature, both shear stiffness and maximum load decrease. The mechanical properties of the sheeting, screw and core material are reduced at elevated temperatures; therefore, the

connection shows less resistance against the shear load. In Figure 6.7, as a sample, the load-displacement curve for the MW sandwich panel is illustrated.

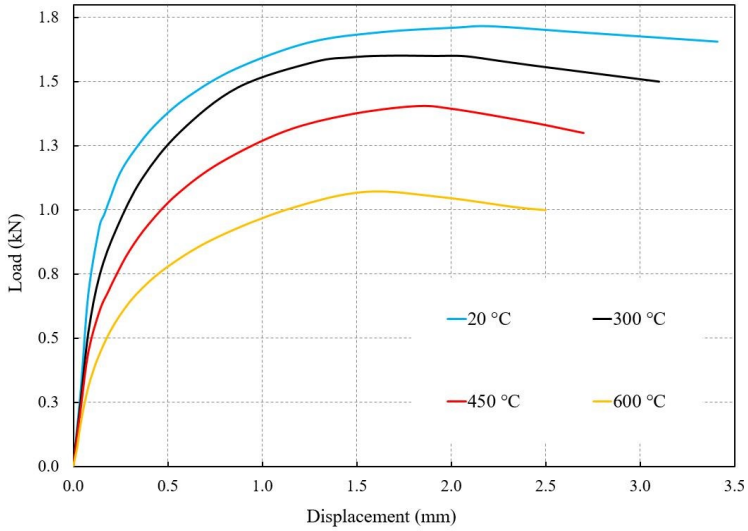

Figure 6.7. Load-displacement curves for MW sandwich panels with 5.5 mm screw diameter and 0.5 mm inner sheet thickness at different temperatures

Figure 6.8 compares the degradation of shear resistance and stiffness of MW and PIR sandwich panels obtained from FE models at ambient and elevated temperatures. As can be seen, the reduction rate of resistance of PIR panels is higher than MW panels. Although PIR panels' shear stiffness at elevated temperatures decreases faster than MW panels, the difference between the two panels for stiffness is not as significant as resistance. The values of stiffness and resistance approximately in all cases for MW panels are higher than in PIR panels.

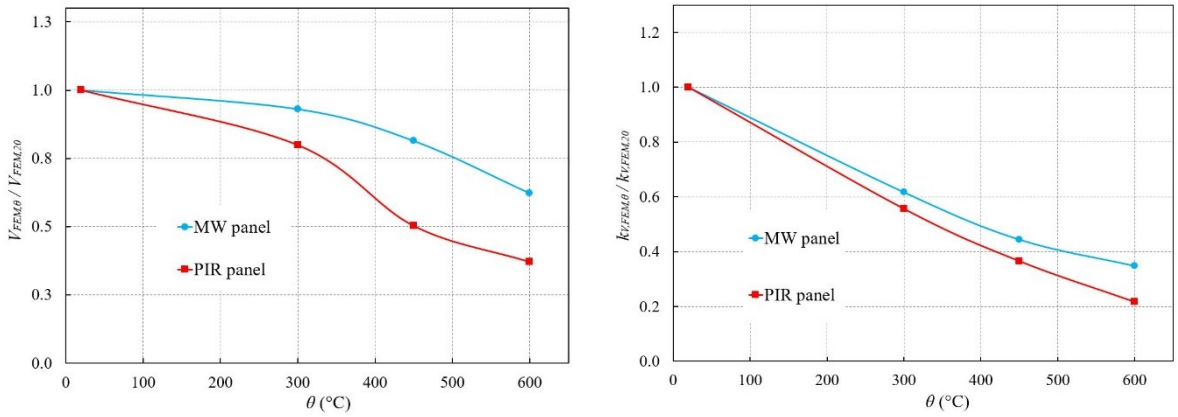

a) b)

Figure 6.8. Degradation of a) shear resistance and b) shear stiffness of MW and PIR panels with 0.5 mm inner sheet thickness and 5.5 mm screw diameter at different temperatures

Figure 6.9 compares the reduction rate of the shear resistance of panels with a 5.5 mm screw diameter with various inner sheet thicknesses at different temperatures. It should be said, the

reduction factor of load-bearing capacity at elevated temperatures, higher than 300 °C, for the thinner thicknesses is greater than for thicker ones.

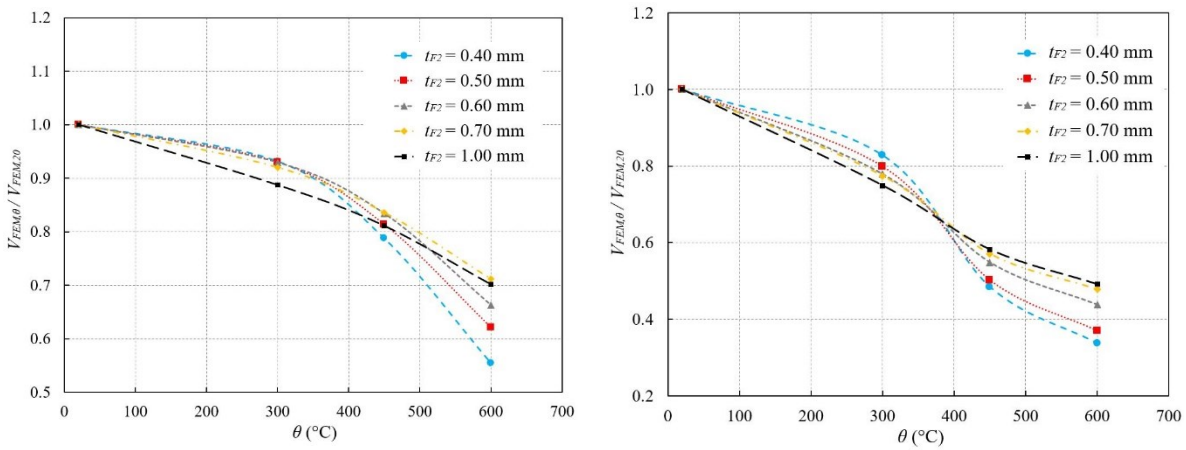

Figure 6.9. Degradation of shear resistance of a) MW panels, b) PIR panels with 5.5 mm screw diameter and various inner sheet thicknesses at elevated temperatures

As the temperature rise, the shear stiffness of sandwich panel connections reduces. Nevertheless, this decrease in different inner sheet thicknesses is not the same. As shown in Figure 6.10, the thinner inner sheets' reduction rate of MW panels is higher than that of thicker ones. The same conclusion is valid for the decrease in shear stiffness of PIR panels.

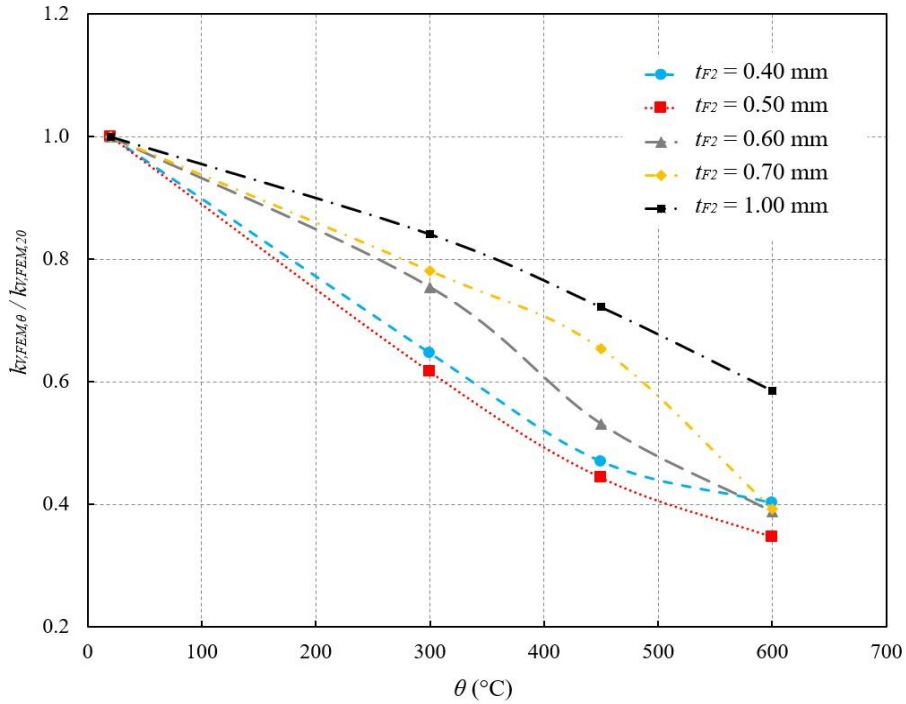

Figure 6.10. Degradation of shear stiffness of MW panels with 5.5 mm screw diameter and various inner sheet thicknesses at different temperatures

As already mentioned, the screw diameter does not substantially influence the load-bearing capacity of panels compared to the inner sheet thickness. However, the results indicate that at

elevated temperatures, the difference in shear resistance of the PIR panels with different screw diameters is even smaller than the ambient temperature (see Figure 6.11). The same conclusion is valid for MW panels.

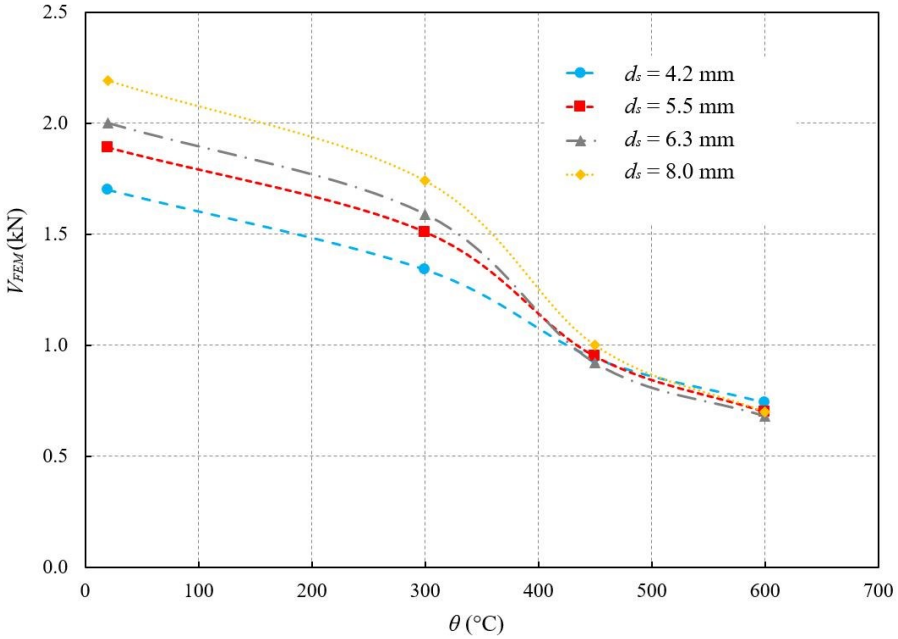

Figure 6.11. Shear resistance of PIR panels with 0.5 mm inner sheet thickness and various screw diameters at different temperatures

6.5 Comparison of numerical results with analytical solutions for shear resistance

In Table 6.2 and Table 6.4, the load-bearing capacity of MW and PIR sandwich panels are compared. Approach 2 is, in most cases, safe. Just for the inner sheet thickness of 1.0 mm at ambient temperatures, the analytical values calculated by Approach 2 exceed the numerical results. At elevated temperatures, this method looks pretty conservative. However, Approach 1 is unsafe for the inner sheet thickness of 0.7 mm to 1.0 mm at ambient temperatures. At the temperatures of 300 °C and 450 °C, and the inner sheet thickness of 0.6 mm to 1.0 mm for PIR panels, and 0.7 mm to 1.0 mm for MW panels, Approach 1 is unsafe. Nonetheless, at 600 °C, Approach 1 is safe for all cases.

As a result, it should be said that both approaches for all MW and PIR are safe for the inner sheet thickness of 0.4 mm and 0.5 mm. Furthermore, at the temperature of 600 °C, all cases are safe.

Figure 6.12 shows V_θ / V_{20} ratios of the analytical Approaches 1 and 2 and the average numerical results of MW and PIR panels at each specific temperature, where V_θ and V_{20} are the shear resistances at elevated and ambient temperatures, respectively. It can be seen that after 100 °C, Approach 2 has the highest reduction rate. Therefore, the analytical solution presented by Approach 2 is more conservative than Approach 1. In addition, the resistance of PIR connections is reduced to a greater extent than MW ones.

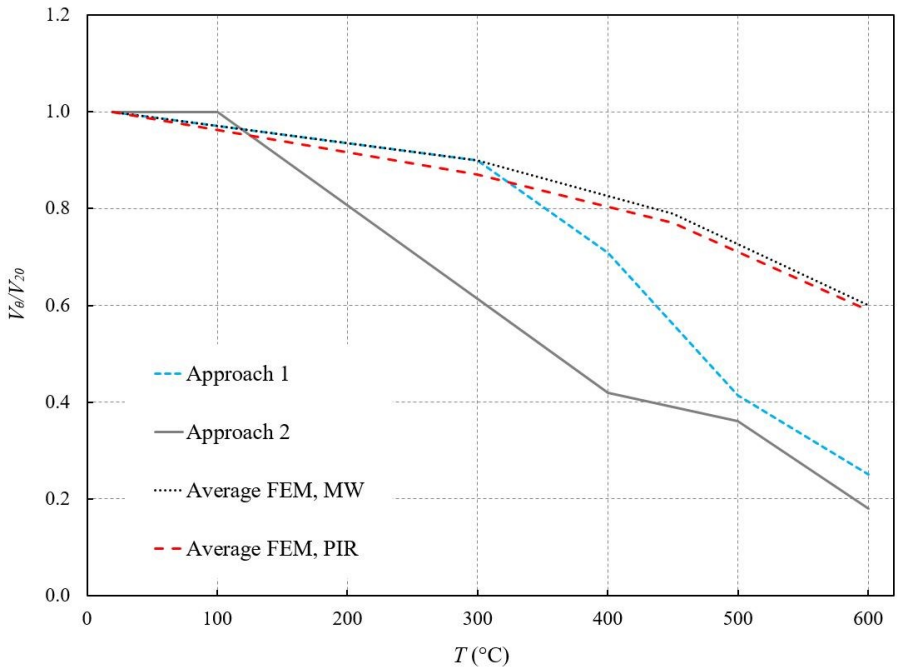

Figure 6.12. Ratios of resistance at ambient and elevated temperatures

6.6 Comparison of numerical results with analytical solutions for shear stiffness

Table 6.3 and Table 6.5 compare the shear stiffness of MW and PIR connections for numerical and analytical results. It should be said that approximately Approach 2 is safe for all specimens. When the screw diameter is 4.2 mm and 5.5 mm, the results calculated by Approach 2 are so conservative. In the case of MW connections, Approach 1 presents safe results except for the screw diameter of 8.0 mm with inner sheet thickness of 0.4 mm and 0.5 mm at 20 °C and 450 °C, and all inner sheet thickness at 300 °C. Approach 1 shows unsafe results for PIR connections with a screw diameter of 8.0 mm at all temperatures. Besides, at 300 °C and 450 °C, the results for PIR connections with a screw diameter of 6.3 mm are also unsafe. It should be noted that the comparison of stiffness is not as strict as for resistance, and a slight overestimation of stiffness is generally accepted. In particular, this research agrees with a 10% overestimation of numerical stiffness by the analytical method.

Figure 6.13 shows $k_{V,\theta}$ /$k_{V,20}$ ratios of the average results of analytical Approaches 1 and 2 and the average numerical results of MW and PIR panels at each specific temperature, where $k_{V,\theta}$ and $k_{V,20}$ are the shear stiffness at elevated and ambient temperatures respectively. It can be seen that after 300 °C, Approach 1 has the highest reduction rate, then PIR and MW connections and Approach 2, respectively. The shear stiffness of PIR connections is reduced to a greater extent than MW ones.

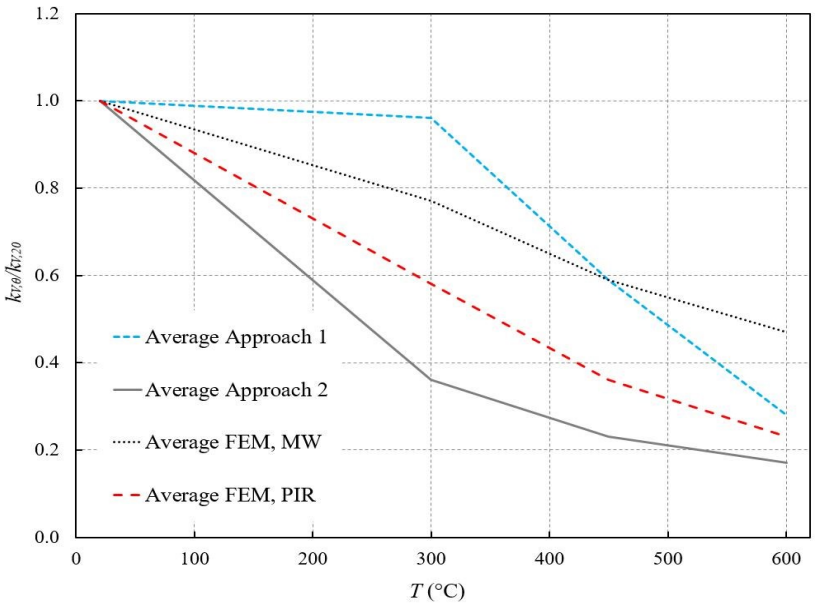

Figure 6.13. Ratios of stiffness at ambient and elevated temperatures

6.7 Alternative solution for shear stiffness of sandwich panel connections

Since changing Young's modulus and the tensile strength of the inner face at different temperatures in Eq. (6.5) is time-consuming, in this section, a simple approach is proposed to calculate the translational stiffness of sandwich panels at elevated temperatures. The approach is designed using the curve-fitting method and developed in two steps.

The first step uses the existing FE results (Section 6.4.1) to determine the so-called stiffness reduction coefficient k_T illustrating the connection's stiffness at a specific temperature to the same connection's stiffness at ambient temperature (20 °C). Figure 6.14 shows the reduction coefficients of MW and PIR connections at different temperatures.

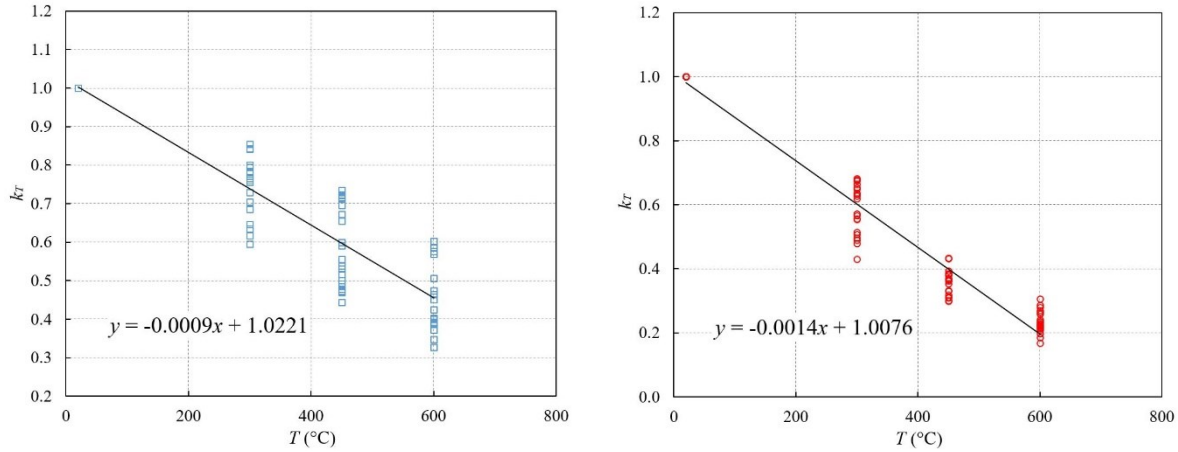

a) b)

Figure 6.14. Temperature reduction coefficients for a) MW panels; b) PIR panels

The second step utilizes the curve-fitting approach to create an algebraic equation to calculate the coefficient k_T. Linear regression is employed to generate Eq. (6.11), which presents the reduction coefficient (k_T).

$$k_T = \beta - \alpha . T . 10^{-5} \tag{6.11}$$

T (°C) is the sandwich panels' inner face temperature, and α and β are according to Table 6.6.

Table 6.6. α and β coefficients for MW and PIR panels

Panel	α (K^{-1})	β
MW	90	1.0221
PIR	140	1.0076

The derived stiffness reduction coefficient (k_T) is applied as an additional multiplier in Eq. (6.5) to calculate the translational stiffness at elevated temperatures. Eq. (6.12) presents the translational stiffness of sandwich panel connections at elevated temperatures. The application range of k_T is according to Table 6.1.

$$k_{v,\theta} = \frac{1}{\frac{x_F}{k_{F2}} + \frac{t_{cor,sup}^2 + 2.(1-x_F).D.t_{cor,sup}}{4C_{sup}} + \frac{3.(1-x_F).D.t_{cor,sup}^2 + t_{cor,sup}^3}{24EI}} . k_T \tag{6.12}$$

6.8 Conclusion

In this chapter, sandwich panels' translational resistance and stiffness under shear loadings at ambient and elevated temperatures were investigated. A comprehensive parametric study was conducted to survey the effect of temperature, inner sheet thickness, and screw diameter on specimens' shear resistance and stiffness. Then, the numerical results were compared with the analytical formulations obtained from the ECCS manual at ambient temperature. Moreover, the

analytical formulations were developed to employ at elevated temperatures. An additional multiplier was added to the translational stiffness formulation at ambient temperature to predict the stiffness at elevated temperatures as a simple alternative solution.

The following conclusions can be drawn:

- It was shown that the shear stiffness and resistance for MW and PIR panels increased by increasing the inner sheet thickness. However, the increase in stiffness was higher than the load-bearing capacity of connections. It should be said that the sandwich panel connections with thinner inner sheets experienced more deformability than thicker ones.
- When the screw diameter increased, the maximum load was raised for both MW and PIR connections. Nevertheless, compared to the inner sheet thicknesses, the maximum load's sensitivity to the screw diameter was not considerable. Moreover, it was observed that the growth rate of shear resistance for thicker inner sheets was slightly higher than the panels with thinner inner sheets. The increase in the screw diameter led to a reduction in the shear stiffness. In fact, a greater screw diameter means a bigger hole in the lower sheet, which negatively influences the shear stiffness of the connection.
- As the temperature is elevated, shear resistance and stiffness of MW and PIR panels decrease due to the degradation of material properties at elevated temperatures. The reduction rate of PIR panels' resistance and stiffness was higher than MW panels. However, the difference between the two panels' shear stiffness was not as significant as shear resistance. Apart from ambient temperature, MW panels showed higher stiffness and resistance than PIR panels. The effect of temperature on stiffness deterioration for the thinner inner sheets was higher than for thicker ones. The results showed that the difference in shear resistance of panels at elevated was even smaller than ambient temperature.
- In the analytical study, two approaches were introduced. Generally, Approach 2 gave more conservative results than Approach 1. To determine shear resistance, it should be said that both approaches for all MW and PIR cases were safe for the inner sheet thickness of 0.4 mm and 0.5 mm, and Approach 1 gave closer outputs to numerical results.
- Approach 2 was safe for all specimens when calculating shear stiffness. In some cases, the results calculated by Approach 2 were very conservative. Approach 1 was also safe for all cases, but for 8.0 mm screw diameter for MW and PIR connections and 8.0 mm and 6.3 mm for PIR connections.

- A reduction coefficient was defined according to the numerical results to simplify the procedure of shear stiffness calculation. This reduction coefficient was added to the shear stiffness formulation as an additional multiplier. This method's advantage over other approaches is that the results are achieved faster and according to simulation outputs. Therefore, this method can also give an acceptable estimation of shear stiffness at elevated temperatures.

Chapter 7: PRACTICAL ASPECTS OF RESEARCH

7.1 Introduction

The purpose of this chapter is to show a practical example of the research. Actually, the effect of replacing bracings with sandwich panels is investigated at ambient and elevated temperatures with an example. The studied models include a single-story building with bracings without any cladding and the same building stabilized with sandwich panels without any bracings. The design of the structure is carried out by RFEM software. Some calculations are conducted in the ABAQUS program. In the following, first, the structure's design is described, and then the stabilization behavior of both systems is compared.

7.2 General information

Figure 7.1 shows the overall view of the frame stabilized with bracings. The length of the building is 49 m, including seven spans of 7 m, and the width is 28 m. The maximum height of the structure is 10 m, while the size of wall columns is 8 m. The inclination of the roof is 8% (Figure 7.2). All members are made of S355 steel. Table 7.1 presents the designed cross-sections applied for the building. The column base connections are modeled as pinned joints, while the beam-to-column connections are rigid. The building stabilized by sandwich panels is illustrated in Figure 7.3. The dimensions of the structure are similar to Figure 7.1.

The structure is designed under permanent and wind loads. Permanent loads include the weight of the roofing with the estimated magnitude of 0.3 kN/m^2 and the self-weight of the steel members, which is automatically calculated by the software. The terrain category III is applied for the structure to consider wind load. Table 7.2 presents the load assumptions parameters which are considered for the design.

Table 7.1. Cross-sections of the members

Member	Profile
Wall column	HEA 320
End column	HEA 200
Purlin	HEA 100
Rafter	IPE 550
Wall brace	RD 30
Roof brace	RD 30

Table 7.2. Load assumptions

Load type	Parameters
Wind load	
Wind zone	Zone 2
Terrain category	Category III
Altitude	70 m
Structure height	10 m
Fundamental wind velocity	25 m/s
Gravity load	
Roofing weight	0.3 kN/m^2
Self-weight	automatically considered

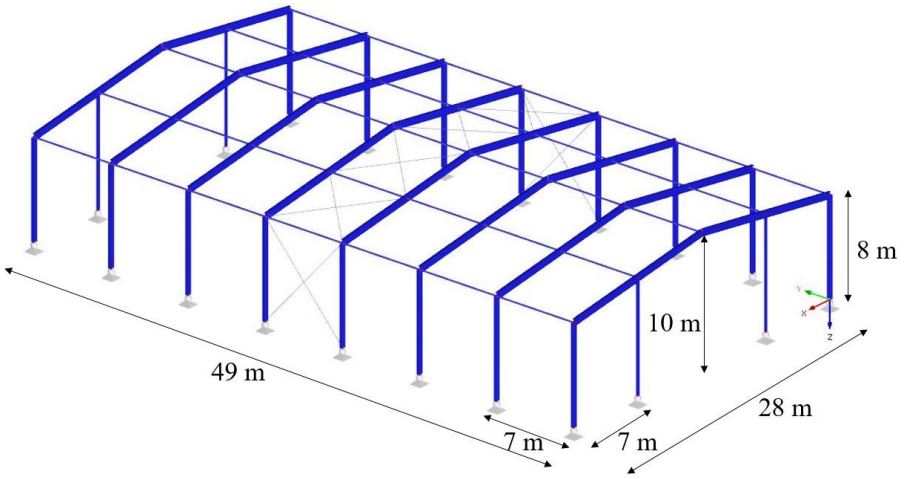

Figure 7.1. Single-story building with bracings (Dimension in m)

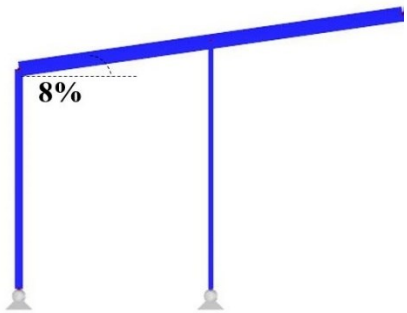

Figure 7.2. Roof inclination

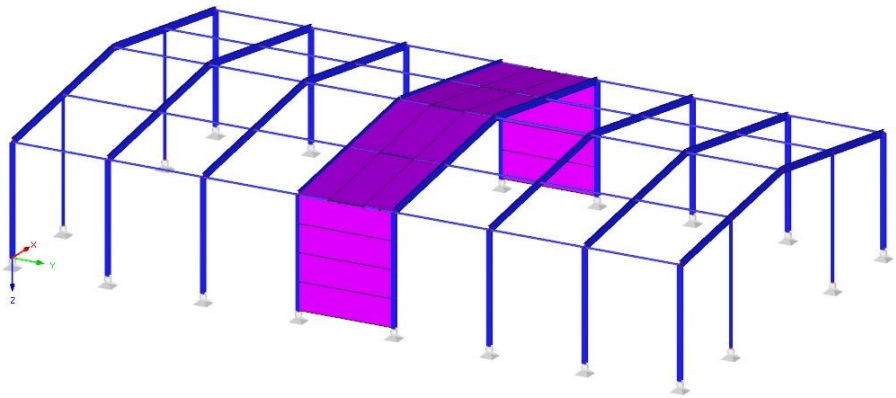

Figure 7.3. Single-story building with sandwich panels

The design outputs, including the different elements, their numbers and types, are summarized in Table 7.3. The employed MW sandwich panels have a size of 7000 mm × 2000 mm × 100 mm. Sandwich panels have an inner sheet thickness of 0.5 mm connected to supporting members by means stainless steel screw of 5.5 mm diameter. Firstly, a single-story building with bracing without claddings is designed under wind and permanent (roofing and self-weight) loads at ambient temperature. The maximum design ratios of the members in ULS (ultimate limit state) are given in Table 7.4. The building fulfills the ULS requirements of the Eurocodes. Then by keeping other elements (columns, rafters and purlins), the bracing of the structure is replaced by sandwich panels. The behavior of the structure is evaluated at ambient and elevated temperatures for both systems.

Table 7.3. Element applied in the single-story building

Element	Cross-section	Length (m)	Number
Wall column	HEA 450	8	16
End column	HEA 280	9	4
Rafter	IPE 550	14.14	16
Purlin	HEA 160	7	35
Wall brace	RD 30	10.63	4
Roof brace	RD 30	9.95	8

Table 7.4. Maximum design ratios of members for the building with bracings

Element	Max Design Ratio
Wall column	0.58
End column	0.92
Rafter	0.79
Purlin	0.86
Wall brace	0.92
Roof brace	0.65

7.3 Stabilization of building at ambient and elevated temperatures

The aim of this section is to compare the stabilization behavior of the buildings with sandwich panels and bracings. Lateral displacements assess stability.

To simplify models, the sandwich panels are considered as shell elements that are rigid in their planes. The panels are located in the same plane as the axes of the columns, considering no eccentricity. Other components, including rafters, columns, purlins and braces, are simulated with wire elements.

The behavior of sandwich panels is incorporated into the structure with fasteners. In other words, the fasteners present the behavior of sandwich panels and their connections to supporting members, which are columns. The resistance and stiffness of spring elements for simulations

are calculated according to the formula from the ECCS manual [9], which determines the shear stiffness and resistance of sandwich panels.

Figure 7.4 shows the spring element, which is the connection between columns and sandwich panels. The properties of the spring element are achieved from the ECCS manual for ambient and elevated temperatures.

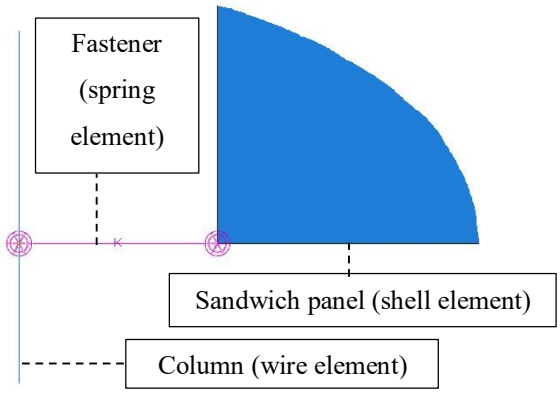

Figure 7.4. Spring element which connects sandwich panels to columns

At elevated temperatures, it is assumed that bracings or sandwich panels are surrounded and affected by the fire. Therefore, Young's modulus and yield stress of fasteners and steel facings of panels and steel bracings are decreased in accordance with the suggested equations and Section 2.5. Figure 7.5 indicates the frame stabilized with bracings and sandwich panels.

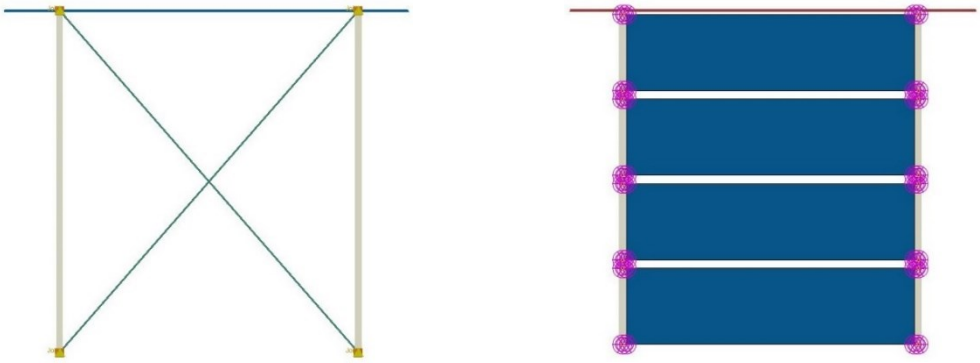

a) b)

Figure 7.5. Frame stabilized with a) bracings, b) sandwich panels

7.4 Results and discussion

In this chapter, two different single-story buildings stabilized with bracings or sandwich panels are compared. The lateral displacement for both structures is calculated and compared with the maximum serviceability limit state (SLS).

In the current example, at ambient temperature, the effect of wind load on stabilized direction is evaluated. The maximum displacement for the structure with sandwich panels is around 38 mm, while the building with bracings shows a displacement of about 25 mm. The maximum serviceability criterion is approximately 67 mm (H/150). Therefore, although the structure with bracings shows stiffer behavior, both systems can meet the suggested requirements. Figure 7.6 compares the lateral displacement for both systems.

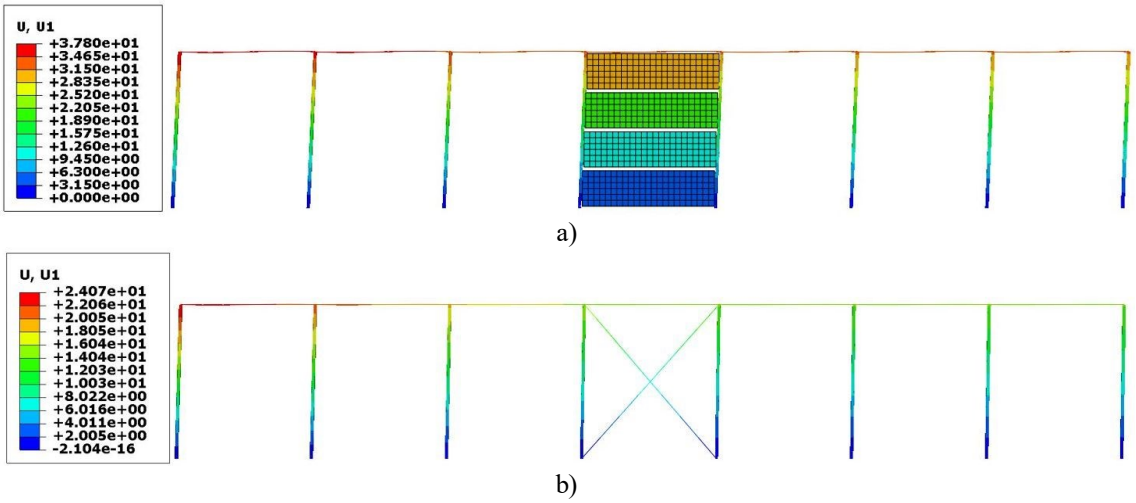

Figure 7.6. Lateral displacement of a) bracings, b) sandwich panels at ambient temperature (in mm)

The sandwich panels are able to provide sufficient lateral restraint to prevent buckling around the weak axis and therefore increase the load-bearing capacity of members. Figure 7.7 illustrates how the sandwich panels can afford excessive lateral restraint to avoid buckling.

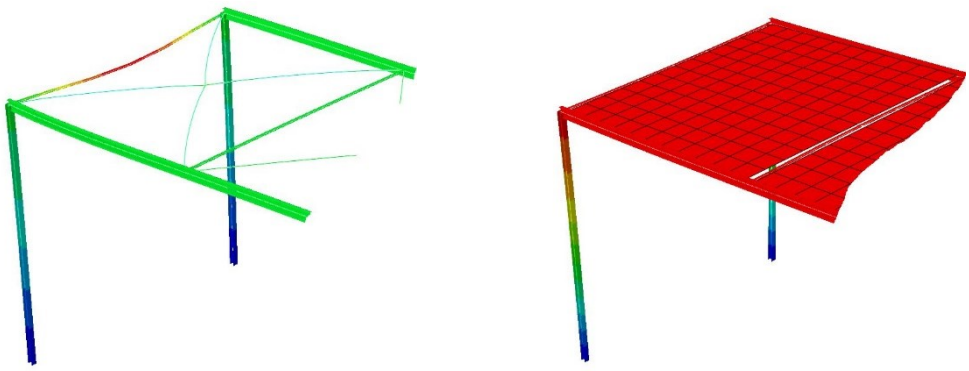

a) b)

Figure 7.7. Buckling around the weak axis of structures stabilized with a) bracings, b) sandwich panels

The building is also analyzed at a temperature of 600 °C. Figure 7.8 shows the deformation of the bracings and sandwich panels under lateral loads. As expected, the maximum displacement of both structures is larger than displacements at ambient temperature. In this case, the maximum displacement for the frame with bracings is around 247 mm, while the building with sandwich panels displays a displacement of about 251 mm. The maximum serviceability

criterion for this example is approximately 333 mm (H/30). As can be seen, the maximum lateral displacement of both structures displays closer values than ones at ambient temperature. Table 7.5 compares the maximum displacement of the frame at ambient and elevated temperatures for both systems.

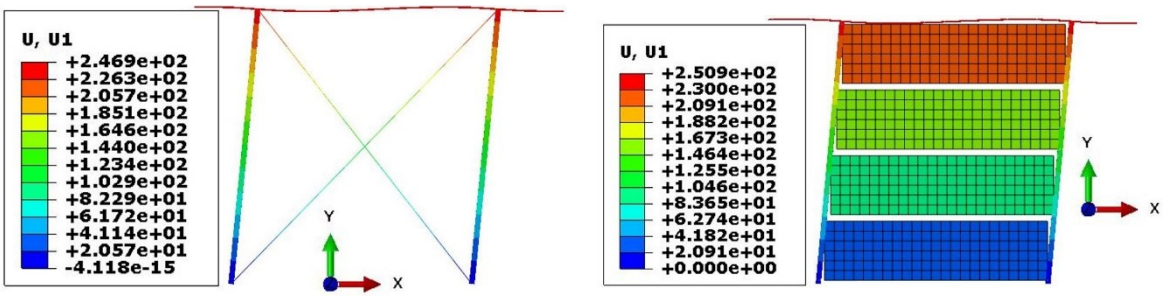

a) b)

Figure 7.8. Lateral displacement of a) bracings, b) sandwich panels (in mm)

Table 7.5. Comparison of maximum displacement at the stabilized direction

Case	Maximum lateral displacement (mm)	Ultimate serviceability criterion (mm)	Temperature (°C)
Building with bracings	25	67	20
Building with bracings	247	333	600
Building with sandwich panels	38	67	20
Building with sandwich panels	251	333	600

In this chapter, the behavior of single-story buildings stabilized with bracings or sandwich panels, for one example, was investigated. The aim of the chapter was to present the practical aspect of the current research. It was shown that sandwich panels might be used as a replacement for diagonal bracings in the structures. Although the bracings demonstrated a stiffer behavior against lateral loads at ambient temperature, both systems fulfilled the Eurocode requirements. At elevated temperatures, both systems exhibited more similar behavior. The possibility to use sandwich panels as stabilizing elements reduces the weight and costs of the frame. Moreover, the implementation of sandwich panels is faster and easier than bracings. Therefore, regarding the economic reasons, the solution to replace diagonal bracings with sandwich panels seems reasonable.

Chapter 8: CONCLUSION AND RECOMMENDATIONS FOR FUTURE RESEARCH

8.1 Summary of work

The thesis includes two parts, the evaluation of sandwich panels under bending and translational loadings. Two different sandwich panels of MW and PIR cores were investigated at ambient and elevated temperatures. The research reviewed the experimental programs shortly and conducted a detailed numerical and analytical study.

Chapter 2 presented a general introduction to sandwich panels and their applications in commercial structures. The performance of sandwich panels under bending, shear and torsional loadings was described. The thermal and mechanical properties of different sandwich panel components were defined. The suggested reduction factors for various parts due to the degradation of material properties at elevated temperatures were introduced.

Chapter 3 presented a short review of the bending test program and provided experimental results. The establishment of numerical models in ABAQUS, including boundary conditions, contact interaction, size, and type of applied elements and employed material properties, was explained. Consequently, the MW and PIR panels' simulations were validated against the experimental results for both mechanical and thermal analyses.

Chapter 4 studied the analytical equations provided by Eurocodes (EN 14509, 2013) to predict the bending stiffness of MW and PIR sandwich panels separately at ambient temperatures. To apply the analytical solution at elevated temperatures, two approaches, "average solution" and "maximum solution," were suggested. Subsequently, a comprehensive parametric study was carried out to investigate the influence of panel thickness, width and span and the facing sheet thickness and temperature on panels' behavior.

Chapter 5 gave a general overview of the translational tests, such as test arrangements, thermal and mechanical loadings and experimental results. The FE models were produced in ABAQUS, and relevant material properties, boundary conditions, contact interactions and elements were assigned. At the end of the chapter, the accuracy of FE models was compared with experimental results.

Chapter 6 studied the ECCS manual's analytical equations to predict the shear resistance and stiffness of MW and PIR sandwich panels at ambient temperatures. Two different approaches, Approach 1 and 2, were proposed to reduce the inner face's tensile strength to enable the ECCS manual's equations to apply at elevated temperatures. Furthermore, an extensive parametric study was performed to assess the effect of different factors such as the screw diameter, the facing sheet thickness and the temperature on connections' behavior. The safety and accuracy of the analytical solutions at elevated temperatures for shear stiffness and resistance were compared with numerical models. At the end of this chapter, an alternative solution was suggested to predict sandwich panel connections' shear stiffness.

Chapter 7 gave an example to present the possibility of using sandwich panels instead of diagonal bracings to stabilize the single-story buildings.

Chapter 8 summarized the works conducted within this thesis and presented the main conclusion and recommendation for future research.

8.2 Main conclusions

Based on the thesis, the following conclusions can be drawn:

- The load-displacement curves of bending models agreed sufficiently well with the tests. The bending resistance of PIR panels at ambient and elevated temperatures was higher than MW panels.
- The panels' inner and outer sheet thicknesses did not play a substantial role in specimens' bending stiffness. For example, an increase of 150% in the inner sheet thickness resulted in just a 7% increase in the bending stiffness of MW panels. On the contrary, the panels' thickness significantly affected the bending stiffness since the thickness parameter greatly influenced the moment of inertia.
- It was found that the width of panels had a direct linear relationship with the bending stiffness while the increase of the span of panels decreased the bending stiffness nonlinearly.
- The bending stiffness and resistance of sandwich panels decreased at elevated temperatures due to the degradation of material properties. Furthermore, it was concluded that the degradation of bending stiffness in the steady-state conditions was independent of panel thickness, width, span and inner and outer thickness of facings.

On the other hand, the panels' geometry did not play an essential role in the reduction rate of bending stiffness.

- At ambient temperature, the bending stiffness of panels was calculated according to equations provided by Eurocodes (EN 14509, 2013) as analytical solutions. In most cases, the analytical solutions gave a reasonable estimation of the numerical results on the safe side. However, some cases showed that analytical results overestimated the bending stiffness; for example, for MW panels with a thickness higher than 160 mm or a width greater than 1800 mm, and PIR panels with a thickness higher than 230 mm or a span shorter than 1500 mm. Nevertheless, this overestimation could be neglected because the difference was insignificant.
- Two approaches called “average solution” and “maximum solution” were suggested to enable the equations of Eurocodes to be applicable at elevated temperatures. The basis of these two methods was according to the reduction of material properties at elevated temperatures. The “average solution” provided an acceptable approximation of numerical results (just for MW panels at temperatures higher than 450 °C, the results were slightly unsafe). In comparison, the “maximum solution” gave extremely conservative results, especially at elevated temperatures. As a result, the “average solution” was recommended to employ at elevated temperatures.
- The FE results of translational models displayed the same failure mode that occurred in the tests, which was a bearing failure of the inner face near the hole of the screw connection. The load-displacement curves provided an excellent agreement between the load-bearing capacities and a reasonable estimation of translational stiffness values. Furthermore, it was found that the reduction in the translational stiffness of panels at elevated temperatures was higher than the shear resistance of panels.
- The results illustrated that sandwich panels' inner sheet thickness was a decisive factor in determining the translational and shear resistance. Even the effect of the inner sheet thickness on the translational stiffness was higher than shear resistance. It was concluded that thinner sheet thicknesses for sandwich panels resulted in higher deformability of connections than thicker inner sheets.
- Although the screw diameter had a slight influence on the load-bearing capacity of connections, the bolts with larger diameters showed higher resistance than the bolts with smaller diameters. Besides, it was observed that the growth rate of shear resistance due to the increase of the screw diameter for panels with thicker inner sheets was higher than

panels with thinner inner sheets. Contrary, the increase in screw diameters led to a reduction in shear stiffness.

- Due to the degradation of material properties at elevated temperatures, shear resistance and stiffness of sandwich panel connections decreased. The PIR sandwich panel connections showed a higher reduction rate of shear resistance and stiffness than MW panels. When the panels had a thinner inner sheet, the decrease rate of shear resistance and stiffness was higher than panels with a thicker inner sheet. The results showed that the influence of screw diameter on the shear resistance at elevated temperatures was less than ambient temperatures.
- According to the ECCS manual, two approaches were introduced in the analytical study to determine the shear stiffness and resistance of sandwich panel connections. In general, Approach 2 was more conservative than Approach 1. For all specimens with an inner sheet thickness of 0.4 mm and 0.5 mm, both approaches provided safe results for shear resistance; however, the outputs obtained from Approach 1 were closer to numerical results. Approach 2 was safe and very conservative when calculating the shear stiffness of panels. Except for 6.3 mm and 8.0 mm screw diameters, Approach 1 gave safe results for all specimens' shear stiffness.
- In this research, a reduction coefficient was defined to simplify the calculation of shear stiffness at elevated temperatures. This reduction factor was obtained from numerical results at different temperatures and added to the equation calculating the shear stiffness. Therefore, Approach 1 was recommended to calculate the shear resistance of panels and the suggested reduction factor as an additional multiplier was found suitable to predict the shear stiffness of panels.
- The single-story buildings were stabilized with two approaches, just with sandwich panels or just with diagonal bracings. In one practical example, it was shown that sandwich panels could be an alternative for bracing systems at ambient and elevated temperatures.
- Since the implementation of diagonal bracing is costly and time-consuming and requires expert workers for preparation and welding, this idea comes to mind to replace them with sandwich panels that are cheaper and faster to install. This research showed that the utility of sandwich panels instead of steel bracing is possible at ambient and elevated temperatures. In addition, since the sandwich panels provide translational stiffness, they can be employed in the case of an earthquake as an alternative for steel bracings.

8.3 Recommendations for future research

The following further research studies may be carried out to improve knowledge in this area:

- Further experimental research studies should be carried out at elevated temperatures, especially in translational tests. By conducting a large number of experimental investigations, the possible inaccuracies caused by initial imperfections are considerably reduced.
- There are still uncertainties associated with MW and PIR mechanical properties at elevated temperatures. Performing tensile and compressive tests at elevated temperatures to achieve accurate mechanical properties is highly recommended.
- The behavior of adhesive materials between cores and facings is not clear at elevated temperatures. Therefore, the decomposition of adhesive materials at elevated temperatures and the consideration of their effect in simulations should be investigated.
- In this research, the interaction between core materials and upper sheets is considered a "Tie." Simulating the exact material properties between facings and cores can influence the results.
- For future studies, it is worth considering specimens' behavior after the maximum load until the final damage.
- The proposed analytical solutions at elevated temperatures consider only the degradation of materials. The initial imperfections due to the elevated temperatures are not considered in these equations. Therefore, the given values are sometimes overestimated. Proposing new equations at elevated temperatures which can consider both material degradation and initial imperfection due to the fire effect is recommended.

REFERENCES

[1] J.M. Davies, Lightweight sandwich construction, Blackwell Science, Oxford, 2001.

[2] A. Rahimijonoush, M. Bayat, Experimental and numerical studies on the ballistic impact response of titanium sandwich panels with different facesheets thickness ratios, Thin-Walled Structures 157 (2020) 107079. https://doi.org/10.1016/j.tws.2020.107079.

[3] J.R. Vinson, The behavior of sandwich structures of isotropic and composite materials, Technomic Publishing Co, Lancaster, Pa., 1999.

[4] A. Farrokhabadi, S. Ahmad Taghizadeh, H. Madadi, H. Norouzi, A. Ataei, Experimental and numerical analysis of novel multi-layer sandwich panels under three point bending load, Composite Structures 250 (2020) 112631. https://doi.org/10.1016/j.compstruct.2020.112631.

[5] A.K. Noor, W.S. Burton, C.W. Bert, Computational Models for Sandwich Panels and Shells, Appl. Mech. Rev 49 (1996) 155–199. https://doi.org/10.1115/1.3101923.

[6] R. Studziński, Z. Pozorski, Experimental and numerical analysis of sandwich panels with hybrid core, Jnl of Sandwich Structures & Materials 20 (2018) 271–286. https://doi.org/10.1177/1099636216646789.

[7] P. van HEES, Fire behaviour of sandwich panels, in: Flammability Testing of Materials Used in Construction, Transport and Mining, Elsevier, 2006, pp. 149–163.

[8] K. Mela, Steel cladding systems for stabilization of steel buildings in fire, STABFI project, 2020.

[9] ECCS, European Recommendations on the Stabilization of Steel Structures by Sandwich Panels, ECCS (2013).

[10] E. Hedman-Petursson, Column buckling with restraint from sandwich wall elements, 2016.

[11] Y.W. Mai, Performance evaluation of sandwich panels subjected to bending compression and thermal bowing, Matériaux et Constructions 13 (1980) 159–168. https://doi.org/10.1007/BF02473562.

[12] K. Cinar, Evaluation of sandwich panels with composite tube-reinforced foam core under bending and flatwise compression, Jnl of Sandwich Structures & Materials 22 (2020) 480–493. https://doi.org/10.1177/1099636218798161.

[13] S.A. Medina, J.M. Meza, L.F. Kawashita, Damage sequence of honeycomb sandwich panels under bending loading: Experimental and numerical investigation, Journal of Reinforced Plastics and Composites 39 (2020) 175–192. https://doi.org/10.1177/0731684419880970.

[14] M.F. Ashby, Hybrids to fill holes in material property space, Philosophical Magazine 85 (2005) 3235–3257. https://doi.org/10.1080/14786430500079892.

[15] M.F. ASHBY, D. CEBON, Materials selection in mechanical design, J. Phys. IV France 03 (1993) C7-1-C7-9. https://doi.org/10.1051/jp4:1993701.

[16] T. Misiek, S. Käpplein, M. Dürr, H. Saal, Stabilisation of beams by sandwich panels - new regulations and recent research results, Karlsruhe, 2010.

[17] Käpplein, S., Misiek, T., EASIE-Connections of sandwich panels: EASIE project Deliverable D3.3 – part 3 (2011).

[18] Z. Pozorski, Numerical analysis of sandwich panels subjected to torsion, in: Selected topics in contemporary mathematical modeling, Publishing Office of Czestochowa University of Technology, Częstochowa, 2017, pp. 109–122.

[19] X. Li, G. Li, C.H. Wang, Optimisation of Composite Sandwich Structures Subjected to Combined Torsion and Bending Stiffness Requirements, Appl Compos Mater 19 (2012) 689–704. https://doi.org/10.1007/s10443-011-9221-z.
[20] M.E. Nemirovskii, Torsional rigidity of outer sheaths of flexible medical endoscopes, Biomed Eng 28 (1994) 262–264. https://doi.org/10.1007/BF00556689.
[21] M. Dürr, Die Stabilisierung biegedrillknickgefährdeter Trager durch Sandwichelemente und Trapezbleche, Karlsruher Institut für Technologie, 2008.
[22] M Georgescu, V Ungureanu, D Dubina, Diaphragm effect in sandwich panel roofing–Experimental approach, 6th European Conference on Steel and Composite Structures, in Hungary, 2011.
[23] M. Georgescu, V. Ungureanu, Stabilisation of continuous Z-purlins by sandwich panels: Full scale experimental approach, Thin-Walled Structures 81 (2014) 242–249. https://doi.org/10.1016/j.tws.2013.09.017.
[24] T.Z. Harmathy, Research, National Research Council of Canada. Division of Building, Design of Buildings for Fire Safety, ASTM International, 1976.
[25] Canadian Wood Council, Fire Safety Design in Buildings, CWC: Canadian Wood Council, 2001.
[26] B. Nagy, E. Tóth, Finite Element Analysis of Composite Ceramic-Concrete Slab Constructions Exposed to Fire, AMM 861 (2016) 88–95. https://doi.org/10.4028/www.scientific.net/AMM.861.88.
[27] TZ Harmathy, Design Approach to Fire Safety in Buildings, fire.tc.faa.gov, 1974.
[28] P.J. Moss, R.P. Dhakal, M.W. Bong, A.H. Buchanan, Design of steel portal frame buildings for fire safety, Journal of Constructional Steel Research 65 (2009) 1216–1224. https://doi.org/10.1016/j.jcsr.2008.09.003.
[29] J. Jiang, Y. Lu, X. Dai, G.-Q. Li, W. Chen, J. Ye, Disproportionate collapse of steel-framed gravity buildings under travelling fires, Engineering Structures 245 (2021) 112799. https://doi.org/10.1016/j.engstruct.2021.112799.
[30] T. Gernay, N.E. Khorasani, Recommendations for performance-based fire design of composite steel buildings using computational analysis, Journal of Constructional Steel Research 166 (2020) 105906. https://doi.org/10.1016/j.jcsr.2019.105906.
[31] L. Chapelle, A. Lyckegaard, Y. Kusano, C. Gundlach, M.R. Foldschack, D. Lybye, P. Brøndsted, Determination of the fibre orientation distribution of a mineral wool network and prediction of its transverse stiffness using X-ray tomography, J Mater Sci 53 (2018) 6390–6402. https://doi.org/10.1007/s10853-018-2044-7.
[32] I.D. Thanasoulas, I.K. Vardakoulias, D.I. Kolaitis, C.J. Gantes, M.A. Founti, Thermal and Mechanical Computational Study of Load-Bearing Cold-Formed Steel Drywall Systems Exposed to Fire, Fire Technol 52 (2016) 2071–2092. https://doi.org/10.1007/s10694-016-0604-4.
[33] F. Liu, F. Fu, Y. Wang, Q. Liu, Fire performance of non-load-bearing light-gauge slotted steel stud walls, Journal of Constructional Steel Research 137 (2017) 228–241. https://doi.org/10.1016/j.jcsr.2017.06.034.
[34] H.B. Wang, Heat transfer analysis of components of construction exposed to fire, University of Salford (United Kingdom) ProQuest Dissertations Publishing, 1995.
[35] M. Gravit, A. Kuleshin, E. Khametgalieva, I. Karakozova, Technical characteristics of rigid sprayed PUR and PIR foams used in construction industry, IOP Conf. Ser.: Earth Environ. Sci. 90 (2017) 12187. https://doi.org/10.1088/1755-1315/90/1/012187.

[36] D. Figueira, J. Sena-Cruz, E. Pereira, I. Valente, J. Barros, F. Castro, D. Soares, Influence of service temperature on shear creep behaviour of a rigid low-density closed-cell PIR foam, Construction and Building Materials 225 (2019) 1052–1063. https://doi.org/10.1016/j.conbuildmat.2019.07.337.
[37] I. Vitkauskiene, R. Makuska, U. Stirna, U. Cabulis, Synthesis and physical-mechanical properties of polyurethane-polyisocyanurate foams based on PET-waste-derived modified polyols, Journal of Cellular Plastics 47 (2011) 467–482. https://doi.org/10.1177/0021955X11409494.
[38] W. Zatorski, Z.K. Brzozowski, A. Kolbrecki, New developments in chemical modification of fire-safe rigid polyurethane foams, Polymer Degradation and Stability 93 (2008) 2071–2076. https://doi.org/10.1016/j.polymdegradstab.2008.05.032.
[39] B. Czupryński, J. Paciorek-Sadowska, J. Liszkowska, Properties of rigid polyurethane-polyisocyanurate foams modified with the selected fillers, J. Appl. Polym. Sci. 115 (2010) 2460–2469. https://doi.org/10.1002/app.30937.
[40] M. Du, C. He, C. Zhou, Flame Retardant Effect of Isocyanate Trimer on Polyisocyanurate Foam, JPSE 1 (2018). https://doi.org/10.24294/jpse.v1i1.320.
[41] K. Chen, C. Tian, F. Cao, S. Liang, X. Jia, J. Wang, Preparation and characterization of highly thermostable polyisocyanurate foams modified with epoxy resin, J. Appl. Polym. Sci. 133 (2016) n/a-n/a. https://doi.org/10.1002/app.43085.
[42] E. Iffa, F. Tariku, W.Y. Simpson, Highly Insulated Wall Systems with Exterior Insulation of Polyisocyanurate under Different Facer Materials: Material Characterization and Long-Term Hygrothermal Performance Assessment, Materials (Basel) 13 (2020) 3373. https://doi.org/10.3390/ma13153373.
[43] Y.C. Wang, A. Foster, Experimental and numerical study of temperature developments in PIR core sandwich panels with joint, Fire Safety Journal 90 (2017) 1–14. https://doi.org/10.1016/j.firesaf.2017.03.003.
[44] N. Boissonnade, Rules for member stability in EN 1993-1-1: Background documentation and design guidelines, European Convention for Constructional Steelwork, Brussels, 2006.
[45] European Committee for Standardisation, EN 1993-1-2: Eurocode 3: Design of steel structures - Part 1-2: General rules - Structural fire design.
[46] H.D. Craveiro, J.P.C. Rodrigues, A. Santiago, L. Laím, Review of the high temperature mechanical and thermal properties of the steels used in cold formed steel structures – The case of the S280 Gd+Z steel, Thin-Walled Structures 98 (2016) 154–168. https://doi.org/10.1016/j.tws.2015.06.002.
[47] J.H. Lee, M. Mahendran, P. Makelainen, Prediction of mechanical properties of light gauge steels at elevated temperatures, Journal of Constructional Steel Research 59 (2003) 1517–1532. https://doi.org/10.1016/S0143-974X(03)00087-7.
[48] J. Outinen, P. Mäkeläinen, Mechanical properties of structural steel at elevated temperatures and after cooling down, Fire Mater. 28 (2004) 237–251. https://doi.org/10.1002/fam.849.
[49] T. Ranawaka, M. Mahendran, Experimental study of the mechanical properties of light gauge cold-formed steels at elevated temperatures, Fire Safety Journal 44 (2009) 219–229. https://doi.org/10.1016/j.firesaf.2008.06.006.
[50] Q. Wu, L. Ma, L. Wu, J. Xiong, A novel strengthening method for carbon fiber composite lattice truss structures, Composite Structures 153 (2016) 585–592. https://doi.org/10.1016/j.compstruct.2016.06.060.

[51] I.G. Colombo, M. Colombo, M. Di Prisco, F. Pouyaei, Analytical and numerical prediction of the bending behaviour of textile reinforced concrete sandwich beams, Journal of Building Engineering 17 (2018) 183–195. https://doi.org/10.1016/j.jobe.2018.02.012.
[52] R. Juntikka, S. Hallstrom, Shear Characterization of Sandwich Core Materials Using Four-point Bending, Jnl of Sandwich Structures & Materials 9 (2007) 67–94. https://doi.org/10.1177/1099636207070574.
[53] S. Huang, B. Samali, J. Li, Numerical and experimental investigations of a thermal break composite façade mullion under four-point bending, Journal of Building Engineering (2020) 101590. https://doi.org/10.1016/j.jobe.2020.101590.
[54] A. Elmushyakhi, Collapse mechanisms of out-of-plane preload composite sandwich beams under in-plane loading, Journal of Building Engineering 26 (2019) 100875. https://doi.org/10.1016/j.jobe.2019.100875.
[55] H. Taghipoor, A. Eyvazian, F. Musharavati, T.A. Sebaey, A. Ghiaskar, Experimental investigation of the three-point bending properties of sandwich beams with polyurethane foam-filled lattice cores, Structures 28 (2020) 424–432. https://doi.org/10.1016/j.istruc.2020.08.082.
[56] M. Kazemi, Experimental analysis of sandwich composite beams under three-point bending with an emphasis on the layering effects of foam core, Structures 29 (2021) 383–391. https://doi.org/10.1016/j.istruc.2020.11.048.
[57] B.P. Russell, T. Liu, N.A. Fleck, V.S. Deshpande, 2011. Quasi-Static Three-Point Bending of Carbon Fiber Sandwich Beams with Square Honeycomb Cores. J. Appl. Mech 78, 031008. https://doi.org/10.1115/1.4003221.
[58] F. Zhang, R. Mohmmed, B. Sun, B. Gu, Damage Behaviors of Foam Sandwiched Composite Materials Under Quasi-Static Three-point Bending, Appl Compos Mater 20 (2013) 1231–1246. https://doi.org/10.1007/s10443-013-9329-4.
[59] C. Yan, X. Song, H. Zhu, C. Jing, S. Feng, Flexural response of carbon fiber reinforced aluminum foam sandwich, Journal of Composite Materials 52 (2018) 1887–1897. https://doi.org/10.1177/0021998317735166.
[60] J.P. Vitale, G. Francucci, J. Xiong, A. Stocchi, Failure mode maps of natural and synthetic fiber reinforced composite sandwich panels, Composites Part A: Applied Science and Manufacturing 94 (2017) 217–225. https://doi.org/10.1016/j.compositesa.2016.12.021.
[61] P. Paczos, R. Wichniarek, K. Magnucki, Three-point bending of sandwich beam with special structure of the core, Composite Structures 201 (2018) 676–682. https://doi.org/10.1016/j.compstruct.2018.06.077.
[62] C.A. Steeves, N.A. Fleck, Collapse mechanisms of sandwich beams with composite faces and a foam core, loaded in three-point bending. Part I: analytical models and minimum weight design, International Journal of Mechanical Sciences 46 (2004) 561–583. https://doi.org/10.1016/j.ijmecsci.2004.04.003.
[63] F. Zhang, W. Liu, L. Wang, Y. Qi, D. Zhou, H. Fang, Flexural behavior of hybrid composite beams with a bamboo layer and lattice ribs, Journal of Reinforced Plastics and Composites 34 (2015) 521–533. https://doi.org/10.1177/0731684415573811.
[64] F. Meraghni, F. Desrumaux, M.L. Benzeggagh, Mechanical behaviour of cellular core for structural sandwich panels, Composites Part A: Applied Science and Manufacturing 30 (1999) 767–779. https://doi.org/10.1016/S1359-835X(98)00182-1.
[65] A.G. Mamalis, K.N. Spentzas, N.G. Pantelelis, D.E. Manolakos, M.B. Ioannidis, A new hybrid concept for sandwich structures, Composite Structures 83 (2008) 335–340. https://doi.org/10.1016/j.compstruct.2007.05.002.

[66] R. Umer, E.M. Waggy, M. Haq, A.C. Loos, Experimental and numerical characterizations of flexural behavior of VARTM-infused composite sandwich structures, Journal of Reinforced Plastics and Composites 31 (2012) 67–76. https://doi.org/10.1177/0731684411431357.
[67] J. Zhang, X. Hu, W. Hong, B. Zhang, C. Zhang, Experimental Study on Bending Performance of Composite Sandwich Panel with New Mixed Core, MATEC Web Conf. 275 (2019) 2018. https://doi.org/10.1051/matecconf/201927502018.
[68] S.V. Iyer, R. Chatterjee, M. Ramya, E. Suresh, K. Padmanabhan, A Comparative Study Of The Three Point And Four Point Bending Behaviour Of Rigid Foam Core Glass/Epoxy Face Sheet Sandwich Composites, Materials Today: Proceedings 5 (2018) 12083–12090. https://doi.org/10.1016/j.matpr.2018.02.184.
[69] F. Mujika, On the difference between flexural moduli obtained by three-point and four-point bending tests, Polymer Testing 25 (2006) 214–220. https://doi.org/10.1016/j.polymertesting.2005.10.006.
[70] O. Murthy, N. Munirudrappa, L. Srikanth, R.M.V.G.K. Rao, Strength and Stiffness Optimization Studies on Honeycomb Core Sandwich Panels, Journal of Reinforced Plastics and Composites 25 (2006) 663–671. https://doi.org/10.1177/0731684406058288.
[71] H. Herranen, O. Pabut, M. Eerme, J. Majak, M. Pohlak, J. Kers, M. Saarna, G. Allikas, A. Aruniit, Design and Testing of Sandwich Structures with Different Core Materials, ms 18 (2012). https://doi.org/10.5755/j01.ms.18.1.1340.
[72] S. Srivaro, N. Matan, F. Lam, Stiffness and strength of oil palm wood core sandwich panel under center point bending, Materials & Design 84 (2015) 154–162. https://doi.org/10.1016/j.matdes.2015.06.097.
[73] A. Petras, M. Sutcliffe, Failure mode maps for honeycomb sandwich panels, Composite Structures 44 (1999) 237–252. https://doi.org/10.1016/S0263-8223(98)00123-8.
[74] L.L. Yan, B. Han, B. Yu, C.Q. Chen, Q.C. Zhang, T.J. Lu, Three-point bending of sandwich beams with aluminum foam-filled corrugated cores, Materials & Design (1980-2015) 60 (2014) 510–519. https://doi.org/10.1016/j.matdes.2014.04.014.
[75] M. He, W. Hu, A study on composite honeycomb sandwich panel structure, Materials & Design (1980-2015) 29 (2008) 709–713. https://doi.org/10.1016/j.matdes.2007.03.003.
[76] T. Kawasaki, M. Zhang, Q. Wang, K. Komatsu, S. Kawai, Elastic moduli and stiffness optimization in four-point bending of wood-based sandwich panel for use as structural insulated walls and floors, J Wood Sci 52 (2006) 302–310. https://doi.org/10.1007/s10086-005-0766-z.
[77] J. Kim, S.R. Swanson, Design of sandwich structures for concentrated loading, Composite Structures 52 (2001) 365–373. https://doi.org/10.1016/S0263-8223(01)00027-7.
[78] J. Daniel Ronald Joseph, J. Prabakar, P. Alagusundaramoorthy, Flexural behavior of precast concrete sandwich panels under different loading conditions such as punching and bending, Alexandria Engineering Journal 57 (2018) 309–320. https://doi.org/10.1016/j.aej.2016.11.016.
[79] M. Mahendran, S. Subaaharan, Shear Strength of Sandwich Panel Systems, Australian Journal of Structural Engineering 3 (2002) 115–126. https://doi.org/10.1080/13287982.2002.11464899.
[80] G. de Matteis, R. Landolfo, Mechanical fasteners for cladding sandwich panels, Thin-Walled Structures 35 (1999) 61–79. https://doi.org/10.1016/S0263-8231(99)00017-8.

[81] T. Misiek, S. Käpplein, D. Ulbrich, Selecting materials for fastening screws for metal members and sheeting, Steel Construction 6 (2013) 39–46. https://doi.org/10.1002/stco.201300009.
[82] W. Lu, Z. Ma, P. Mäkeläinen, J. Outinen, Design of shot nailed steel sheeting connection at ambient and elevated temperatures, Engineering Structures 49 (2013) 963–972. https://doi.org/10.1016/j.engstruct.2012.12.034.
[83] C.A. Rogers, G.J. Hancock, Failure Modes of Bolted-Sheet-Steel Connections Loaded in Shear, J. Struct. Eng. 126 (2000) 288–296. https://doi.org/10.1061/(ASCE)0733-9445(2000)126:3(288).
[84] K. Chung, K. Ip, Finite element investigation on the structural behaviour of cold-formed steel bolted connections, Engineering Structures 23 (2001) 1115–1125. https://doi.org/10.1016/S0141-0296(01)00006-2.
[85] T. Soo Kim, H. Kuwamura, Finite element modeling of bolted connections in thin-walled stainless steel plates under static shear, Thin-Walled Structures 45 (2007) 407–421. https://doi.org/10.1016/j.tws.2007.03.006.
[86] T.S. Kim, B.S. Han, Numerical Simulation and Effect of Curling on Bolted Connections in Cold-formed Stainless Steel, ISIJ Int. 47 (2007) 920–929. https://doi.org/10.2355/isijinternational.47.920.
[87] S. Yan, B. Young, Tests of single shear bolted connections of thin sheet steels at elevated temperatures—Part I: Steady state tests, Thin-Walled Structures 49 (2011) 1320–1333. https://doi.org/10.1016/j.tws.2011.05.013.
[88] W. Lu, P. Mäkeläinen, J. Outinen, Z. Ma, Design of screwed steel sheeting connection at ambient and elevated temperatures, Thin-Walled Structures 49 (2011) 1526–1533. https://doi.org/10.1016/j.tws.2011.07.014.
[89] W. Lu, P. Makelainen, J. Outinen, Finite Element Modeling of Single Lap Shear Screw Connection in Steel Sheeting in Fire, TOBCTJ 2 (2008) 257–261. https://doi.org/10.2174/1874836800802010257.
[90] Cábová K., Arha T., Lišková N., Wald F., Experimental investigation of stiffness in bending of sandwich panels at elevated temperatures, The 6th international Applications of Structural Fire Engineering (ASFE'19) (2019), in Singapore, p. 1-6.
[91] H. Pasternak, A. Shoushtarian Mofrad, Numerical and Analytical Study on Bending Stiffness of Sandwich Panels at Ambient and Elevated Temperatures, Construction of Unique Buildings and Structures 94 (2021) 9405. https://doi.org/10.4123/CUBS.94.5.
[92] M. Alzerreca, M. Paris, O. Boyron, D. Orditz, G. Louarn, O. Correc, Mechanical properties and molecular structures of virgin and recycled HDPE polymers used in gravity sewer systems, Polymer Testing 46 (2015) 1–8. https://doi.org/10.1016/j.polymertesting.2015.06.012.
[93] L.H. Sperling, Introduction to physical polymer science, fourth ed., Wiley, New York, Chichester, 2006.
[94] I. Gnip, S. Vėjelis, V. Keršulis, S. Vaitkus, Strength and deformability of mineral wool slabs under short-term compressive, tensile and shear loads, Construction and Building Materials 24 (2010) 2124–2134. https://doi.org/10.1016/j.conbuildmat.2010.04.047.
[95] E. Mıhlayanlar, Ş. Dilmaç, A. Güner, Analysis of the effect of production process parameters and density of expanded polystyrene insulation boards on mechanical properties and thermal conductivity, Materials & Design 29 (2008) 344–352. https://doi.org/10.1016/j.matdes.2007.01.032.
[96] Dassault Systemes, ABAQUS, Version 2017.

[97] J.-B. Yan, H.-N. Guan, T. Wang, Finite element analysis for flexural behaviours of SCS sandwich beams with novel enhanced C-channel connectors, Journal of Building Engineering 31 (2020) 101439. https://doi.org/10.1016/j.jobe.2020.101439.
[98] W.-J. Mao, W.-D. Wang, W. Xian, Numerical analysis on fire performance of steel-reinforced concrete-filled steel tubular columns with square cross-section, Structures 28 (2020) 1–16. https://doi.org/10.1016/j.istruc.2020.08.043.
[99] Z. Li, W. Chen, H. Hao, Numerical study of sandwich panel with a new bi-directional Load-Self-Cancelling (LSC) core under blast loading, Thin-Walled Structures 127 (2018) 90–101. https://doi.org/10.1016/j.tws.2018.02.003.
[100] A. Pournaghshband, S. Afshan, M. Theofanous, Elevated temperature performance of restrained stainless steel beams, Structures 22 (2019) 278–290. https://doi.org/10.1016/j.istruc.2019.08.015.
[101] R. Ding, S. Fan, G. Chen, C. Li, E. Du, C. Liu, Fire resistance design method for restrained stainless steel H-section columns under axial compression, Fire Safety Journal 108 (2019) 102837. https://doi.org/10.1016/j.firesaf.2019.102837.
[102] CEN European Committee for Standardization, EN 14509, 2013. Self-supporting double skin metal faced insulating panels — Factory made products — Specifications: BS. Brussels, 2013.
[103] V. Saxena, M. Krief, L. Adam (Eds.), Handbook of Borehole Acoustics and Rock Physics for Reservoir Characterization, Elsevier Science, San Diego, CA, USA, 2018.
[104] T.N. Chakherlou, M.J. Razavi, B. Abazadeh, Finite element investigations of bolt clamping force and friction coefficient effect on the fatigue behavior of aluminum alloy 2024-T3 in double shear lap joint, Engineering Failure Analysis 29 (2013) 62–74. https://doi.org/10.1016/j.engfailanal.2012.11.004.
[105] Käpplein S, Misiek T. Ensuring advancement in sandwich construction through innovation and exploitation (EASIE). Deliverable D3.3 – part 3. Connections of sandwich panels. Karlsruhe: Karlsruhe Institute of Technology (KIT); 2011.

APPENDICES

Appendix A. CALCULATION EXAMPLE OF PREDICTING BENDING STIFFNESS OF MW PANELS AT AMBIENT AND ELEVATED TEMPERATURES

The parameters of the MW panel at ambient temperature:

L=7000 mm, D=100 mm, B=1200 mm, t_{F1}=0.6 mm, t_{F2}=0.5 mm, E_f=200000 MPa, E_c=4.47 MPa, G_c=2.17 MPa, v_c=0.03, θ=20 °C.

$$k_b = \frac{F}{v_{max}} = \frac{q.L}{v_{max}} = \frac{384B_s}{5L^3(1+3.2k)}$$

$$B_S = e^2 \frac{E_{F1}A_{F1}.E_{F2}A_{F2}}{(E_{F1}A_{F1}+E_{F2}A_{F2})}$$

$$k = \frac{3B_S}{L^2G_cA_c} = \frac{3B_S}{L^2G_cBD}$$

$$B_S = 100.55^2 \times \frac{200000 \times 0.6 \times 1200 \times 200000 \times 0.5 \times 1200}{(200000 \times 0.6 \times 1200 + 200000 \times 0.5 \times 1200)} = 6.6176 \times 10^{11}$$

$$k = \frac{3 \times 6.6176 \times 10^{11}}{(7000 - 2 \times 75)^2 \times 2.17 \times 1200 \times 100} = 0.16248$$

$$k_{b,20} = \frac{384 \times 6.6176 \times 10^{11}}{5 \times 6850^3 \times (1 + 3.2 \times 0.16248)} = 104.0304\ N/mm = 0.104\ kN/mm$$

The parameters of the MW panel at 600 °C:

L=7000 mm, D=100 mm, B=1200 mm, t_{F1}=0.6 mm, t_{F2}=0.5 mm, E_f=200000 MPa, E_c=4.47 MPa, G_c=2.17 MPa, v_c=0.03, θ=600 °C.

$$B_{S,\theta} = e^2 \frac{E_{F1}A_{F1}.E_{F2,\theta}A_{F2}}{(E_{F1}A_{F1}+E_{F2,\theta}A_{F2})}$$

$$k_\theta = \frac{3B_{S,\theta}}{L^2G_{c,\theta}A_c} = \frac{3B_{S,\theta}}{L^2G_{c,\theta}BD}$$

$$k_{b,\theta} = \frac{384B_{s,\theta}}{5L^3(1+3.2k_\theta)}$$

$$B_{S,600} = 100.55^2 \times \frac{200000 \times 0.6 \times 1200 \times 200000 \times 0.0305 \times 0.5 \times 1200}{(200000 \times 0.6 \times 1200 + 200000 \times 0.0305 \times 0.5 \times 1200)}$$

$$= 2.9504 \times 10^{11}$$

$$E_{c,600,avg} = \frac{3.2 \times 1.11 + 0.8 \times 1.67 + 0.4 \times 2.23 + 0.6 \times 4.47}{5} = 1.68$$

$$E_{c,600,max} = 0.25 \times 4.47 = 1.11$$

$$k_{600,avg} = \frac{3 \times 2.9504 \times 10^{11}}{(7000 - 2 \times 75)^2 \times 0.8155 \times 1200 \times 100} = 0.192755$$

$$k_{600,max} = \frac{3 \times 2.9504 \times 10^{11}}{(7000 - 2 \times 75)^2 \times 0.5388 \times 1200 \times 100} = 0.29173$$

$$k_{b,600,avg} = \frac{384 \times 2.9504 \times 10^{11}}{5 \times 6850^3 \times (1 + 3.2 \times 0.192755)} = 43.603209\ N/mm = 0.043\ kN/mm$$

$$k_{b,600,max} = \frac{384 \times 2.9504 \times 10^{11}}{5 \times 6850^3 \times (1 + 3.2 \times 0.29173)} = 36.4604\ N/mm = 0.036\ kN/mm$$

Appendix B. CALCULATION EXAMPLE OF PREDICTING BENDING STIFFNESS OF PIR PANELS AT AMBIENT AND ELEVATED TEMPERATURES

The parameters of the PIR panel at ambient temperatures:

L=7000 mm, D=100 mm, B=1000 mm, t_{Fl}= 0.5 mm, t_{F2}=0.4 mm, E_f=200000 MPa, E_c=9 MPa, G_c=3.48 MPa, v_c=0.03, e=108.18 mm, θ=20 °C.

$$k_b = \frac{384B_s}{5L^3(1+3.2k)(1-\beta)}$$

$$\beta = \frac{B_{F1}}{B_{F1} + \frac{B_s}{1+3.2k}}$$

$$B_{F1} = E_{F1}I_{F1}$$

$$B_S = e^2 \frac{E_{F1}A_{F1}.E_{F2}A_{F2}}{(E_{F1}A_{F1} + E_{F2}A_{F2})}$$

$$k = \frac{3B_S}{L^2G_cA_c} = \frac{3B_S}{L^2G_cBD}$$

$$B_S = 108.18^2 \times \frac{200000 \times 0.5 \times 1000 \times 200000 \times 0.4 \times 1000}{(200000 \times 0.5 \times 1000 + 200000 \times 0.4 \times 1000)} = 5.5652 \times 10^{11}$$

$$k = \frac{3 \times 5.5652 \times 10^{11}}{(7000 - 2 \times 150)^2 \times 3.48 \times 1000 \times 100} = 0.106627$$

$$B_{F1} = 200000 \times 73089.4 = 14617880000\ N.mm^2$$

$$\beta = \frac{14617880000}{14617880000 + \frac{5.5652 \times 10^{11}}{1 + 3.2 \times 0.106627}} = 0.034027$$

$$k_{b,20} = \frac{384 \times 5.5652 \times 10^{11}}{5 \times 6700^3 \times (1 + 3.2 \times 0.106627) \times (1 - 0.034027)} = 109.697\ N/mm$$

$$= 0.109\ kN/mm$$

The parameters of the PIR panel at 300 °C:

L=7000 mm, D=100 mm, B=1000 mm, t_{Fl}= 0.5 mm, t_{F2}=0.4 mm, E_f=200000 MPa, E_c=9 MPa, G_c=3.48 MPa, v_c=0.03, e=108.18 mm, θ=300 °C.

$$k_{b,\theta} = \frac{384B_{s,\theta}}{5L^3(1+3.2k_\theta)(1-\beta_\theta)}$$

$$\beta_\theta = \frac{B_{F1}}{B_{F1} + \frac{B_{S,\theta}}{1+3.2k_\theta}}$$

$$B_{F1} = E_{F1}I_{F1}$$

$$B_{S,\theta} = e^2 \frac{E_{F1}A_{F1}.E_{F2,\theta}A_{F2}}{(E_{F1}A_{F1} + E_{F2,\theta}A_{F2})}$$

$$k_\theta = \frac{3B_{S,\theta}}{L^2G_{c,\theta}A_c} = \frac{3B_{S,\theta}}{L^2G_{c,\theta}bD}$$

$$B_{S,300} = 108.18^2 \times \frac{200000 \times 0.5 \times 1000 \times 200000 \times 0.703 \times 0.4 \times 1000}{(200000 \times 0.5 \times 1000 + 200000 \times 0.703 \times 0.4 \times 1000)}$$

$$= 4.4482 \times 10^{11}$$

$$E_{c,300,avg} = \frac{1 \times 4.5 + 1 \times 5.5 + 1 \times 6 + 1 \times 6.5 + 1 \times 8}{5} = 6.1$$

$$E_{c,600,max} = 0.45 \times 9 = 4.05$$

$$k_{300,avg} = \frac{3 \times 4.4482 \times 10^{11}}{(7000 - 2 \times 150)^2 \times 2.36 \times 1000 \times 100} = 0.12573$$

$$k_{300,max} = \frac{3 \times 4.4482 \times 10^{11}}{(7000 - 2 \times 150)^2 \times 1.57 \times 1000 \times 100} = 0.18937$$

$$B_{F1} = 200000 \times 73089.4 = 14617880000\ N.mm^2$$

$$\beta_{300,avg} = \frac{14617880000}{14617880000 + \frac{4.4482 \times 10^{11}}{1 + 3.2 \times 0.12573}} = 0.044$$

$$\beta_{300,max} = \frac{14617880000}{14617880000 + \frac{4.4482 \times 10^{11}}{1 + 3.2 \times 0.18937}} = 0.05013$$

$$k_{b,300,avg} = \frac{384 \times 4.4482 \times 10^{11}}{5 \times 6700^3 \times (1 + 3.2 \times 0.18937) \times (1 - 0.044)} = 84.7287\ N/mm$$

$$= 0.084\ kN/mm$$

$$k_{b,300,max} = \frac{384 \times 4.4482 \times 10^{11}}{5 \times 6700^3 \times (1 + 3.2 \times 1.7563) \times (1 - 0.05013)} = 74.4578\ N/mm$$

$$= 0.074\ kN/mm$$

Appendix C. CALCULATION EXAMPLE OF PREDICTING SHEAR RESISTANCE AND STIFFNESS OF PANELS AT AMBIENT TEMPERATURES

The parameters of the sandwich panel at ambient temperatures:

L=7000 mm, D=100 mm, B=1000 mm, t_{F1}= 0.5 mm, t_{F2}=0.4 mm, E_f=200000 MPa, d_S=5.5 mm, $t_{cor,sup}$=8 mm, $f_{u,F2}$=500.8 MPa, $f_{y,F2}$=301.5 MPa, θ=20 °C.

$$V_{ECCS} = 4.2\sqrt{t_{cor,F2}^3 . d_1} . f_{u,F2}$$

$V_{1,ECCS} = 4.2 \times \sqrt{(0.4 - 0.04)^3 \times 0.9 \times 5.5} \times 500.8 = 1010.81\ N = 1.01\ kN$ when $f_{u,F2}$=500.8 MPa

$V_{2,ECCS} = 4.2 \times \sqrt{(0.4 - 0.04)^3 \times 0.9 \times 5.5} \times 1.25 \times 301.5 = 760.68\ N = 0.76\ kN$ when $f_{u,F2}$=1.25$f_{y,F2}$=1.25×301.5=376.87 MPa

$$k_v = \frac{1}{\frac{x_F}{k_{F2}} + \frac{t_{cor,sup}^2 + 2.(1 - x_F).D.t_{cor,sup}}{4C_{sup}} + \frac{3.(1 - x_F).D.t_{cor,sup}^2 + t_{cor,sup}^3}{24EI}}$$

$$x_F = 1 - \frac{\frac{1}{k_{F2}} - \frac{D.t_{cor,sup}}{2C_{sup}} - \frac{D.t_{cor,sup}^2}{8EI}}{\frac{1}{k_{F2}} + \frac{D^2}{C_{sup}} + \frac{D^2.(2D + 3t_{cor,\mathrm{sup}})}{6EI}}$$

$$EI = 200000N/mm^2 . \frac{\pi . d_s^4}{64}$$

$$C_{sup} = 2400N/mm^2 . \sqrt{t_{cor,sup} . d_1^5}$$

$$k_{F2} = \begin{cases} 6.93. \dfrac{f_{u,F2} . \sqrt{t_{cor,F2}^3 . d_1}}{0.26mm + 0.8t_{F2}} & for\ 0.40mm \le t_{cor,F2} \le 0.70mm \\ 4.20. \dfrac{f_{u,F2} . \sqrt{t_{cor,F2}^3 . d_1}}{0.373mm} & for\ 0.70mm\ \le t_{cor,F2} \le 1.00mm \end{cases}$$

$$C_{sup} = 2400N/mm^2 \times \sqrt{8 \times (0.9 \times 5.5)^5} = 370057.52$$

$$EI = 200000N/mm^2 \times \frac{(0.9 \times 5.5)^5}{64} = 5894143.29$$

$$k_{F2} = 6.93 \times \frac{500.8 \times \sqrt{(0.4 - 0.04)^3 \times (0.9 \times 5.5)}}{0.26 + 0.8 \times (0.4 - 0.04)} = 3043.5$$

$$x_F = 1 - \frac{\frac{1}{3043.5} - \frac{100 \times 8}{2 \times 370057.52} - \frac{100 \times (8)^2}{8 \times 5894143.29}}{\frac{1}{3043.5} + \frac{100^2}{370057.52} + \frac{100^2 \times (2 \times 100 + 3 \times 8)}{6 \times 5894143.29}} = 1.00$$

$k_{v1} = 2726.81 \frac{N}{mm} = 2.73\ kN/mm$ when $f_{u,F2}$=500.8 MPa

$k_{v2} = 2055.63\ N/mm$=2.10 kN/mm when $f_{u,F2}$=1.25$f_{y,F2}$=1.25×301.5=376.87 MPa

Appendix D. CALCULATION EXAMPLE OF PREDICTING SHEAR RESISTANCE AND STIFFNESS OF PANELS AT ELEVATED TEMPERATURES

The parameters of the sandwich panel at ambient temperatures:

L=7000 mm, D=100 mm, B=1000 mm, t_{F1}= 0.5 mm, t_{F2}=0.4 mm, E_f=200000 MPa, d_S=5.5 mm, $t_{cor,sup}$=8 mm, $f_{u,F2,600}$=125.8 MPa, $f_{y,F2}$=56.1 MPa, θ=600 °C.

$$V_{ECCS,\theta} = 4.2\sqrt{t_{cor,F2}^3 . d_1} . f_{u,F2,\theta}$$

$V_{1,ECCS,600} = 4.2 \times \sqrt{(0.4-0.04)^3 \times 0.9 \times 5.5} \times 125.8 = 253.91\ N = 0.25\ kN$ when $f_{u,F2}$=125.8 MPa

$V_{2,ECCS,600} = 4.2 \times \sqrt{(0.4-0.04)^3 \times 0.9 \times 5.5} \times 56.1 = 113.23\ N = 0.11\ kN$ when $f_{u,F2}$=$f_{y,F2}$=56.1 MPa

$$k_{v,\theta} = \frac{1}{\frac{x_{F,\theta}}{k_{F2,\theta}} + \frac{t_{cor,sup}^2 + 2.(1-x_{F,\theta}).D.t_{cor,sup}}{4C_{sup}} + \frac{3.(1-x_{F,\theta}).D.t_{cor,sup}^2 + t_{cor,sup}^3}{24EI_\theta}}$$

$$x_{F,\theta} = 1 - \frac{\frac{1}{k_{F2,\theta}} - \frac{D.t_{cor,sup}}{2C_{sup}} - \frac{D.t_{cor,sup}^2}{8EI_\theta}}{\frac{1}{k_{F2,\theta}} + \frac{D^2}{C_{sup}} + \frac{D^2.(2D+3t_{cor,\mathrm{sup}})}{6EI_\theta}}$$

$$EI_\theta = 61000N/mm^2 . \frac{\pi . d_s^4}{64}$$

$$C_{sup} = 2400N/mm^2 . \sqrt{t_{cor,sup} . d_1^5}$$

$$k_{F2,\theta} = \begin{cases} 6.93.\dfrac{f_{u,F2,\theta} . \sqrt{t_{cor,F2}^3 . d_1}}{0.26mm + 0.8t_{F2}} & for\ 0.40mm \le t_{cor,F2} \le 0.70mm \\ 4.20.\dfrac{f_{u,F2,\theta} . \sqrt{t_{cor,F2}^3 . d_1}}{0.373mm} & for\ 0.70mm\ \le t_{cor,F2} \le 1.00mm \end{cases}$$

$$C_{sup} = 2400N/mm^2 \times \sqrt{8 \times (0.9 \times 5.5)^5} = 370057.52$$

$$EI_{600} = 61000N/mm^2 \times \frac{(0.9 \times 5.5)^5}{64} = 1797713.70$$

$$k_{F2,600} = 6.93 \times \frac{125.8 \times \sqrt{(0.4 - 0.04)^3 \times (0.9 \times 5.5)}}{0.26 + 0.8 \times (0.4 - 0.04)} = 764.52$$

$$x_{F,600} = 1 - \frac{\frac{1}{764.5} - \frac{100 \times (8)}{2 \times 370057.52} - \frac{100 \times (8)^2}{8 \times 1797713.70}}{\frac{1}{764.5} + \frac{100^2}{370057.52} + \frac{100^2 \times (2 \times 100 + 3 \times 8)}{6 \times 1797713.70}} = 1.00$$

$k_{v1,600} = 733.72 \frac{N}{mm} = 0.73\ kN/mm$ when $f_{u,F2}$=125.8 MPa

$k_{v2,600} = 335.63\ N/mm$=0.34 kN/mm when $f_{u,F2}$=$f_{y,F2}$=56.1 MPa

Appendix E. LOAD-DISPLACEMENT CURVES OF SANDWICH PANELS UNDER BENDING LOADING

The load-displacement curves for MW panels under bending loading obtained from FE models:

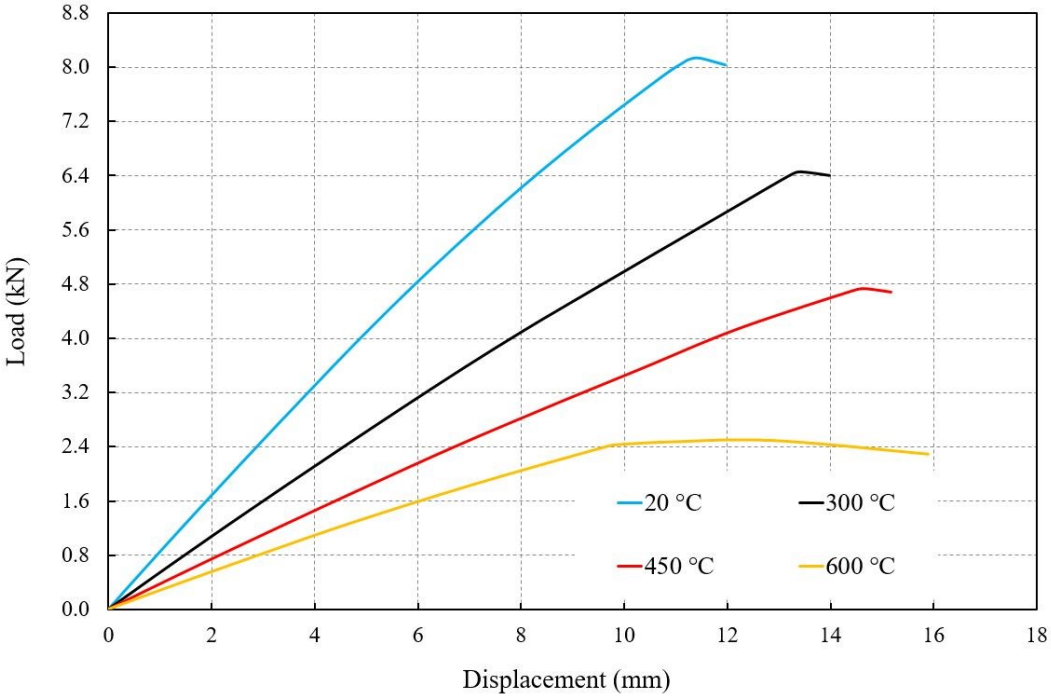

Figure E.1. Load-displacement curves for MW-1200-100-2500-0.4-0.6-θ

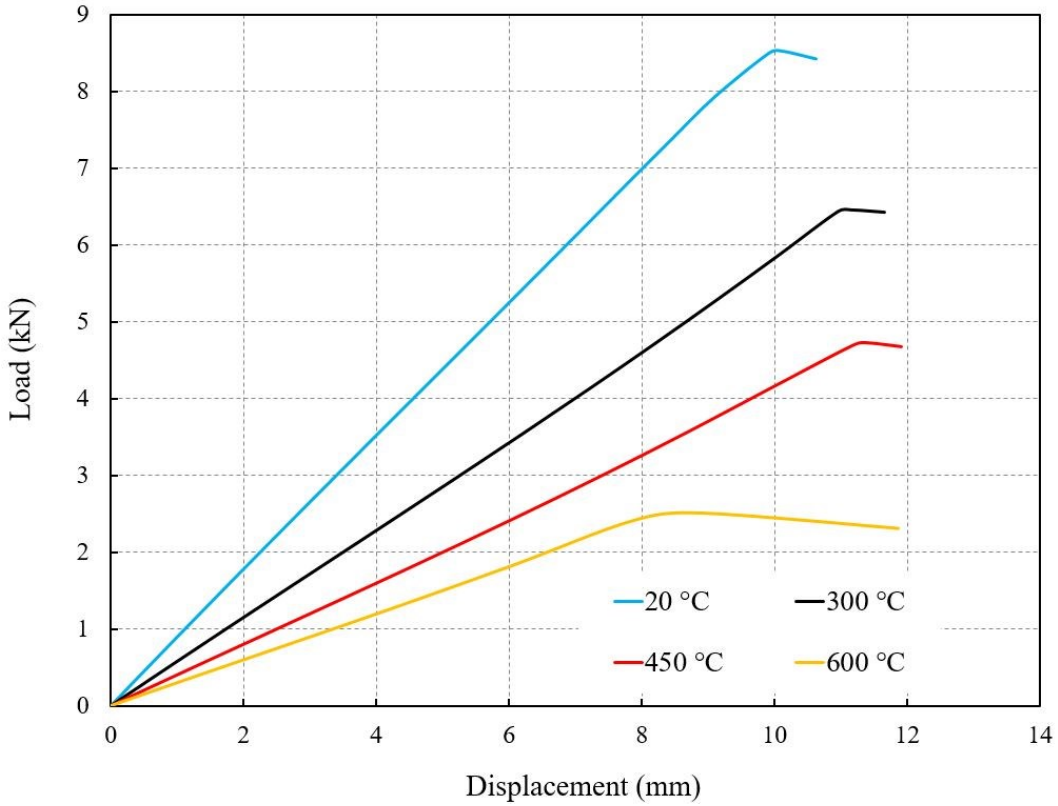

Figure E.2. Load-displacement curves for MW-1200-100-2500-1.0-0.6-θ

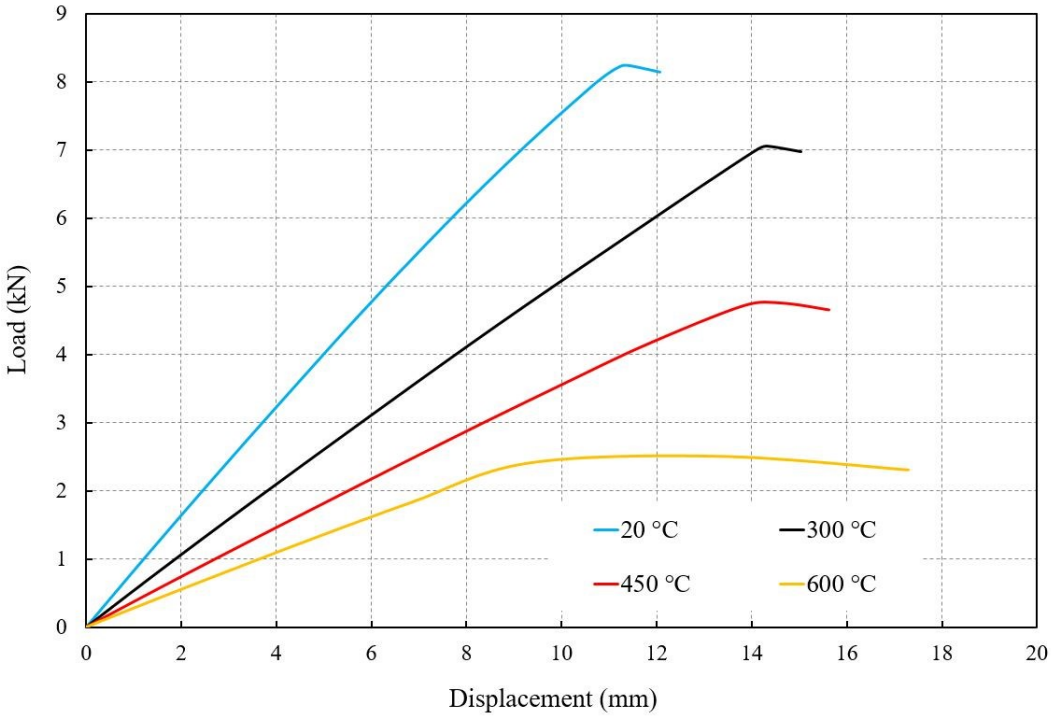

Figure E.3. Load-displacement curves for MW-1200-100-2500-0.5-0.4-θ

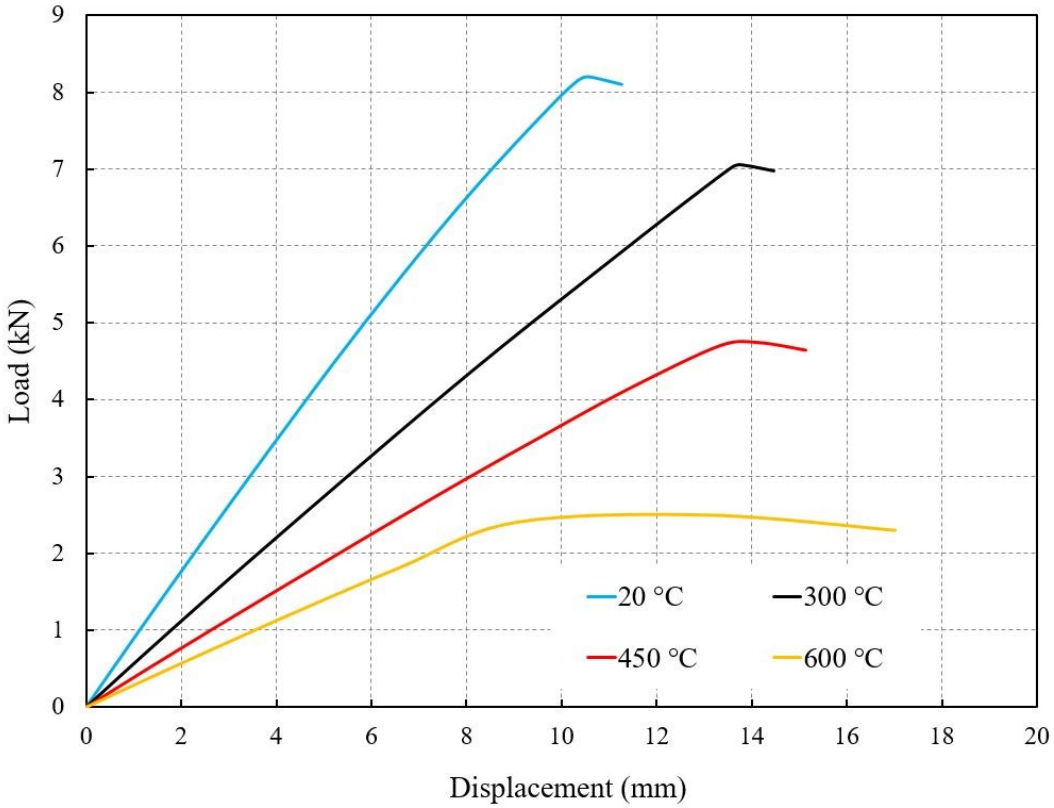

Figure E.4. Load-displacement curves for MW-1200-100-2500-0.5-1.0-θ

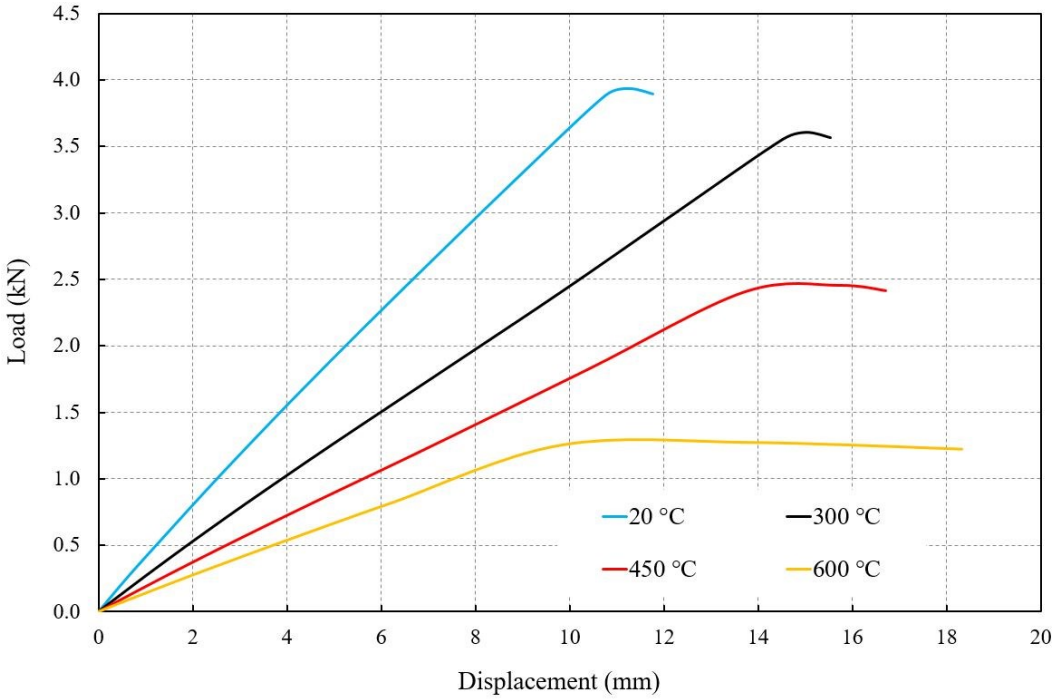

Figure E.5. Load-displacement curves for MW-1200-50-2500-0.5-0.6-θ

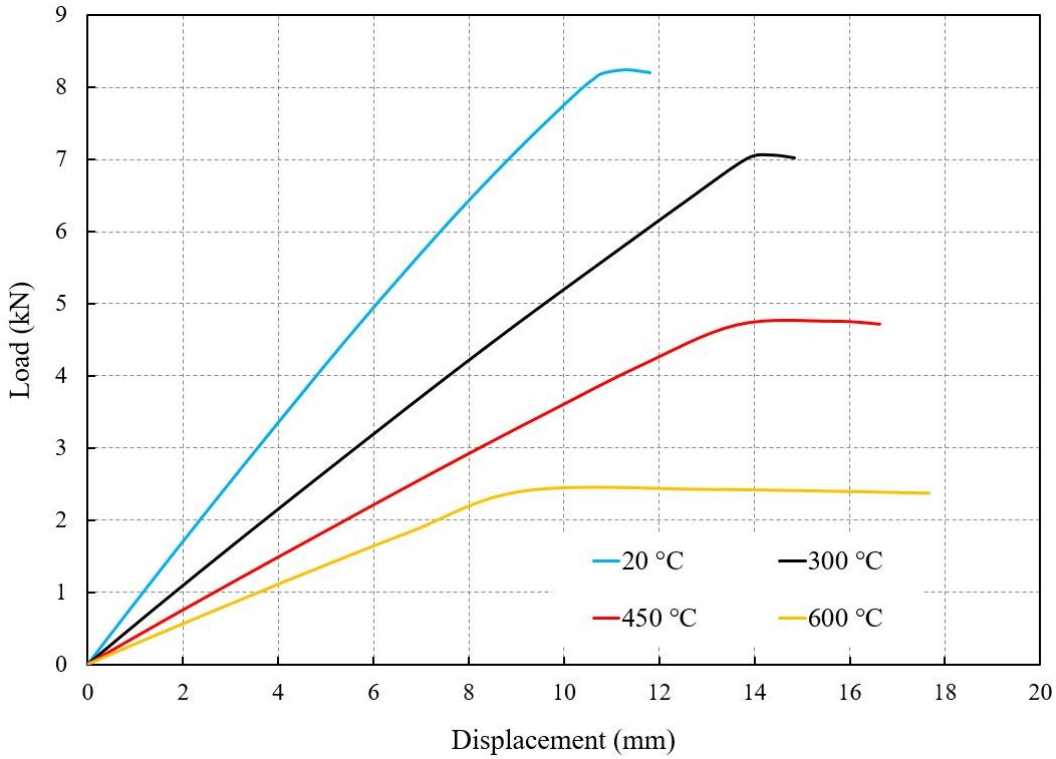

Figure E.6. Load-displacement curves for MW-1200-100-2500-0.5-0.6-θ

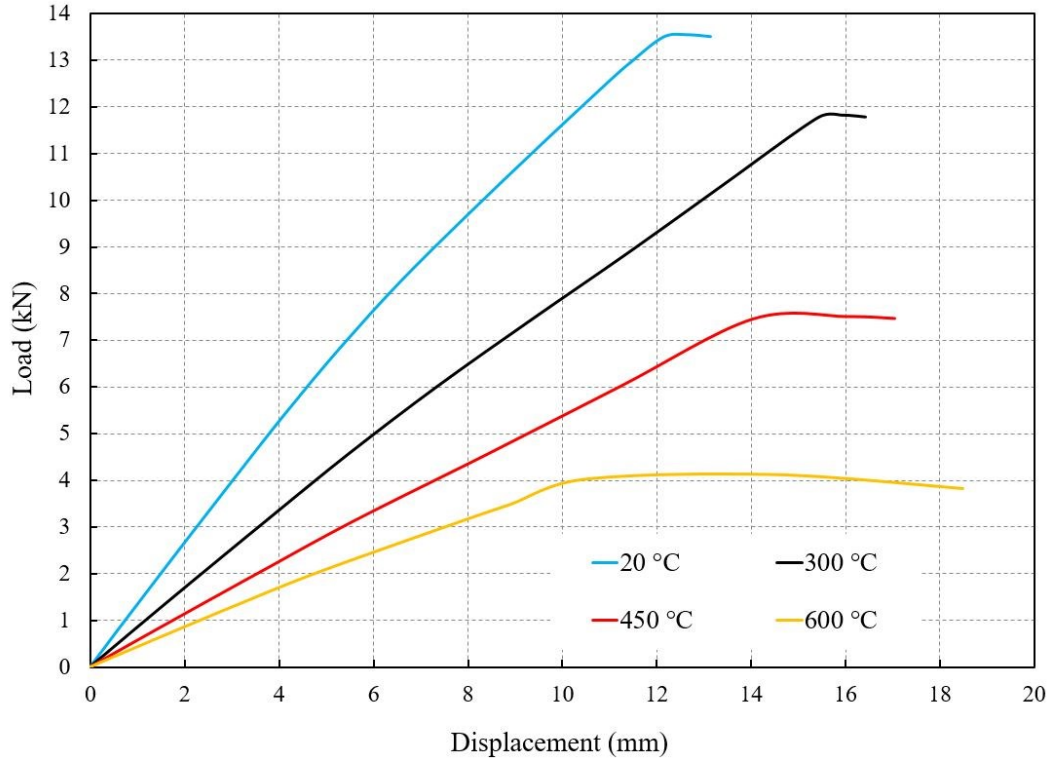

Figure E.7. Load-displacement curves for MW-1200-160-2500-0.5-0.6-θ

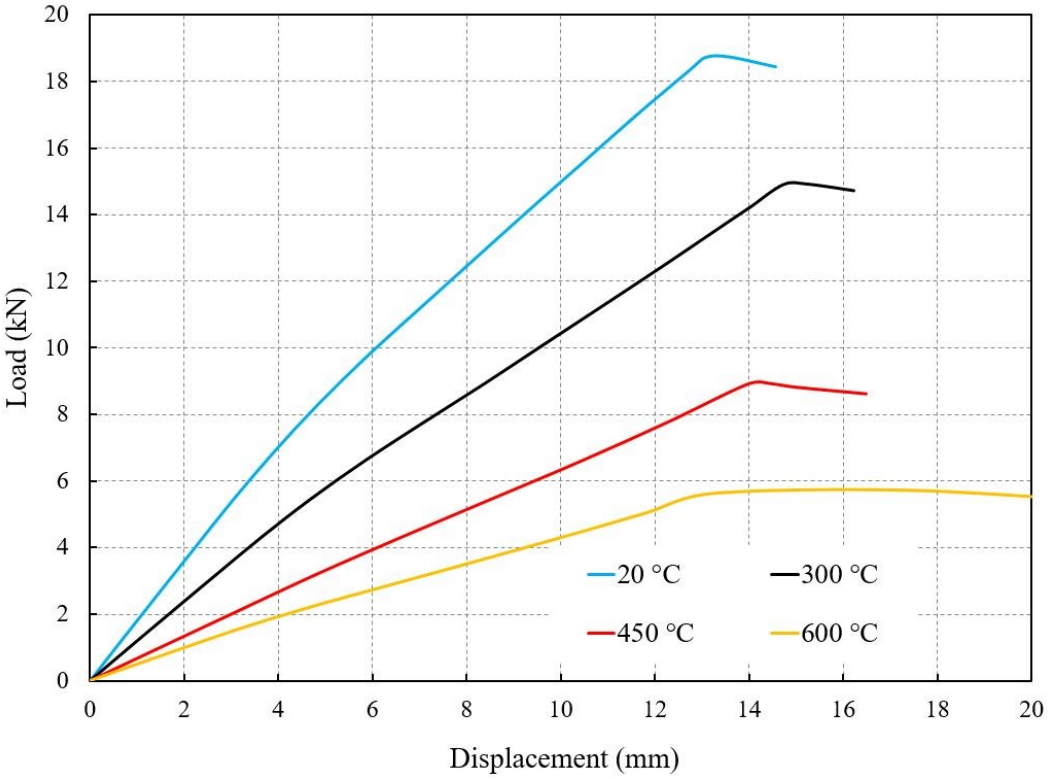

Figure E.8. Load-displacement curves for MW-1200-230-2500-0.5-0.6-θ

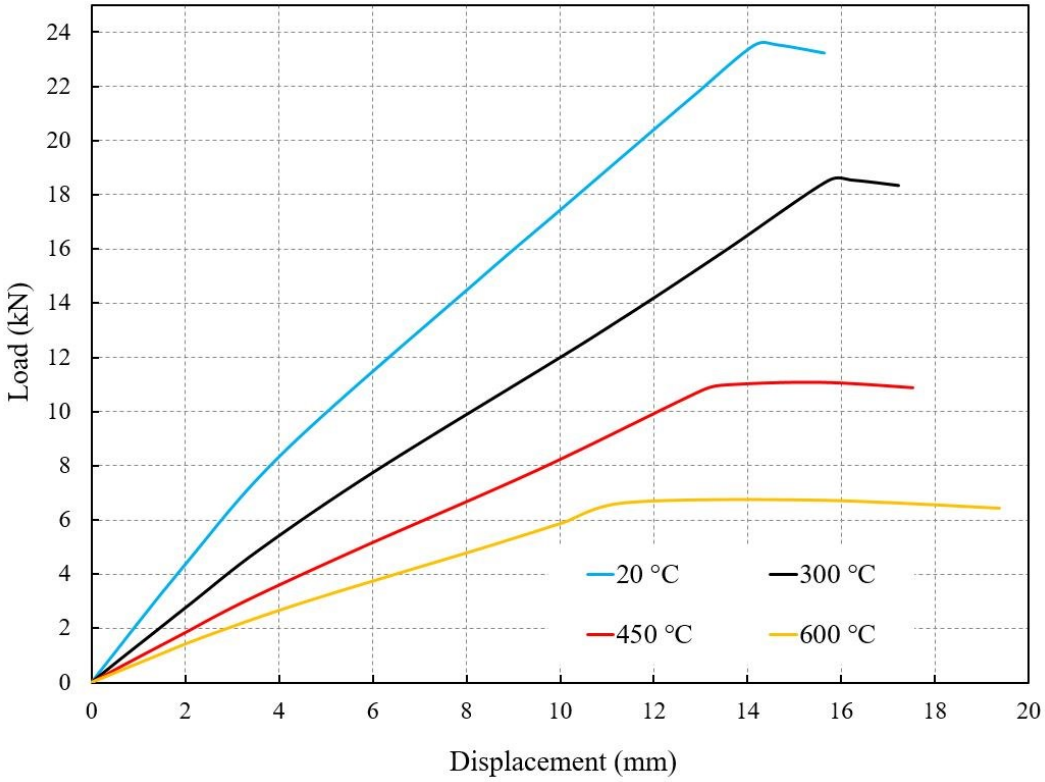

Figure E.9. Load-displacement curves for MW-1200-300-2500-0.5-0.6-θ

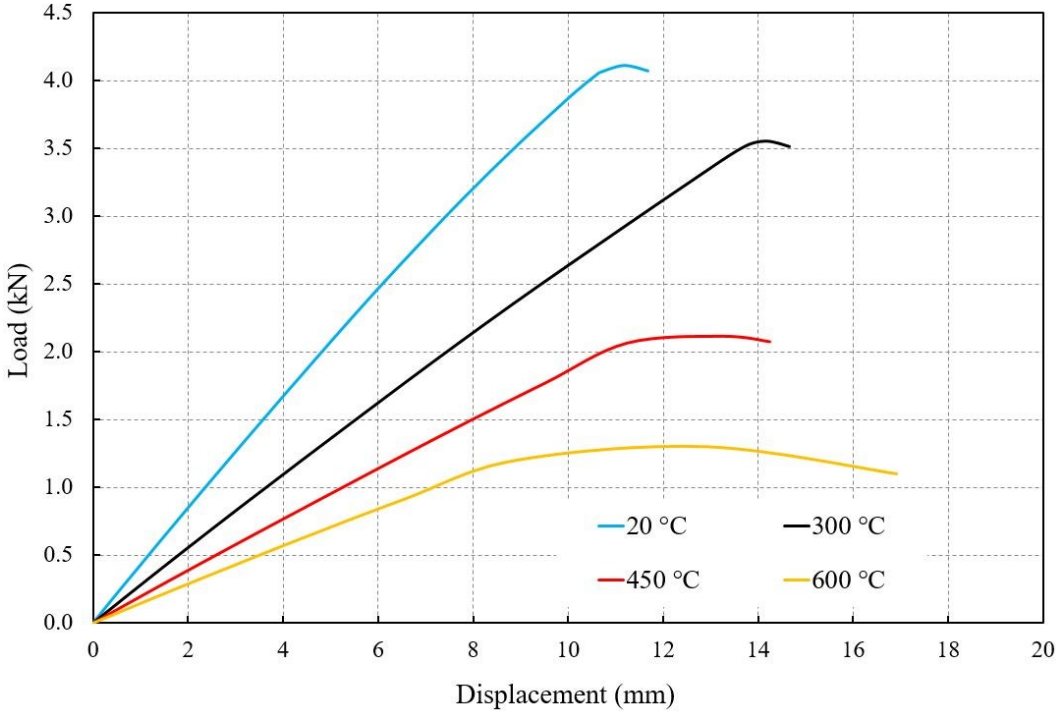

Figure E.10. Load-displacement curves for MW-600-100-2500-0.5-0.6-θ

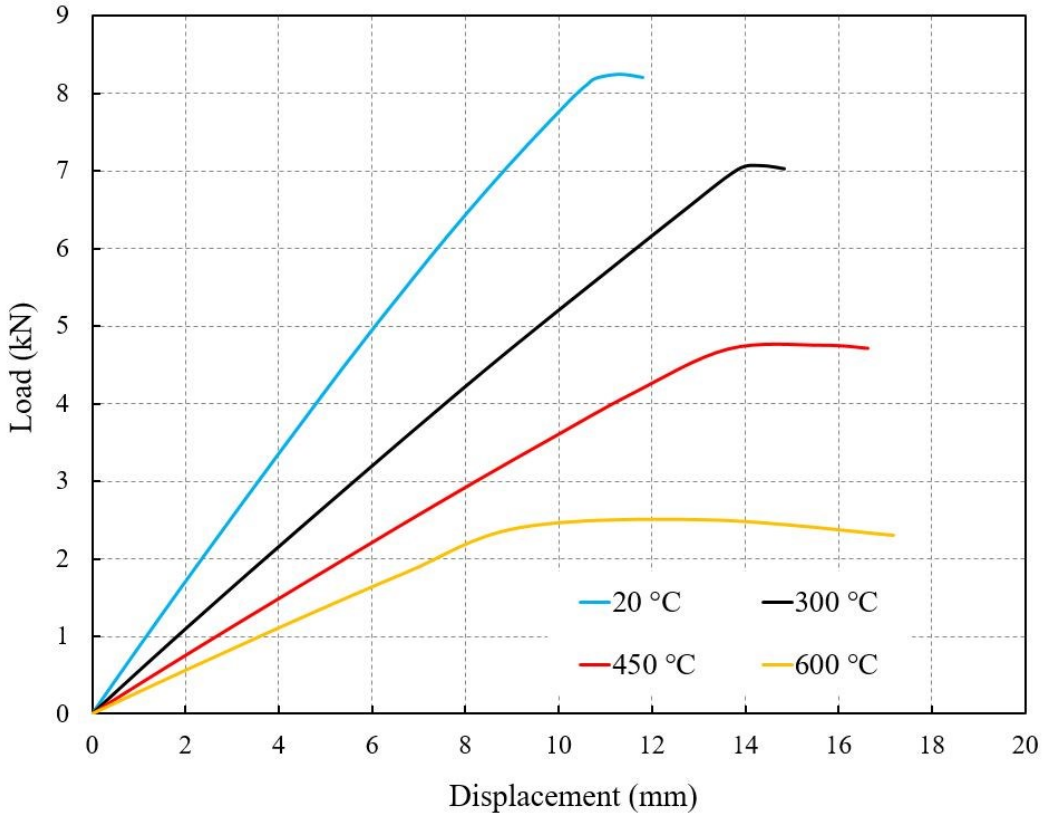

Figure E.11. Load-displacement curves for MW-1200-100-2500-0.5-0.6-θ

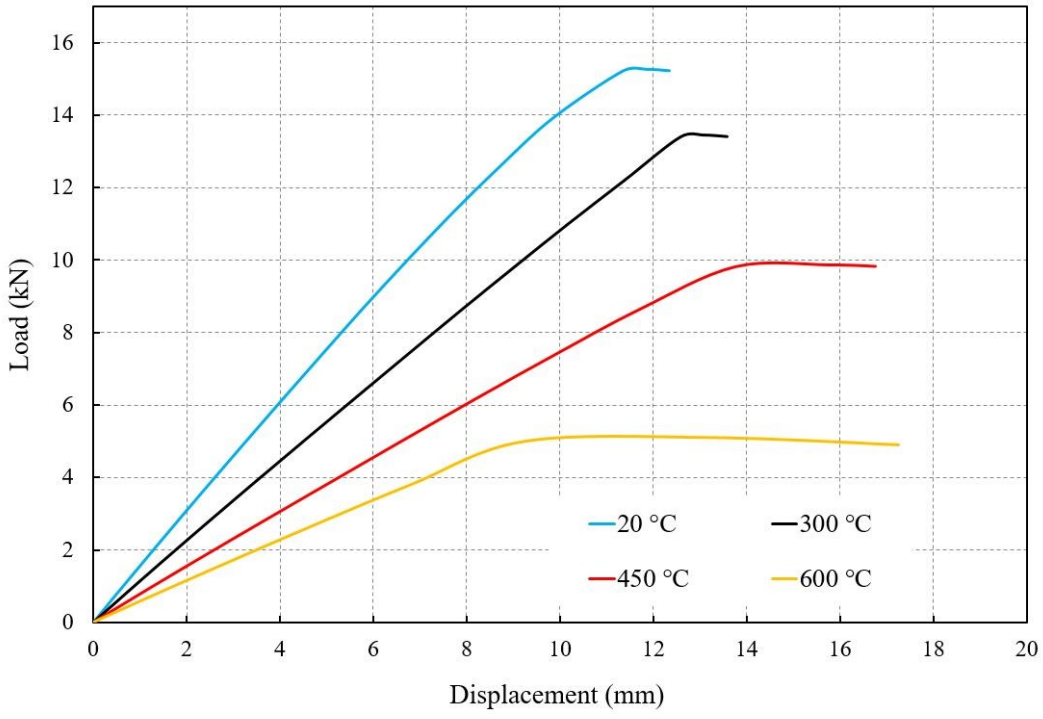

Figure E.12. Load-displacement curves for MW-2500-100-2500-0.5-0.6-θ

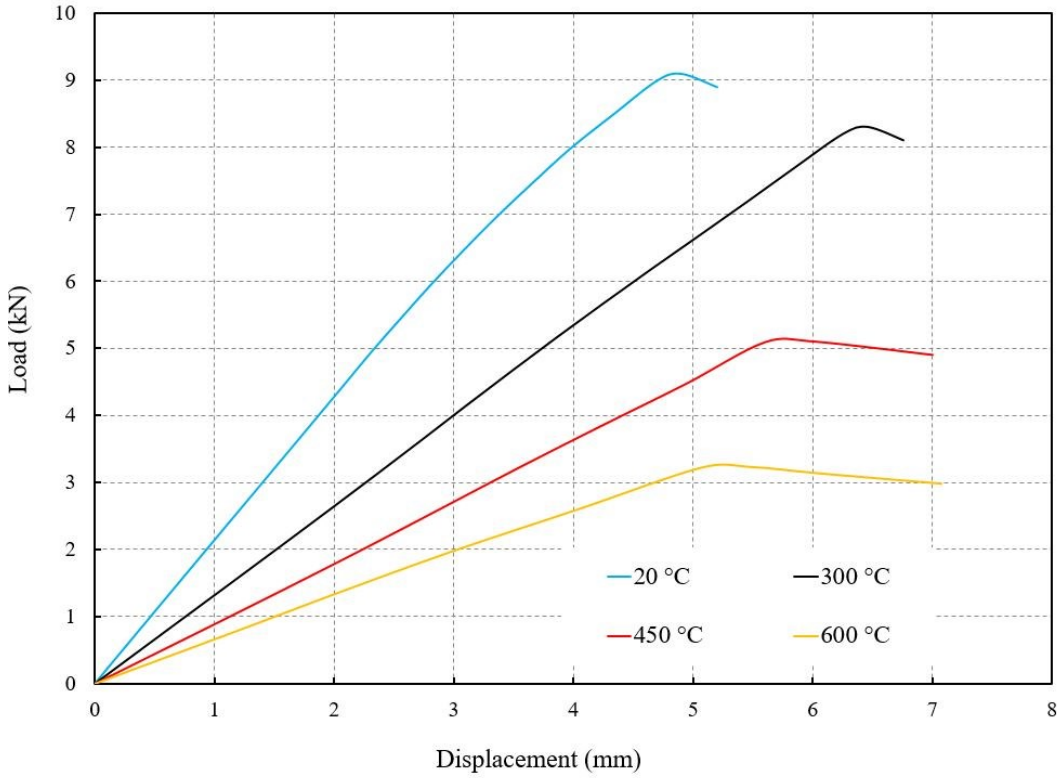

Figure E.13. Load-displacement curves for MW-1200-100-1000-0.5-0.6-θ

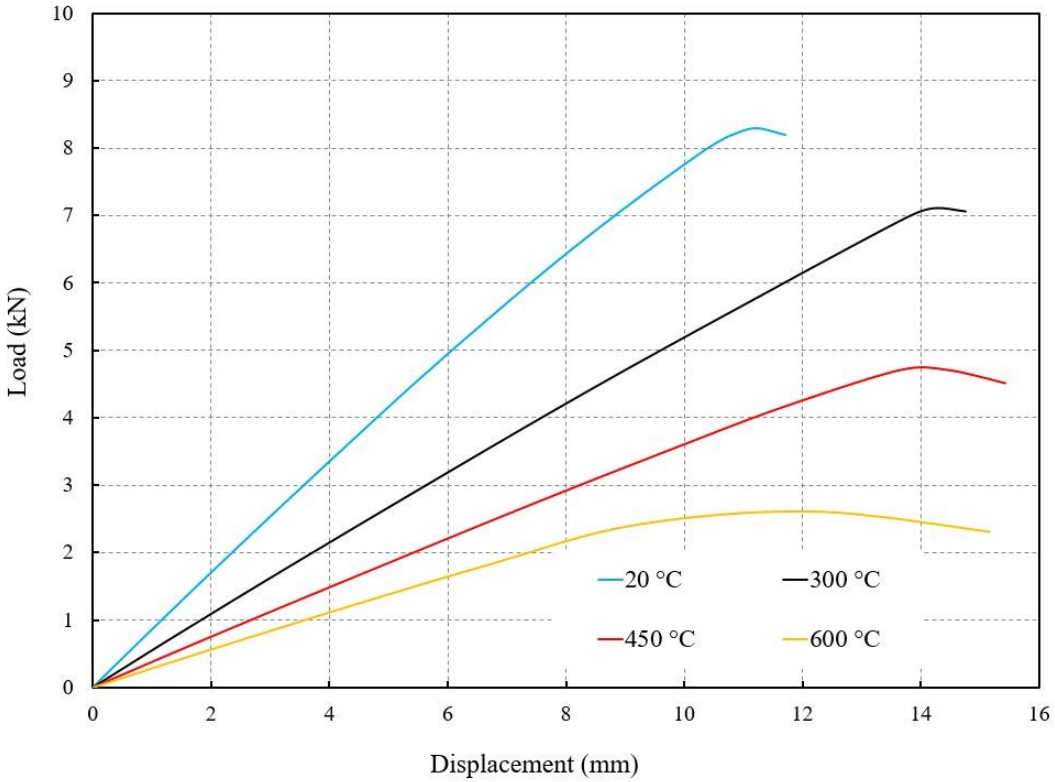

Figure E.14. Load-displacement curves for MW-1200-100-2500-0.5-0.6-θ

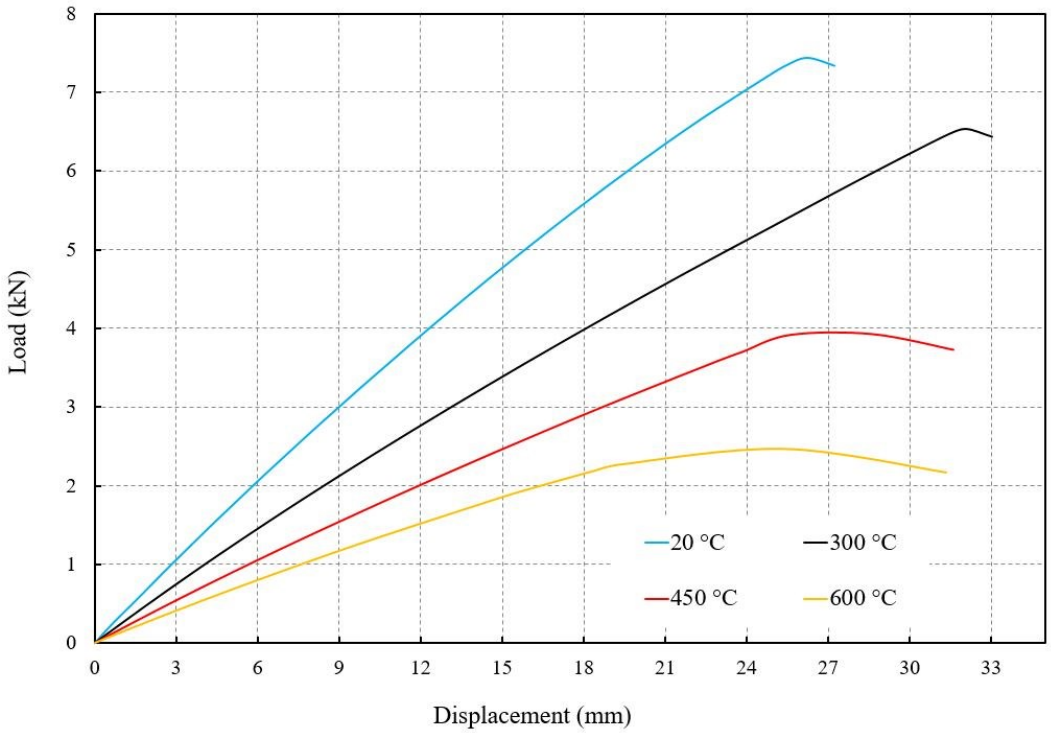

Figure E.15. Load-displacement curves for MW-1200-100-4500-0.5-0.6-θ

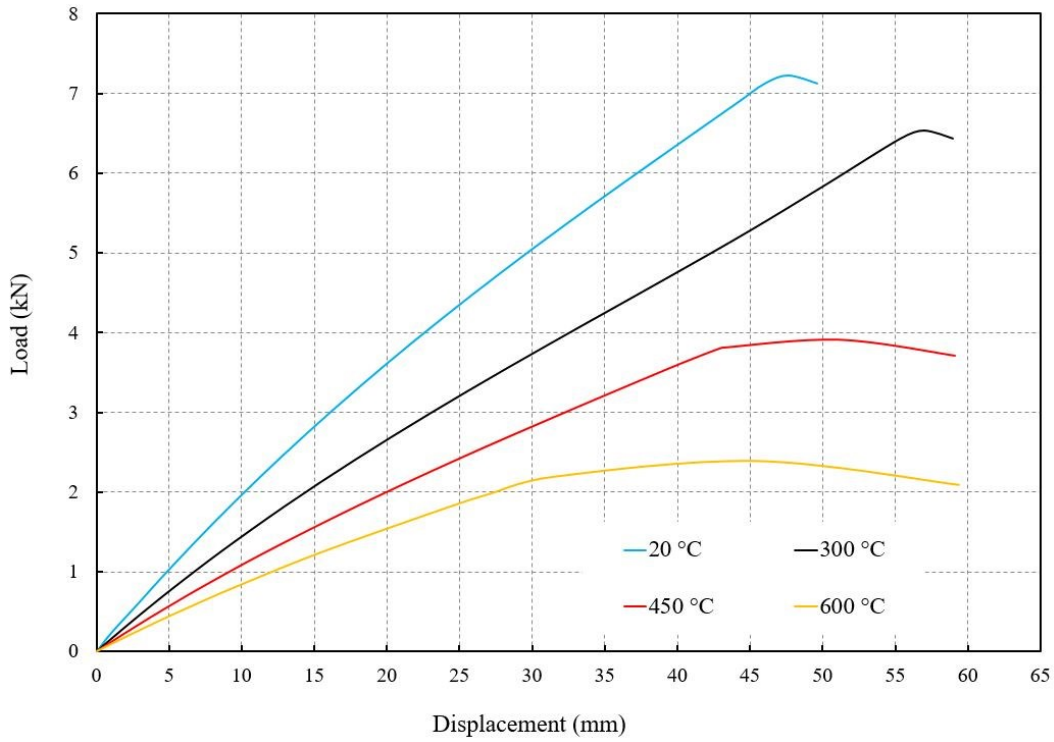

Figure E.16. Load-displacement curves for MW-1200-100-6000-0.5-0.6-θ

The load-displacement curves for PIR panels under bending loading obtained from FE models:

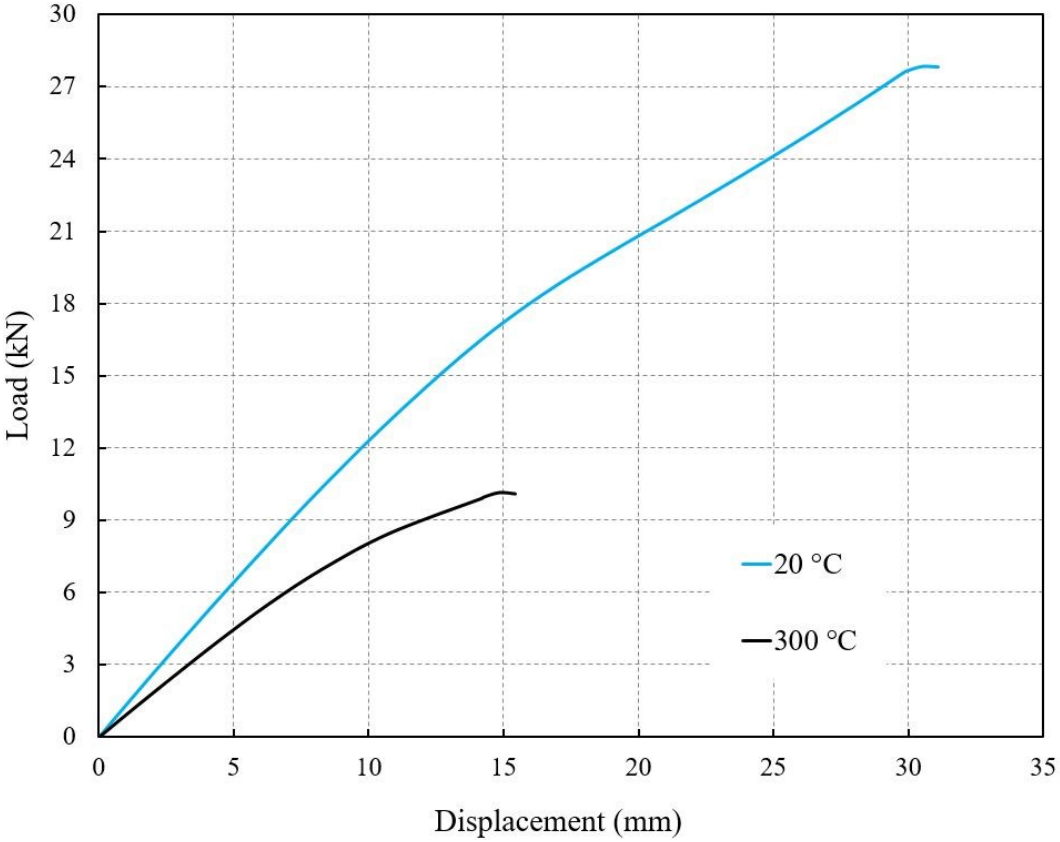

Figure E.17. Load-displacement curves for PIR-1200-100-2500-0.4-0.5-θ

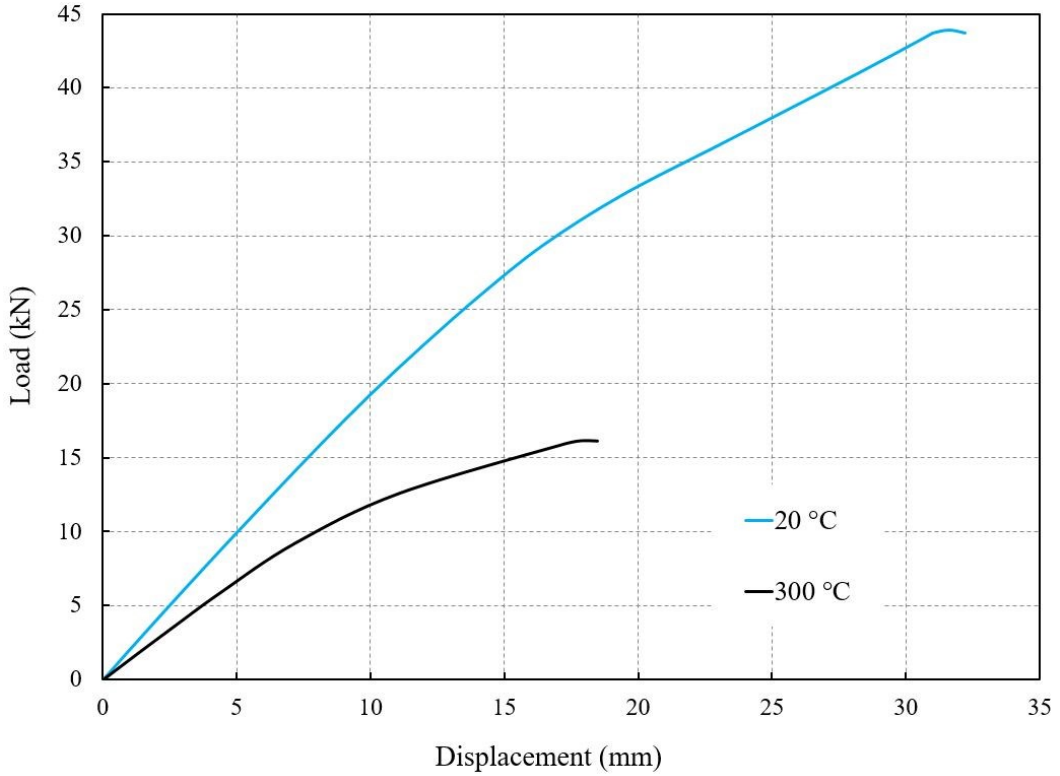

Figure E.18. Load-displacement curves for PIR-1200-160-2500-0.4-0.5-θ

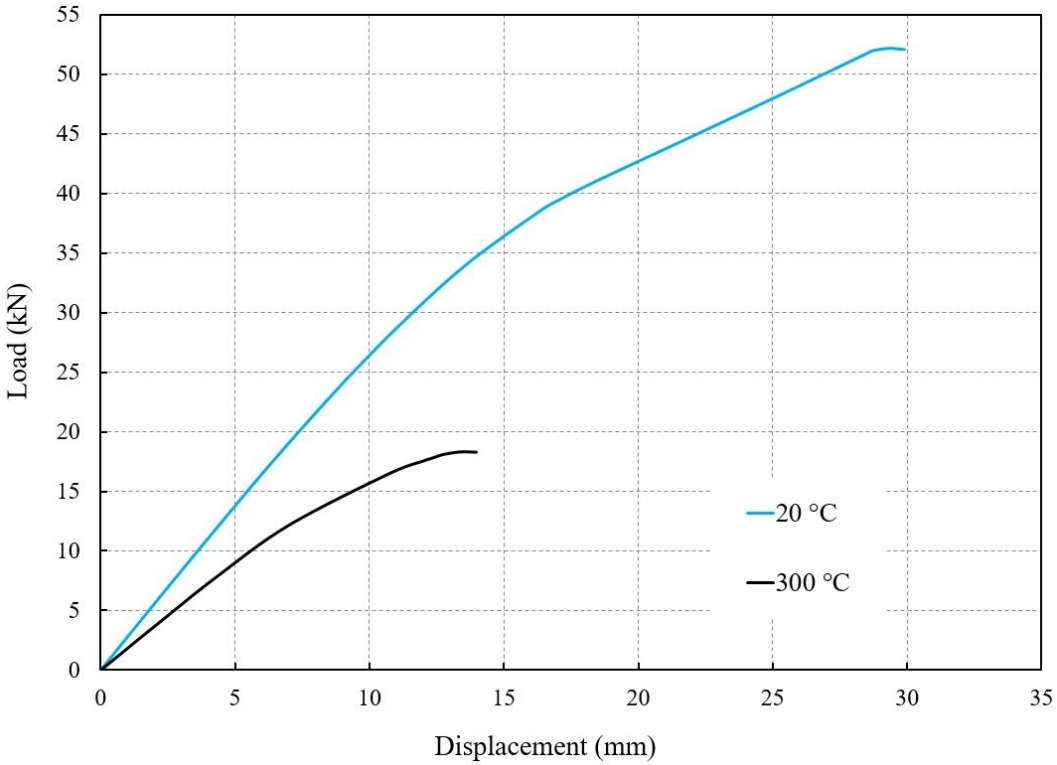

Figure E.19. Load-displacement curves for PIR-1200-230-2500-0.4-0.5-θ

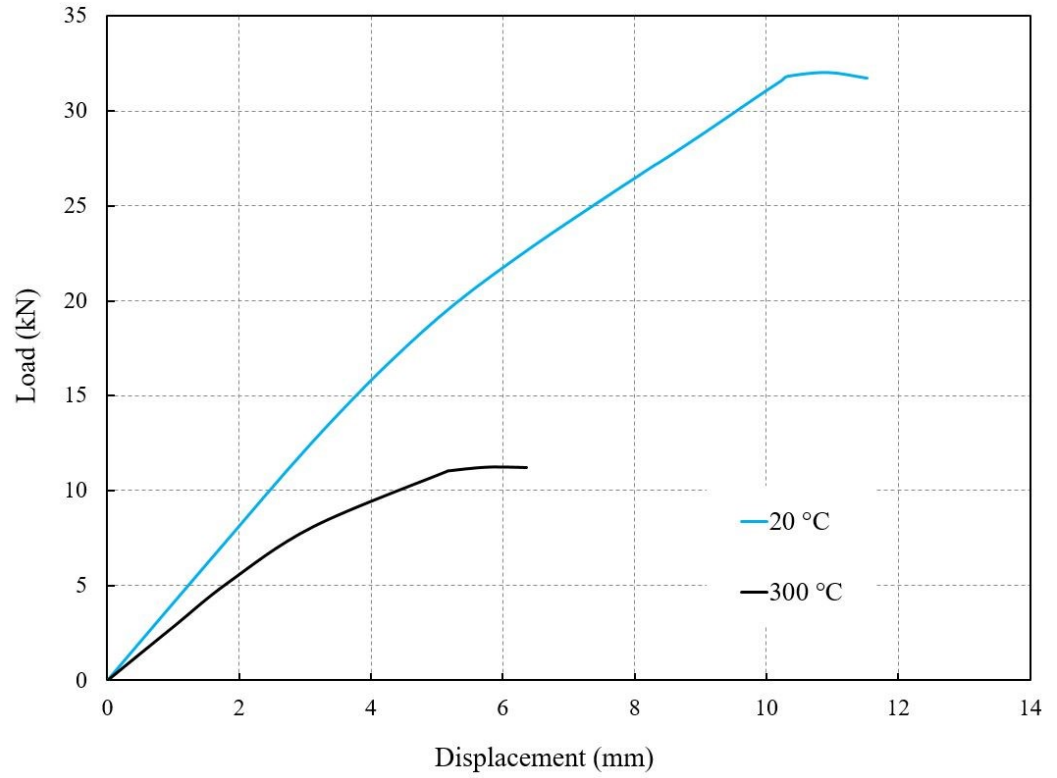

Figure E.20. Load-displacement curves for PIR-1200-100-1000-0.4-0.5-θ

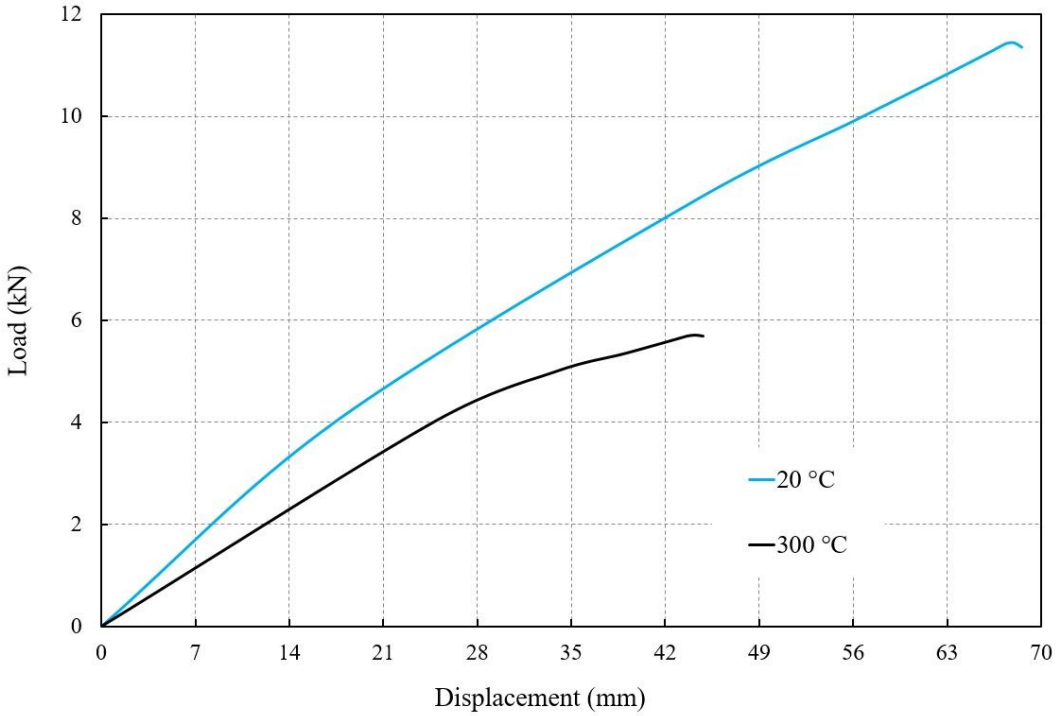

Figure E.21. Load-displacement curves for PIR-1200-100-6000-0.4-0.5-θ

Appendix F. LOAD-DISPLACEMENT CURVES OF SANDWICH PANELS UNDER SHEAR LOADING

The load-displacement curves for MW panels under shear loading obtained from FE models:

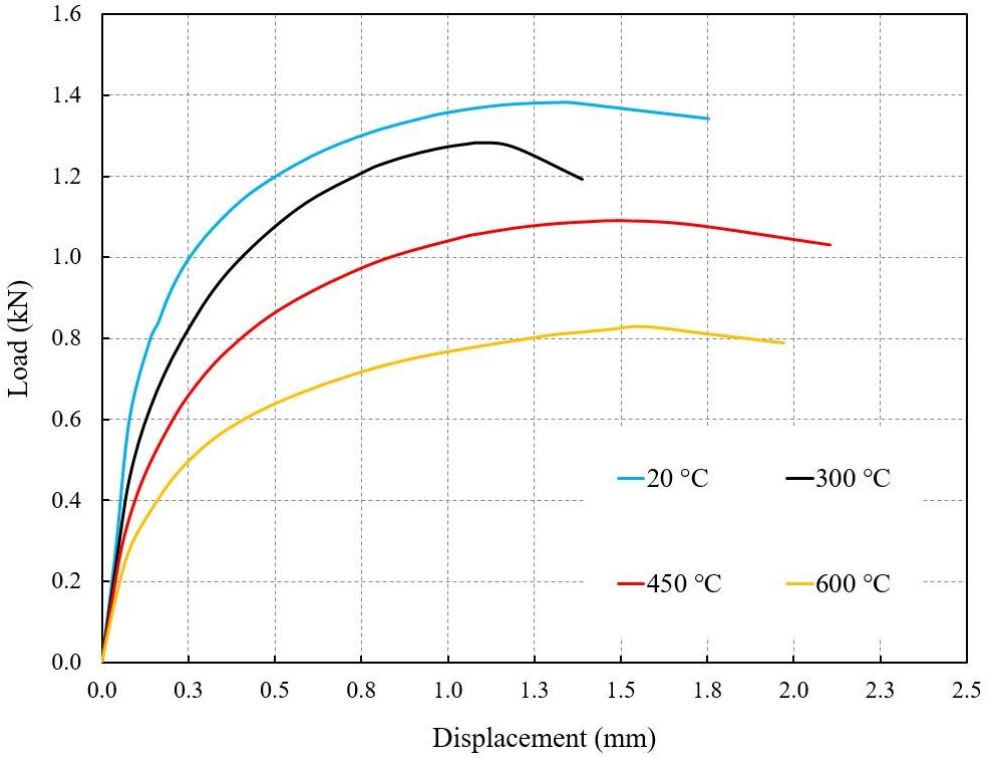

Figure F.1. Load-displacement curves for MW sandwich panels with 4.2 mm screw diameter and 0.4 mm inner sheet thickness at different temperatures

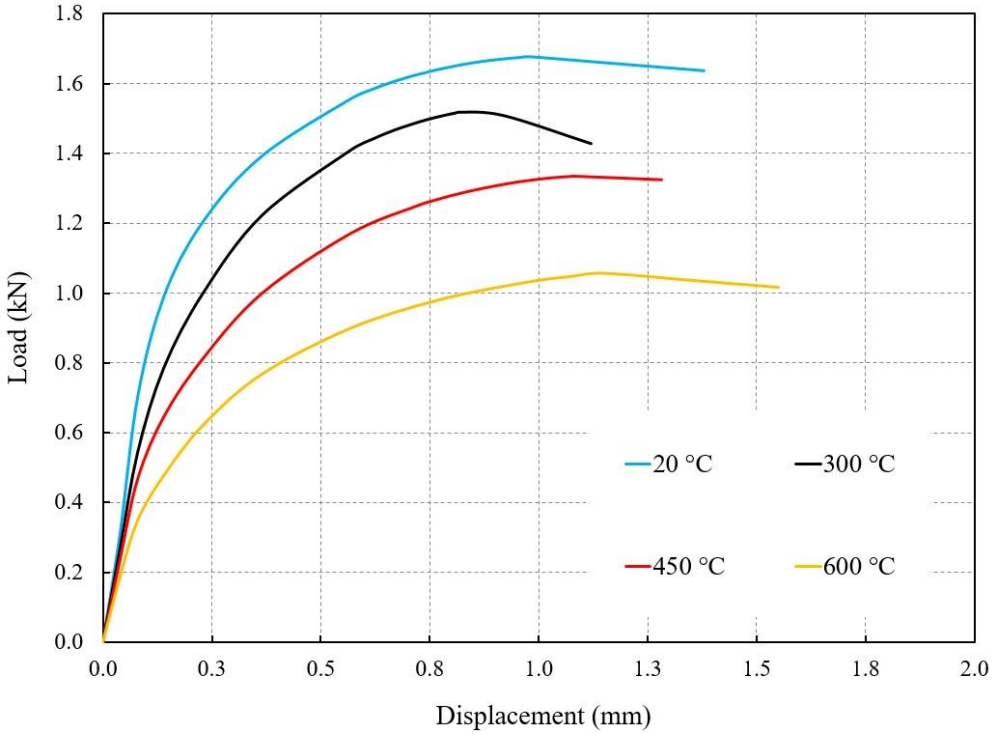

Figure F.2. Load-displacement curves for MW sandwich panels with 4.2 mm screw diameter and 0.5 mm inner sheet thickness at different temperatures

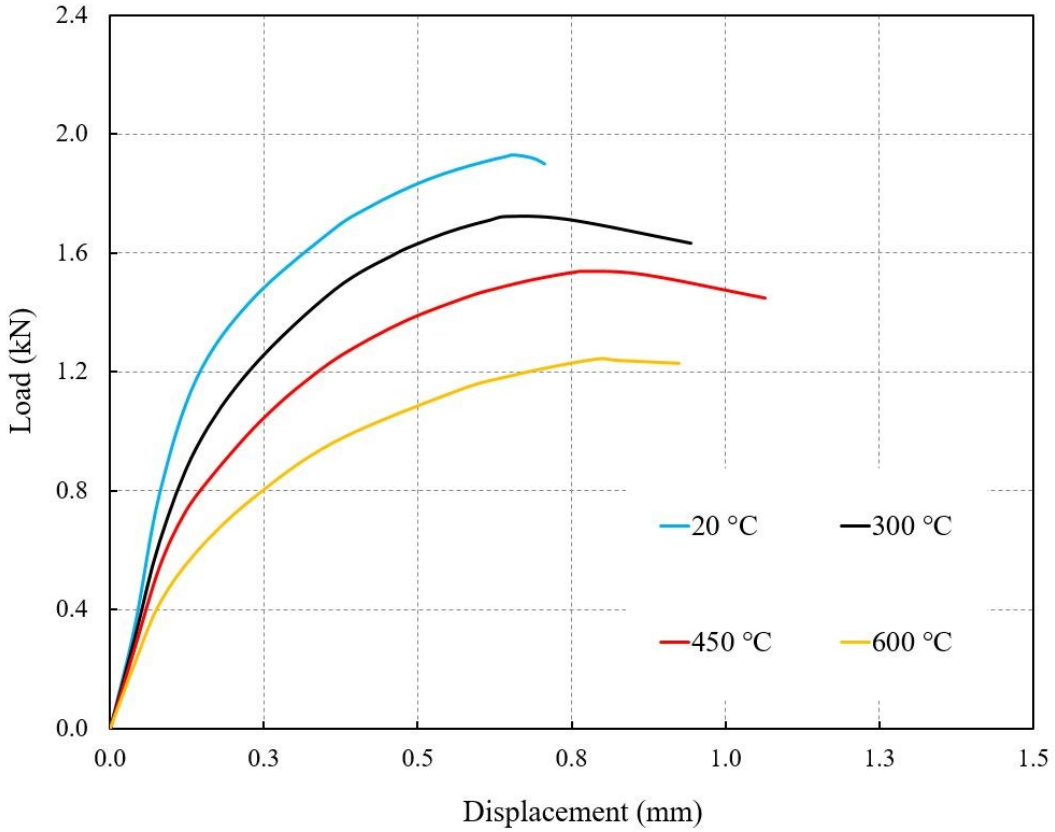

Figure F.3. Load-displacement curves for MW sandwich panels with 4.2 mm screw diameter and 0.6 mm inner sheet thickness at different temperatures

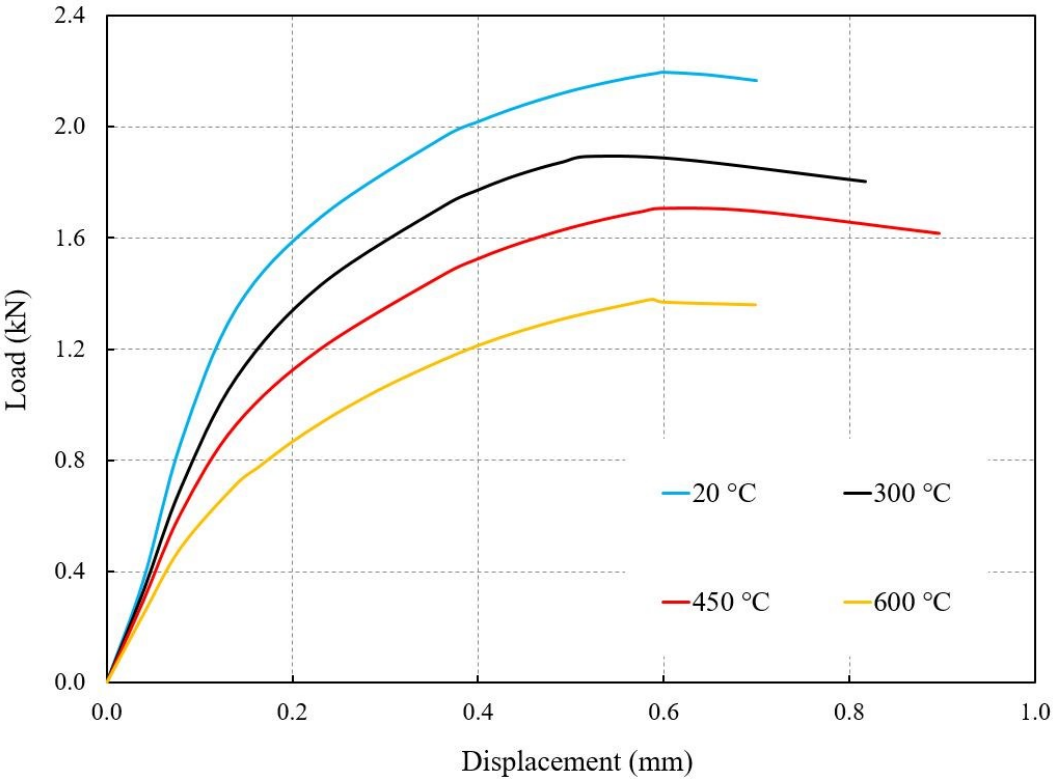

Figure F.4. Load-displacement curves for MW sandwich panels with 4.2 mm screw diameter and 0.7 mm inner sheet thickness at different temperatures

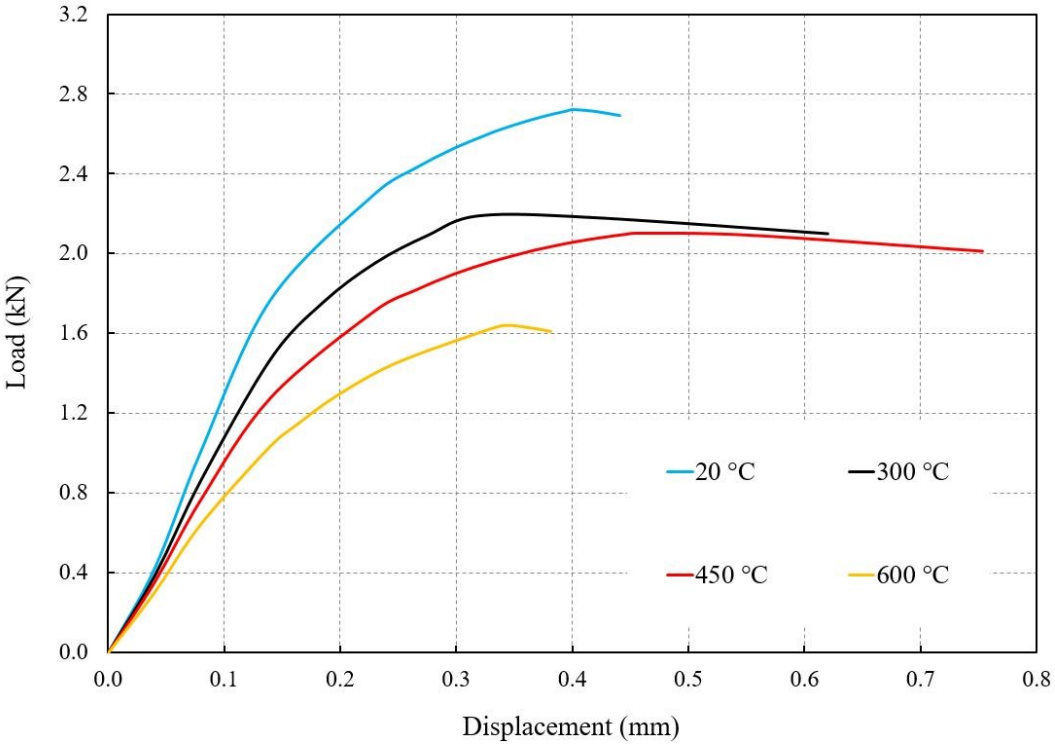

Figure F.5. Load-displacement curves for MW sandwich panels with 4.2 mm screw diameter and 1.0 mm inner sheet thickness at different temperatures

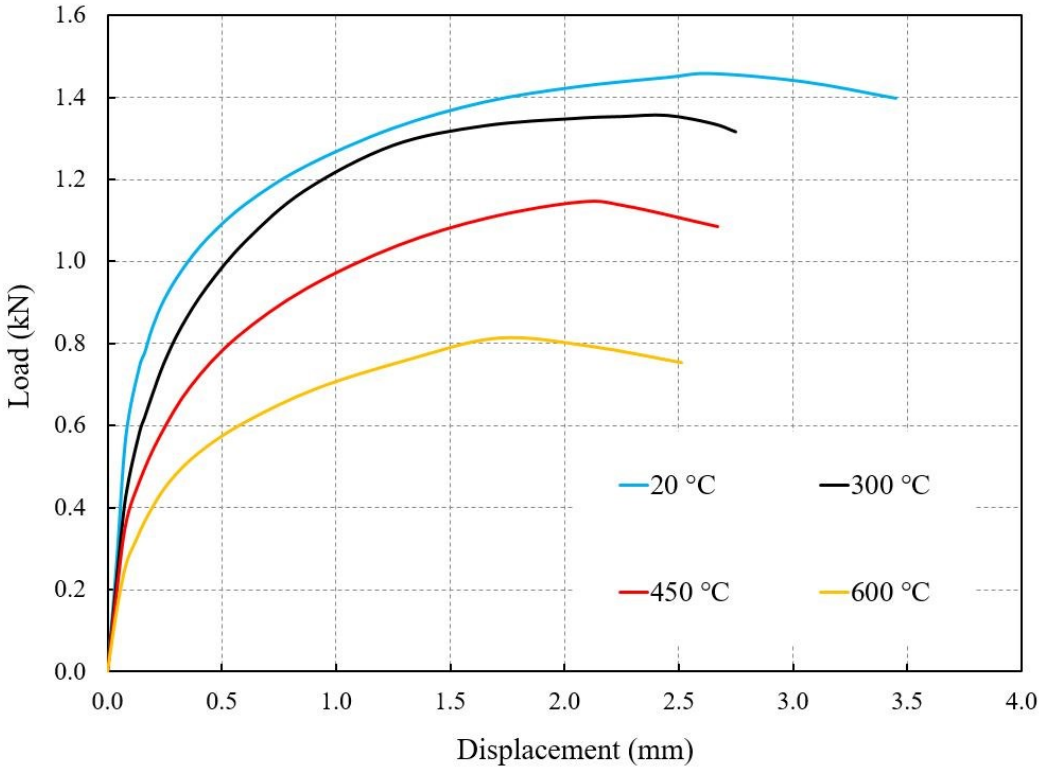

Figure F.6. Load-displacement curves for MW sandwich panels with 5.5 mm screw diameter and 0.4 mm inner sheet thickness at different temperatures

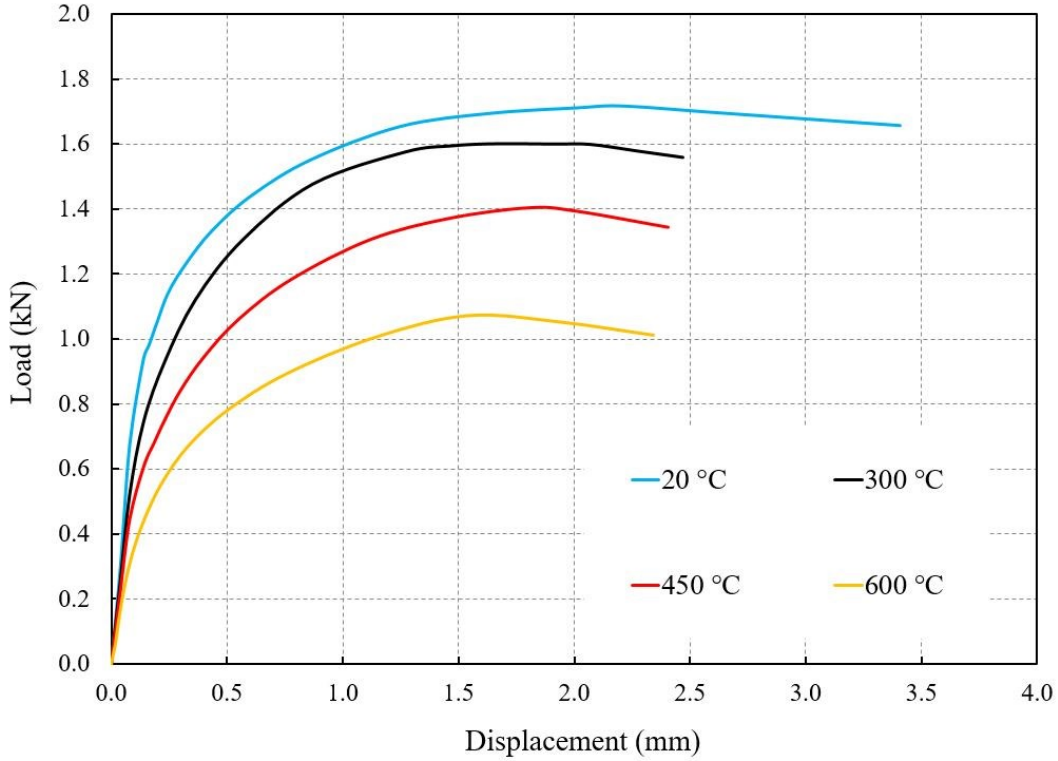

Figure F.7. Load-displacement curves for MW sandwich panels with 5.5 mm screw diameter and 0.5 mm inner sheet thickness at different temperatures

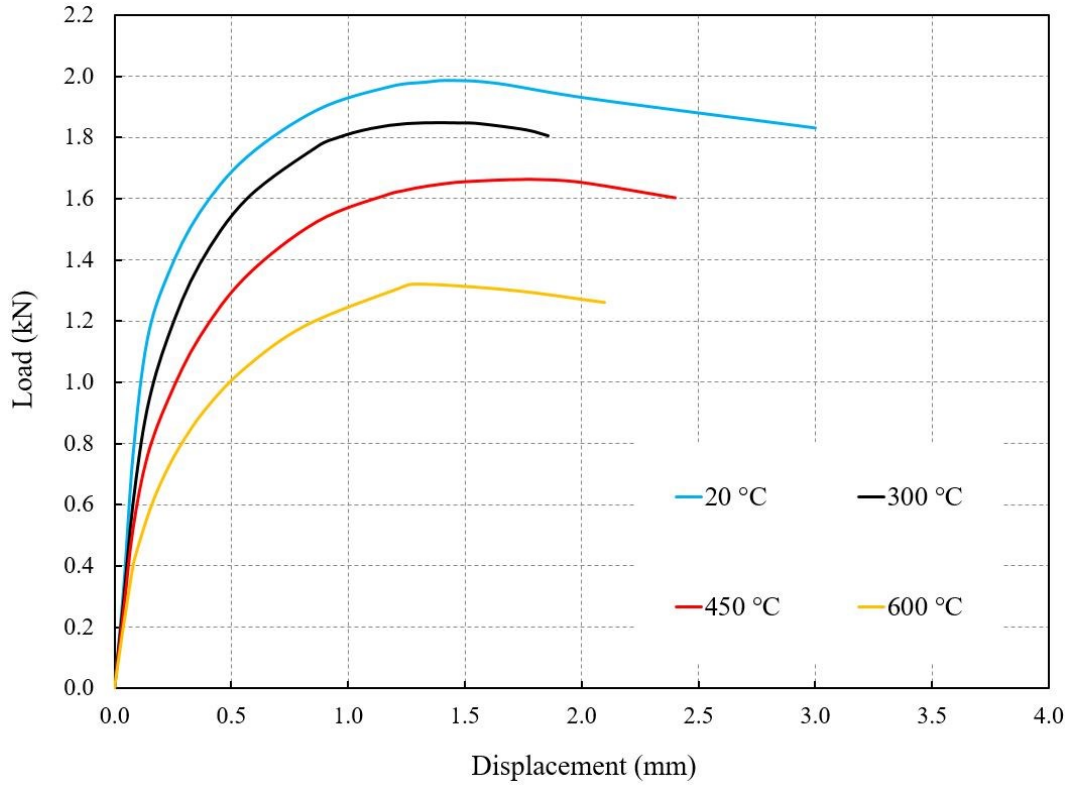

Figure F.8. Load-displacement curves for MW sandwich panels with 5.5 mm screw diameter and 0.6 mm inner sheet thickness at different temperatures

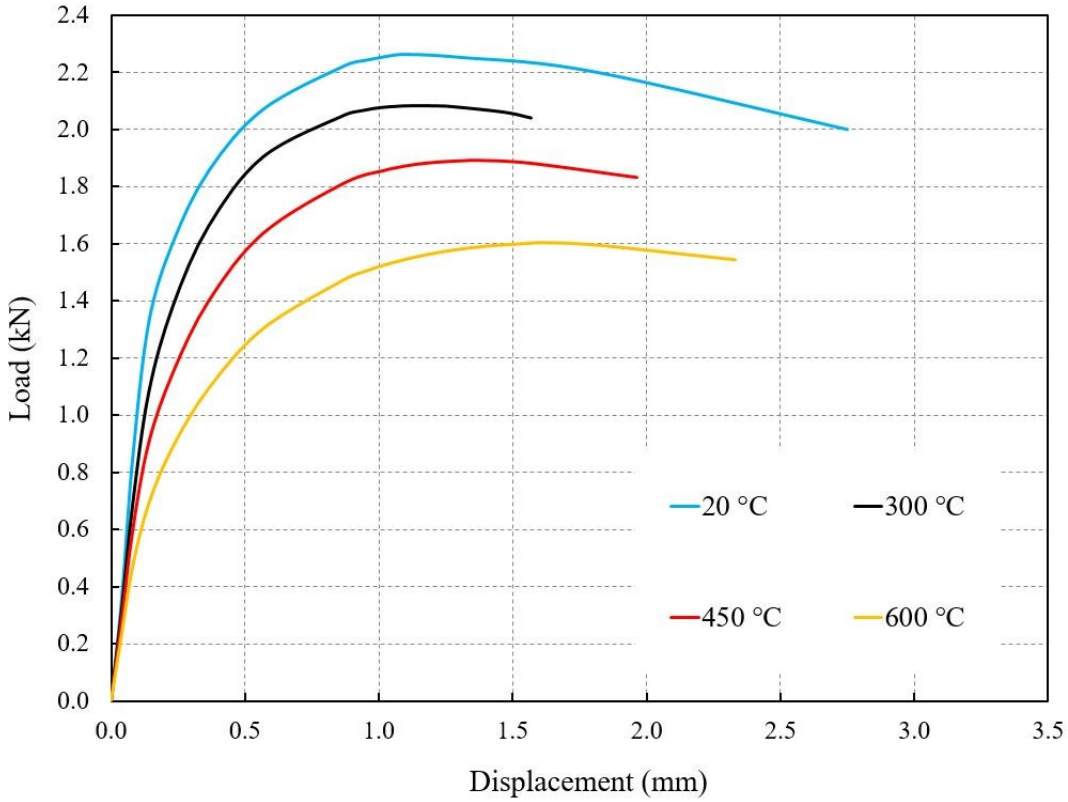

Figure F.9. Load-displacement curves for MW sandwich panels with 5.5 mm screw diameter and 0.7 mm inner sheet thickness at different temperatures

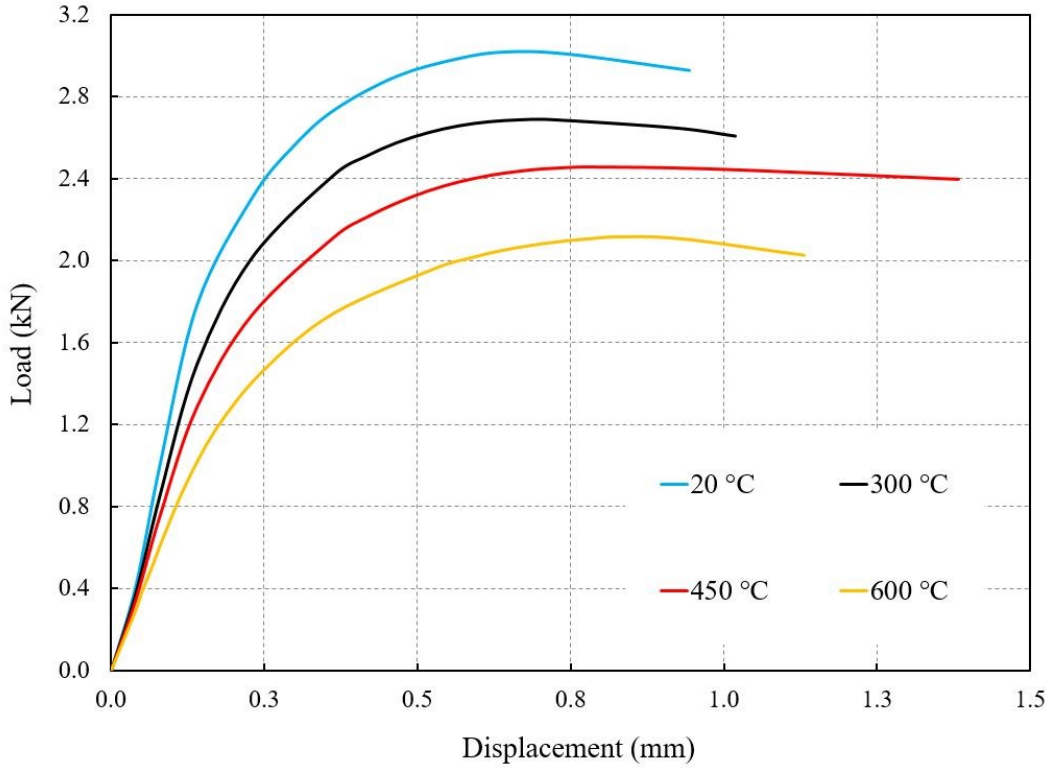

Figure F.10. Load-displacement curves for MW sandwich panels with 5.5 mm screw diameter and 1.0 mm inner sheet thickness at different temperatures

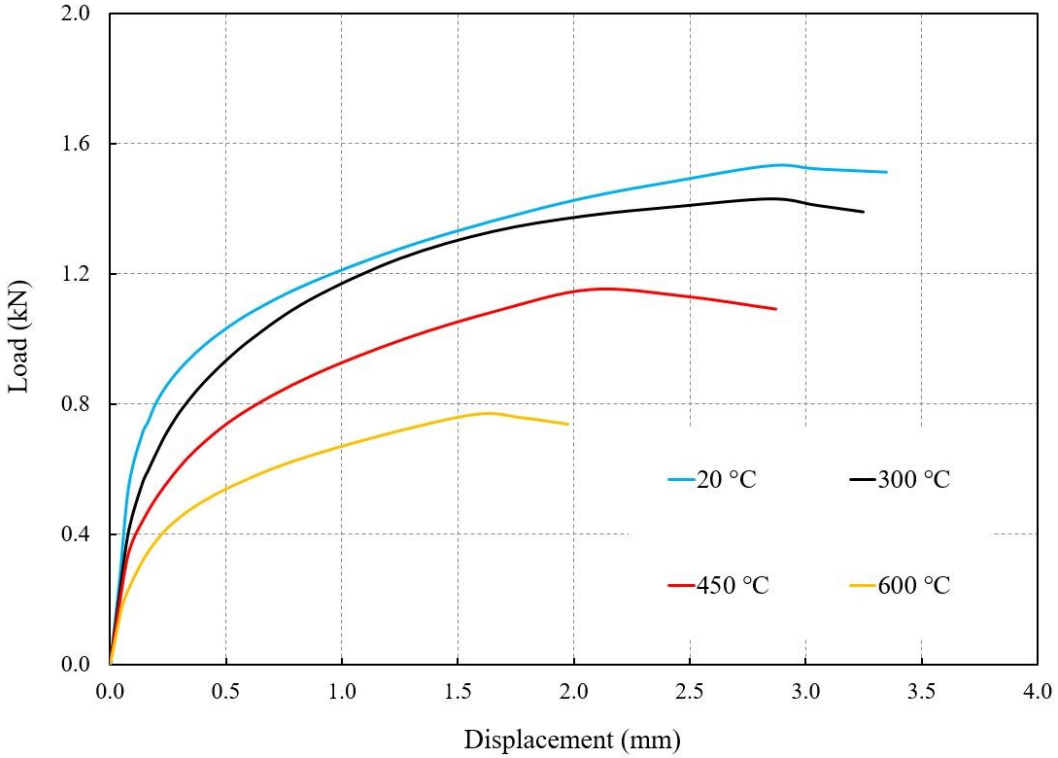

Figure F.11. Load-displacement curves for MW sandwich panels with 6.3 mm screw diameter and 0.4 mm inner sheet thickness at different temperatures

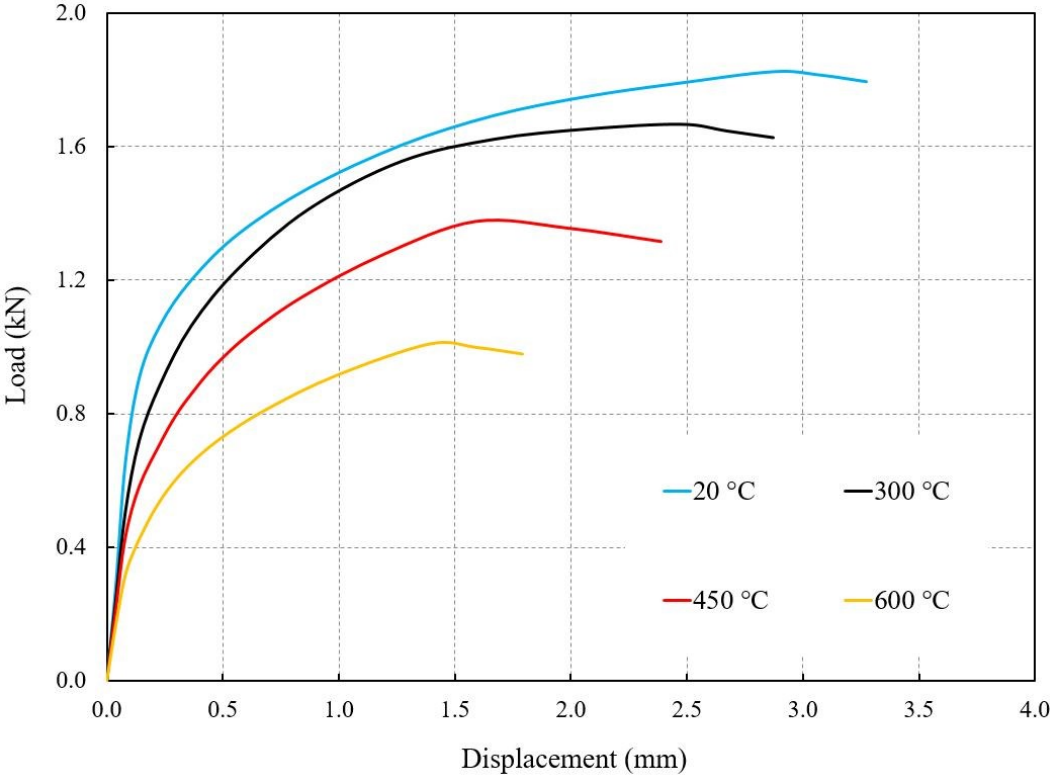

Figure F.12. Load-displacement curves for MW sandwich panels with 6.3 mm screw diameter and 0.5 mm inner sheet thickness at different temperatures

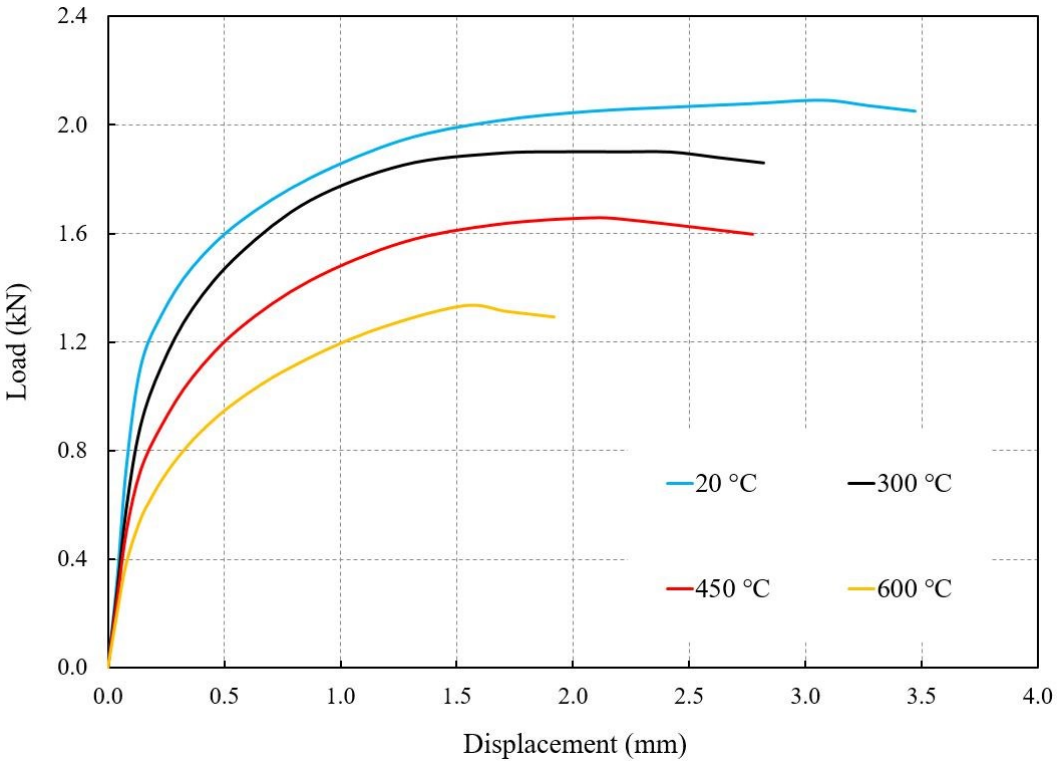

Figure F.13. Load-displacement curves for MW sandwich panels with 6.3 mm screw diameter and 0.6 mm inner sheet thickness at different temperatures

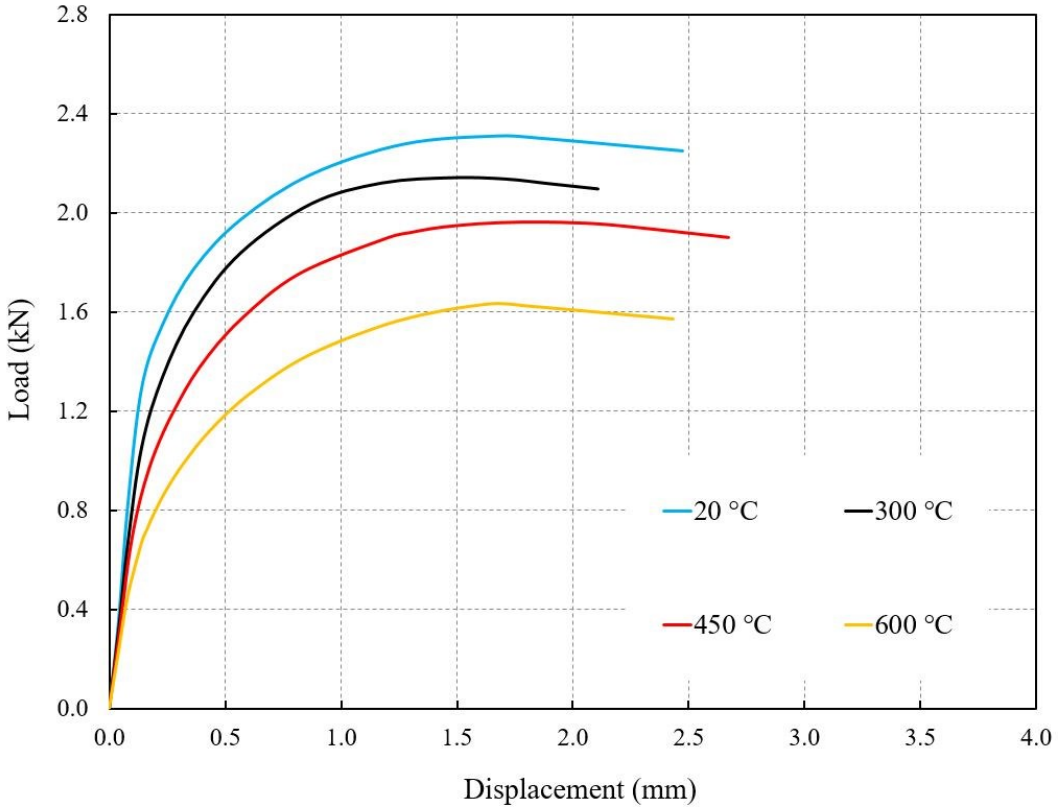

Figure F.14. Load-displacement curves for MW sandwich panels with 6.3 mm screw diameter and 0.7 mm inner sheet thickness at different temperatures

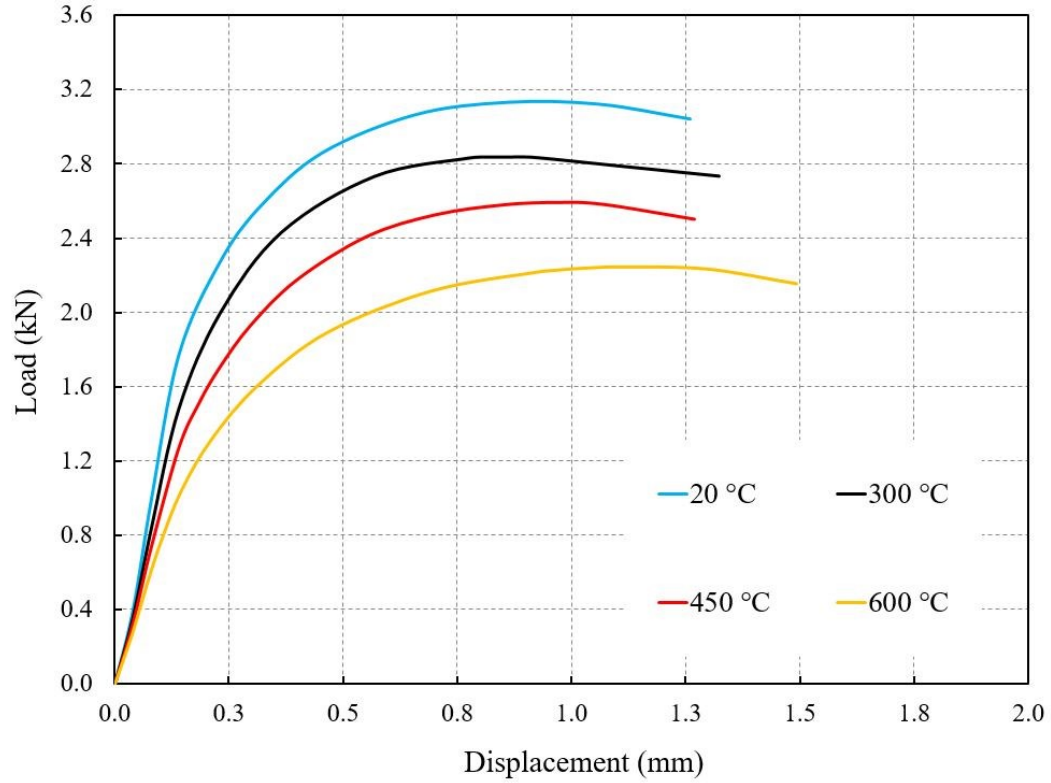

Figure F.15. Load-displacement curves for MW sandwich panels with 6.3 mm screw diameter and 1.0 mm inner sheet thickness at different temperatures

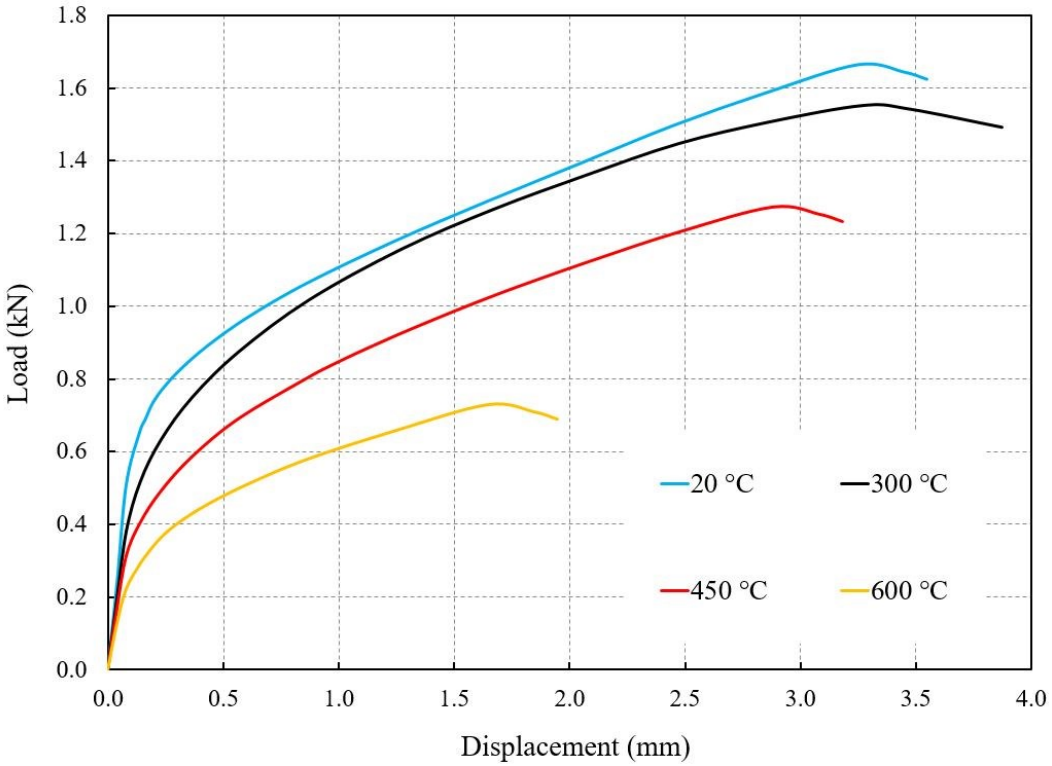

Figure F.16. Load-displacement curves for MW sandwich panels with 8.0 mm screw diameter and 0.4 mm inner sheet thickness at different temperatures

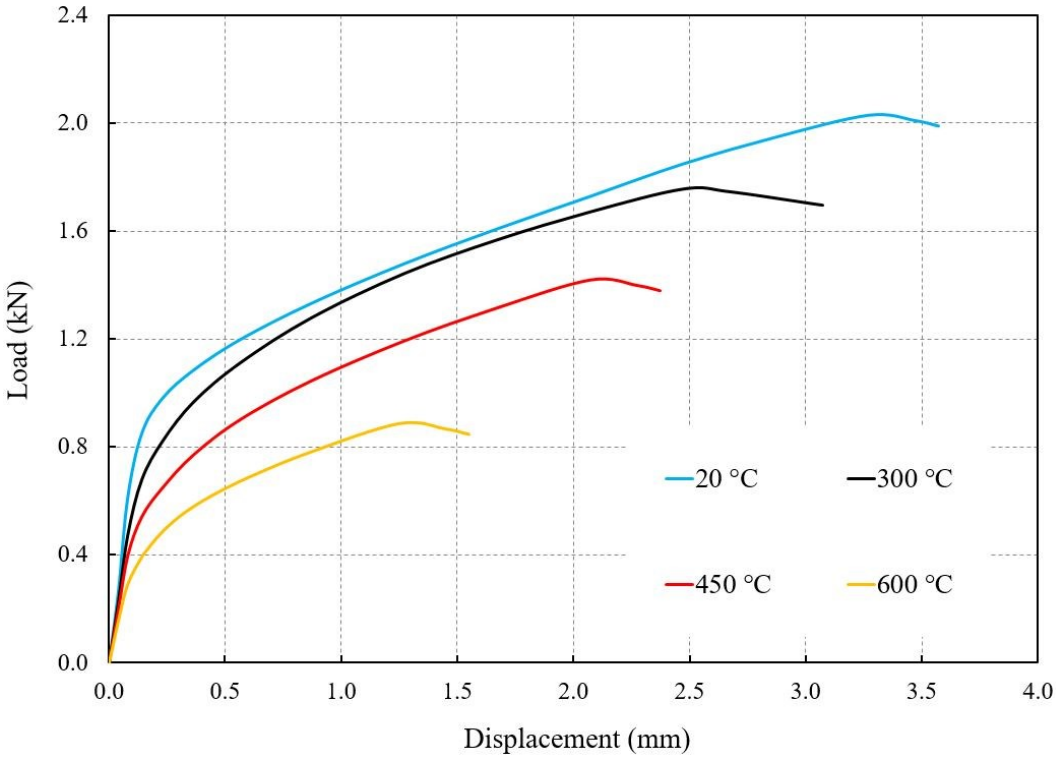

Figure F.17. Load-displacement curves for MW sandwich panels with 8.0 mm screw diameter and 0.5 mm inner sheet thickness at different temperatures

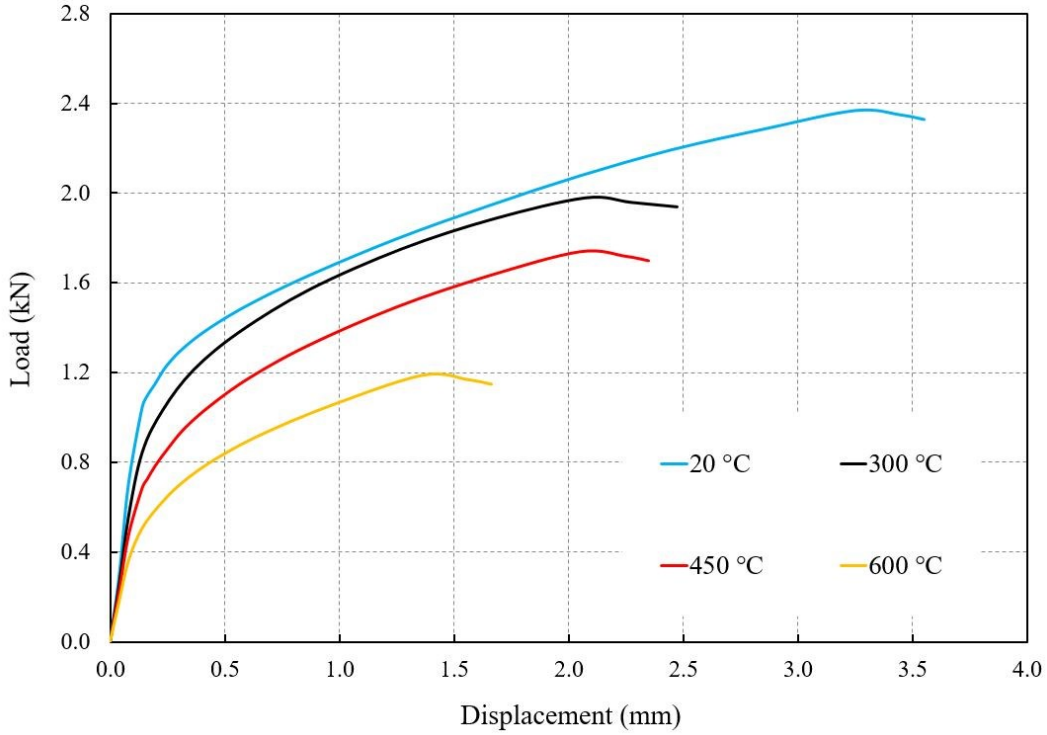

Figure F.18. Load-displacement curves for MW sandwich panels with 8.0 mm screw diameter and 0.6 mm inner sheet thickness at different temperatures

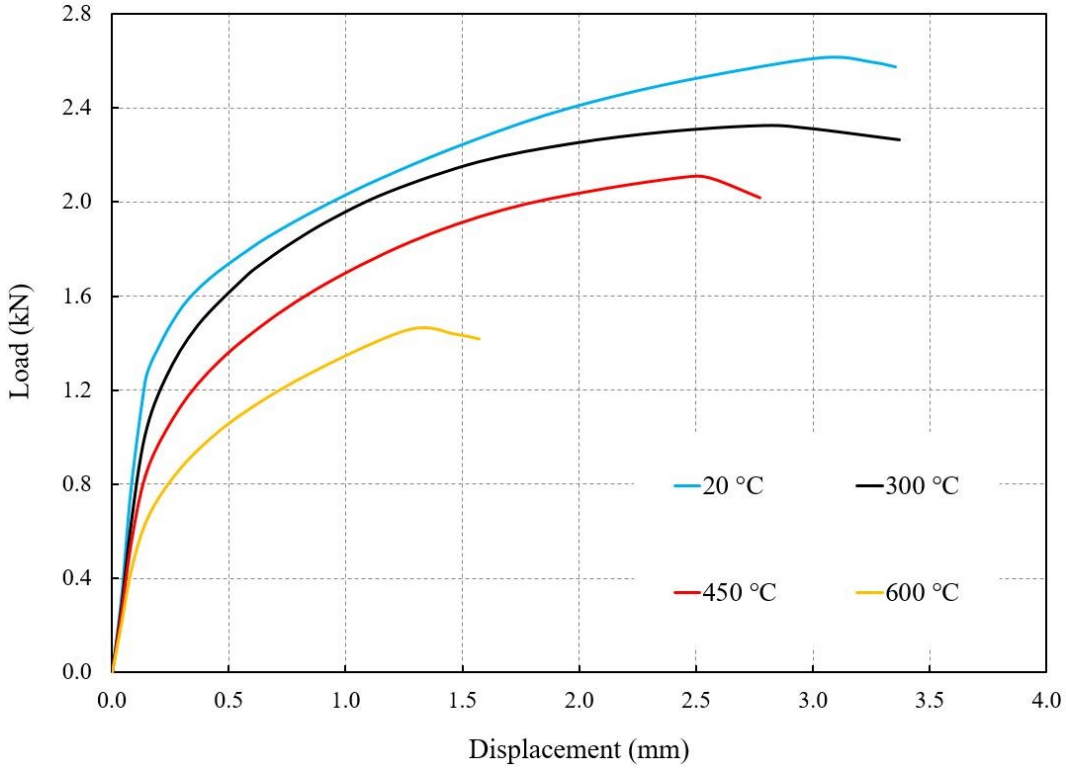

Figure F.19. Load-displacement curves for MW sandwich panels with 8.0 mm screw diameter and 0.7 mm inner sheet thickness at different temperatures

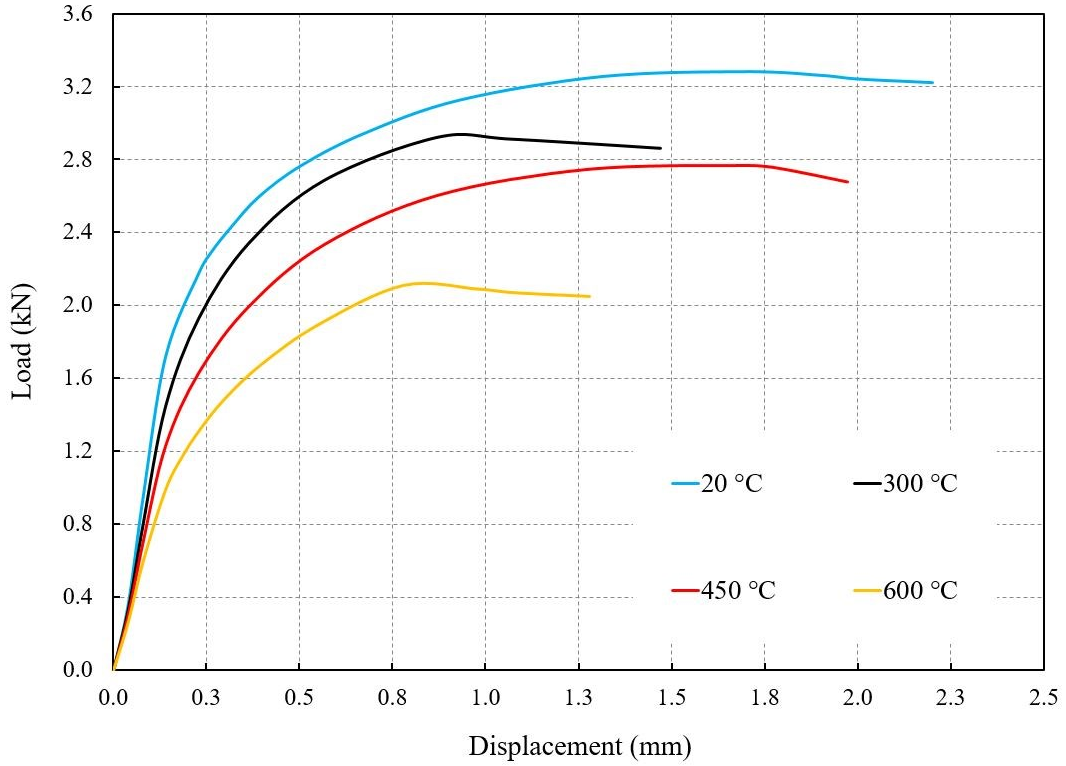

Figure F.20. Load-displacement curves for MW sandwich panels with 8.0 mm screw diameter and 1.0 mm inner sheet thickness at different temperatures

The load-displacement curves for PIR panels under shear loading obtained from FE models:

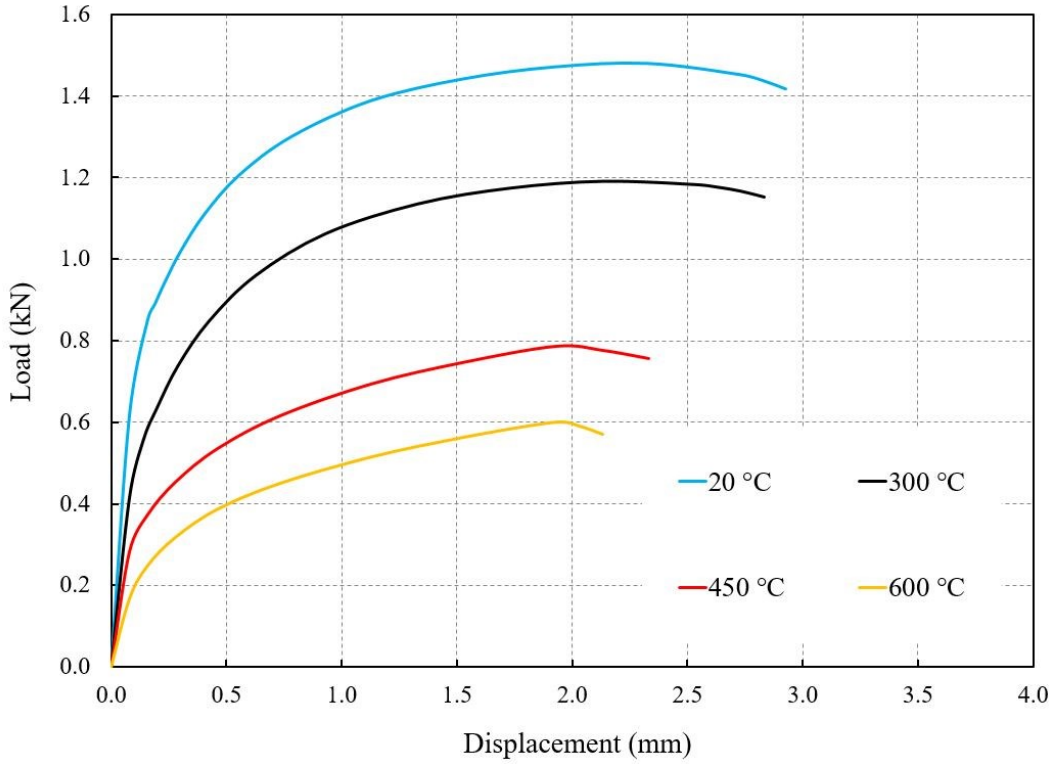

Figure F.21. Load-displacement curves for PIR sandwich panels with 4.2 mm screw diameter and 0.4 mm inner sheet thickness at different temperatures

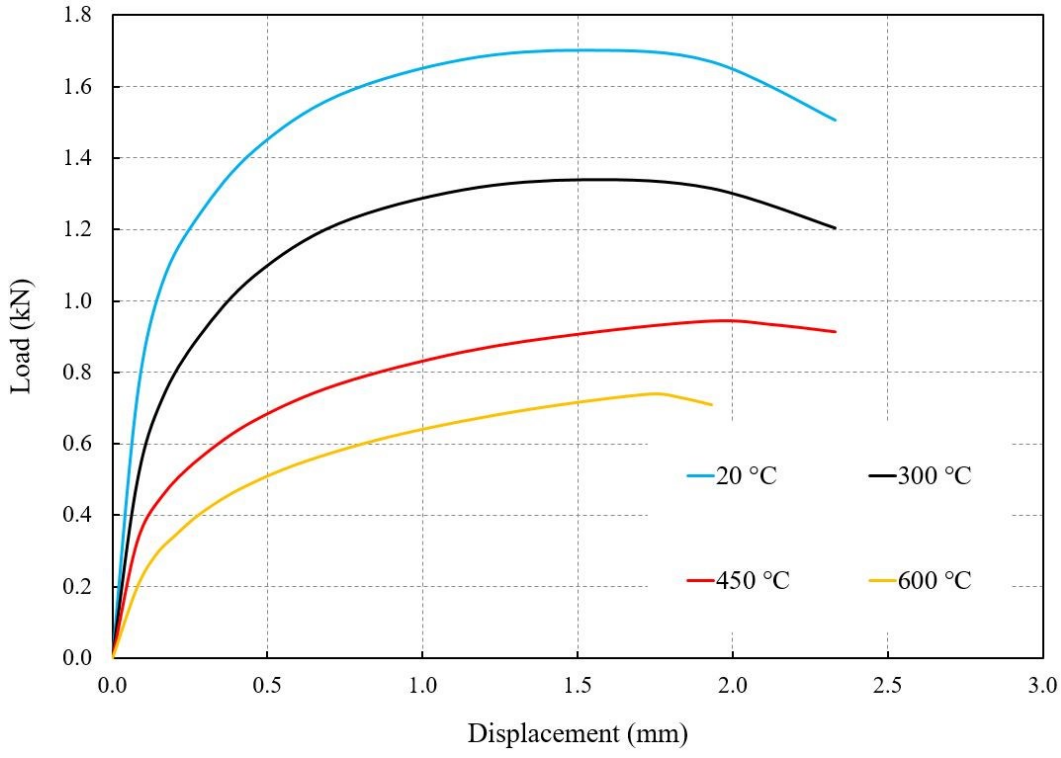

Figure F.22. Load-displacement curves for PIR sandwich panels with 4.2 mm screw diameter and 0.5 mm inner sheet thickness at different temperatures

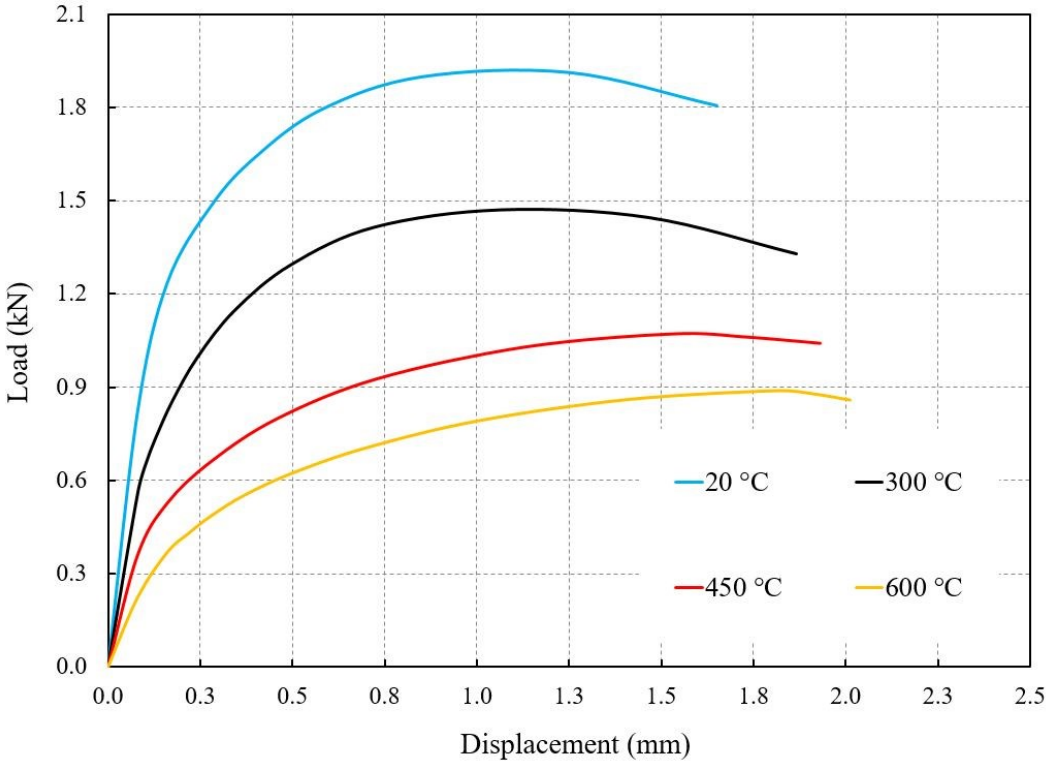

Figure F.23. Load-displacement curves for PIR sandwich panels with 4.2 mm screw diameter and 0.6 mm inner sheet thickness at different temperatures

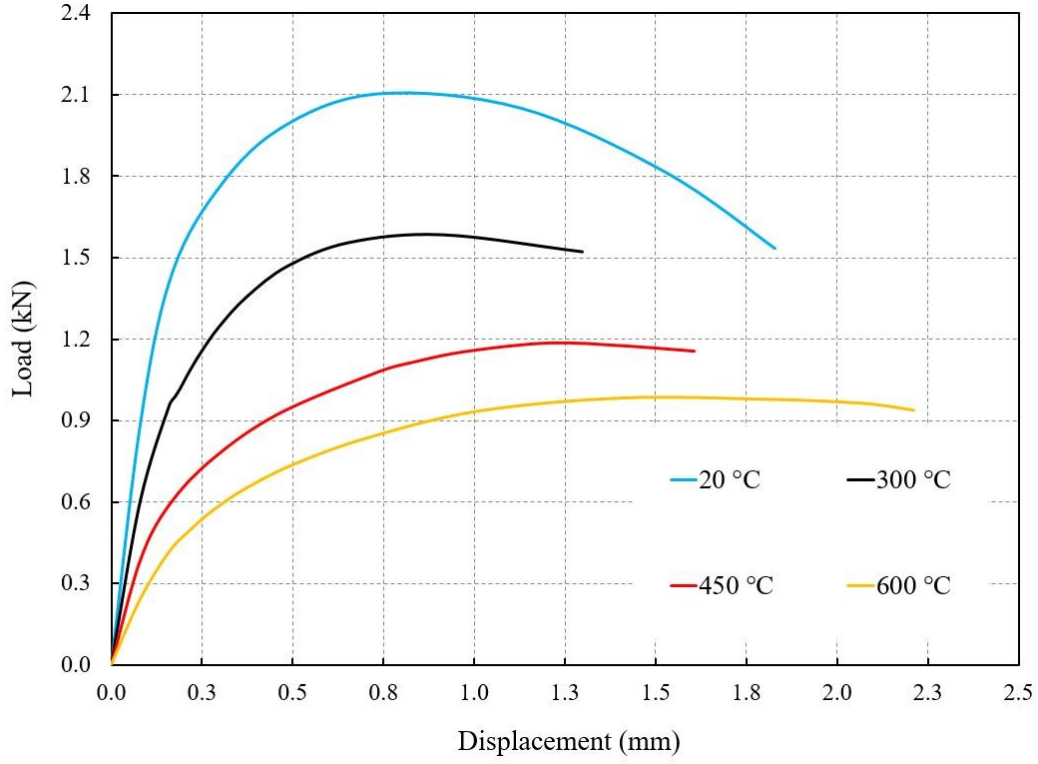

Figure F.24. Load-displacement curves for PIR sandwich panels with 4.2 mm screw diameter and 0.7 mm inner sheet thickness at different temperatures

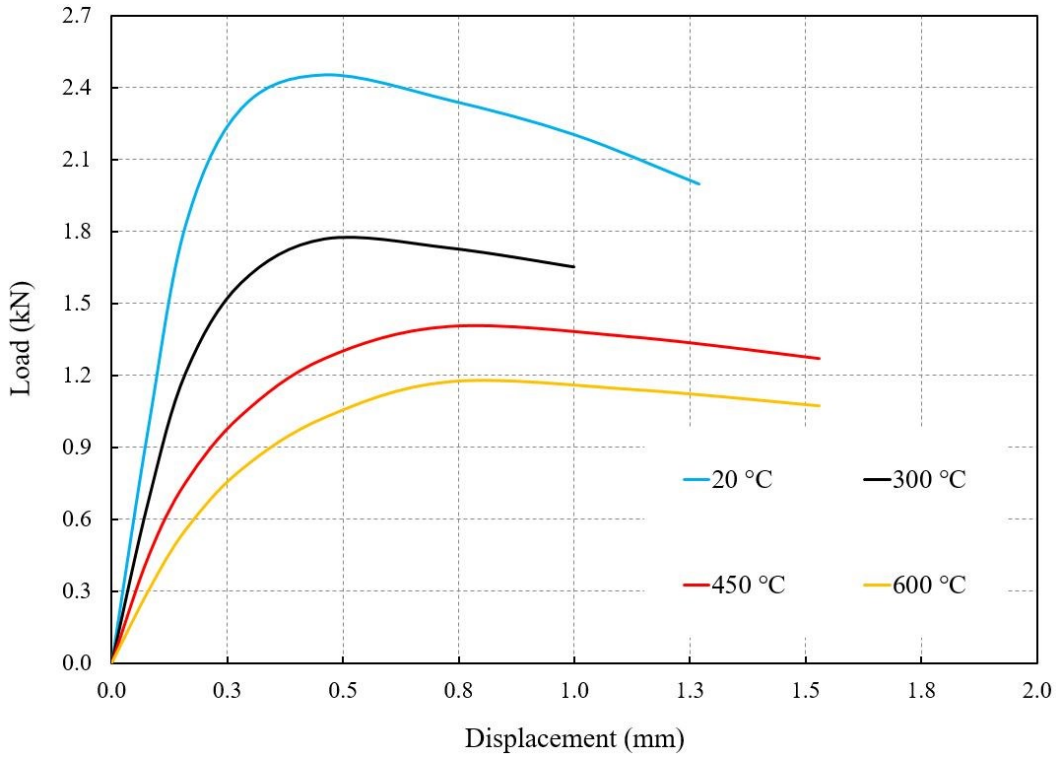

Figure F.25. Load-displacement curves for PIR sandwich panels with 4.2 mm screw diameter and 1.0 mm inner sheet thickness at different temperatures

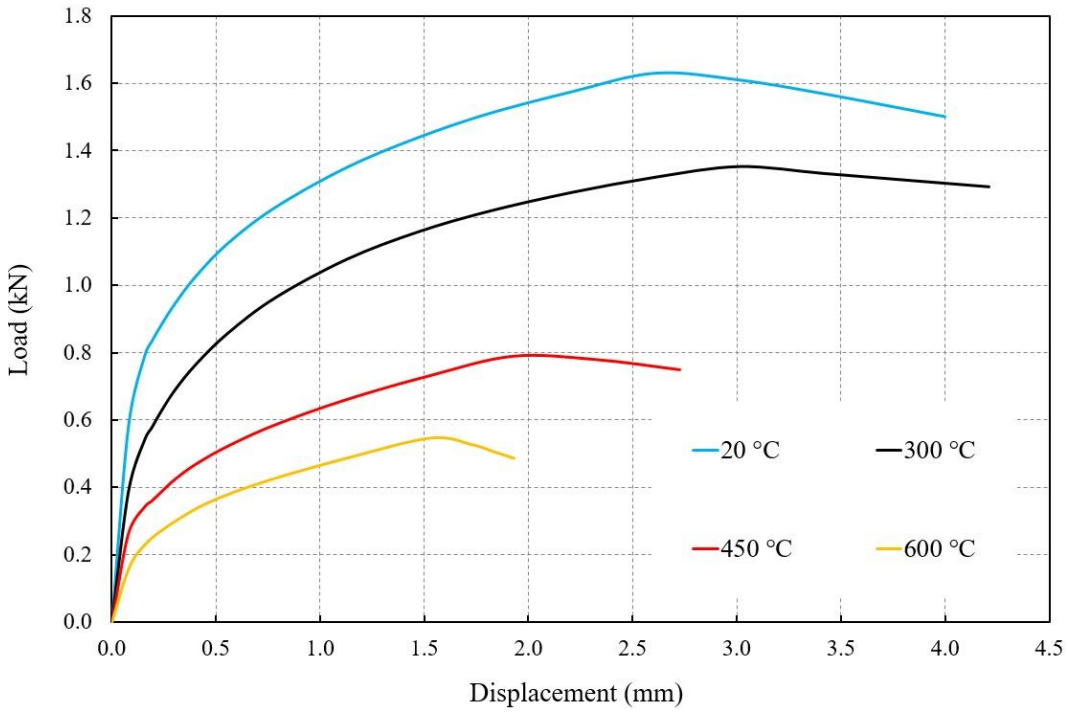

Figure F.26. Load-displacement curves for PIR sandwich panels with 5.5 mm screw diameter and 0.4 mm inner sheet thickness at different temperatures

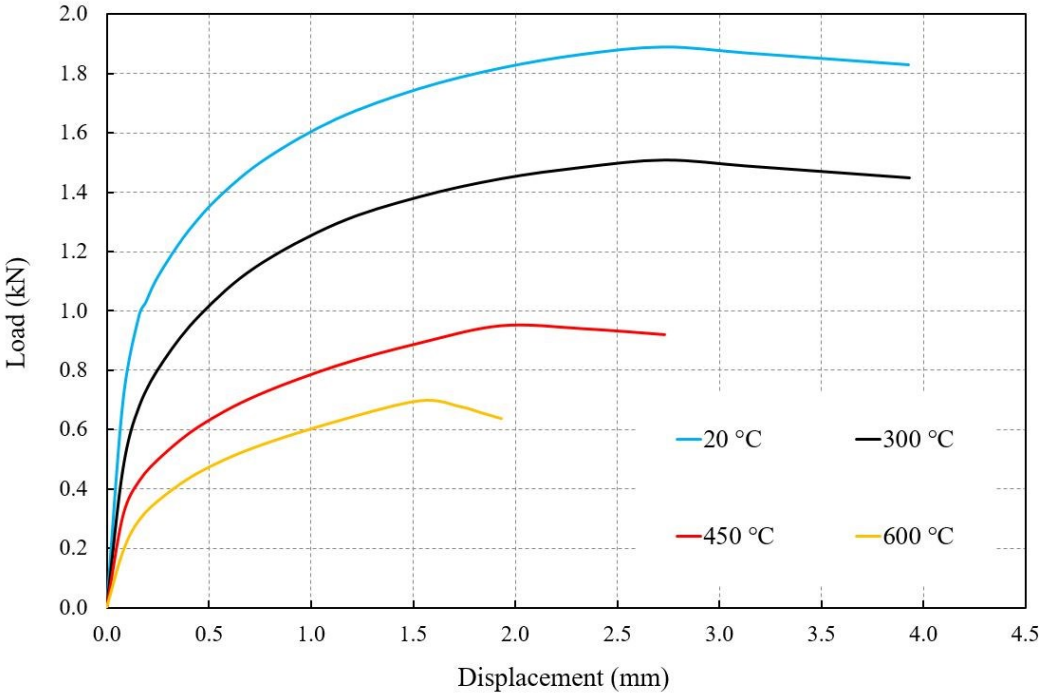

Figure F.27. Load-displacement curves for PIR sandwich panels with 5.5 mm screw diameter and 0.5 mm inner sheet thickness at different temperatures

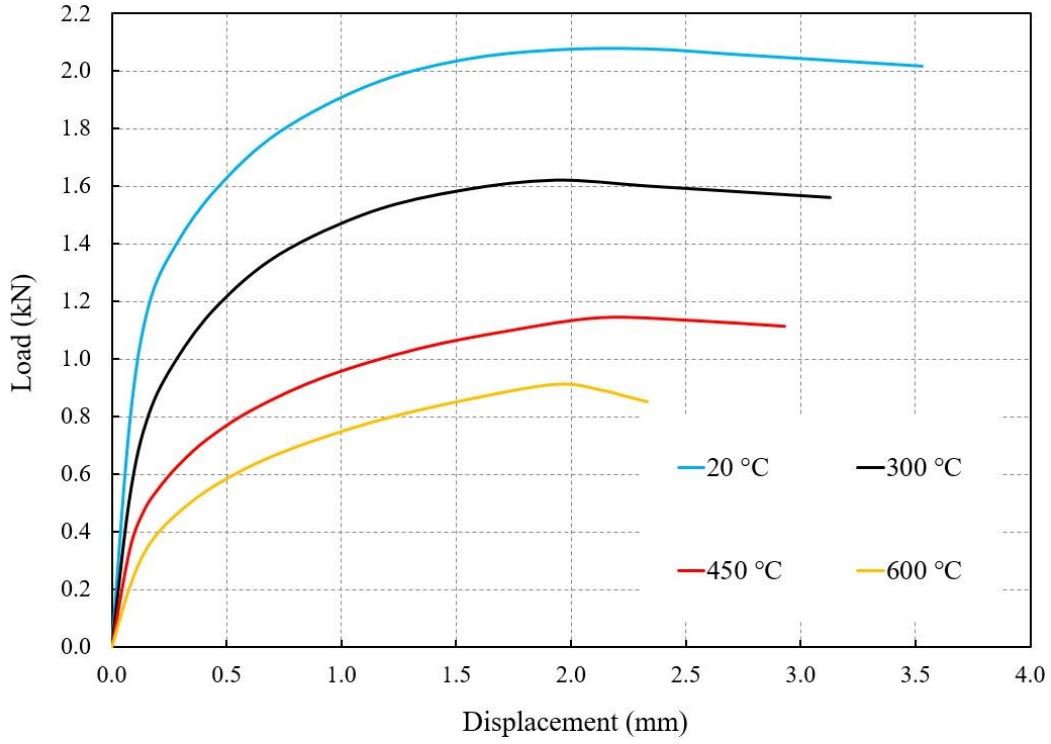

Figure F.28. Load-displacement curves for PIR sandwich panels with 5.5 mm screw diameter and 0.6 mm inner sheet thickness at different temperatures

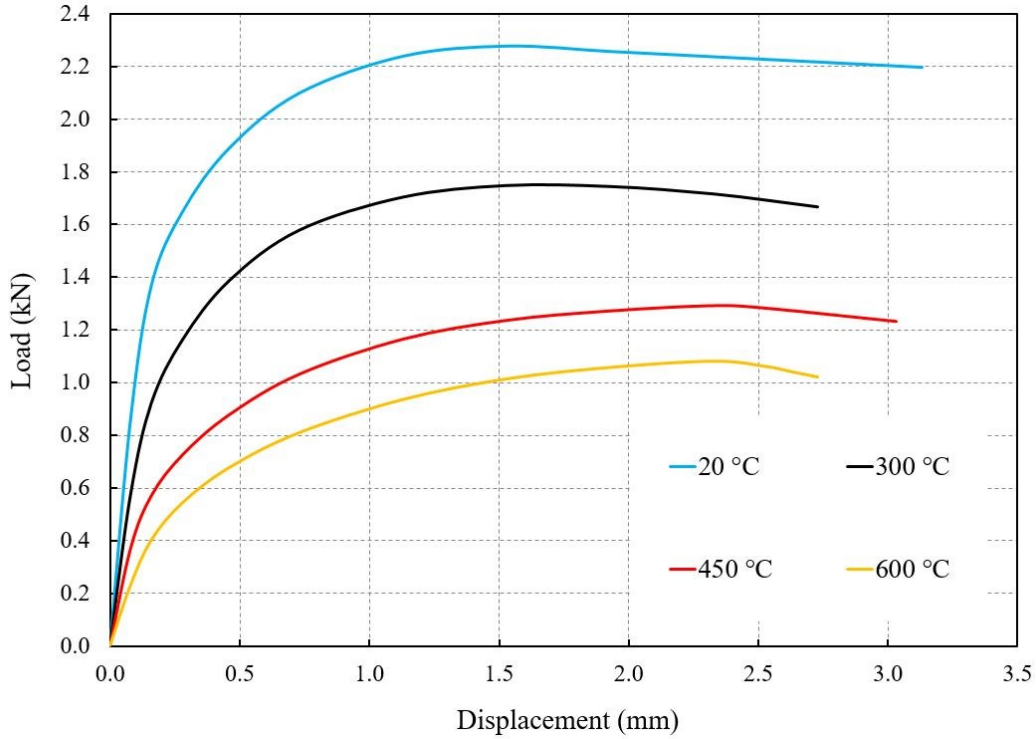

Figure F.29. Load-displacement curves for PIR sandwich panels with 5.5 mm screw diameter and 0.7 mm inner sheet thickness at different temperatures

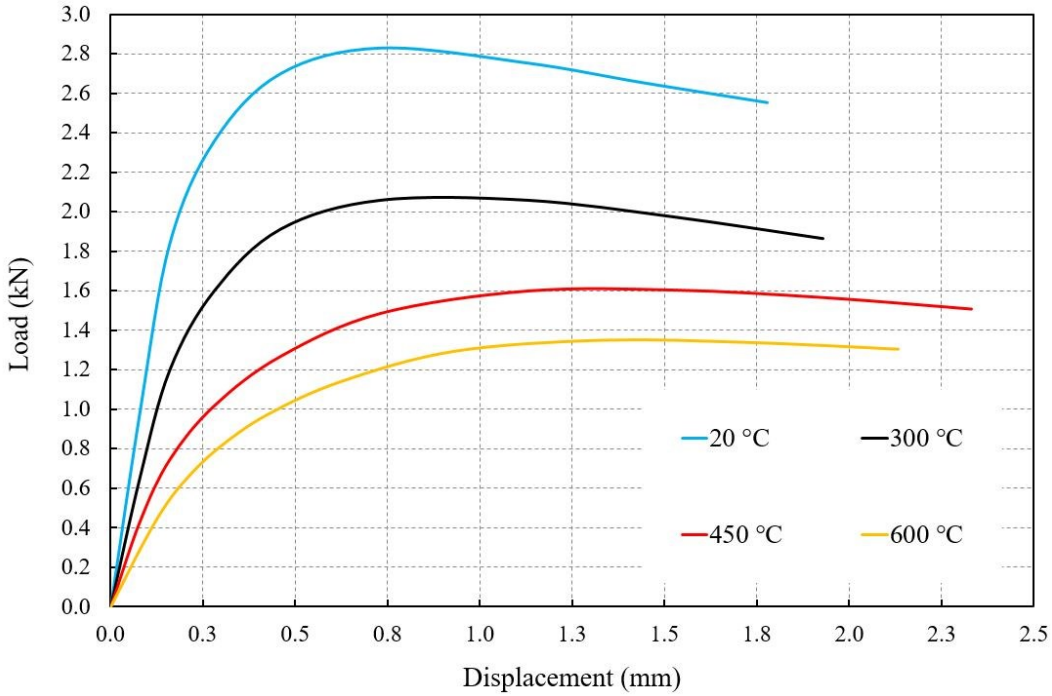

Figure F.30. Load-displacement curves for PIR sandwich panels with 5.5 mm screw diameter and 1.0 mm inner sheet thickness at different temperatures

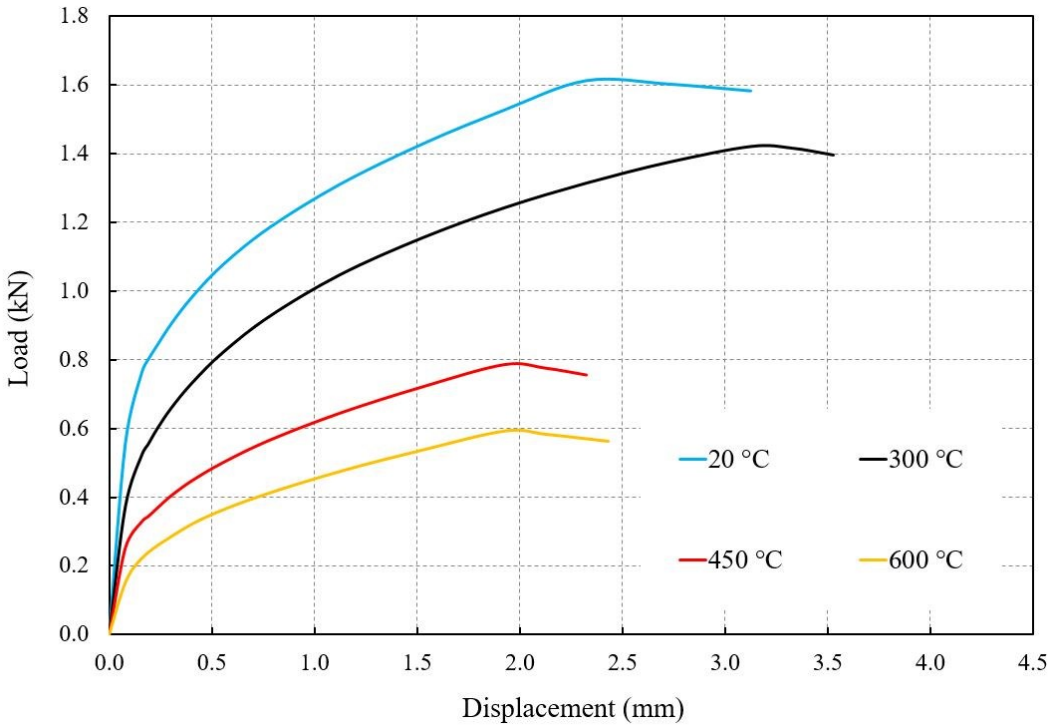

Figure F.31. Load-displacement curves for PIR sandwich panels with 6.3 mm screw diameter and 0.4 mm inner sheet thickness at different temperatures

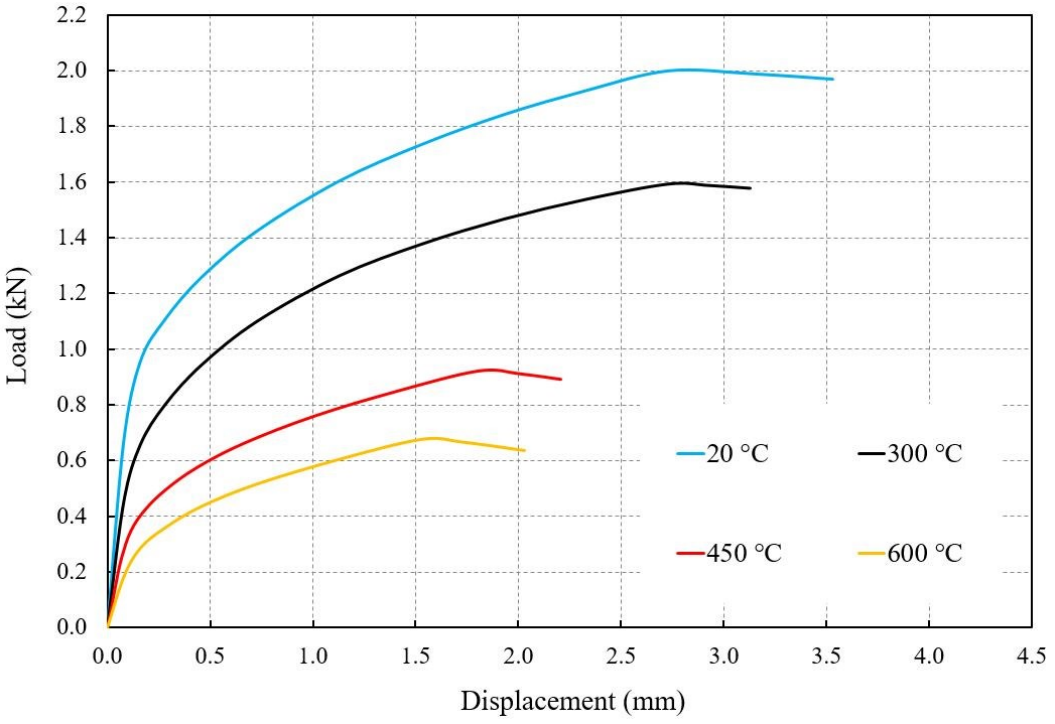

Figure F.32. Load-displacement curves for PIR sandwich panels with 6.3 mm screw diameter and 0.5 mm inner sheet thickness at different temperatures

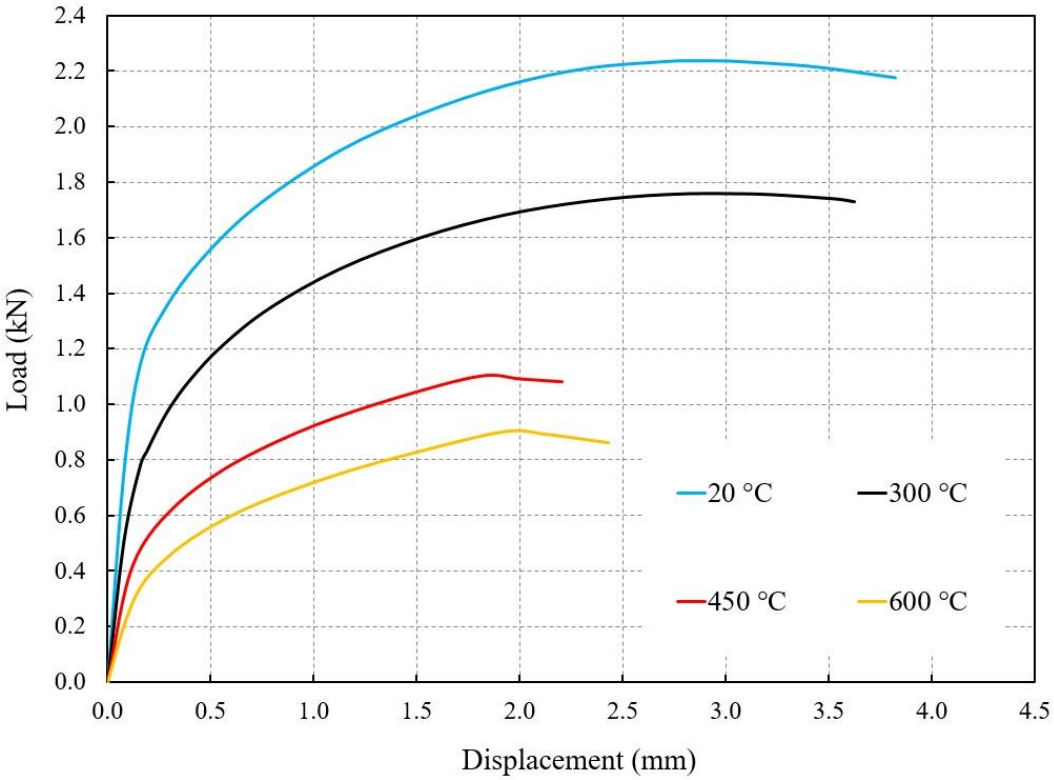

Figure F.33. Load-displacement curves for PIR sandwich panels with 6.3 mm screw diameter and 0.6 mm inner sheet thickness at different temperatures

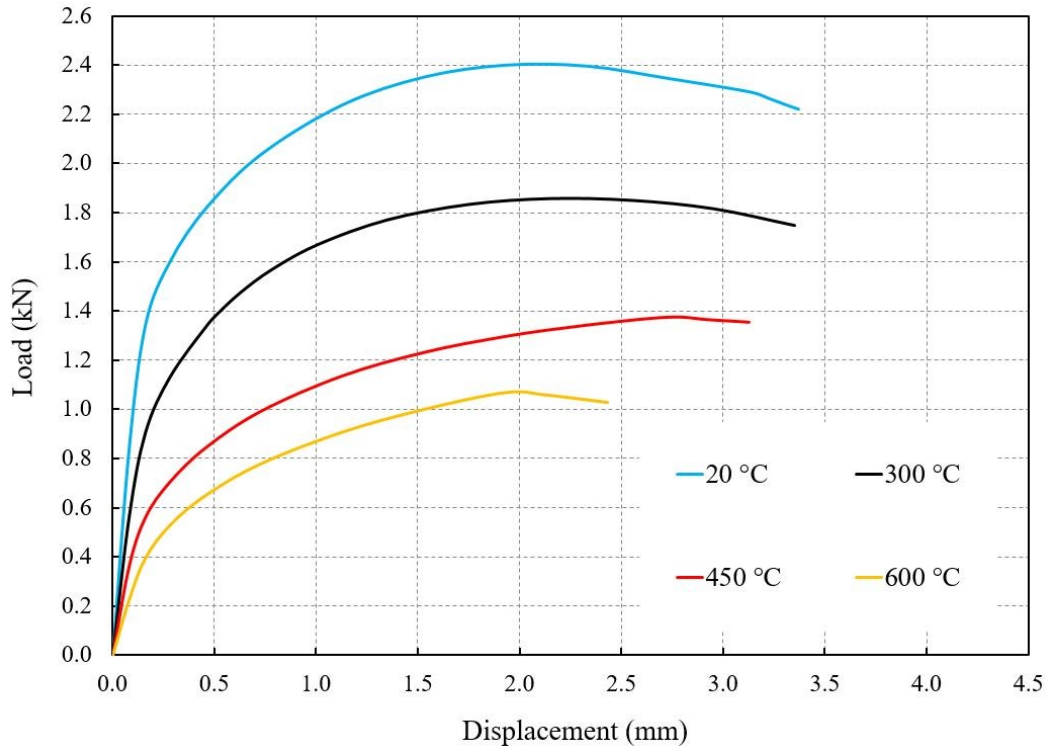

Figure F.34. Load-displacement curves for PIR sandwich panels with 6.3 mm screw diameter and 0.7 mm inner sheet thickness at different temperatures

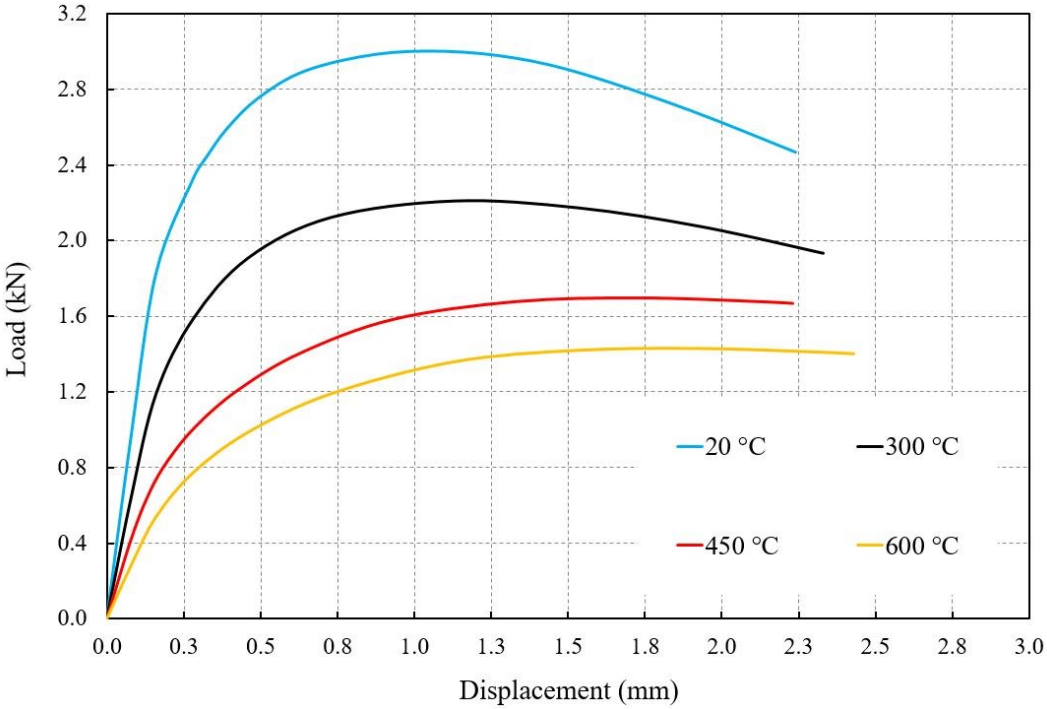

Figure F.35. Load-displacement curves for PIR sandwich panels with 6.3 mm screw diameter and 1.0 mm inner sheet thickness at different temperatures

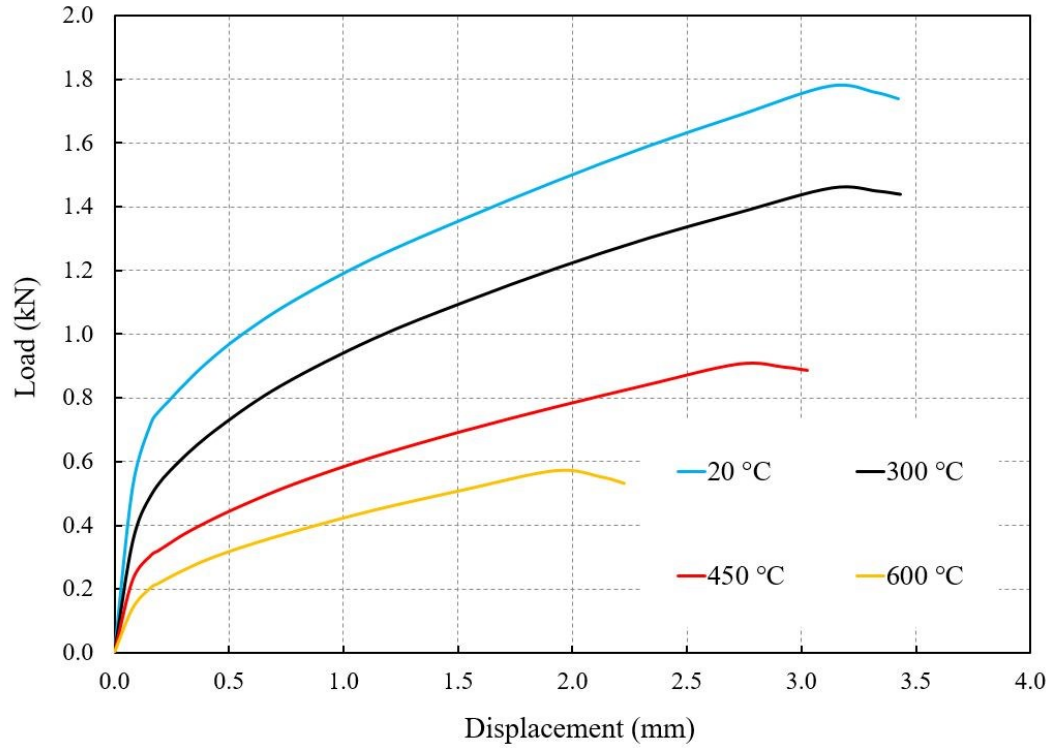

Figure F.36. Load-displacement curves for PIR sandwich panels with 8.0 mm screw diameter and 0.4 mm inner sheet thickness at different temperatures

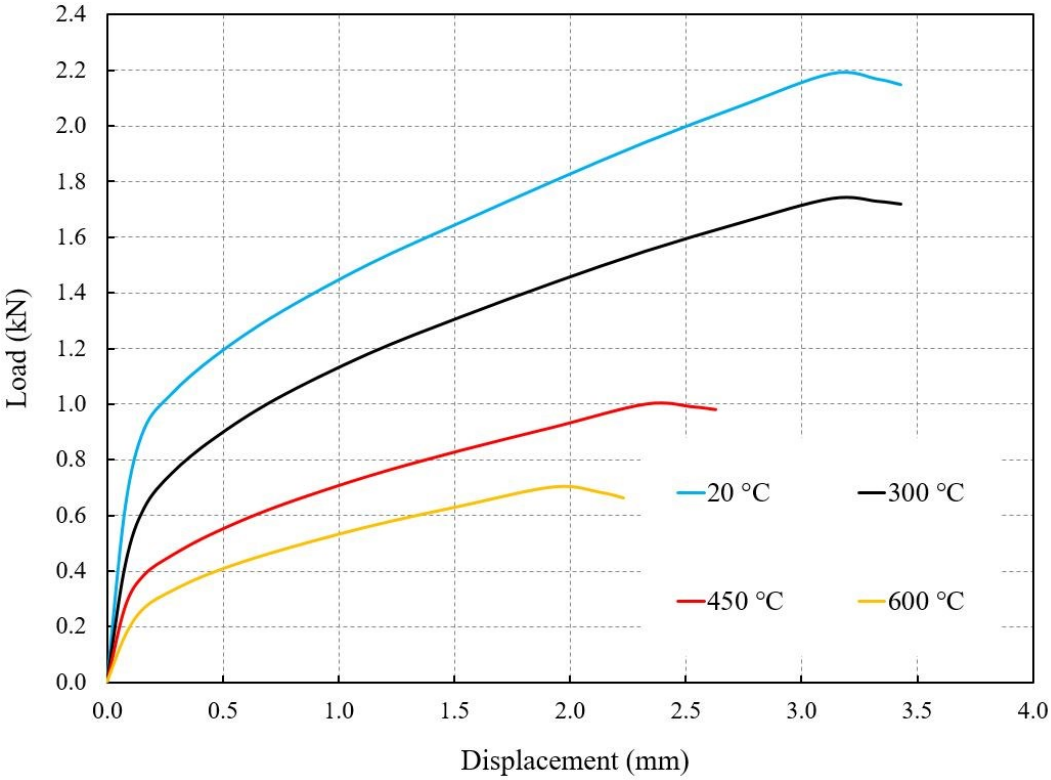

Figure F.37. Load-displacement curves for PIR sandwich panels with 8.0 mm screw diameter and 0.5 mm inner sheet thickness at different temperatures

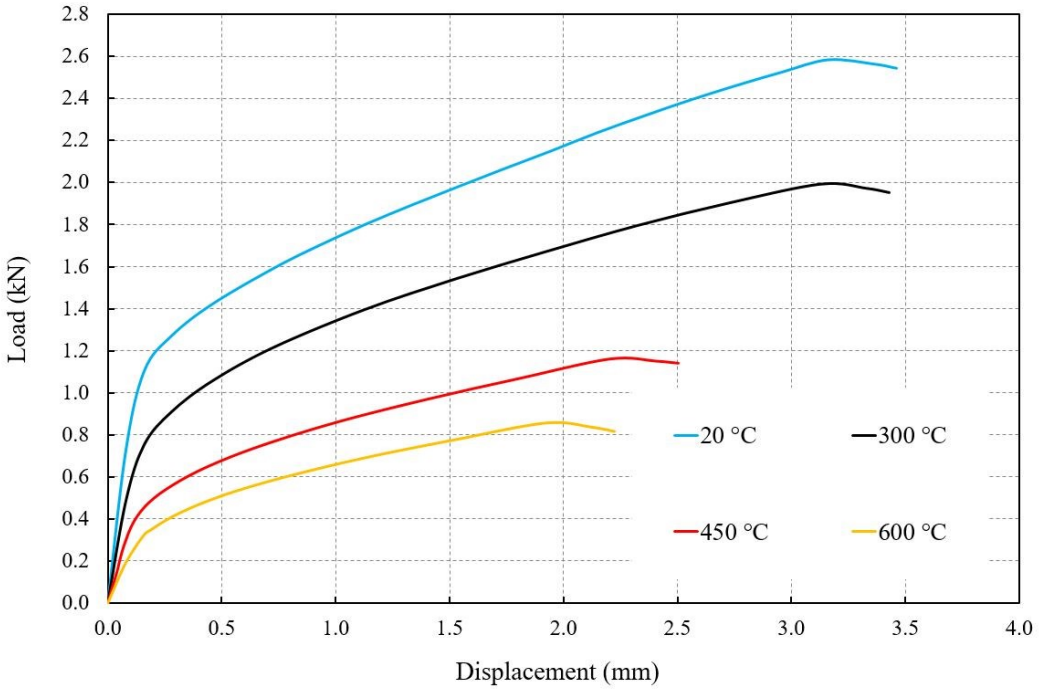

Figure F.38. Load-displacement curves for PIR sandwich panels with 8.0 mm screw diameter and 0.6 mm inner sheet thickness at different temperatures

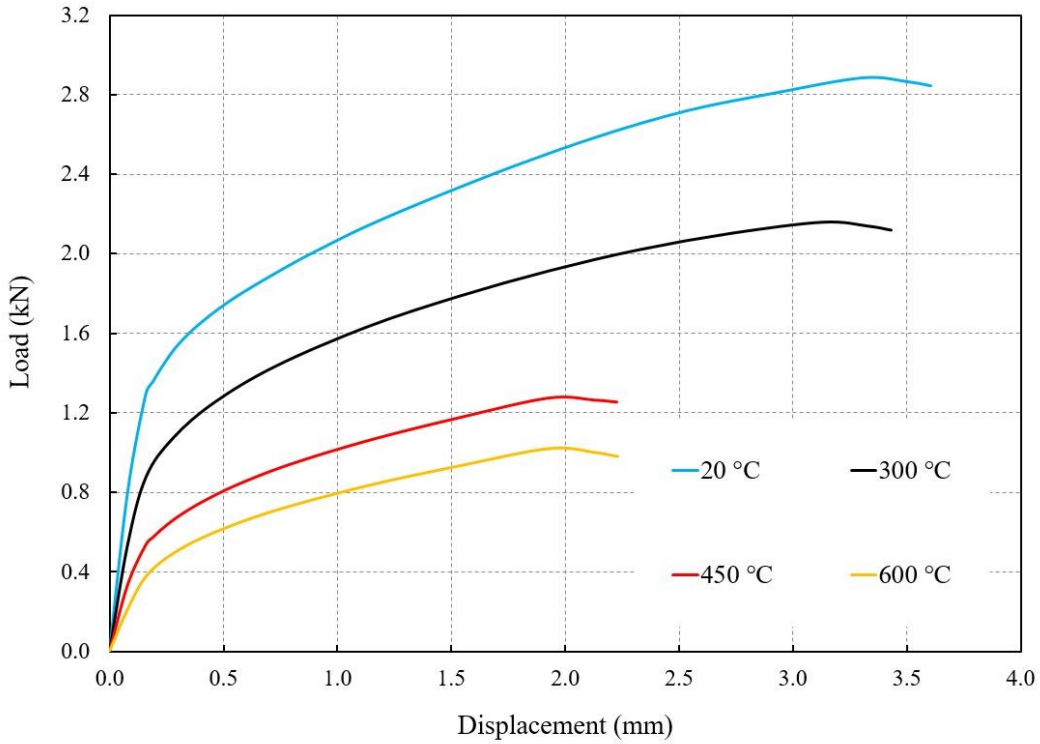

Figure F.39. Load-displacement curves for PIR sandwich panels with 8.0 mm screw diameter and 0.7 mm inner sheet thickness at different temperatures

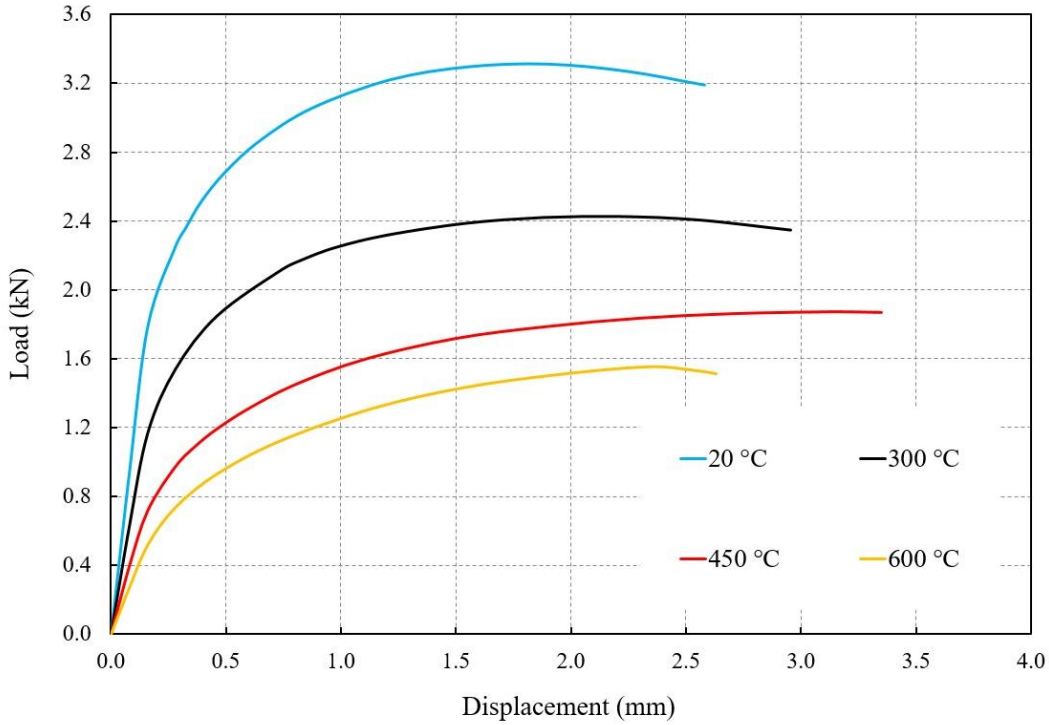

Figure F.40. Load-displacement curves for PIR sandwich panels with 8.0 mm screw diameter and 1.0 mm inner sheet thickness at different temperatures